INFORMATION TO USERS

This manuscript has been reproduced from the microfilm master. UMI films the text directly from the original or copy submitted. Thus, some thesis and dissertation copies are in typewriter face, while others may be from any type of computer printer.

The quality of this reproduction is dependent upon the quality of the copy submitted. Broken or indistinct print, colored or poor quality illustrations and photographs, print bleedthrough, substandard margins, and improper alignment can adversely affect reproduction.

In the unlikely event that the author did not send UMI a complete manuscript and there are missing pages, these will be noted. Also, if unauthorized copyright material had to be removed, a note will indicate the deletion.

Oversize materials (e.g., maps, drawings, charts) are reproduced by sectioning the original, beginning at the upper left-hand corner and continuing from left to right in equal sections with small overlaps.

Photographs included in the original manuscript have been reproduced xerographically in this copy. Higher quality 6" x 9" black and white photographic prints are available for any photographs or illustrations appearing in this copy for an additional charge. Contact UMI directly to order.

SYNTHESIS AND PHOTOPHYSICS OF MONO-DIPERSE PHENYLENE
ETHYNYLENE OLIGOMERS THAT FEATURE Ru(II), Os(II) AND Re(I)
POLYPYRIDINE COMPLEXES

By

YITING LI

A DISSERTATION PRESENTED TO THE GRADUATE SCHOOL
OF THE UNIVERSITY OF FLORIDA IN PARTIAL FULFILLMENT
OF THE REQUIREMENTS FOR THE DEGREE OF
DOCTOR OF PHILOSOPHY

UNIVERSITY OF FLORIDA

2001

UMI Number: 3027544

UMI®

Copyright 2001

by

Yiting Li

Dedicated to my family for their love and support

ACKNOWLEDGMENTS

I am grateful to the chairman of my committee, Dr. Kirk S. Schanze, who introduced this area of research to me. I would also like to thank him for his guidance, both professionally and personally, and also for his tremendous encouragement, advice and support during my doctoral work.

I would also like to thank the other members of my committee, Dr. William R. Dolbier, Dr. Kenneth B. Wagener, Dr. David E. Richardson, and Dr. Bruce F. Carroll, for their valued advice, expertise, and support which helped in the development of this research project.

I would also like to thank Dr. Yibing Shen and Dr. Yingsheng Wang for all their help and continued friendship.

I would also like to thank Dr. Shujun Jiang and Dr. Yao Liu for their help in my work.

I would also like to thank all members (or former members) of the Schanze Group, Shengxia Liu, Kevin Ley, Keith Walters, Ed Whittle, Chunyan Tan, Eric Silverman, Ksenija Glusac, and Benjamin Harrison.

Last, but not least, I would like to thank my husband, Tianhong Jiang, for his love, support and understanding during the most trying years of my life and to my family in Pennsylvania, Minnesota, and China for their love and support.

iv

TABLE OF CONTENTS

Abstract of Dissertation Presented to the Graduate School
of the University of Florida in Partial Fulfillment of the
Requirements for the Degree of Doctor of Philosophy

SYNTHESIS AND PHOTOPHYSICS OF MONO-DIPERSE PHENYLENE
ETHYNYLENE OLIGOMERS THAT FEATURE Ru(II), Os(II) AND Re(I)
POLYPYRIDINE COMPLEXES

By

Yiting Li

August, 2001

Chairman: Kirk S. Schanze
Major Department: Chemistry

There has been a surge of interest concerning the synthesis and properties of π-conjugated polymers that contain transition metal complexes. The integration of transition metal chromophores with metal-to-ligand charge transfer (MLCT) excited states into the polymers permits easy variation of their optical properties by changing ligands or the metal chromophore. However, their photophysical properties were not the major focus of the reported research. With this in mind, the synthesis and photophysics of two different types of metal-organic polymers and oligomers are presented.

First, a series of mass exact PPE-type aryleneethynylene oligomers with the $Ru^{II}(bpy)_2$ chromophore incorporated via a 2,2'-bipyridyl unit were synthesized. Organic-based fluorescence is quenched, and is replaced by an MLCT-based emission. Photoluminescence and transient absorption photophysics are dominated by ^{3}MLCT excited state. But the energy levels of ^{3}MLCT and $^3\pi,\pi^*$ excited states are very close and

there is equilibrium between these two manifolds. To gain a further understanding of the interaction between the PPE backbone and the metal center, electron withdrawing substituents were introduced into the bipyridine group on $Ru^{II}(bpy)_2$ chromophore. The observed MLCT emission quenching is attributed to the presence of a ligand-to-ligand charge-transfer state in the excited state manifold. Also the PPE oligomers containing different metal centers, $Os^{II}(bpy)_2$ and $Re(CO)_3(MQ^+)$, were synthesized. By incorporation of low oxidation potential osmium metal, the MLCT state is separated from $^3\pi,\pi^*$ states and the "unperturbed" MLCT emission is observed. The MLCT state gives rise to a luminescence and lifetime that are typical for the $Os(bpy)_3$ chromophore. The introduction of $Re(CO)_3(MQ^+)$ chromophore into the PPE backbone shifts the MLCT state to higher energy. And the $^3\pi,\pi^*$ state becomes dominant at photoluminescence and transient absorption spectra.

Second, a mass exact PPVE-type aryleneethynylene vinylene oligomer that incorporates $Ru(bpy)_2$ chromophore is synthesized. The introduction of vinylene bond into PPE backbone decreases the energy level of $^3\pi,\pi^*$ state and the photoluminescence and transient absorption are dominated by $^3\pi,\pi^*$ phosphorescence.

CHAPTER 1
INTRODUCTION

Conjugated oligomers and polymers are macromolecules that, in a formal sense, possess π-orbitals that are delocalized along the entire backbone of the molecule.[1] Such oligomers and polymers have received considerable attention owing to their unique optical and electrooptical device applications. Prime examples are organic-based light-emitting diodes (LEDs),[2-3] photoconductive or photorefractive devices,[4-5] chemical sensors,[6-8] and molecular electronic devices.[9-10] During the past decade, considerable research effort has explored the properties of organic-based π-conjugated oligomers and polymers. The class of conjugated polymers which has found the most attention in the past is undoubtedly the poly(*p*-phenylenevinylene)s (PPVs). However, the structurally close relative to PPV, the poly(phenyleneethylene)s (PPEs), have attracted much less attention in the polymer community, despite their fascinating properties. The synthesis and photophysics of PPE oligomers and polymers are considered here. Conjugated materials incorporating redox-active transition metal center will be discussed here also because of their unique properties.

Sonogashira Cu-Pd-Catalyzed Alkyne Coupling Reaction and Synthesis of PPE Polymers

Carbon-carbon bond-forming reactions are of crucial importance to the practicing organic chemist. One such reaction which is technically simple, efficient, and high-yielding is the Sonogashira copper-palladium-catalyzed coupling of terminal alkynes to aromatic halides.[11,12] The reaction was developed in 1975 by Sonogashira et al.[11] at the same time as both Dieck and Heck[13] and Cassar[14] reported a similar process which did

1

not involve copper catalyst but which required much more forcing conditions. This coupling is useful for forming C-C single bonds between sp- and sp^2-hybridized carbon centers and for synthesis of PPE based polymers (Figure 1-1) because it removes the requirement for the quite serious technical difficulties involved in the preparation and safe handling of copper acetylides and allows a huge range of substrates to couple under very mild conditions.

X = Cl, Br or I
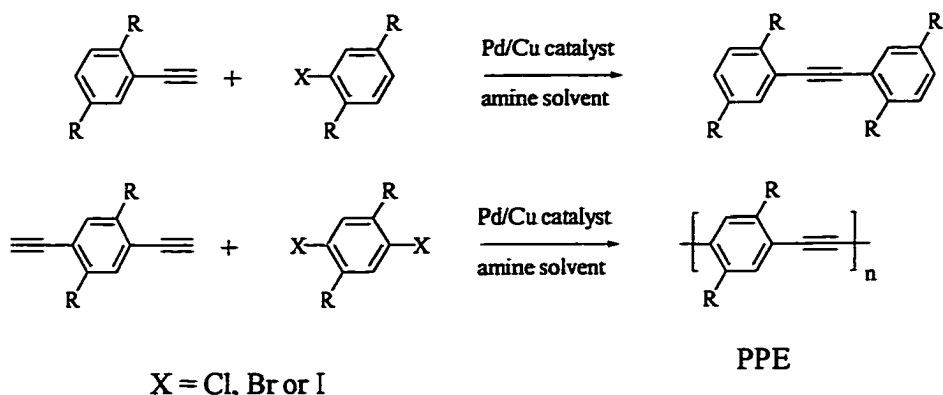
Figure 1-1: General reaction scheme of Sonogashira coupling reaction.

The generally accepted mechanism of this reaction is depicted in Figure 1-2.[15] In most cases the commercially available $Pd(PPh_3)_2Cl_2$ is the catalytic source of Pd, largely due to the air stability of $Pd(PPh_3)_2Cl_2$ relative to the other Pd^0 catalysts. Pd in its oxidized form is inactive. It is generally believed that substitution occurs through the initial formation of a bis(triphenylphosphine)dialkynylpalladium^{II} complex (**B**), which gives the active catalytic species bis(triphenylphosphine)palladium^0 complex (**C**), through reductive elimination of a 1,3-butadiyne. Subsequent oxidative addition of an aryl halide to (**C**), followed by an alkynylation of the adduct (**D**), gives an aryl-derivative of palladium (**E**). The latter regenerates the original bis(triphenylphosphine)palladium^0

(C) through reductive elimination of the desired coupling products. The alkynylation of the starting catalyst (A), or an oxidative adduct (D) in the catalytic cycle, is catalyzed by cuprous iodide in the presence of an amine based solvent, typically triethylamine. Several of the critical factors that affect the reaction are the choice of the aryl halide, substituent choice on the haloarene, the type and amount of starting catalyst as well as the choice of solvents.
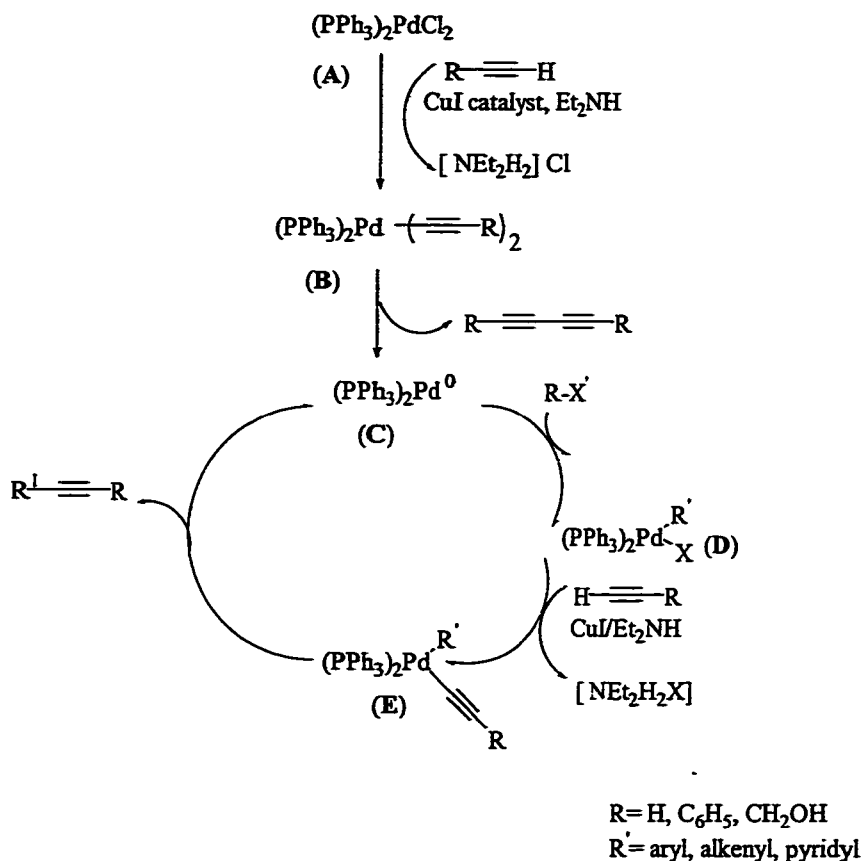
Figure 1-2: Proposed mechanism for the palladium mediated coupling of a terminal acetylene with an aryl halide (Ref. 15).

Choice of Halide

The most commonly used form of the Sonogashira reaction is that in which an aromatic idode is coupled with a terminal alkyne. The reaction takes place readily at room temperature (Figure 1-3). Aromatic bromides react much less readily than the corresponding iodides and will generally require solvents at reflux in order to effect reaction. The reaction of aromatic chlorides with alkynes under Sonogashira conditions is much more restricted in the nature of substrate which will participate in the process. Only those benzenoid aromatic chlorides which also processes suitably sited electron-withdrawing groups – particularly nitro – are likely to react to any appreciable extent.[16] It is proposed that the oxidative addition of C is more facile for aryliodides than for the bromides. The relative ease of oxidative addition of the aryliodide to C is a function of the lower bond dissociation energy of the aryliodide compared to the arylbromide. As a consequence polymer formation can be conducted under mild conditions when iodides are used so that problems including cross-linking and formation of defects are minimized.
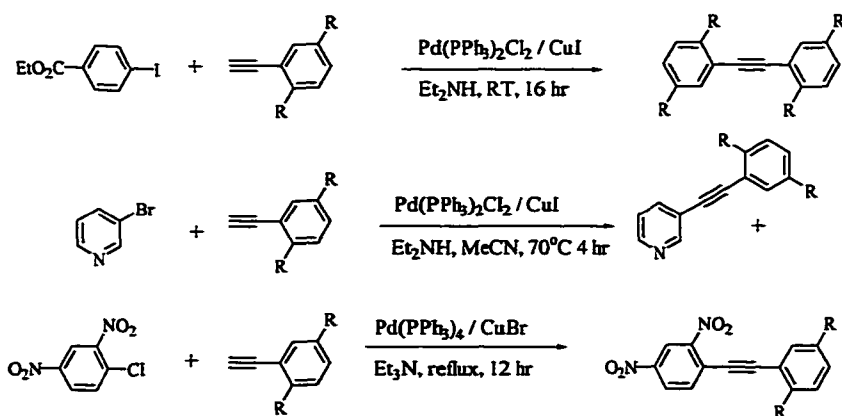
Figure 1-3: Sonogashira coupling reaction (Ref. 17).

Substituents on the Haloarene

The active catalyst of **C** is an electron-rich species, and as a consequence, oxidative addition, i.e., the formation of **D**, is dramatically influenced by the nature of the substituents Y on the aromatic nucleus. The more electron –withdrawing Y is, the faster its oxidative addition to the electron rich Pd^0 proceeds. Consequently, an electron-withdrawing substituent Y on the halide improves both the rate and yield of these coupling reactions. *Ortho-* and *para-* positioned acceptor substituents are more efficient than ones placed in the meta-position.

Catalyst

Most frequently 0.1-5 mmol% $Pd(PPh_3)_2Cl_2$ and varying amounts of CuI are used in both small-molecule and polymer-forming reactions. The small-molecule couplings for iodoarenes take approximately 1-2 hr until they are complete. But for polymerization, it is necessary to stir the reaction mixture for extended periods of time (24-48 hr) to ensure the consumption of the monomers. It was noted that the formation of high molecular weight polymers was difficult using $Pd(PPh_3)_2Cl_2$ since the activation step uses up some of the alkyne present in the reaction mixture and a small percentage of butadiyne defects was incorporated in the polymer[18,19]. This problem can be circumvented by using $Pd(PPh_3)_4$.[6, 20-21] But extreme caution must be taken to eliminate even trace amounts of oxygen to produce high molecular weight polymers.

Solvents

Generally, the yield and purity of the coupling products are very dependent upon careful choice of amine and cosolvent. The amine base must be readily able to deprotonate the terminal alkyne at elevated temperature, allowing for addition of the alkyne to the Pd^0 catalyst. Cosolvent is necessary to ensure solubility of the formed

polymer. A good choice of amine seems to be diisopropylamine and triethylamine and THF and toluene as cosolvent.[15] Other bases such as piperidine, pyrrolidine, and morpholine have been used with success in small molecule synthesis but have had little success in large molecule (PPE) polymer synthesis.[22]

Transition Metal-Containing π-Conjugated Oligomers and Polymers

There has been a surge of interest concerning the synthesis and properties of π-conjugated polymers that contain transition metal complexes.[23-28] Much of the work in this area has focused on new materials for application such as light-emitting diodes, photorefractivity, photoconductivity, electrochromism, and chemical sensing.

To reap the greatest rewards of a transition metal/conjugated polymer hybrid, the ideal structure would have the metal centers directly affixed to, and in direct electronic communication with, the polymer backbone. There are only a few reported examples of conjugated polymers where metal centers are in conjugation with the polymer's π-system. All of these systems possess metal centers coordinated to bidentate, nitrogen-containing, heterocyclic units(2,2'-bithiazole, 2,2-bipyridyl, or Schiff base) incorporated into the polymer backbone.

Such design concepts were first reported utilizing 2,2'-bithiazole and 2,2'-bipyridine units, respectively, as postpolymerization metal coordination sites.[29-32] A poly-2,2'-bipyridine (**PBpy**) linear polymer was synthesized by dehalogenation polycondensation of dihaloaromatic compounds. The bipyridine repeat unit allows easy ligation of ruthenium, nickel, copper, and iron chromophores, as shown with the $Ru^{II}(bpy)_2^{2+}$ chromophore in Fig 1-4. The UV-visible spectrum of the methanol solution gives rise to an absorption band at about 450 nm overlapped with a tail of the π-π*

7

absorption of **PBpy** at 373 nm. The photoluminescence spectrum of the polymer gives rise to a strong emission band at 640 nm, which is attributed to MLCT based emission. The cyclic voltammetry of the **Pbpy-Ru** complex was composed of the $Ru^{II} \rightarrow Ru^{III}$ oxidation peaks which were shifted to lower potentials and all the redox peaks are broadened compared to the redox peaks of $[Ru(bpy)_3]^{2+}$. These results suggest the presence of electronic interactions between the Ru species through electronically conductive polymer chain. The photophysics of Yamamoto's **PBpy-Ru** polymer were largely neglected due to the polymer's insolubility, as well as the fact that the author's objectives for studying the **PBby-Ru** polymers were aimed at examining their photocatalytic and photoelectrochemical properties.
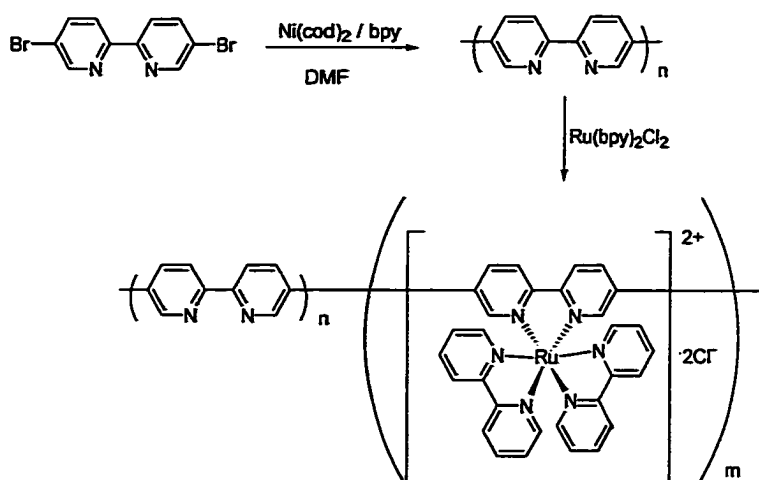
Figure 1-4: Poly(arylene) polymer synthesized by Yamamoto incorporating a $Ru(bpy)_3^{2+}$ MLCT chromophore (Ref. 30).

Cameron and Pickup[33] synthesized polymer based on the complexation of poly[2-(2-pyridyl)-bibenzimidazole] with $Ru(bpy)_2^{2+}$ (Figure 1-5). The polymer exhibits an absorption due to the π,π^* transition at $\lambda_{max} = 401$ nm in DMF. They found that there is

Reproduced with permission of the copyright owner. Further reproduction prohibited without permission.

electronic communication between metal centers through the conjugated backbone. Electron transport in the new polymer is enhanced by communication through the backbone.
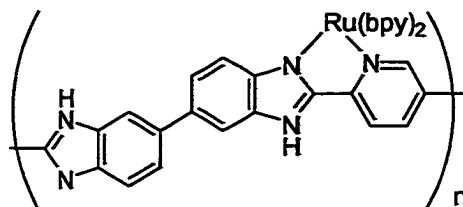
Figure 1-5: poly[2-(2-pyridyl)-bibenzimidazole] with Ru(bpy)$_2{}^{2+}$ (Ref. 33).

Subsequently, poly(p-phenylenevinylene)-based polymers containing ionic ruthenium and osmium centers bound to bipyridyl (**bpy**) units incorporated into the polymer backbone were reported (Figure 1-6) by Yu's group.[23,24,34] These polymers exhibit interesting photoconductivity, photorefractivity, and NLO properties. The all-organic polymer I (x = 0, y =1 in Figure 1-6) exhibits an intense π,π^* transition absorption at 470 nm, while the all-ruthenium polymer II (x =1, y = 0) has a 550 nm "MLCT" absorption. The absorption spectrum of a mixed polymer III (x = 0.1, y = 0.9) exhibits properties of these polymers listed above. For polymer IV the absorption spectrum shows similar π,π^* transition absorption and an absorption tail extending to 750 nm which can be assigned to the spin-forbidden ^{3}MLCT. To further tune the optical and electronic properties of this kind of material, they continued to synthesize similar PPV polymer in which ruthenium complexes containing β-diketonate and hydroxyquinoline ligands are intergrated into polymer main chains.[35] The presence of σ-donating diketonate and phenolate groups in ligands substantially lowered the Ru$^{II}\rightarrow$ Ru^{III}

potentials relative to analogous polypyridyl complexes. This MLCT band red-shifted toward lower energy ($\lambda_{max} = 551 - 708$ nm) due to the reduction of the ligand-field strength. But Yu's group never really extensively probe the basic photophysical properties of the polymer excited states.

R = n-heptyl
R' = n-hexyl

Polymer I: M = Ru, x = 0, y =1
Polymer II: M = Ru, x =1, y =0
Polymer III: M = Ru, x = 0.1, y = 0.9
Polymer IV: M = Os, x = 0.05, y = 0.95
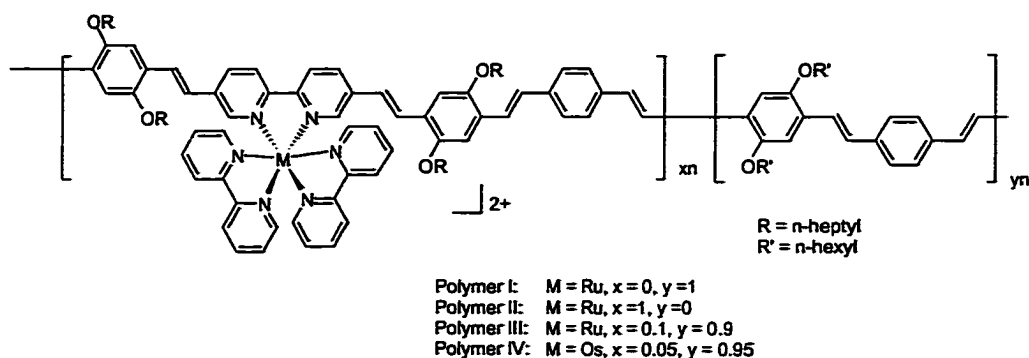
Figure 1-6: Ru(bpy)$_3^{2+}$ - containing PPV polymer (Ref. 23).

An elegant study showing the sensitivity of a bipyridine-containing, pseudo-poly(phenylenevinylene) system capable of complexing various metal ions followed.[8,36] In this work, conformational changes of the polymer, which are associated with the coordination of the metal ions, afforded a system that can toggle between its conjugated and nonconjugated forms (Figure 1-7).
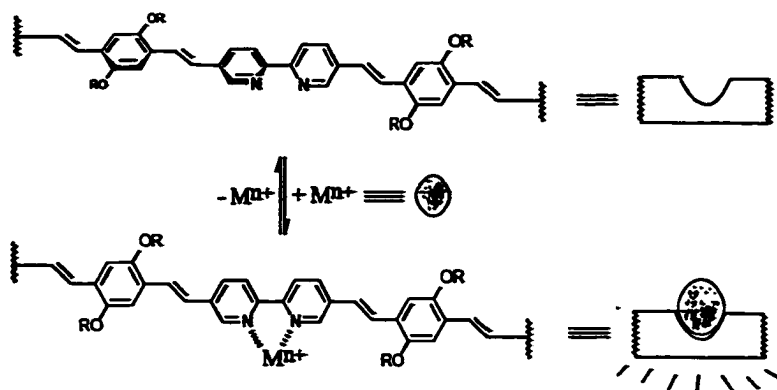
Figure 1-7: PPV metal ion sensing polymers synthesized by Wasielewski and coworkers (Ref. 36).

The choice of the 2,2'-bipyridine ring was based on its high binding constants to a variety of transition metal and main group metal ions. When a metal ion coordinates to the 2,2'-bipyridine, ring enhancement in the conjugation is observed within the polymer backbone. This is due to the fact that the unmetallated PPV polymer exhibits a conjugation break due to the lack of planarity of the 2,2'-bipyridine ring. When a metal ion coordinates to the bipyridine ring, the once non-planar bipyridine rings are forced planar due to the binding needs of the metal. This conjugation increase led to differing photophysical properties that signal the presence of the analyte ion (e.g., red-shifted absorption and emission bands) due to a lowering of the HOMO – LUMO gap. For example, when nickel(II), zinc(II), or palladium(II) ions were titrated into a solution containing the 2,2'-bipyridine-containing PPV, the polymer π,π^* 450 nm absorbance red-shifted between 50 – 100 nm depending on the metal ion. The ionochromic effect has demonstrated a new approach to sensitive, selective, and highly reversible metal ion responsive polymers and can be used for metal ion sensor studies.

Kimura and coworkers also used a PPV polymer containing the terpyridyl ligand in the side chain as chemical sensor to test several kinds of transition metals (Figure 1-8).[37] The visible spectrum of this polymer features a strong band at 450 nm in CHCl₃-MeOH (9:1 v/v), which is attributed to the absorption of the conjugated backbone. With the addition of Fe^{2+}, a new peak at 568 nm appeared which is caused by the formation of bis(terpyridyl)metal complex. Also the fluorescence of the polymer was quenched completely by Fe^{2+}, Fe^{3+}, Ni^+, Cu^{2+}, Cr^{2+}, Mn^{2+} and Co^{2+}.
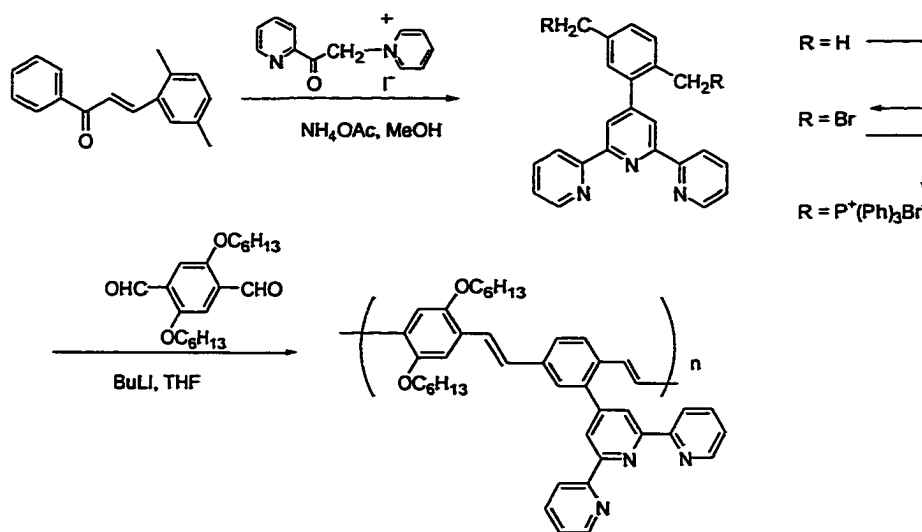
Figure 1-8: PPV metal ion sensing polymers (Ref. 37).

In the work of the PPV research, other π-conjugated polymers containing inorganic MLCT chromophores have also been investigated. Rasmussen et al.[38] prepared a bpy-containing conjugated polymer system, poly[1-(2,2'-bipyridine-4-yl)-1,4-diazabutadiene-4,4'-diyl] (polyazabpy), and its polymetalated ruthenium complex. This polymer was synthesized by polymeric condensation fashioned after that of the polymer polyazine (Figure 1-9). The excited state polymer is short-lived and develops weaker

emission relative to Ru(bpy)$_3^{2+}$, presumably due to the lower energy gap. The emission

lifetime for the polymer is similar to that for a dimeric model oligomer, indicating that

there are no ground state/excited interactions across the dimer ligand or by adjacent metal

centers in the polymer systems.
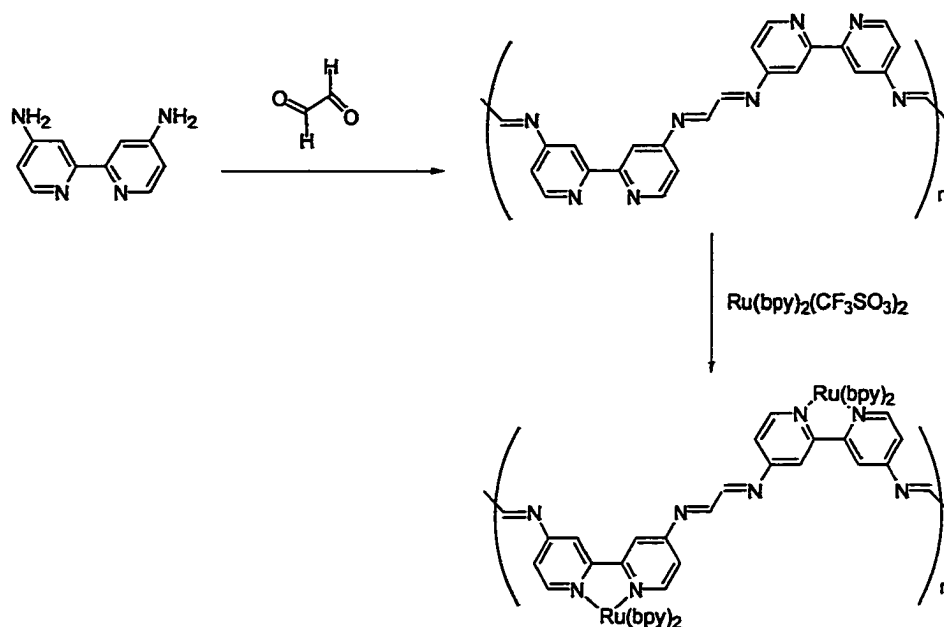
Figure 1-9: Ruthenium – containing diazabutadiene polymer (Ref. 38).

Introducing MLCT chromophore into thiophene-based polymer has also been

studied, but to a lesser degree than the PPV-based polymers. Zhu et al.[39,40] synthesized a

Ru(bpy)$_2^{2+}$-containing polythiophene via ligation to a 2,2'-bipyridine polymer subunit,

as seen in Figure 1-10. The monomer repeat unit of the polymer exhibited a sharp 400 nm

absorption in dicholoromethane, which is blue-shifted from the estimated native

polythiophene (490 nm). Further work by Zhu et al.[41,42] focused on polymetallorotaxane

by electrochemical polymerization of metallorotaxanes (Figure 1-11). Poly(1) shows red

absorption at 501 nm. The metal-free polyrotaxane is produced by rinsing Poly(1) with a

$H_2O/NH_2CH_2CH_2NH_2$ (3:1) solution, and it changes to yellow ($\lambda_{max} = 467$ nm).
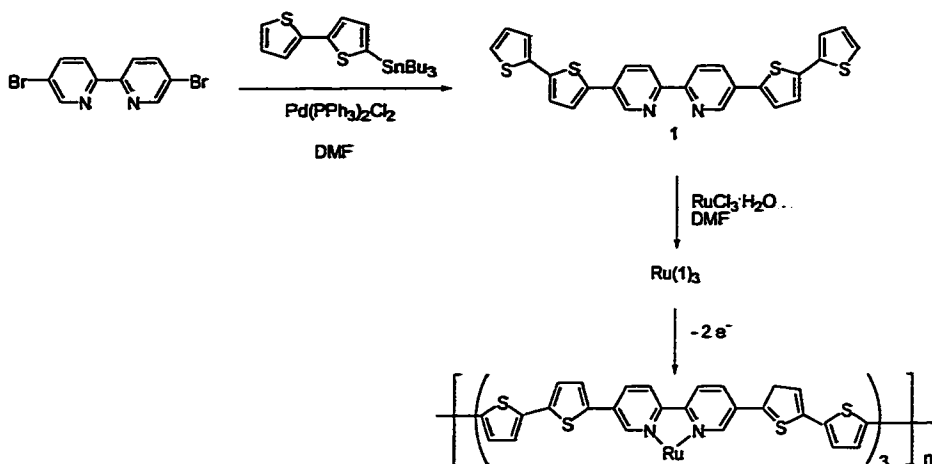
Figure 1-10: Ru(bpy)$_3^{2+}$-substituted polythiophene (Ref. 39).
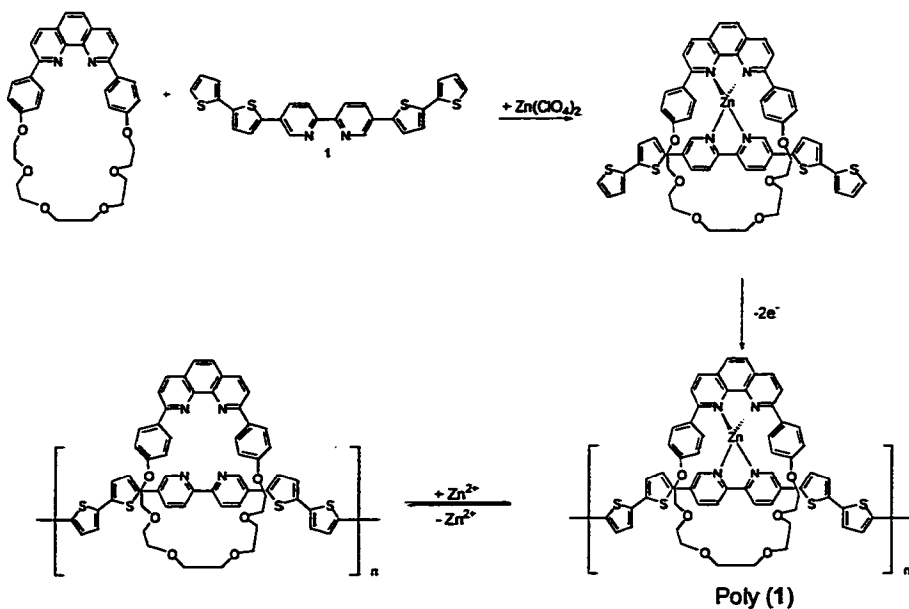
Figure 1-11: Metallorotaxane-thiophene polymers (Ref. 41).

Trouillet et al.[43] and Walters et al.[44] synthesized polymers based on regioregular

3-(octylthiophene) tetramers alternated with either bpy or the corresponding $Ru(bpy)_2^{2+}$

complexes and $Os(bpy)_2^{2+}$ complexes by Pd-catalyzed Stille cross-coupling reactions

(Figure 1-12). UV-visible experiments indicated that the delocalization of π-orbitals

occurs efficiently in the conjugated structures and involves both oligothiophene and

ruthenium chelating bipyridine units. The absorption is dominated by a broad band at 475

nm in CH_3CN which is due to the superposition of π,π^* transition of the conjugated

backbone and the MLCT transition. In the $Os(bpy)_2^{2+}$ complexes, the low-energy MLCT

transitions are clearly observed on the red-side of the π,π^* transition.
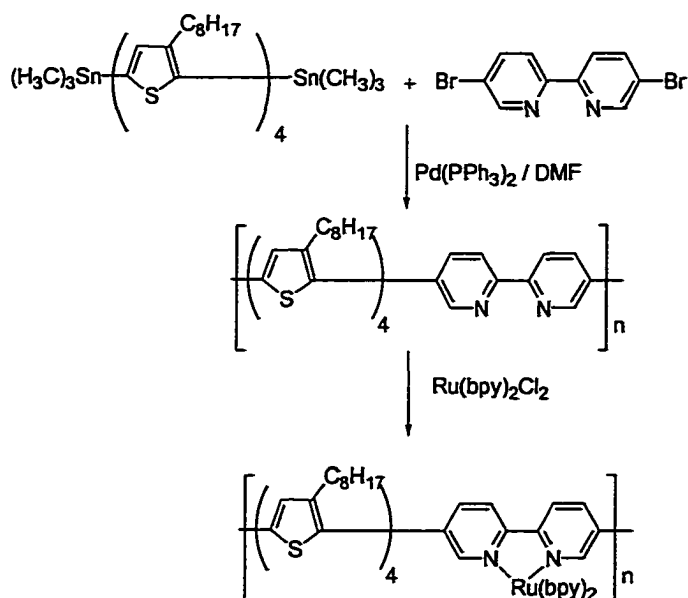
Figure 1-12: $Ru(bpy)_3^{2+}$ - substituted polythiophene (Ref. 43).

Reddinger and Reynolds[45,46] synthesized another novel thiophene-based polymer

containing MLCT chromophores. The polymer is centered around

bis(salicylidene)thienyl cores that can undergo site-directed electro-polymerization to

yield phenylene- or thineylene-linked polymers. In these polymers, a nickel or copper

chromophore was complexed to a SALOTH ligand that was incorporated into the thiophene backbone as shown in Figure 1-13. This polymer showed excellent conductivity properties, but again its photophysics were not the major focus of the reported research.
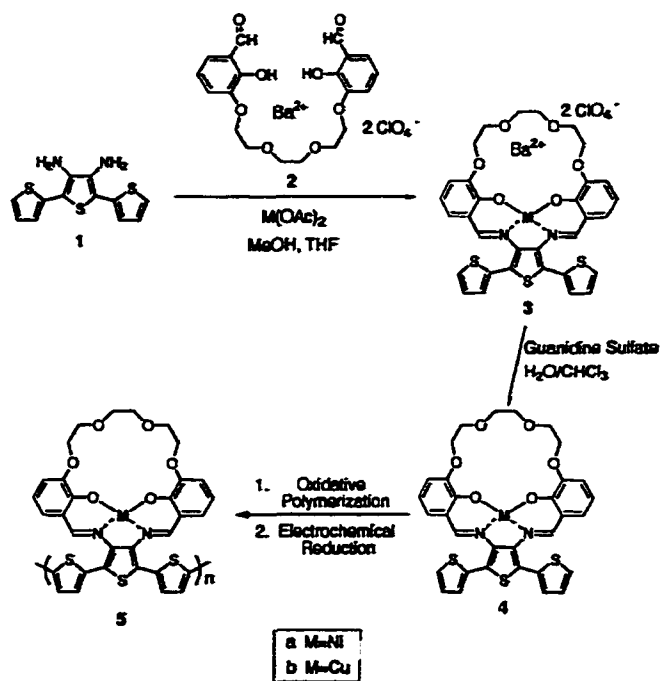
Figure 1-13: SALOTH thiophene polymer (M = Ni^{2+} and Cu^{2+}, Ref. 46).

An alternative method for introducing transition metal chromophores into π-conjugated polymers involves direct metal center substitution into the polymer chain. Wittmann and coworkers[47] synthesized aryleneethynylene-based polymers containing Pd[P(C$_4$H$_9$)$_3$]$_2$ or Pt[P(C$_4$H$_9$)$_3$]$_2$ subunits as shown in Figure 1-14.
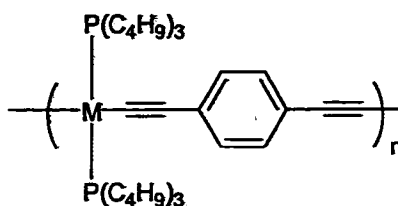
Figure 1-14: Aryleneethylylene-based polymers containing platinum subunits (M = Pd or Pt, Ref. 47).

This synthetic approach produces very consistent polymer products and interesting photophysical results. An intense 380 nm singlet and weaker 510 nm triplet ground state absorption were observed in solution studies of this polymer, which is red-shifted from the model monomer spectrum (345 nm). This red-shift reflects a clear increase in delocalization across adjacent π orbitals in the polymer backbone. A broad 520 nm luminescence was also observed from the polymer sample. However, due to their position within the polymer backbone these metal chromophores lack the "tunability" options available in other MLCT-based chromophores that are attached to the polymer backbone.

Photophysics of PPE Polymers

The absorption spectrum for the polymer shown in Figure 1-15 exhibits a sharp 452 nm band that is assigned as a π,π* transition of the conjugated backbone. A corresponding sharp fluorescence emission band with a 482 nm maximum is observed, as shown in Figure 1-16. This polymer exhibits high fluorescence quantum yield (0.5).[48]
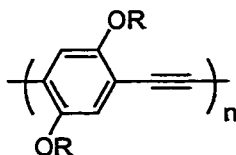
Figure 1-15: Aryleneethynylene-based polymer structure (R = n-octadecyl, Ref. 48).

Keeping the "molecular wire" idea in mind, Swager and coworkers synthesized aryleneethynylene-based polymers containing varying amounts of anthracene repeat units as shown in Figure 1-17.[49] Photophysical studies of these polymers showed that excitation into absorption bands associated with the polymer backbone produced emission typically observed for anthracene and a dramatic reduction in the polymer-based fluorescence. For example, a polymer with a structure corresponding to $x = 0.17$ has the absorption and emission spectra shown in Figure 1-18 and the quantum yield decreases from 0.4 to 0.09.
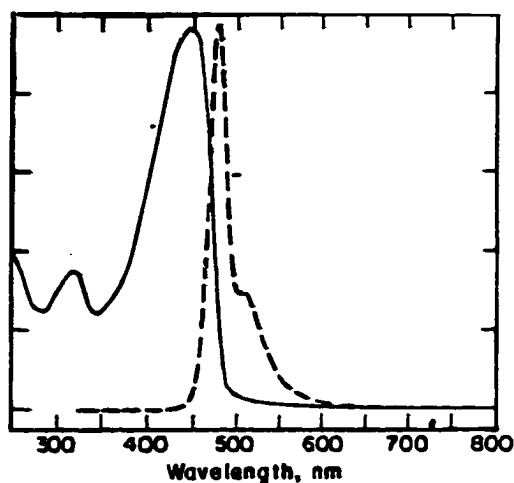
Figure 1-16: PPE absorption (solid line) and emission (dashed line) spectra in chloroform (Ref. 48).
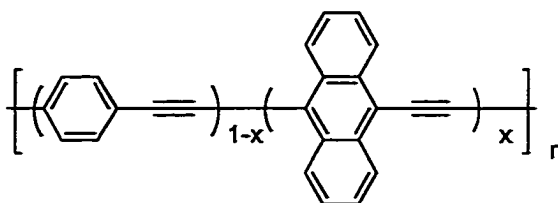
Figure 1-17: Anthracene-containing aryleneethynylene polymer (Ref. 49).

This mixed polymer exhibited the same absorption and emission observed for the PPE polymer (Figure 1-16), but the presence of new absorption and emission bands at 527 and 549 nm, respectively, result from the anthracene moiety. This observation suggests that the excitation is efficiently "trapped" by the anthracene subunits. This trapping could lead to emission or energy transfer to other substituents, and the polymers could be utilized in LED or NLO applications.
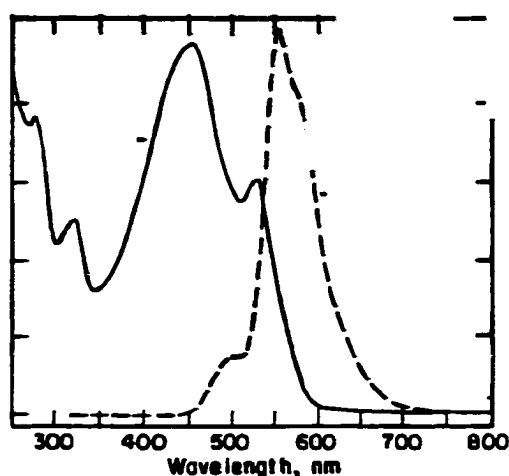
Figure 1-18: Absorption (solid line) and emission (dashed line) spectra in chloroform of the polymer in Figure 1-17 with x = 0.17 (Ref. 49).

Photophysics of Metal Coordination Complexes

Inorganic photochemists have long been fascinated by the photophysics of polypyridyl complexes of Re^I, Ru^{II}, and Os^{II}, largely because of their highly versatile luminescent and photoredox properties. The polypyridine complexes of Re^I, Ru^{II}, and Os^{II} are of octahedral symmetry and the metal centers are d^6 systems. A schematic orbital and state energy level diagram for a typical $(d\pi)^6$-polypyridyl complex is shown in Figure

1-19. Here the π and π^* are the π-bonding and π^*-antibonding orbitals of aromatic system of the ligand. The $d\pi$ and $d\sigma$ are the t_{2g} and e_g levels originating of 4d orbitals of metal.
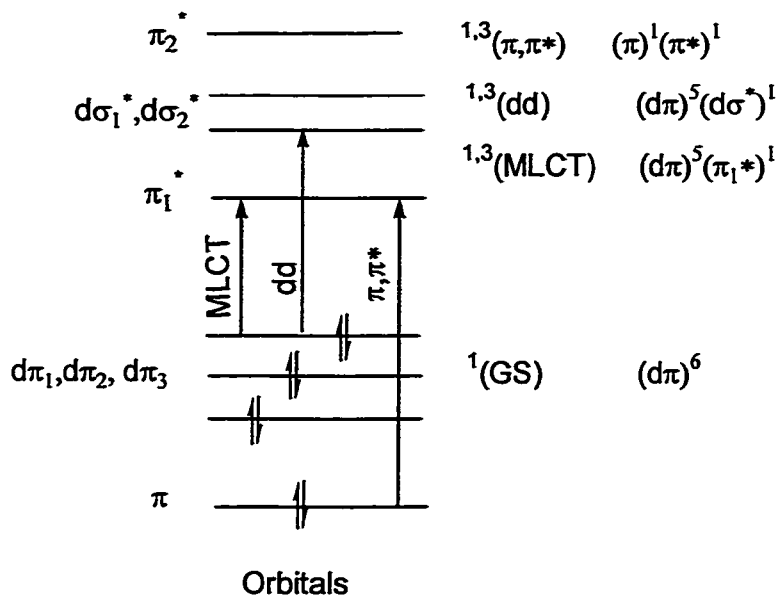
Figure 1-19: Simplified molecular orbital diagram for d^6 metal complexes in octahedral symmetry showing the three types of electronic transitions occurring at low energies.

The excited states of these complexes are of three types: 1) metal-centered ligand-field (M(d-d)) excited states; 2) metal-to-ligand charge-transfer (MLCT) excited states; and 3) intraligand (L($\pi \rightarrow \pi^*$)) excited states.[50]

Promotion of an electron from a $d\pi$ to $d\sigma^*$ orbitals gives rise to metal centered dd excited states. This transition is a weak Laporte forbidden absorption ($\varepsilon \approx 100$ $M^{-1}cm^{-1}$) that leads to a short-lived excited state.[51] And this transition is not generally observed in the absorption spectra of $(d\pi)^6$ polypyridyl complexes. However, because of the significant differences in structure along the metal-ligand bond axes between the $(d\pi)^6$ and $(d\pi)^5(d\sigma^*)^1$ configurations, when thermally equilibrated, dd excited states appear at

much lower energies. That's why the photophysical properties of ruthenium complexes are sometimes quite complex because the energies of the relaxed MLCT and dd state are comparable.

Excitation of an electron from a $d\pi$ metal orbital to π^* ligand orbitals results in an allowed metal-to-ligand charge transfer (MLCT) excited state ($\varepsilon \approx 20,000 \ M^{-1}cm^{-1}$).[51] In general, visible light absorption is usually dominated by transitions to MLCT excited states which are largely singlet in character $^1[(d\pi)^5(\pi^*)^1]$. And the lowest excited state is a ^{3}MLCT which undergoes relatively slow radiationless transitions and thus exhibits a long lifetime and intense luminescence emission.

Ligand centered π,π^* excited states can be obtained by promoting an electron from a polypyridine localized π orbital to π^* orbital. These transitions appear to vary somewhat in energy with the metal and its oxidation state but generally appear at ~ 300 nm ($\pi \rightarrow \pi_1^*$) and ~ 240 nm ($\pi \rightarrow \pi_2^*$). Because of the lack of charge transfer character for the $\pi \rightarrow \pi^*$ transitions, $\pi \rightarrow \pi^*$ excited states are relative insensitive to solvent variations and at low temperatures vibrational structure arising from aromatic ring based stretching modes can appear in their emission spectra.

The energy-level sequence in Figure 1-19 is schematic only. The relative ordering can be altered by switching metal ions, and exchanging or modifying ligands, and ligands. Changes in the ligand which influence either the basicity of the donor or the energetics of the unoccupied orbitals will therefore have an impact on the excited-state properties of the molecule. Exploitation of these effects has served as the basis for synthetic tuning of excited-state properties.

The energy gap law has been observed for families of aromatic hydrocaron.[52-55] It predicts there is an inverse correlation between the rates of non-radiative transitions involving the lowest states of similar molecules and the difference in energy between the $v = 0$ levels (initial potential energy) of the states involved.[56] In other words, the smaller the energy gap the larger the rate. It can be understood that as the gap increases the radiationless transition from a given level of state 1 will be to an increasingly high vibrational level of state 2, with reduced vibrational overlap and a correspondingly reduced rate constant.

Meyer's group first applied the energy gap law in the transition metal complexes.[57] In comparing a series of related excited state of mono- and bis-2,2'-bipyridine or 1,10-phenanthroline complexes of Os(II), they found there is a proportionality between the logarithm of the nonradiative rate constant k_{nr} and the emission energy:

$$\ln k_{nr} \propto E_{em} \qquad\qquad 1\text{-}1$$

They derived this expression[57] by the form derived by Englman, Freed, and Jortner which described multiphonon nonadiabatic electron transfer.[58-61]

$$k_{nr} = \left(\frac{2\pi V^2}{\hbar}\right)\left(\frac{1}{2\pi\hbar\omega_M \Delta E}\right)^{1/2} \exp\left(-S\right)\exp\left(\frac{-\gamma\Delta E}{\hbar\omega_M}\right) \qquad 1\text{-}2$$

In equation 1-2 ΔE is the internal energy gap between the upper and lower states, ω_M is the frequency of the deactivating mode or modes, and V is the electron tunneling matrix element. The terms γ and S are defined in equation 1-3 and 1-4, respectively, and Δ_j is the

dimensionless fractional displacement between the equilibrium nuclear configuration of the ground and excited state for the complex's jth normal mode.

$$\gamma = \ln\left(\frac{2\Delta E}{\sum_j \hbar\omega_j \Delta j^2}\right) - 1 \qquad \text{1-3a}$$

$$\gamma \sim \ln\left(\frac{2\Delta E}{\hbar\omega_M \Delta M^2}\right) - 1 \qquad \text{1-3b}$$

$$s = 1/2\sum_j \Delta j^2 \qquad \text{1-4}$$

Equation 1-2 can be further simplified as equation 1-5 if the deactivation mode or modes remain common and if variations in V and in S are relatively small. Although ΔE appears both in β and γ in equation, both are slowly varying functions of ΔE compared with the term $\dfrac{\gamma\Delta E}{\hbar\omega_M}$ and equation predicts that $\ln k_{nr}$ should vary linearly with E_{em}.

$$\ln k_{nr} = (\ln\beta - S) - (\frac{\gamma\Delta E}{\hbar\omega_M}) \qquad \text{1-5}$$

$$\beta = \left(\frac{2\pi V^2}{\hbar}\right)\left(\frac{1}{2\pi\hbar\omega_M\Delta E}\right)^{1/2} \qquad \text{1-6}$$

Nonradiative decay from MLCT states to the ground state is typically dominated by energy loss into a series of medium-frequency ring-stretching vibrations with energy spacings between 1000 and 1600 cm^{-1}.[62] They further simplified this equation into equation 1-7 by assumption that these vibrations can be approximated as a single averaged mode of quantum spacing $\hbar\omega_M$ and electron-vibrational coupling constant S_M. S_M is related to the change in equilibrium displacement between the ground and excited

state, ΔQ_e, and the reduced mass, M by equation 1-9. Upon above assumption this equation is only valid in the limit that $\Delta E \gg \hbar \omega_M$ and $S_M \hbar \omega_M \gg k_B T$.

$$\ln k_{nr} = A - (\frac{\gamma \Delta E}{\hbar \omega_M})$$ 1-7

$$\gamma = \ln(\frac{E_0}{S_M \hbar \omega_M}) - 1$$ 1-8

$$S_M = \frac{1}{2}\left(\frac{M \omega_M}{\hbar}\right)(\Delta Q_e)^2$$ 1-9

From above discussion, we know that the energy gap influences vibrational overlap between the initial and final states in the "acceptor modes". The linear relation between $\ln k_{nr}$ and the energy gap predicted by the energy gap law has been observed in a series of MLCT excited state of Ru(II), Os(II), and Re(I). The energy gap can be varied by changing the temperature,[63] coordinated ligand,[57,64] the counter ion in dichlormethane solution,[65] and solvent variation.[66]

Despite its many successes, the energy gap law must be applied with care because a change in equilibrium the displacement (ΔQ_e) also influences vibrational overlap (Figure 1-20).[67,68] As ΔQ_e increases, vibrational overlap between two states increases, so does k_{nr}.
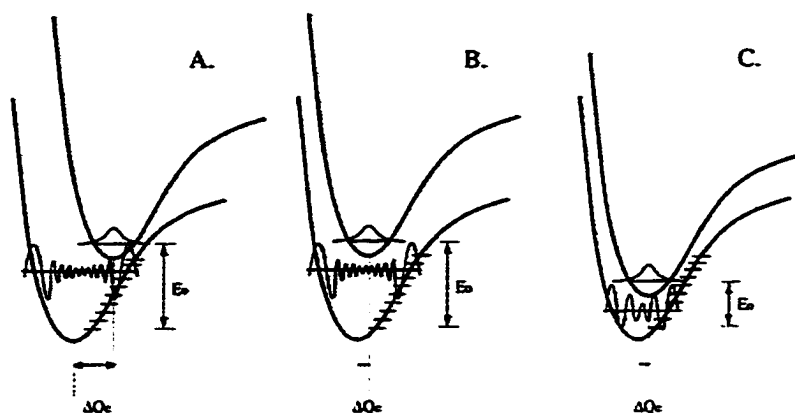
Figure 1-20: Graphical illustration of the factor influencing vibrational overlap for non-radiative excited-state decay (Ref. 68).

One way to decrease ΔQ_e is by delocalization. For linear conjugated polymers, α,ω-diphenylpolyenes, or benzenoid hydrocarbons, including benzene, naphthalene, and anthracene, as the number of conjugated π-bonds is increased in organic radical anions, bond orders increase and bond distance differences between the neutral and anions decrease.[50] The added electron is dispersed over the π-bonding framework, more bonds are distorted and the average displacement change is decreased. Meyer's group has synthesized a ruthenium complex which has conjugated **bbpe** ligand (trans-1,2-bis-(4-(4'-methyl)-2,2'-bipyridyl)ethene ligand) (Figure 1-21).[68] Compared to related complexes having comparable energy gaps, the lifetimes of this ruthenium complex are unusually long ($\tau = 1.31$ μs in CH_3CN at 298 K). The extended lifetime is believed to be due to a delocalization effect caused by decreased bond displacement changes in the excited state. This decreases vibrational overlap between states, and the rate constants for nonradiative decay.

[(dmb)₂Ru(μ-bbpe)Ru(dmb)₂]⁴⁺
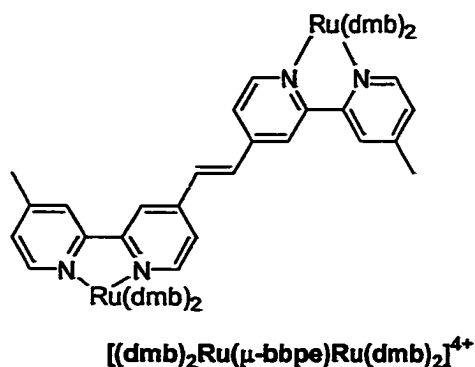
Figure 1-21: Structure of [(dmb)$_2$Ru(μ-bbpe)Ru(dmb)$_2$]$^{4+}$ (Ref. 68).

Previous Group Work and Object of Present Study

In view of the rich and varied photophysical properties of π-conjugated materials and d^6 transition metal complexes, it is of interest to combine these two molecular systems in order to produce new "hybrid" metal-organic π-conjugated systems that might have unusual and possibly useful optical and photophysical properties.

Despite the increasing attention that has been given to the synthesis and properties of metal-organic π-conjugated polymers, comparatively few studies have been carried out to define the fundamental optical properties of the metal-organic chromophores. Much of the difficulty with examining the photophysical properties of these systems results from the difficulty in relating complex photophysical results to poorly defined structures or the poor solubility of the polymers.

A series of π-conjugated aryleneethynylene oligomers with various lengths of the repeat structure incorporated -(bpy)Re^I(CO)$_3$Cl chromophore were synthesized via Sonogashira coupling and their photophysical properties were investigated in our lab (Figure 1-22).[26,69] The repeat units and geometries of the oligomers were varied to see

how these changes affect the observed photophysics. These compounds feature a rich manifold of excited states based on the π-conjugated electron systems as well as charge transfer excited states arising from the transition metal-chromophores. Long-lived (i.e., ns - μs) photoluminescent excited states are observed. Careful analysis of the properties of these long-lived states suggests that they can be assigned either to the $^3\pi,\pi^*$ or ^{3}MLCT manifolds, or in special cases to an equilibrium distribution of these two excited states.
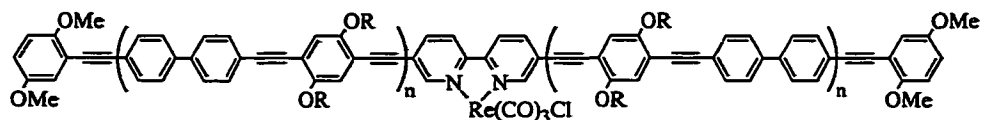
Figure 1-22: Structures of rhenium complexes (Ref. 26).

To further explore the photophysical properties of metal-organic π-conjugated polymers, a series of PPE-type conjugated oligomers that contain Ru^{II}, Os^{II}, and Re^{I} tranistion metal complexes were synthesized. Accordingly, through a judicious choice of ligand, the redox and photophysical properties of the ground and excited states of complexes were tuned. Many spectroscopic techniques were utilized to probe the molecular excited states.

CHAPTER 2
SYNTHESIS AND PHOTOPHYSICS OF PHENYLENE ETHYNYLENE OLIGOMERS THAT CONTAIN THE Ru(bpy)$_2^{2+}$ CHROMOPHORE

Introduction

Inorganic photochemists have long been fascinated by the photophysics of transition metal complexes such as Ru(bpy)$_3^{2+}$ and its analogs. It has been established that the photophysical properties of the MLCT excited states (i.e., the emission energy, emission quantum yield and lifetime) are determined largely by the energy gap between the ground and excited states and also by the extent by which the excited electron is delocalized in the acceptor ligand.

It would be interesting to study how the electron delocalization affects MLCT excited state properties of ruthenium polypyridyl complexes. There are two key questions concerning the effect of delocalization on the photophysical properties of the excited state, (1) to what extent is the MLCT state "delocalized" by the π-conjugated system and (2) is there a systematic relationship between the structure of the π-conjugated system and the extent of delocalization. In order to address this question, we embarked on the synthesis and optical characterization a series of π-conjugated oligomers that containing PPE type repeating structure. The structures of the 5-L oligomers and (L)Ru^{II}(bpy)$_2$ complexes are shown in Fig 2-1.

By comparing the photophysical properties of the (L)Ru^{II}(bpy)$_2$ complexes with the structurally similar (L)Re^{I}(CO)$_3$Cl complexes synthesized by our lab, it will produce more insight into the excited state properties of this type of metal-organic material.

27

These oligomers were synthesized via Sonogashira coupling, an iterative sequence involving palladium-mediated cross coupling of a terminal actylene and aryl halide. Triple bonds are introduced into this system therefore, these oligomers have well defined (and controllable) structures at the molecular level because there is no structural isomerization in comparison to double bond linked oligomers. A detailed description of the improved synthetic methodology used to create these oligomers and their photophysical properties is presented in this chapter which afford us the opportunity to systematically explore relationships between structure and photophysical properties at the molecular level.
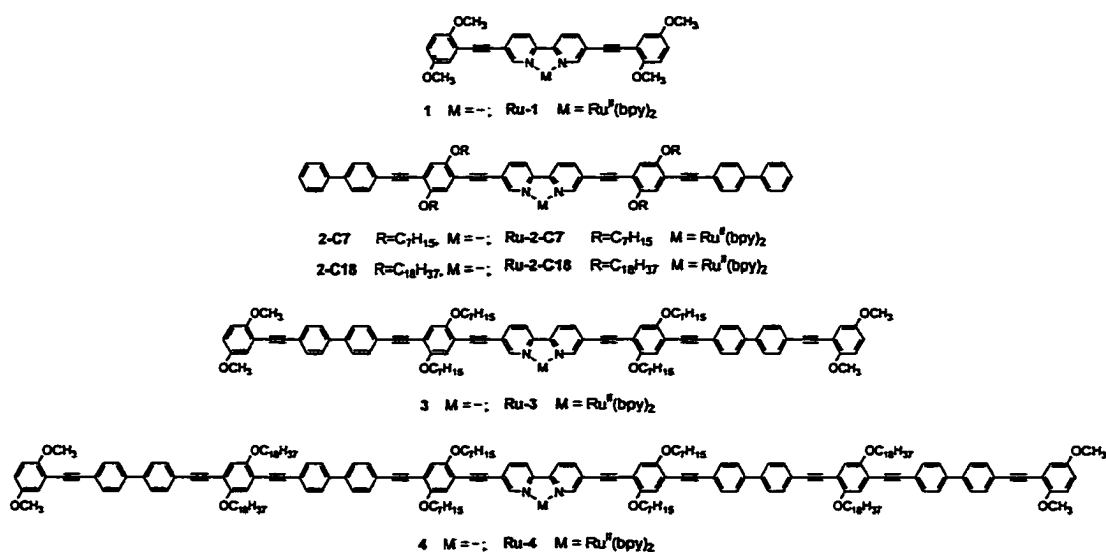
Figure 2-1: 5-L oligomer and (L)Ru^{II}(bpy)$_2$ structures.

Synthesis

cis-**Ru(bpy)₂Cl₂** is a useful starting material for the preparation of mixed ligand

complexes of **(L)Ruᴵᴵ(bpy)₂**. We tried two ways to make this starting compound. First,

the modification of the procedure developed by Sullivan was utilized.[70] Commercial

RuCl₃·3H₂O was refluxed with 2 equivalent of 2,2'-bipyridine to give good yields of the

complex (70%). This complex was also prepared by using 'ruthenium-blue' solution, an

activated species generated from hydrated ruthenium chloride with 84% yield.[71] Both of

these two ways work well and the product has the desired purity.

Early in the project, preparation of uncomplexed oligomer series 1-4 used an

iterative Pd-mediated (Sonogashira) coupling chemistry[11,12] to extend the PPE backbone

outward from a 2,2'-bipyridine-5,5'-diyl 'core'. The key starting compound is 5,5'-

dibromo-2,2'- bipyridine (6) which is obtained by modification of a procedure developed

by Ziessel and coworkers[72] (Figure 2-2). Further treatment of 6 with

trimethylsilylacetylene in the presence of Pd(PPh₃)₂Cl₂ catalyst yielded 5,5-diethynyl-

2,2'-bipyridine (8) in high yield.
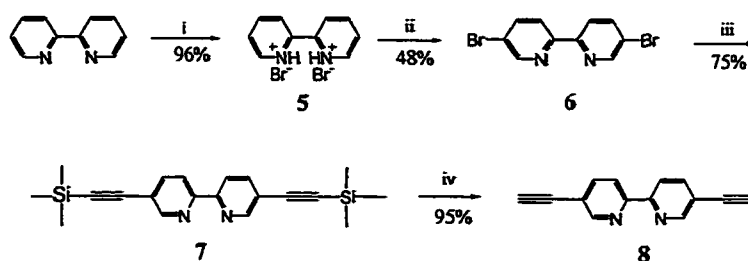
i. Acetyl bromide, MeOH; ii. Br₂, 180°C, 4 days; iii. TMSC≡CH (4 eq.) Pd/Cu (Cat.),
heat, 20 hr; iv. KOH, THF-MeOH.

Figure 2-2: Synthesis of model compounds.

Synthesis of oligomer **1** is straightforward (Figure 2-3). Endcapping of **8** with

two equivalents of 1-iodo-2,5-dimethoxybenzene affords dimethoxyphenylethynyl

bipyridine (**1**) in a 75% yield, and subsequent metallation of **1** with 1.2 equivalents of *cis*-

Ru(bpy)₂Cl₂ in refluxing THF/CH₃OH yields model compound **Ru –1** in reasonable

yield.
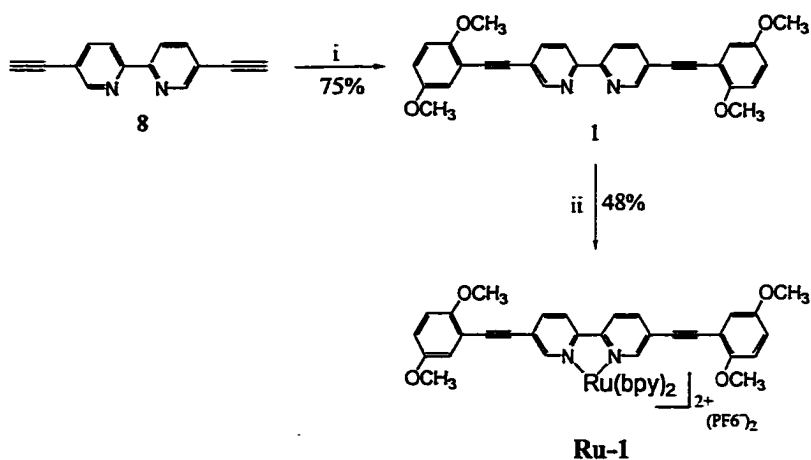
i.1-Iodo-2,5-dimethoxybenzene (2 eq.), Pd/Cu (Cat.); ii. *cis*-**Ru(bpy)₂Cl₂** (1eq.), MeOH-
THF, heat, 24 hr.

Figure 2-3: Synthesis of model compounds.

For oligomer **2**, two analogs with different alkoxy side chains on the benzene

ring, **2-C₇** and **2-C₁₈**, were synthesized (Figure 2-1). How the side chains affect the

solubility, disturb the solvation environment and affect MLCT excited state properties is

of interest.

The synthesis of 1,4-diiodo-2,5-diheptyloxybenzene (**9**) was straightforward,

alkylation of 1,4-hydroquinone followed by iodination (Figure 2-4). The synthesis of 1,4-

diiodo-2,5-dioctadecyloxybenzene (**12**) was effected by modification of a procedure

reported by Swager and coworkers[73] (Figure 2-5). Synthesis of **2-C₁₈** still follow the same

methodology as making of **Ru-1**, extending the PPE backbone outward from a 2,2'-bipyridine-5,5'-diyl 'core'. 1,4-Diiodo-2,5-dialkoxybenzene is coupled with 1 equivalent of 2-methyl-3-butyn-2-ol (**2-MP**) to produce **13** (Figure 2-6). This compound is readily separated from unreacted starting material owing to the polar **2-MP** functionality. Reaction of 2.0 equivalents of **13** with 5,5'-diethynyl-2,2'-bipyridine (**8**) affords **14**, which is deprotected to **15** with KOH, toluene and heat. Finally, **15** is coupled with 4-bromobiphenyl to produce **2-C₁₈**.
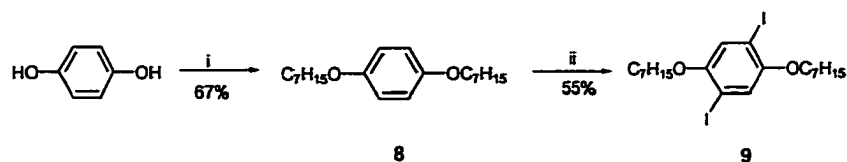
i. 1-bromoheptane, DMF, KOH; ii. I₂, KIO₃, HOAc, H₂SO₄.

Figure 2-4: Synthesis of 1,4-diiodo-2,5-diheptyloxybenzene.
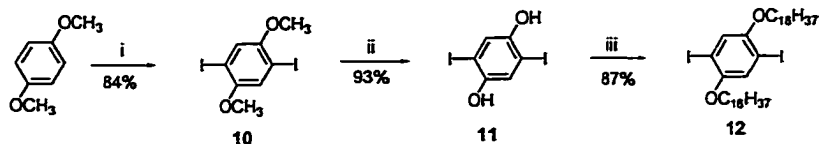
i. I₂, KIO₃, HOAc, H₂SO₄; ii. BBr₃, CH₂Cl₂; iii. 1-bromooctadecane, DMF, KOH.

Figure 2-5: Synthesis of 1,4-diiodo-2,5-dioctadecyloxybenzene.

A very useful synthetic technique for the preparation of ruthenium complex is the use of $[Ag^+(CF_3SO_3^-)]$ to remove chloride ligands to form labile solvated complex intermediates (Figure 2-7).[70] **2-C₁₈** is conveniently metallated by using *cis*-**Ru(bpy)₂Cl₂** in the presence of Ag(CF₃SO₃) to afford **Ru-2-C18** (Figure 2-8).
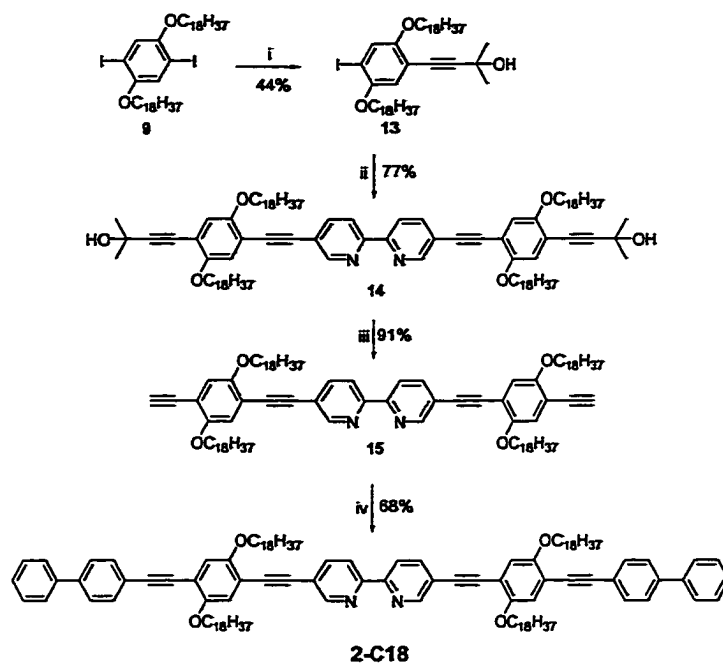
i. HC≡CMe₂OH (1 eq.), Pd/Cu (Cat.); ii. 5,5'-diethynyl-2,2'-bipyridine (0.5 eq.), Pd/Cu (Cat.); iii. KOH, toluene, reflux; iv, 4-bromobiphenyl, Pd/Cu (Cat.).

Figure 2-6: Synthesis of **2-C18**.
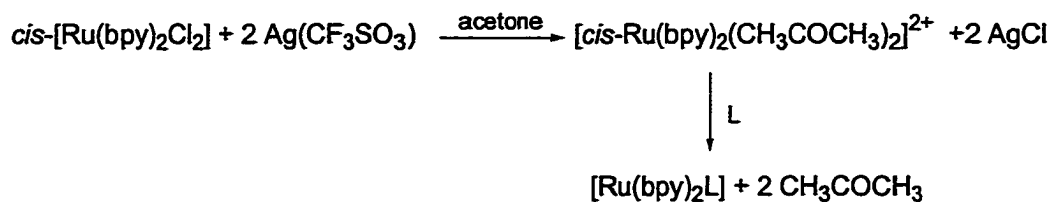
Figure 2-7: Synthesis strategy for **(L)Ru^{II}(bpy)₂** (Ref. 70).

When we started to make **Ru-2-C7**, we chose a new approach by synthesizing a two component system, 1) an "outer" peripheral segment, and 2) a central bipyridine

"core". We hoped to be able to make the central "core" and outer segments separately. By making the different lengths outer segment, we can extend the molecule more efficiently than via the sequential approach developed by Ley in our group.[74] As molecule becomes bigger it becomes harder to extend the PPE backbone outward from the 2,2'-bipyridine-5,5'-diyl 'core'. For example, the high temperature necessary to remove the tertiary alcohol acetylene protecting group proved to provide an easy route for the terminal acetylene to dimerize, producing butadiynes. In order to implement this new strategy, we selected compound 16 as the 'core' (Figure 2-9). Compound 16 features a central 2,2'-bipyridine-5,5'-diyl and a reactive aryl iodide periphery which in turn can be coupled to any acetylene product. We can make the "outer" segment (18) in high quantity without the need to use 2,2'-bipyridine-5,5'-diyl 'core' (Figure 2-11). In essence, this strategy is more convenient, an it minimizes the need to synthesizes large quantities of 5,5'-diethynyl-2,2'-bipyridine which is a tedious starting material to prepare.

2-C18

i | 40%
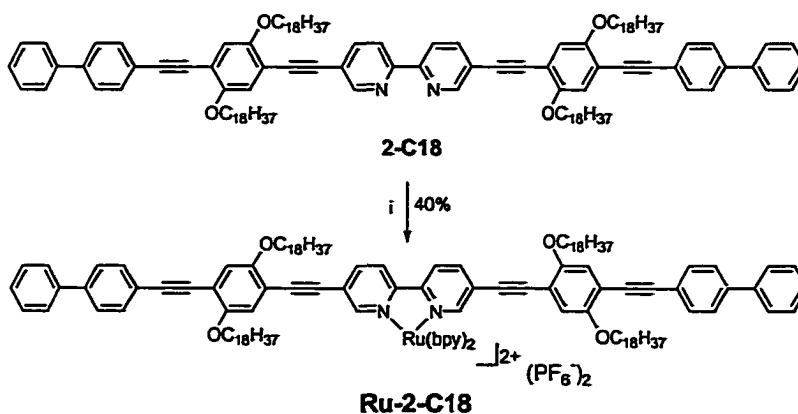
Ru-2-C18

i. *cis*-Ru(bpy)$_2$Cl$_2$ (1 eq.), Ag(CF$_3$SO$_3$), acetone-2-methoxyethanol, heat, 24 hr.

Figure 2-8: Synthesis of Ru-2-C18.
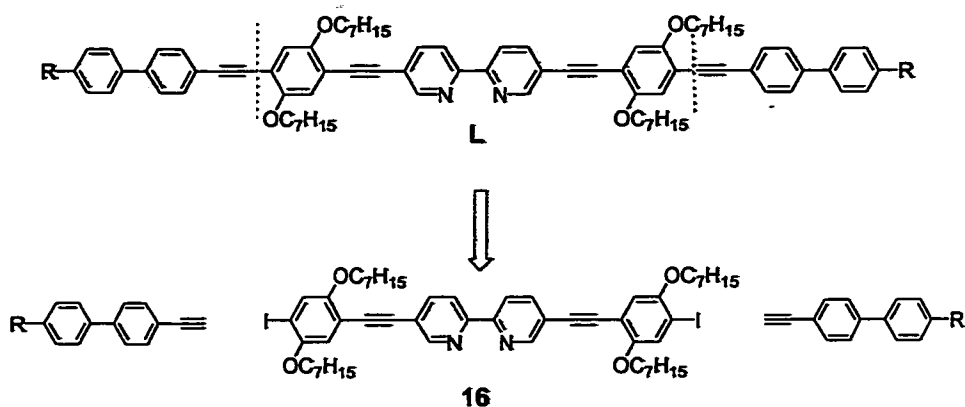
Figure 2-9: Synthesis strategy for ligand.

New 'core' **16** is prepared by coupling 1,4-diiodo-2,5-diheptyloxybenzene with

0.25 equivalents of 5,5'-diethynyl-2,2'-bipyridine with 35% yield (Figure 2-10). By using

excess 1,4-diiodo-2,5-diheptyloxybenzene, the amount of oligomer formed can be

reduced. The excess starting compound can be separated from product relatively easily

by silica gel chromatography and recovered to recycle.
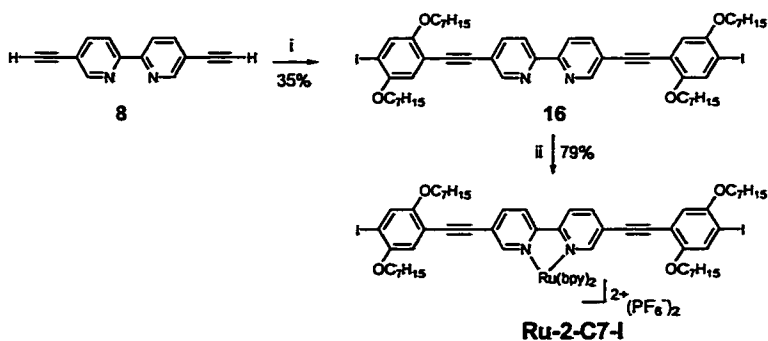
i. 1,4-Diiodo-2,5-diheptyloxybenzene (4 eq.), Pd/Cu (Cat.), heat, 20 hr; ii. *cis*-
Ru(bpy)₂Cl₂ (1eq.), Ag(CF₃SO₃), acetone, 2-methoxyethanol, heat, 24 hr.

Figure 2-10: Synthesis of **Ru-2-C7-I**.

The synthesis of outer segment **18** is quite straightforward. 4-Bromobiphenyl is coupled with 1 equivalent of 2-methyl-3-butyn-2-ol (**2-MP**) to produce **17** (Figure 2-11). This compound is readily separated from unreacted starting material then followed by deprotection to **18** with KOH, toluene and heat.
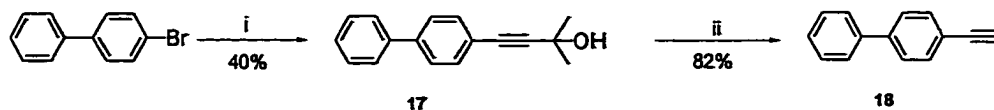
i. HC≡CMe₂OH (1 eq.), Pd/Cu (Cat.); ii. KOH, toluene, reflux.
Figure 2-11: Synthesis of model compounds.

Instead of the direct coupling reaction between **16** and **18** to yield **2-C7**, **16** is metallated with *cis*-**Ru(bpy)₂Cl₂** in the presence of Ag(CF₃SO₃) to form **Ru-2-C7-I** first (Figure 2-10). Endcapping of **Ru-2-C7-I** with **18** produces **Ru-2-C7** directly (Figure 2-12). The yield of this two step reaction is improved to 60% compared with the 50% yield from direct coupling and subsequent metallation. This improvement in coupling yield is probably due to the electron withdrawing ability of ruthenium metal center.
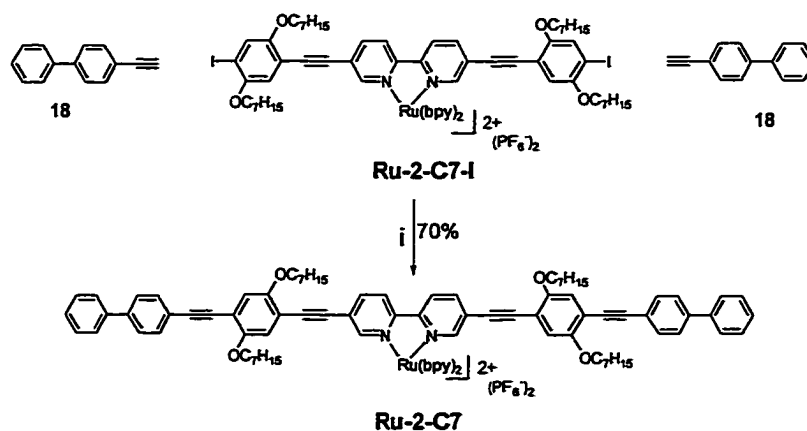
i. Pd/Cu (Cat.), heat, 20 hr.

Figure 2-12: Synthesis of **Ru-2-C7**.

Synthesis of **Ru-3** and **Ru-4** can be effected by the same strategy in this case, by endcapping the 'core' **Ru-2-C7-I** with the corresponding outer segments **22** and **25** (Figure 2-13). Starting material **20** for the synthesis of **22** is available in multigram quantities (Figure 2-13). In a two-step, one-pot procedure, 4,4'-diiodobiphenyl is reacted with TMSC≡CH and then with 2-methyl-3-butyn-ol (**2-MP**) to afford **19**. The **2-MP** protecting group in **19** allows this compound to be separated from the reaction by-products by silica gel chromatography. The separation is facile because the by-products have significantly higher or lower R_f value compared to compound **19** owing to the polar **2-MP** protecting group. Selective removal of the TMS group from **19** with KOH/MeOH produces mono-protected compound **20** in 24% overall yield from the starting diiodobiphenyl. The reaction of **20** with 1-iodo-2,5-dimethoxy benzene produces **21**, which is subsequently deprotected with KOH/MeOH to yield **22**. Endcapping of **Ru-2-C7-I** with **22** produces **Ru-3** directly (Figure 2-14). The synthesis of the outer segment of **Ru-4** proved to be much more time consuming (Figure 2-13). Coupling of compound **20** with 1.0 equivalent of 1,4-diiodo-2,5-dioctadecyloxybenzene yielded the protected oligomer **23** in modest yield, which in turn is coupled with 1.0 equivalent of **22** yielding the protected oligomer **24**. Deprotection of **24** affords the desired "peripheral" segment in reasonable yield. Coupling of **Ru-2-C7-I** with the end segment **25** proceeded smoothly, yielding **Ru-4** directly in 70% yield based on **25** (Figure 2-15).
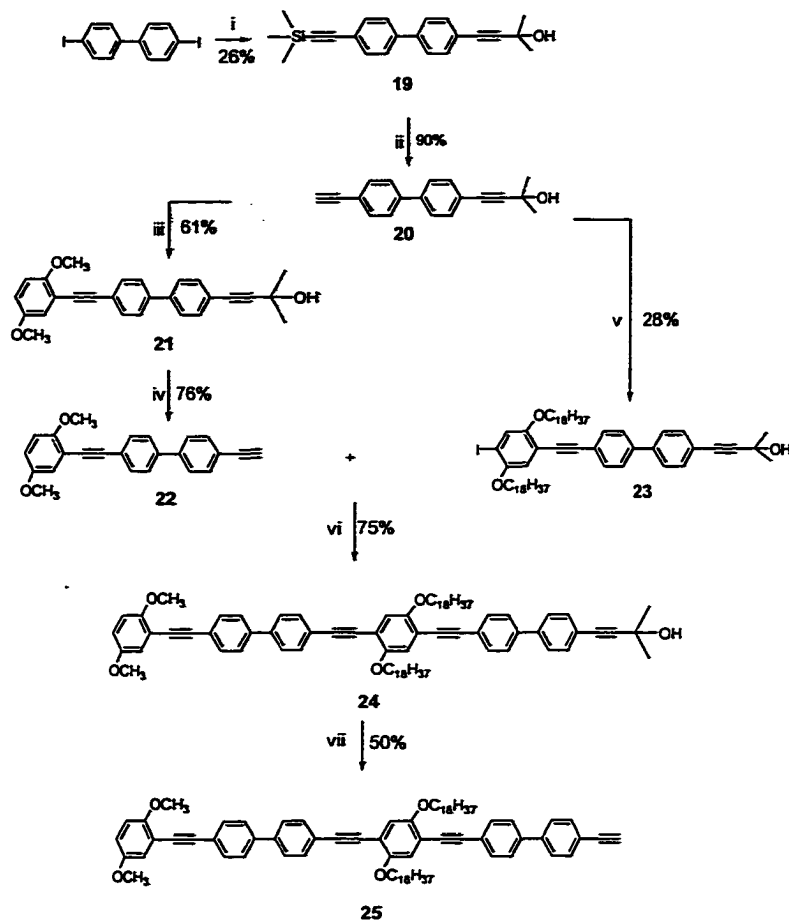
i. TMSC≡CH (1eq.) Pd/Cu (Cat.), heat, 3 hr, then HC≡CCMe₂OH(excess), heat, 17 hr; ii. KOH, THF/MeOH; iii. 1-iodo-2,5-dimethoxybenzene (2 eq.), Pd/Cu (Cat.); iv, KOH, toluene, reflux; v. 1,4-diiodo-2,5-dioctadecyloxybenzene (1 eq.), Pd/Cu (Cat.); vi. Pd/Cu (Cat.); vii. KOH, toluene, reflux.

Figure 2-13: Synthesis of model compounds.

For **Ru-4**, two different length alkoxy side chains, C_7 and C_{18}, are introduced on the two benzene rings, which greatly increases the solubility of this large conjugated oligomer.
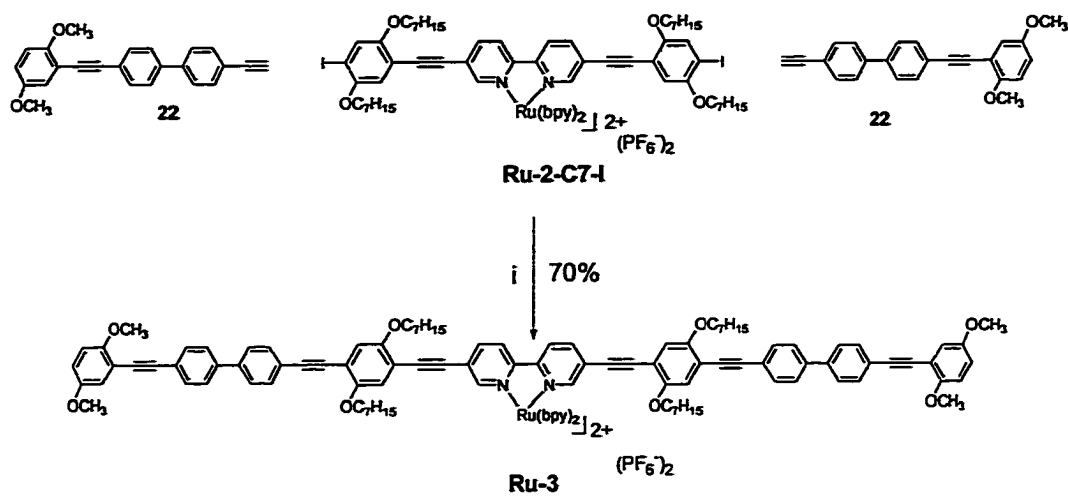
i. Pd(PPh₃)₄, CuI, THF, (i-Pr)₂NH.

Figure 2-14: Synthesis of **Ru-3**.
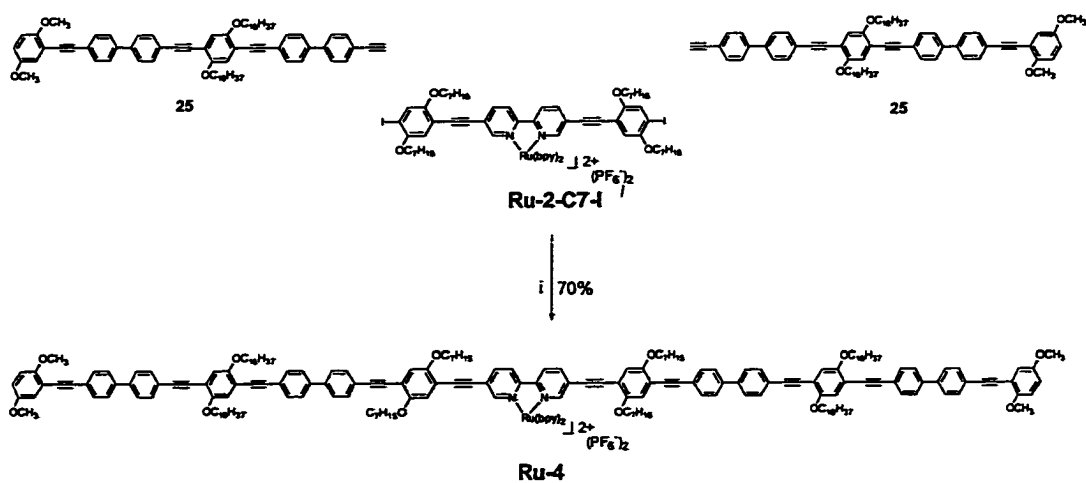
i. Pd(PPh₃)₄, CuI, THF, (i-Pr)₂NH.

Figure 2-15: Synthesis of **Ru-4**.

Results

Absorption Spectra

Absorption spectra were obtained on dilute THF solutions of the various

oligomers and dilute CH_2Cl_2 solutions of ruthenium complexes. Absorption spectra for

the free ligand 1-4 and (L)Ru^{II}(bpy)$_2$ (Ru-1 – Ru-4) are shown in Figure 2-16 and Table

2-1 contains a listing of the absorption bands and extinction coefficients. For comparison,

the absorption spectra of (L)Re^{I}(CO)$_3$Cl (Re-1 – Re-4) in THF solution are also shown

in Figure 2-16.

The free oligomers exhibit two strong absorption bands in 300-400 nm region.

The lowest energy band is assigned to the long-axis polarized π,π^* (HOMO → LUMO)

transition, while the second band is assigned to the short-axis polarized π,π^* transition.

The low energy band red-shifts considerably from 1 to 2, but the position and bandshape

of the transition remains relatively constant in 2-4, indicating that the bandgap of the

oligomers (effective conjugation length) is defined very early in the series. This

observation contrasts with observations made on PPE oligomers that contain phenylene

repeats (as opposed to the biphenyl and bipyridyl repeats present in 1-4), in which the

bandgap continues to decrease for 10 or more repeat units.[75-77] This suggests that the poor

electronic coupling between the non-coplanar phenyl (and pyridyl) rings in the biphenyl

and bipyridyl units in 2-4 restricts the conjugation length. However, the oscillator

strength of the π,π^* transition increases substantially with increasing oligomer length.

Similar observations have been reported with structurally-similar PPE oligomers and

polymers.[78]

Table 2-1: Near UV-visible absorption bands of $(L)Ru^{II}(bpy)_2$.[a]

Complex	λ_{max} /nm $(\varepsilon_{max}/$ mM^{-1}cm$^{-1})$	Assignment
Ru-1	290 (81.2)	π,π^* (bpy)
	326 (54.3)	π,π^* (1)
	422 (46.2)	π,π^* (1) & MLCT
Ru-2-C7	290 (78.5)	π,π^* (bpy)
	342 (64.3)	π,π^* (2-C$_7$)
	458 (48.7)	π,π^* (2-C$_7$) & MLCT
Ru-2-C18	290 (86.2)	π,π^* (bpy)
	344 (74.0)	π,π^* (2-C$_{18}$)
	458 (60.9)	π,π^* (2-C$_{18}$) & MLCT
Ru-3	290 (78.2)	π,π^* (bpy)
	356 (107.2)	π,π^* (3)
	458 (55.5)	π,π^* (3) & MLCT
Ru-4	290 (117.9)	π,π^* (bpy)
	338 (146.2)	π,π^* (4)
	388 (171.3)	π,π^* (4) & MLCT
	458 (77.8)	

[a] Measurements were conducted on CH_2Cl_2 solutions at 25°C.

Emission Spectra

Emisson studies were carried out on each of the $(L)Ru^{II}(bpy)_2$ complexes; emission maxima at 298 and 80 K are given in Table 2-2. Excitation of $(L)Ru^{II}(bpy)_2$ at 450 nm at room temperature in CH_3CN produces a moderately intense emission at $\lambda_{max} \approx$ 689 nm (Figure 2-17). All of these complexes feature a broad emission band with well-defined (0,0) and (0,1) vibronic components. This emission is clearly due to the $d\pi(Ru) \rightarrow \pi^*(L)$ MLCT excited state.

41
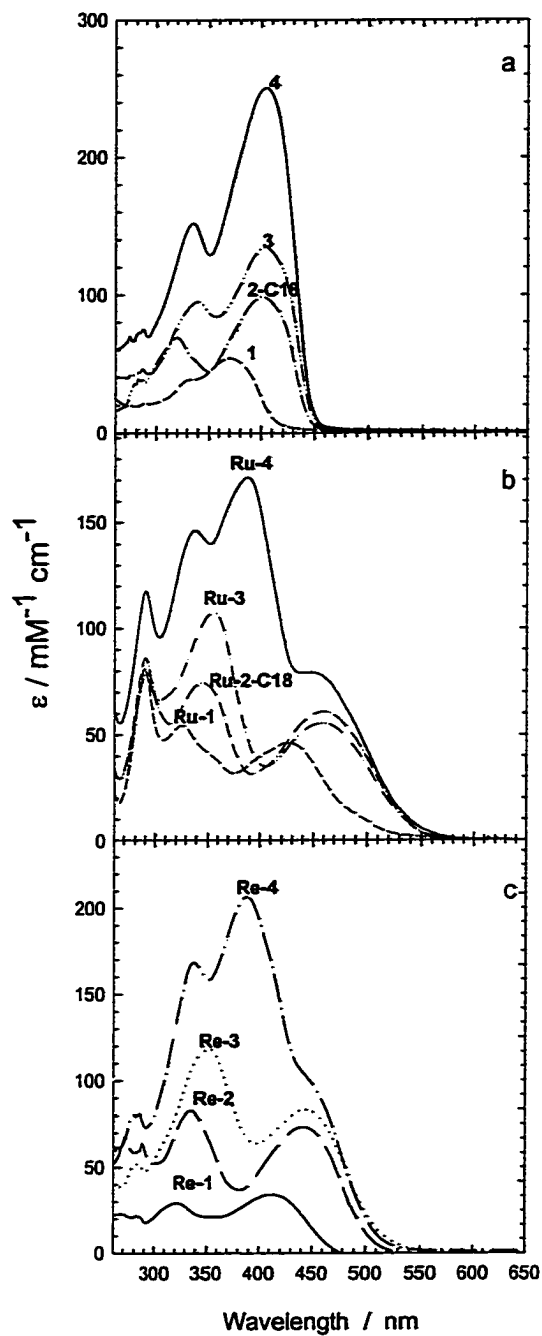
Figure 2-16: Absorption spectra of free oligomers and metal complexes. (a) 1 – 4 in THF; (b) **Ru-1** - **Ru-4** in CH₂Cl₂; (c) **Re-1** - **Re-4** in THF.

42
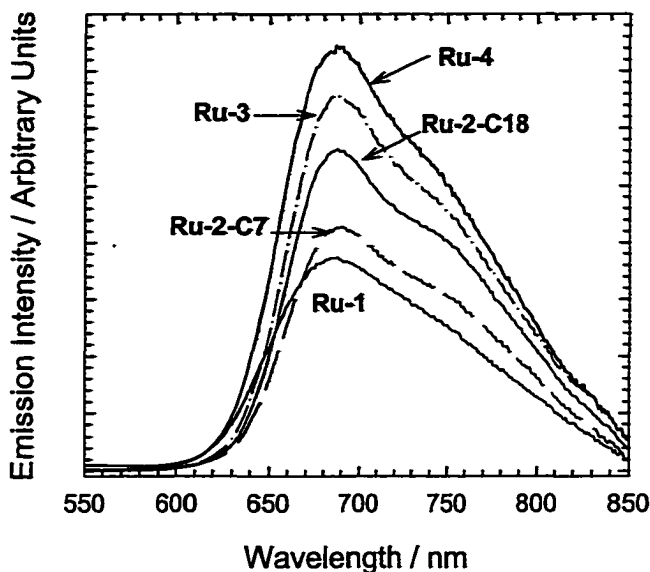
Figure 2-17: Emission spectra of $(L)Ru^{II}(bpy)_2$ in CH_3CN at room temperature.

In Figure 2-18 are shown temperature-dependent emission spectra of **Ru-1 – Ru-4** in 4:1 (v/v) EtOH/MeOH and 2-methyltetrahydrofuran (2-MTHF) solutions through the glass-to-fluid transition region from 80 to 298 K. The emission intensity increases substantially upon cooling (a 5-fold increase on cooling from 298 to 80 K is typical). The emission spectra of **Ru-1 – Ru-4** are similar to one another. At 80 K, all these complexes feature a vibronic structure that is very well resolved in the long oligomers, especially **Ru-3**. As temperature increases, the band red-shifted and it becomes broad at 298 K. Excitation spectra probing this emission (not shown) agree well with the absorption spectra, suggesting efficient electronic communication between the π,π^* oligomer and

dπ(Ru) → π*(MLCT) excited states.
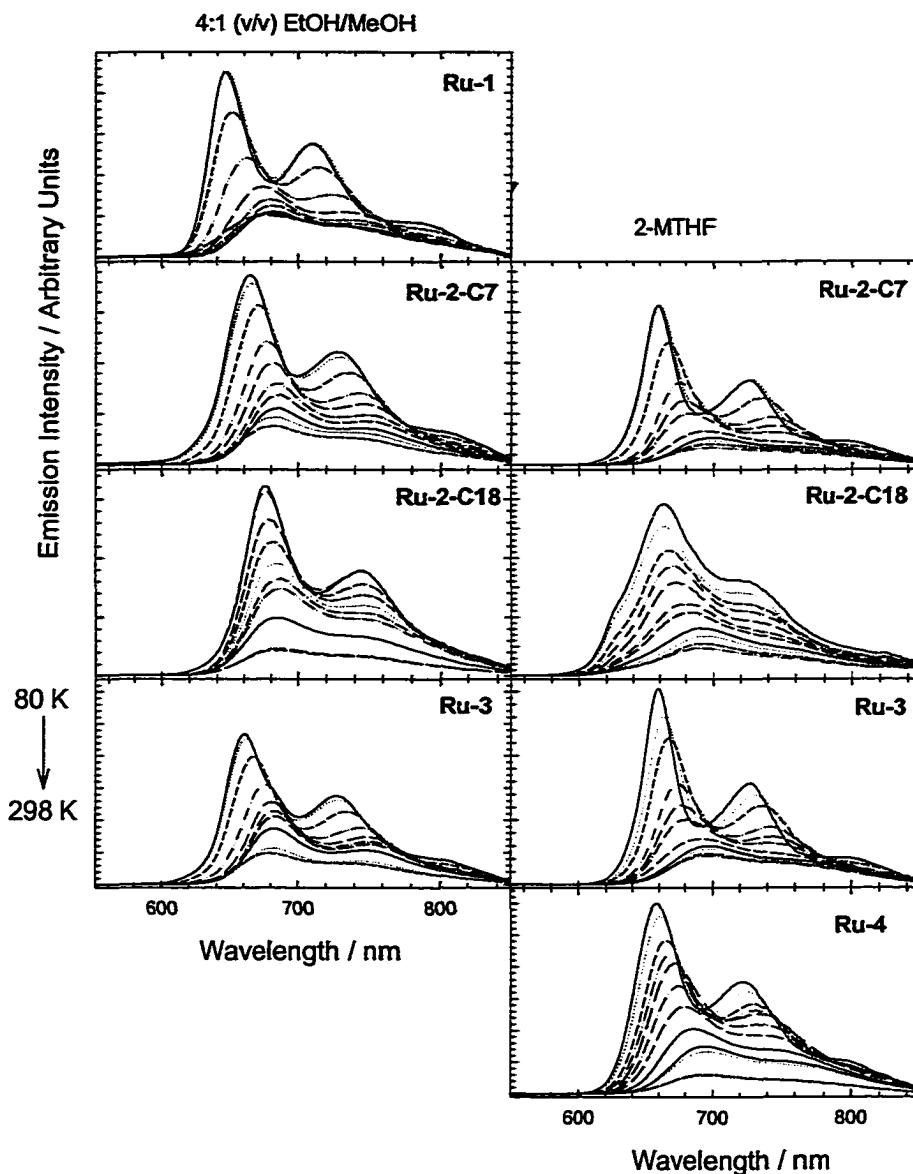
Figure 2-18: Emission spectra of **(L)Ru^{II}(bpy)$_2$** complexes in 2-MTHF and 4:1 (v/v) EtOH/MeOH solvents (450 nm excitation) at temperatures varying from 80 to 298 K. Emission intensity increases with decreasing temperature, and spectra are in 20 K increments.

Table 2-2: Photophysical properties of $(L)Ru^{II}(bpy)_2$ complexes.

| complex | 298 K[a] | | | | | | λ_{max}^{em} / nm | | | |
	λ_{max}^{em} nm	τ_{em}[b] ns	ϕ_{em}	$10^4 k_r$[c] s^{-1}	$10^6 k_{nr}$[c] s^{-1}	τ_{TA}[d] ns	EtOH/MeOH[e] 80 K	298 K	2-MTHF[e] 80 K	298 K
Ru(bpy)$_3$[f]	619	855	0.062	7.7	0.48	–	582	–	–	–
Ru-1	687	670	0.039	5.9	1.4	650	647	677	–	–
Ru-2-C7	690	706	0.034	4.4	1.3	990	664	686	658	701
Ru-2-C18	687	825	0.033	4.1	1.2	960	676	686	658	692
Ru-3	691	811	0.037	4.6	1.2	810	660	682	658	698
Ru-4	689	722	0.029	3.8	1.3	710	–	–	660	682

[a] Measurements were conducted on argon bubble-degassed CH_3CN solution at 298 K. [b] The lifetimes are monoexponetial. [c] $k_r = \phi_{em} / \tau$; $k_{nr} = 1/\tau_{em}(1-\phi_{em})$. It is assumed that the emitting state is produced with $\phi = 1$. [d] Decay lifetimes of transient absorption. [e] Samples were freeze-pump-thaw degassed. [f] Data from ref. [79-80].

44

The emission maximum shifts noticeably with temperature and solvents. This thermally-induced Stokes shift that occurs upon cooling is consistent with the "rigidochromic" effect observed for MLCT emissions of other polypyridine d^6 metal complexes[81] and further supports the assignment of the luminescence to the $d\pi(Ru) \rightarrow \pi^*(L)$ MLCT excited state. Figure 2-19 shows the thermally-induced Stokes shift of $(L)Ru^{II}(bpy)_2$ complexes in 4:1 (v/v) EtOH/MeOH and 2-MTHF solutions from 80 to 298 K. The ΔEs is the emission energy difference between 298 K and 80 K, $\Delta Es = E_{em}(80\ K) - E_{em}(298\ K)$, where $E_{em}(T) = 1/\lambda_{max}(T)$. The larger ΔEs value, the smaller Stoke shift.

The interesting point is that this thermally-induced Stokes shift is solvent and structure dependent. Three trends are readily observed with this data. 1) As the ligand becomes more conjugated, there is a smaller observed shift because of the smaller structural distortion of excited state. 2) As the side alkyl chain length of ligand increases, there is a smaller observed shift. From 80 K to 298 K, the emission maxima for **Ru-2-C7** in 4:1 (v/v) EtOH/MeOH red shifts 22 nm. And **Ru-2-C18**, which has long C18 chain on the ligand features only a very small thermally – induced Stokes shift (8 nm). 3) The thermally – induced Stokes shift is larger in the less polar solvent (2-MTHF). For example, the Stokes shift for **Ru-2-C7** is 43 nm in 4:1 (v/v) EtOH/MeOH compared to 22 nm in 2-MTHF.
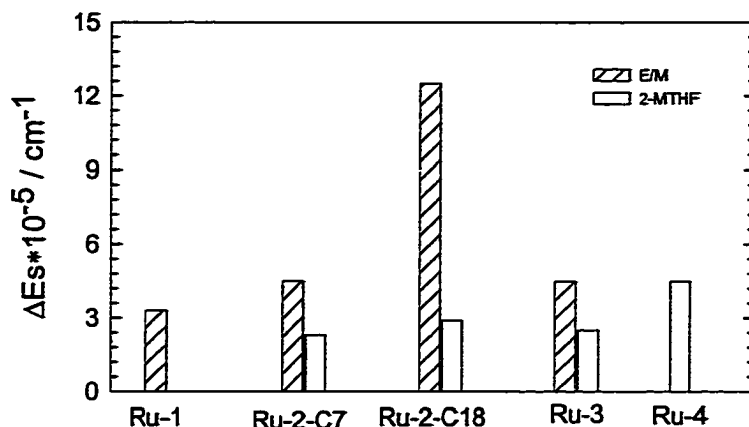
Figure 2-19: Thermally-induced Stokes shift of $(L)Ru^{II}(bpy)_2$ from 80 K to 298 K.

Emission Decays

Emission decays were monitored by using time-correlated single photon counting.[82] The emission decay profiles of **Ru-1 – Ru-4** in CH_3CN at room temperature are monoexponential. The lifetimes are listed in Table 2-2. Figure 2-20 shows the decay observed for **Ru-1** in CH_3CN solution on a logarithmic scale along with the excitation lamp profile and the computer calculated fit.
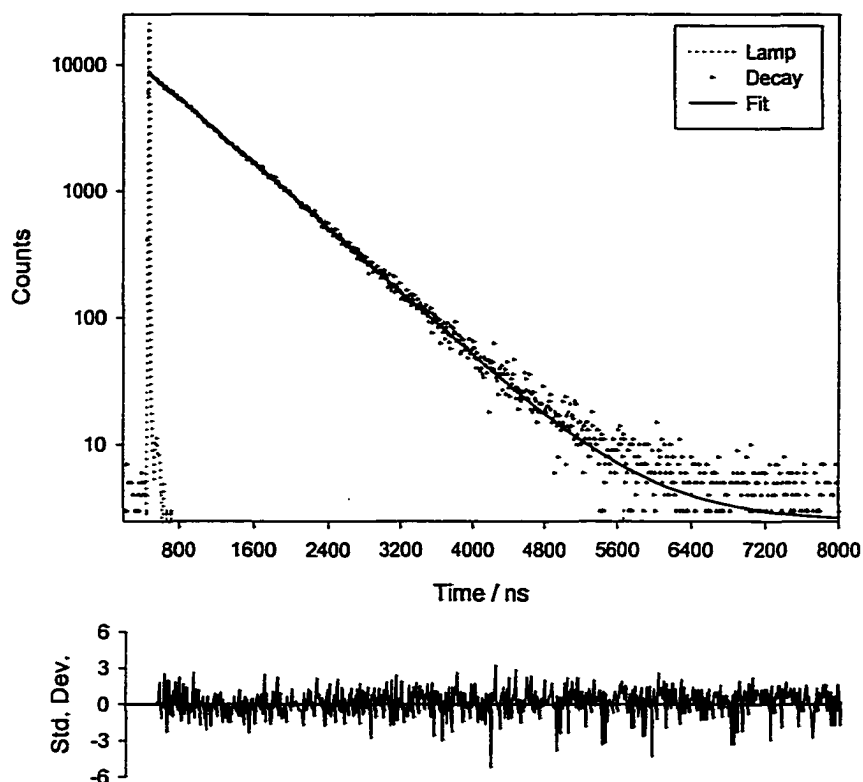
Figure 2-20: Time resolved emission decay of **Ru-1** in CH$_3$CN at room temperature. Upper box shows the emission decay (Δ) and the excitation lamp profile (dash line) along with the computer-calculated fit (solid line). Lower box show plots of the residuals indicating the quality of the calculated fit.

Emission quantum yields (ϕ_{em}) were measured for **(L)Ru^{II}(bpy)$_2$** complexes in CH$_3$CN at 298 K, and the values are listed in Table 2-2. Radiative and apparent nonradiative decay rates (k$_r$ and k$_{nr}$) were computed for all these complexes using the ϕ_{em} and τ_{em} values from equation 2-1, and these parameters are also listed in the table. The apparent k$_{nr}$ values

$$k_r = \phi_{em} / \tau \qquad\qquad \text{2-1a}$$

$$k_{nr} = 1/\tau_{em} - k_r \qquad\qquad \text{2-1b}$$

represent the sum of the rate of the "intrinsic" nonradiative decay process and the rate of internal conversion to the dd excited state. In addition, there may be further complication in the excited-state decay kinetics arising from the close energetic proximity of a L-centered $^3\pi,\pi^*$ state.

The quantum yields and lifetimes for these complexes are smaller than those for Ru(bpy)$_3$[79,80] (Table 2-2). The decreases in ϕ_{em} and τ_{em} values for the complexes arise mainly from increases in the apparent rates of nonradiative decay and decreases in the rates of radiative decay. Compared to **Ru-2** and **Ru-3**, there is slight depression in ϕ_{em} and τ_{em} for **Ru-4** which suggests that an additional, non-radiative decay path is operative in **Ru-4**.

Emission decay measurements at 650 nm for the **(L)Ru^{II}(bpy)$_2$** complexes were also performed in 4:1 (v/v) EtOH/MeOH and 2-MTHF as a function of temperature. For all of these complexes, both monoexponential and muliexponential decays were observed. Multiexponential fits were performed using equation 2-2,[82,83] yielding decay times (τ_i) and normalized amplitudes (α_i). Table 2-3 contains parameters for multiexponential fits of the emission from **Ru-1** – **Ru-4** complexes in 4:1 (v/v) EtOH/MeOH and 2-MTHF solutions at 80 and 298 K.

$$I(t) = \sum_i^n \alpha_i \exp\left\{\frac{-t}{\tau_i}\right\} \qquad 2\text{-}2$$

Figure 2-21 shows the decay observed for **Ru-1** and **Ru-2-C18** in 4:1 (v/v) EtOH/MeOH glass at 80 K on a logarithmic scale along with the excitation lamp profile and the computer calculated fit.

The emission kinetics of ruthenium complexes was obtained by calculating a weighted-average (mean) decay lifetime ($<\tau>$). The mean decay lifetime, $<\tau>$, was calculated using the multiexponential decay data according to the equation 2-3 and listed in the Table 2-3.

$$<\tau> = \sum_{i}^{n} \alpha_i \tau_i \qquad 2\text{-}3$$

In both 4:1 (v/v) EtOH/MeOH and 2-THF solvents the lifetimes are relatively long, consistent with assignment of the emission to a MLCT excited state with a large degree of triplet character.

Table 2-3: Emission lifetime data.[a]

complex	Solvent	80K					298 K				
		τ_1, μs (α_1,%)	τ_2, μs (α_2,%)	τ_3, μs (α_3,%)	$<\tau>^b$ μs	$\chi^{2\,c}$	τ_1, μs (α_1, %)	τ_2, μs (α_2, %)	τ_3, μs (α_3, %)	$<\tau>^b$ μs	$\chi^{2\,c}$
Ru-1	E/M	1.7 (100)	–	–	1.7	1.3	0.65 (100)	–	–	0.65	1.3
Ru-2-C7	E/M	1.0 (13)	4.0 (87)	–	3.6	1.3	0.52 (29)	1.0 (43)	2.1 (28)	1.2	1.2
	2-MTHF	2.7 (56)	10.6 (44)	–	6.2	2.7	1.0 (15)	2.1 (34)	4.1 (51)	3.0	1.6
Ru-2-C18	E/M	1.2 (38)	2.4 (48)	4.8 (14)	2.3	3.5	0.52 (5)	1.0 (11)	2.1 (84)	1.9	15.7
	2-MTHF	0.9 (26)	5.3 (74)	–	4.1		0.4 (63)	2.6 (37)	–	–	–
Ru-3	E/M	7.1 (29)	2.9 (71)	–	4.1	1.1	0.21 (15)	0.86 (85)	–	0.8	1.3
	2-MTHF	0.98 (8)	3.9 (92)	–	3.7	1.1	0.25 (56)	1.1 (47)	–	0.65	1.1
Ru-4	2-MTHF[d]	2.0 (4)	8.1 (78)	4.1 (18)	7.2	1.5	–	–	–	–	–
	2-MTHF	1.7 (1)	3.4 (53)	6.7 (46)	3.1	1.3	0.7 (58)	2.8 (42)	–	1.61	1.2

[a] 405 nm excitation. Decays were recorded at 650 nm. Lifetime and relative biexponential fits were performed with equation 2-2. [b] The mean decay lifetime, $<\tau>$, was calculated using the multiexponential decay data according to the equation 2-3. [c] χ^2 is used to evaluate the quality of the calculated fit. $\chi^2 = 1$ means the best fit. [d] Decays were recorded at 600 nm..

50
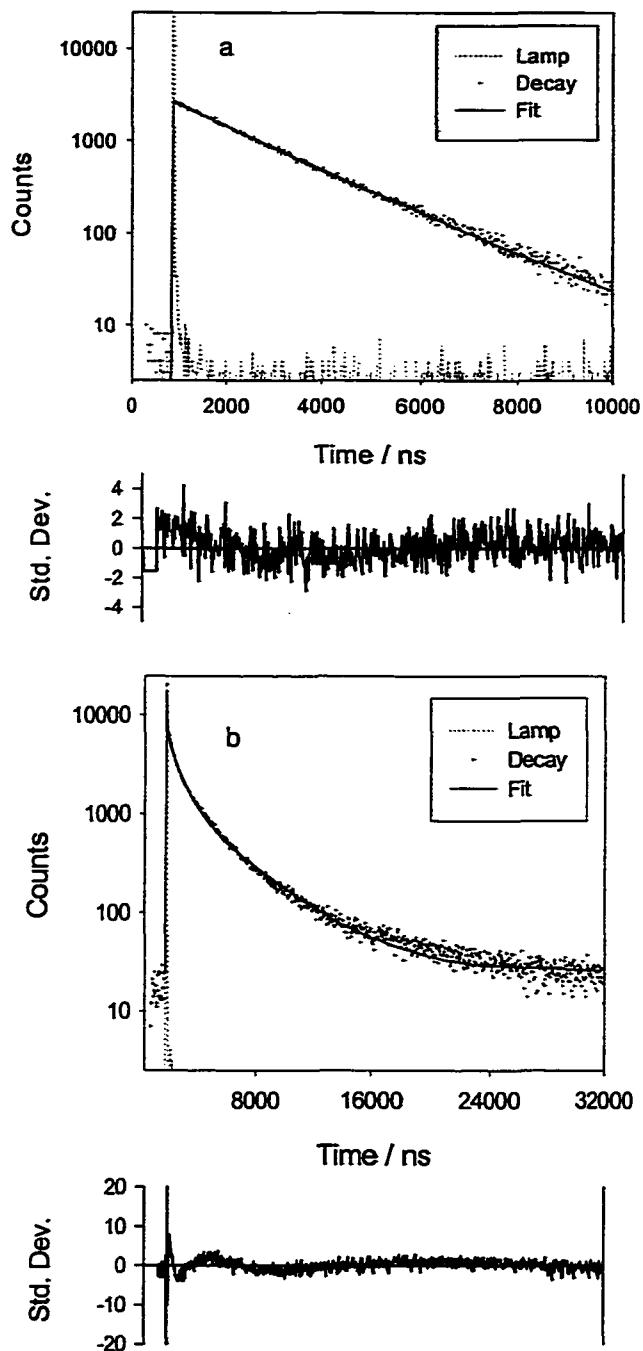
Figure 2-21: Time resolved emission decay. Upper box shows the emission decay (Δ) and the excitation lamp profile (dash line) along with the computer-calculated fit (solid line). Lower box show plots of the residuals indicating the quality of the calculated fit. (a) **Ru-1** in 4:1 (v/v) EtOH/MeOH glass at 80 K; (b) **Ru-2-C18** in 4:1 (v/v) EtOH/MeOH glass at 80 K.

The temperature dependences of the mean decay lifetimes for $(L)Ru^{II}(bpy)_2$ complexes could be satisfactorily fit by assuming a single thermally activated nonradiative decay path exists for the emitting excited state (equation 2-4),[84] where k^1 is the sum of the intrinsic radiative and nonradiative decay rate constants of the emitting state. If the state populated in the surface crossing is not in equilibrium with the emitting state, then k^0 and ΔE_1 represent the prefactor and activation barrier for the process. If the two states are in equilibrium, the k^0 is a function of the prefactors for both forward and back internal conversion between the equilibrated states and the decay rate of the nonemitting state and ΔE_1 equals the energy difference between the two states. The kinetic decay parameters so obtained and temperature range are collected in Table 2-4, where $\tau_0(T)$ uses the mean decay lifetime $<\tau>$.

$$[\tau_0(T)]^{-1} = k^1 + k^0 \exp(-\Delta E_1/RT) \qquad 2\text{-}4$$

Table 2-4: Kinetic parameters for excited-state decay.

	Temp range K	E/M (4:1) $k^0 \times 10^{-6}$ s^{-1}	$k^1 \times 10^{-5}$ s^{-1}	ΔE_1 cm^{-1}	2-MTHF $k^0 \times 10^{-6}$ s^{-1}	$k^1 \times 10^{-5}$ s^{-1}	ΔE_1 cm^{-1}
Ru-1	80 – 200	6.6	1.9	190	–	–	–
Ru-2-C7	80 – 200	6.8	3.5	271	2.5	1.2	204
Ru-2-C18	80 - 298	–	–	–	1.5	0.33	116
Ru-3	80 - 200	5.1	3.7	265	1.6	2.3	172
Ru-4	80 - 298	–	–	–	1.6	2.6	198

Emission Spectra Fitting

Emission spectral profiles were analyzed by comparing experimental spectra with spectra generating by using equation 2-5.[85]

$$I(\upsilon) = \sum_{v_M=0}^{5} \left[\left(\frac{E_0 - \upsilon_M \hbar \varpi_M}{E_0} \right)^3 \times \frac{S_M^{v_M}}{\upsilon_M!} \times \exp\left\{ -4\ln 2 [(\frac{\upsilon - E_0 + \upsilon_M \hbar \varpi_M}{\Delta v_{1/2}})^2 \} \right] \right] \qquad \text{2-5}$$

This equation results from a standard Frank-Condon analysis and expresses the energy dependence of the emission intensity (in cm^{-1}, relative to the intensity of the 0 – 0 transition) in terms of four parameters: E_0, $\hbar\varpi$, S, $\Delta v_{1/2}$. Vibronic contributions are included as a single, averaged mode of quantum spacing $\hbar\varpi$ and electron-vibrational coupling constant S. The electron-vibrational coupling constant is related to the change in equilibrium displacement between states, ΔQ_e, and reduced mass, μ, by S = $(1/2)(\mu\omega/\hbar)(\Delta Q_e)^2$ as described in equation 1-2. The summation in equation 2-5 was performed over the first five quantum levels. The full width at half-maximum, $\Delta v_{1/2}$, includes contributions from low-frequency inner- and outer- sphere modes treated classically. The energy quantity, E_0, is the energy difference between the $v^* = 0 \rightarrow v = 0$ vibrational levels in the excited and ground states as described in equation 1-1. Figure 2-22 illustrates the spectral parameters E_0, $\hbar\varpi$, and $\Delta v_{1/2}$. The magnitude of S determines the relative intensities of the individual components in the vibrational progression. $I(\upsilon)$ is the relative emitted light intensity at energy υ in their lowest energy vibrational levels. The parameter υ_M is the vibrational quantum number for the medium frequency acceptor mode, and S_M is the corresponding electron-vibrational coupling constant or Huang-Rhys factor.
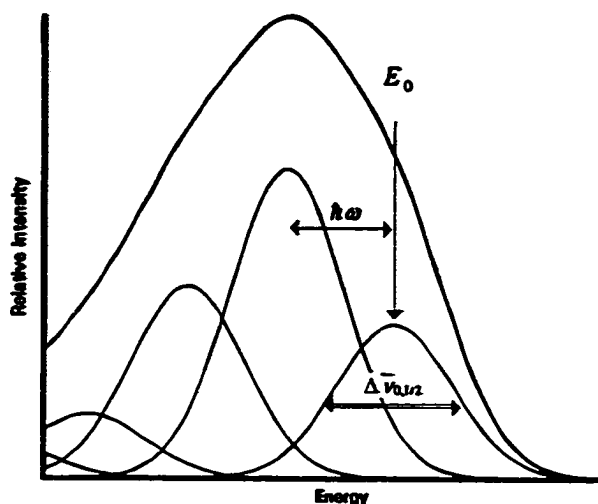
Figure 2-22: Graphical depiction of parameters used in emission spectral fitting showing deconvolution into four vibronic components (Ref. 85).

The details of the fit of an emission spectrum are therefore going to be a function of the nature of the vibrational modes that are coupled to the transition (e.g., $\hbar\omega_M$), the relative vertical and horizontal positions of the excited-state and ground-state potential energy surfaces (E_0 and S_M, respectively), and effects due to the surrounding medium.

Results of these analyses are given in Table 2-5 while a representative example of such a fit is illustrated in Figure 2-23 of **Ru-2-C7** in 4:1 (v/v) EtOH/MeOH at 80 K. The spectral fit diagrams of other complexes at 80 K and 298 K will be displayed in appendix A. Initially, the parameters E_{00}, $\hbar\omega$, and S_M were estimated from the energy at one-quarter intensity on the high-energy side of the first vibrational component (E_{00}), the spacing between observable medium-frequency vibration progression ($\hbar\omega$), and the ratio of peak height for the two highest energy vibration progressions (S_M).

It can be seen from Table 2-5 that there is a small drop in S_M from **Ru(4,4'-dmb)$_3$** (**4,4'-dmb** is 4,4'-dimethyl-2,2'-bipyridine) (1.05) to **Ru-1** (0.95) at room temperature.

This change in the Huang-Rhys factor originating from difference in ΔQ_e between the two complexes and is therefore directly related to changes in the equilibrium geometries of the excited states of the compounds. There is also a noticeable decrease in $\Delta \nu_{1/2}$.
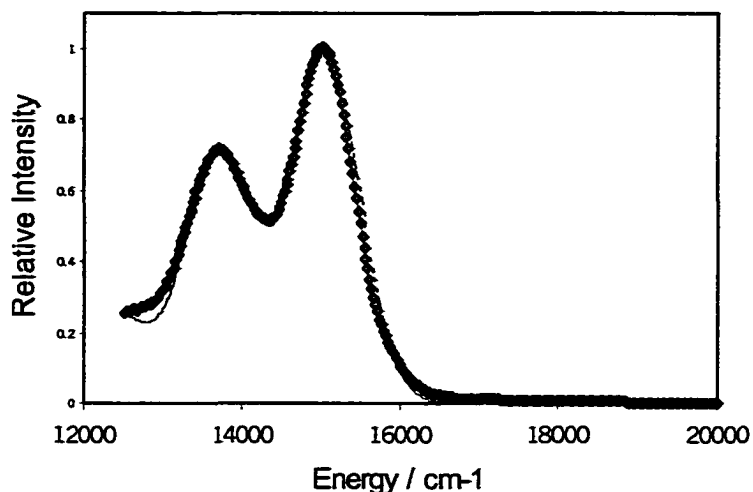
Figure 2-23: Spectral fitting results for low-temperature (80 K) emission of Ru-2-C7 in 4:1 (v/v) EtOH/MeOH (450 nm excitation). Points are experimental-determined data, while the lines are Frank-Condon bandshape analysis fits as described in the text.

In order to further probe the superimposed emission spectra at low temperatures, excitation polarization studies were conducted on Ru-2-C7 and Ru-2-C18. Wavelength-resolved polarization anisotropies ($r(\lambda)$) were calculated with equation 2-6.[83]

$$r(\lambda) = \frac{I_{vv} - GI_{vh}}{I_{vv} + 2GI_{vh}}$$

2-6

where G is $\dfrac{I_{HV}}{I_{HH}}$ and I_{XY} is the emission intensity with the excitation and emission polarizers adjusted according to x and y, respectively (e.g., I_{HV} is the emission intensity with horizontally polarized excitation light and vertically polarized emission detection).

Anisotropy measures the polarized light component ratio to its total intensity and is a direct indication of the angle between absorption and emission dipoles, α. Anisotropy values vary from 0.4 ($\alpha = 0°$) to -0.2 ($\alpha = 90°$), with an anisotropy value of zero statistically representing unpolarized light (e.g.; a uniform statistical distribution of emitting dipole angles relative to the absorption dipole).

The excitation polarization anisotropy, $r(\lambda)$ for **Ru-2-C7** and **Ru-2-C18** was measured at 125 K, recorded at the maximum of the structured emission (660 nm), and plots of $r(\lambda)$ are shown in Figure 2-24 along with their absorption spectra. In such a rigid solution, depolarization arising from rotational diffusion is eliminated. The anisotropy value is high for the lowest-energy absorption band (0.12), which suggests that the absorbing and emitting states are the same (i.e., little electronic rearrangement occurs between the absorbing and emitting states). As expected, the anisotropy value drops as the excitation wavelength decreases, since the absorbing state is now a higher-energy excited state than the emitting state. The excited complex must undergo internal conversion in this situation to reach the emitting state, which would certainly change the transition dipole and, consequently, the observed anisotropy. The negative anisotropy value (-0.1) remains constant over 350-450 nm range, which suggests that the angle between absorption and emission dipole is almost perpendicular. Since this region absorption is assigned as the π,π^* transition originating from the complexed oligomer, the structured emission observed at low temperature is ^{3}MLCT. This conclusion is based on the fact that the transition dipoles for the π,π^* and MLCT transitions are perpendicular.

Table 2-5: Parameters obtained by emission spectral fitting.

Compound	solvent	80 K				298 K			
		E_{00} cm^{-1}	ϖ cm^{-1}	S_M	$\Delta\nu_{1/2}$ cm^{-1}	E_{00} cm^{-1}	$h\varpi$ cm^{-1}	S_M	$\Delta\nu_{1/2}$ cm^{-1}
Ru(bpy)$_3$[a]	Propylene Carbonate	-	-	-	-	16300	1350	0.99	1700
Ru(4,4'-dmb)$_3$[b]	CH$_3$CN	-	-	-	-	15980	1330	1.05	1750
Ru-1	E/M	15450	1390	0.96	870	14750	1340	0.95	1420
Ru-2-C7	E/M	15060	1350	0.95	1020	14684	1280	0.99	1190
	2-MTHF	15174	1380	0.85	830	14245	1300	0.9	1380
Ru-2-C18	E/M	14770	1350	0.90	920	14530	1275	1.0	1265
	2-MTHF	15220	1360	0.80	1200	14420	1530	0.78	1600
Ru-3	E/M	15150	1400	0.96	900	14730	1380	1.0	1280
	2-MTHF	15170	1400	0.85	780	14490	1350	0.9	1420
Ru-4	2-MTHF	15170	1360	0.92	950	14340	1280	0.92	1330

[a] Data from ref. [66]. [b] Data from ref. [67].

57
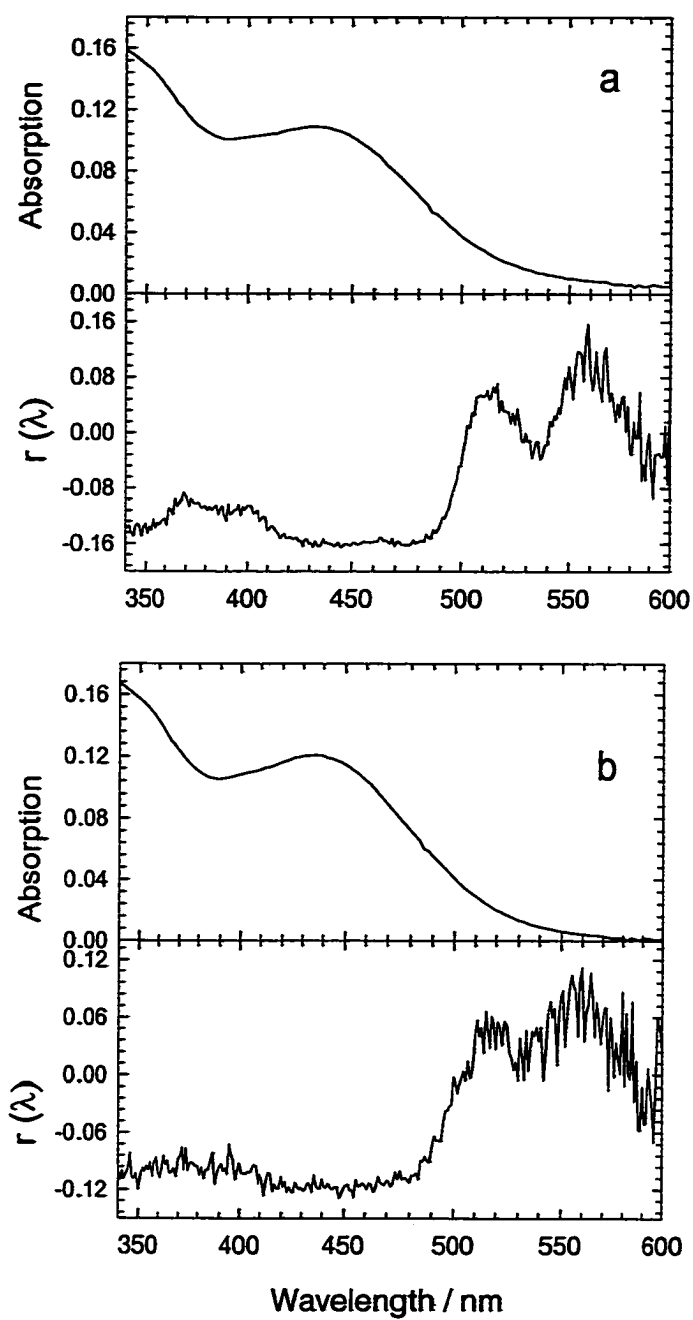
Figure 2-24: Excitation polarization r(λ) spectra acquired from 2-MTHF solution at 125 K with an emission wavelength of 660 nm for (a) **Ru-2-C7** and (b) **Ru-2-C18** along with their absorption spectra.

Transient Absorption

Transient absorption spectroscopy in the ns – μs time domain was carried out on all of the complexes to provide further information concerning the electronic structure of the long-lived excited states. Transient absorption spectra of $(L)Ru^{II}(bpy)_2$ complexes following pulsed laser excitation at 355 nm are shown in Figure 2-25 along with the ground-state absorption spectra. All the transient absorption spectra feature ground-state bleaching between 300 and 400 nm and strong absorbance around 520 nm, and a second broad absorption band that extends into the near-IR. Equivalent first order decays were observed for all features of the various transient absorption spectra. Excited state lifetimes obtained from factor analysis and global decay fitting are listed in Table 2-2. The transition absorption decays lifetime and that of the luminescence are approximately equivalent. This correspondence suggests that the transient absorption arises from the emitting ^{3}MLCT excited state.
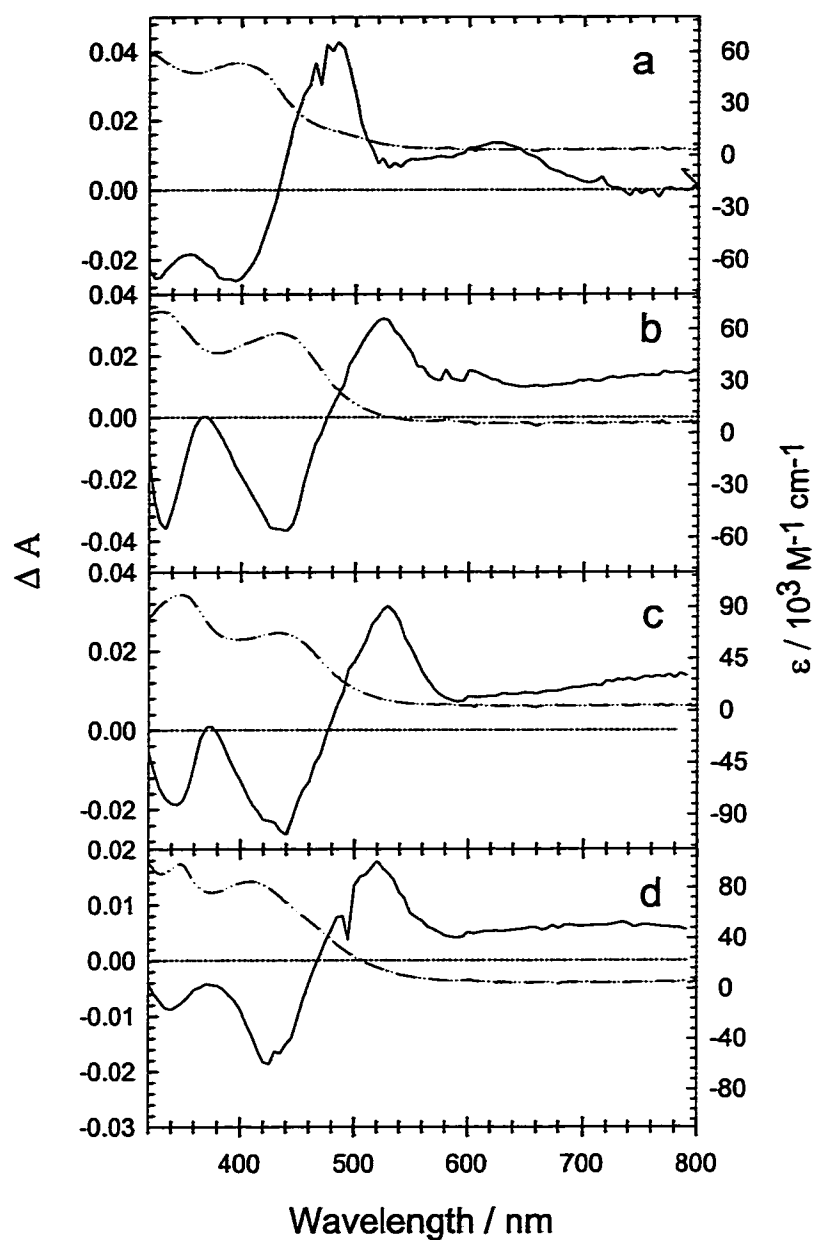
Figure 2-25: Transient absorption difference following 355 nm pulsed laser excitation (5 mJ dose) acquired from CH_3CN solution is plotted as a solid line with axis on left and the absorption spectra is plotted as a dash-dot-dot line with axis on right for (a) **Ru-1**; (b) **Ru-2-C7**; (c) **Ru-3** and (d) **Ru-4**.

Electrochemistry

Cyclic voltammetry was carried out on all the metal complexes. For **Ru-1** CH_3CN /0.1 M TBAH was used as the solvent for measurement. Owing to the solubility of **Ru-2** – **Ru-4**, CH_2Cl_2/0.1 M TBAH was used as the solvent. The relevant oxidation and reduction half-wave potentials are listed in Table 2-6. For comparison, redox potentials for $Ru(bpy)_3^{2+}$ in CH_3CN /0.1 M TBAH[87] are also included. Figure 2-26 illustrates the cyclic voltammogram of **Ru-1**, **Ru-2-C7** and **Ru-4**.

The one-electron oxidation is generally reversible in the cyclic voltammograms of all complexes with a half-wave potential ($E_{1/2}^{ox}$) in the region of $1.3 - 1.5$ V vs. SCE. For each of the complexes the first reduction occurs with $E_{1/2} \approx -1.0$ V (see Table 2-6) and the wave is quasi-reversible. Comparison of the redox potentials of the $(L)Ru^{II}(bpy)_2$ complexes reveals that their first oxidation and reduction are shifted anodically (i.e., to more positive potentials) relative to those of $Ru(bpy)_3^{2+}$. The shifts are consistent with the conjugation on the bpy ligands acting as moderate π-electron acceptors and the aryl-ethynyl moieties that are at the 5,5' position on the bpy stabilize the reduced complex. It's difficult to determine whether the first oxidation wave corresponds to the Ru(II/III) couple or the oxidation of ligand. Since the first oxidation potential of 1,4-dimethoxybenze in CH_3CN solution is 1.34 V,[88] the oxidation potential of the conjugated ligand probably will occur in the same potential region. The shape of the cyclic voltammogram of **Ru-1** is different from those of the other two complexes.

Table 2-6: Electrochemical data[a] for $(L)Ru^{II}(bpy)_2$ complexes and thermodynamics and kinetics of electron transfer[b] from excited-state $(L)Ru^{II}(bpy)_2$ systems to PQ^{2+} and DMA.

compound	$E_{0,0}^c$ eV	$E_{1/2}$, ox V	$E_{1/2}$, red V	$E_{1/2}(*Ru^{2+/3+})$ V	$E_{1/2}(*Ru^{2+/+})$ V	$10^8 k_q / PQ^{2+}$ $M^{-1} s^{-1}$	$10^9 k_q / DMA$ $M^{-1} s^{-1}$	$\Delta G_{ET} / PQ^{2+\,d}$ V	$\Delta G_{ET} / DMA^e$ V
$Ru(bpy)_3^{2+\,f}$	2.10	1.29	-1.33	-0.81	0.77	2.4	0.07	-0.35	-0.05
Ru-1	1.79	1.43[g]	-0.98[g]	-0.36	0.81	1.6	2.1	0.1	-0.09
Ru-2-C7	1.82	1.37[g]	-0.91[g]	-0.45	0.91	3.8	-	0.01	-0.19
Ru-2-C18	1.82	1.43[h]	-	-0.39	-	3.6	3.2	0.07	-
Ru-3	1.82	1.45[h]	-0.91[h]	-0.37	0.91	5.3	4.6	0.09	-0.19
Ru-4	1.81	1.47[h]	-0.93[h]	-0.34	0.87	1.4	-	0.12	-0.15

[a] Estimated error in $E_{1/2}$ values is ± 0.05 V for reversible waves. Recorded in CH_3CN or CH_2Cl_2 solution with 0.1 M TBAH as supporting electrolyte with a Pt working electrode, a Pt auxiliary electrode, and Ag/Ag^+ reference electrode. Potentials are referenced to a ferrocene internal standard and reported in V vs. SCE along with their assigned redox couples. $Fc^+/Fc = 0.425$ V was assumed in CH_3CN, and 0.45 V in CH_2Cl_2.[86] [b] Measurements were conducted in CH_3CN solution. [c] $E_{0,0}$ is estimated from computer fits of the corrected emission spectra of $(L)Ru^{II}(bpy)_2$. [d] Computed by using the equation $\Delta G_{ET} = E_{1/2}(*Ru^{2+/3+}) - E_{1/2}(PQ^{2+/+})$. [e] Computed by using the equation $\Delta G_{ET} = E_{1/2}(DMA^{+/0}) - E_{1/2}(*Ru^{2+/+})$. [f] Data from ref.[87] [g] Measurements were conducted in CH_3CN solution. [h] Measurements were conducted in CH_2Cl_2 solution.

62
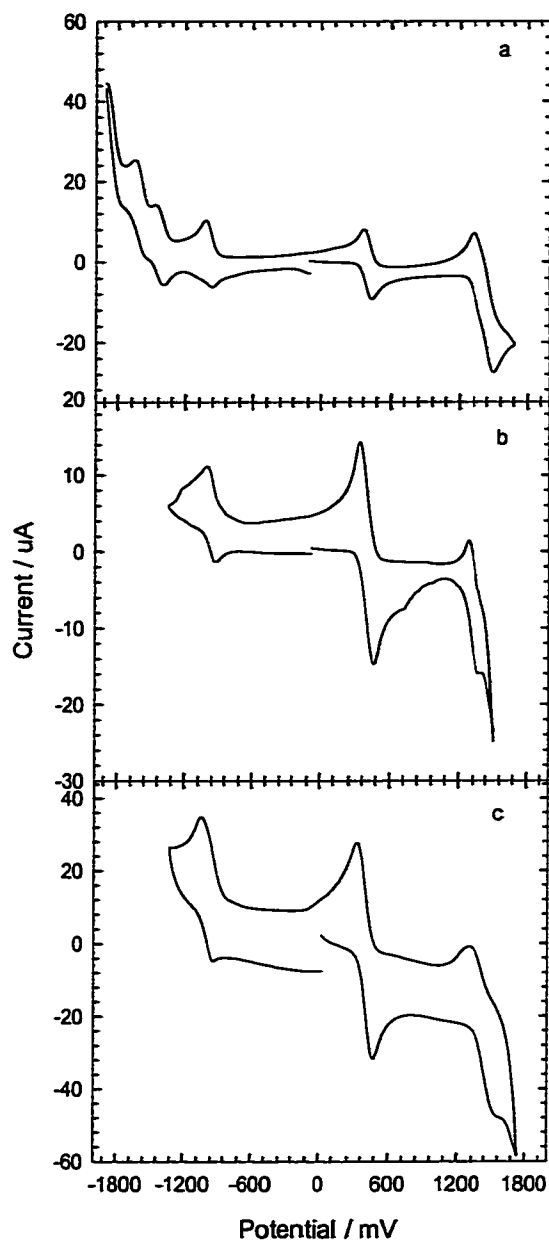
Figure 2-26: Cyclic voltammetry of $(L)Ru^{II}(bpy)_2$. (a) **Ru-1** in CH_3CN; (b) **Ru-2-C7** in CH_2Cl_2; (c) **Ru-4** in CH_2Cl_2.

Quite clearly the first reduction of all these complexes is localized on the conjugated ligand, i.e.

$$[(L)Ru^{II}(bpy)_2]^{2+} + e^- \rightarrow [(L^-)Ru^{II}(bpy)_2]^+$$
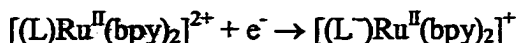
The electron probably is not delocalized significantly since the reduction potentials are almost the same for all these complexes.

In order to obtain the proper redox potentials for the metal complex excited state, the excited state energy must be included with the redox measurements as described in equation 2-7.[89]

Excited state oxidation potentials: $\quad E_{1/2}(*Ru^{2+/3+}) = E_{1/2}(Ru^{2+/3+}) - E_{0,0}$ $\qquad$ 2-7a

Excited state reduction potentials: $\quad E_{1/2}(*Ru^{2+/+}) = E_{1/2}(Ru^{2+/+}) + E_{0,0}$ $\qquad$ 2-7b

In equation 2-7, E_{00} is the zero-zero excitation energy of the excited state transition (i.e., the MLCT transition) and it can be approximated from computer fits of the corrected emission spectra. By using the photophysical and redox data complied for the $(L)Ru^{II}(bpy)_2$ complexes, excited-state redox potentials have been calculated (see Table 2-6). Because of its overall higher energy content than the ground state, the excited state is both a stronger oxidant and reductant than is the ground state from which it originated.[90] Compared with $Ru(bpy)_3^{2+}$, in general complexes are much weaker reductants and similar oxidants.

Excited State Electron Transfer Quenching.

In an effort to investigate the propensity of the excited-state metal complexes to undergo photoinduced electron transfer (ET) and to characterize the spectroscopic properties of the oxidized and/or reduced forms of the complexes, quenching experiments

were carried out on all the complexes in the presence of N,N'-dimethylanine (DMA, a reductive quencher) and N,N'-dimethyl-4,4'-bipyridinium (PQ^{2+}, an oxidative quencher) (Figure 2-27).

$$^*[(L)Ru^{II}(bpy)_2]^{2+} + PQ^{2+} \xrightarrow{k_q} [(L)Ru^{III}(bpy)_2]^{3+} + PQ^{+\cdot}$$

$[(L)Ru^{II}(bpy)_2]^{2+} + PQ^{2+}$
oxidative ET quenching

PQ^{2+}
$E_{1/2} = -0.46\ V^{90}$

$$^*[(L)Ru^{II}(bpy)_2]^{2+} + DMA \xrightarrow{k_q} [(L^{\cdot-})Ru^{II}(bpy)_2]^+ + DMA^{\cdot+}$$

$[(L)Ru^{II}(bpy)_2]^{2+} + DMA$
reductive ET quenching

DMA
$E_{1/2} = 0.72\ V^{90}$
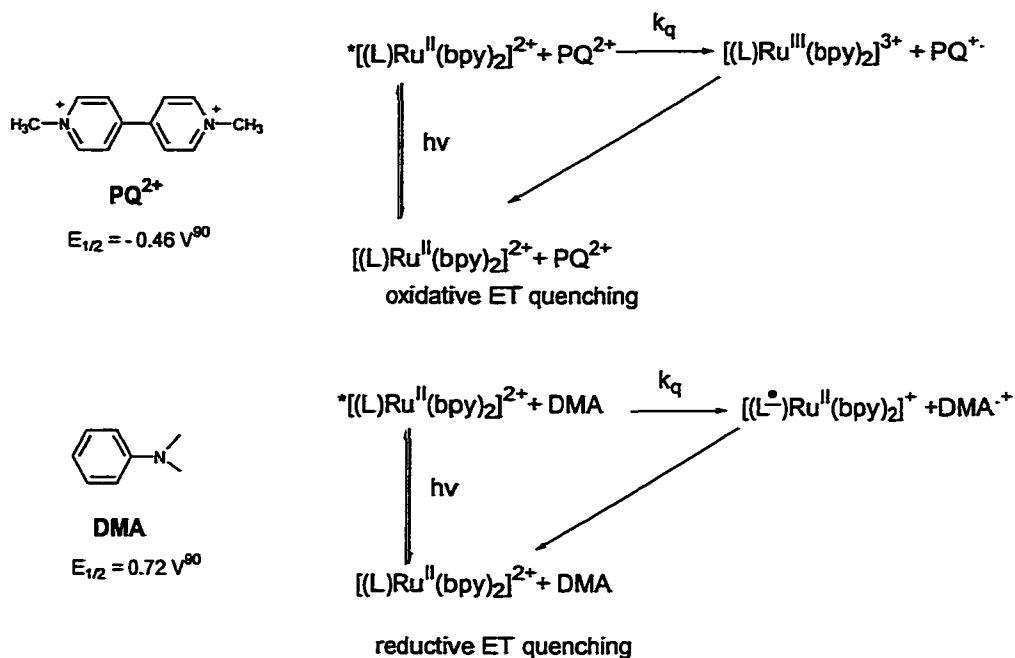
Figure 2-27: Photoinduced electron transfer reactions of $(L)Ru^{II}(bpy)_2$.

The thermodynamics for electron transfer quenching in the $(L)Ru^{II}(bpy)_2$ complexes by DMA and PQ^{2+} can be estimated from electrochemical and spectroscopic data by using equation 2-8.

$$\Delta G_{ET}\ /\ DMA = E_{1/2}(DMA^{+/0}) - E_{1/2}(^*Ru^{2+/+}) \qquad \text{2-8a}$$

$$\Delta G_{ET}\ /\ PQ^{2+} = E_{1/2}(^*Ru^{2+/3+}) - E_{1/2}(PQ^{2+/+}) \qquad \text{2-8b}$$

where $E_{1/2}(^*Ru^{2+/+})$ is the first excited reduction potential of the Ru^{II} chromophore, $E_{1/2}(DMA^{+/0})$ is the first oxidation potential of the electron donor, $E(^*Ru^{2+/3+})$ is the first

excited state oxidation potential of the Ru^{II} chromophore, and $E_{1/2}(PQ^{2+/+})$ is the first reduction potential of the electron acceptor. The results are shown in Table 2-6. It is clear that the reactions of $(L)Ru^{II}(bpy)_2^{2+}*$ with DMA are exothermic, while oxidative quenching of $(L)Ru^{II}(bpy)_2^{2+}*$ by PQ^{2+} is endothermic.

The results of the quenching experiments are shown in Table 2-6 for **DMA** and PQ^{2+} quenchers. Both **DMA** and PQ^{2+} quench the luminescence of all the complexes. The data were plotted according to the Stern-Volmer equation, $I_0/I = 1 + k_q\tau_0[Q]$ where k_q is the experimental quenching rate constant, I_0 is the intensity of light emitted at a fixed wavelength in the absence of quencher, and I is the emitted intensity in solutions with added quencher. The plots were linear over a range of quencher concentrations (0 – 20 mM) and the intercepts were unity as expected. A representative example of Stern-Volmer plots of **Ru-2-C18** is shown in Figure 2-28; k_q values were determined from the slope of lines and the lifetime.
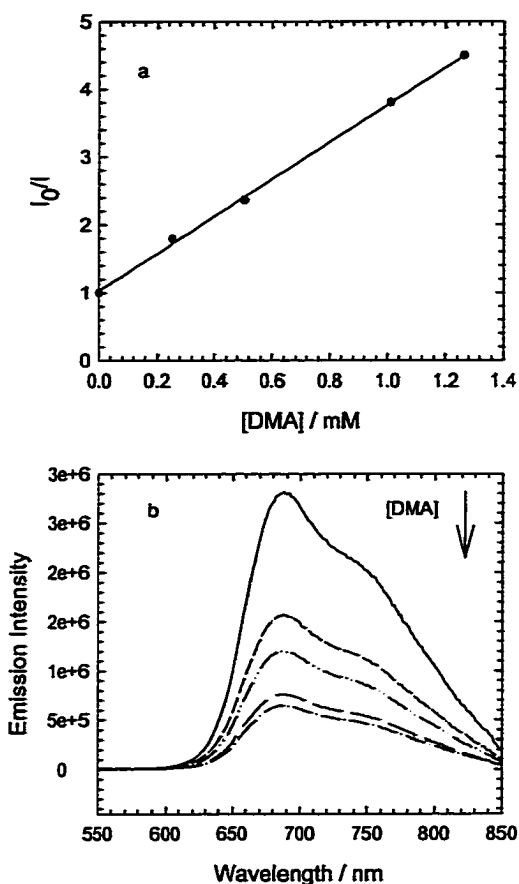
Figure 2-28: **DMA** quenching of **Ru-2-C18** in CH₃CN. (a) Stern-Volmer plot; (b) emission intensity quenched by **DMA**.

Figure 2-29a illustrates the difference spectra when a solution of **Ru-2-C18** and 11 mM **PQ^{2+}** is subjected to 355 nm excitation. The experiments were carried out at relatively high quencher concentrations so that excitation of the Ru^{II} chromophore and electron transfer quenching occurs during the flash, and the expected redox products are observed following the flash. At early times after excitation, the first transient was formed with 213 ns lifetime which is the absorption of the MLCT excited state; however over the course of its lifetime, the second transient formed and spectrum evolves into one that is characterized by bleaching for $\lambda < 360$ nm, a strong absorption at $\lambda_{max} = 370$ and

395 nm, weak bleaching between 410 and 480 nm, and a broad band at $\lambda_{max} = 520$ nm. This difference spectrum is clearly due to a superposition of absorption bands characteristic of the oxidized Ru^{III} complex and viologen radical cation, PQ^{+}.[90] The second transient decays on a longer time scale ($\tau_{1/2} \approx 32$ μs), consistent with disappearance of the radical ions via diffusion-controlled back-ET.

The transient absorption difference spectra of **Ru-2-C18** in the presence of 3 mM **DMA** are illustrated in Figure 2-29b. In this experiment quenching also leads to the production of long-lived transient absorption ($\tau_{1/2} \approx 29$ μs) that clearly arises from the products of bimolecular photoinduced ET. The new broad band appears at $\lambda_{max} = 600$ nm is clearly due to the absorption of **DMA**$^{+}$.[90]

The transient absorption spectra of other ruthenium complexes in the presence of different concentration **PQ**$^{2+}$ and **DMA** are shown in appendix B.
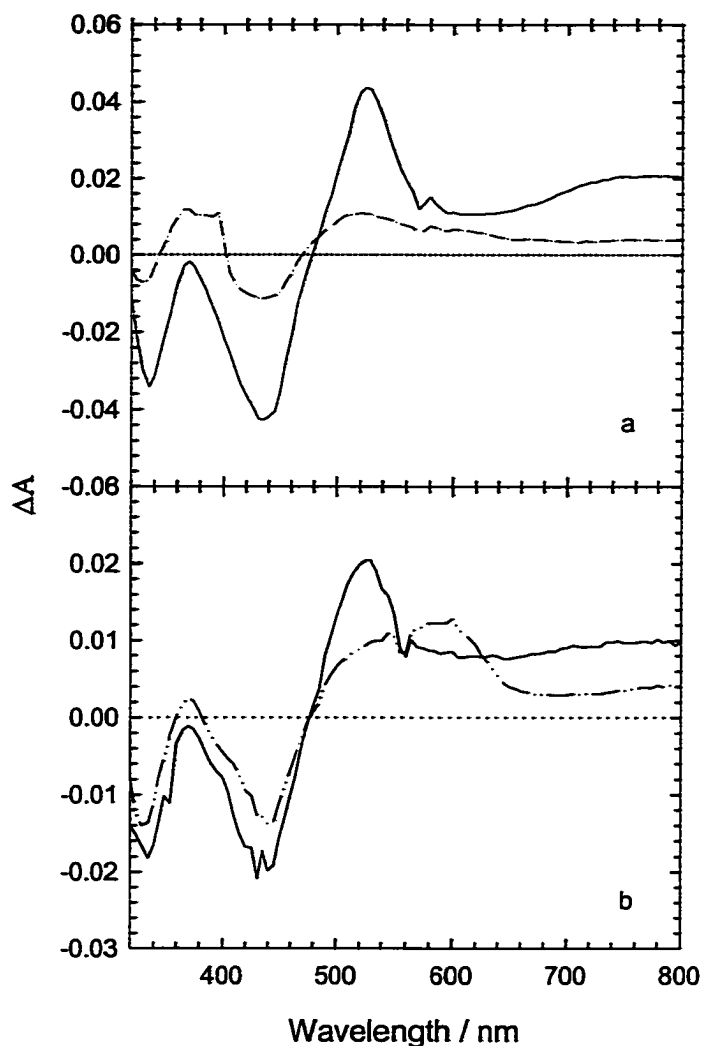
Figure 2-29: Transient absorption difference spectra following 355 nm pulsed laser excitation (5 mJ dose) of **Ru-2-C18** (1.0×10^{-5}M) in CH_3CN. (a) with 11 mM **PQ^{2+}**. The solid line is the first transient formed with short lifetime ($\tau = 213$ ns) and the dash-dot-dot line is the long-lived transient ($\tau = 32$ μs); (b) with 3 mM **DMA**. The solid line is the first transient formed with short lifetime ($\tau = 835$ ns) and the dash-dot-dot line is the long-lived transient ($\tau = 29$ μs).

There are several significant features with respect to the ET quenching experiments. Although the excited state oxidation potentials for **(L)Ru^{II}(bpy)$_2$** complexes are considerably less negative than Ru(bpy)$_3$$^{2+}$ and the quenching rates for **Ru-1** and **Ru-**

4 by PQ^{2+} are only slightly smaller than the rate by which PQ^{2+} quenches $Ru(bpy)_3^{2+}$ and

the quenching rates for **Ru-2 and Ru-3** are even bigger than that of $Ru(bpy)_3^{2+}$. This is

probably caused by the conjugation of ligand which stabilizes the Ru^{III} excited state and

makes electron transfer easy to happen. On the contrary, the excited state reduction

potentials for **(L)Ru^{II}(bpy)$_2$** are only slightly positive than that of $Ru(bpy)_3^{2+}$ which

imply that **(L)Ru^{II}(bpy)$_2$** are better oxidizing agents than $Ru(bpy)_3^{2+}$. The quenching

rates for all the **(L)Ru^{II}(bpy)$_2$** complexes are more than an order of magnitude bigger

than that of $Ru(bpy)_3^{2+}$.

Discussion

UV-Visible Absorption Spectra

For the **1 – 4** oligomers, recall that following an initial red-shift from **1** to **2** (370

nm → 400 nm), the lower-energy π,π^* transition remained at a constant wavelength for

oligomers **2 – 4**, suggesting that oligomer bandgap had been reached. The extent of

oligomer conjugation is dominated by "breaks" caused by twists in the bipyridine and

biphenyl subunits of the oligomer backbone. These twists are induced by steric effects

due to the close proximity of α-hydrogens on adjacent phenyl rings. It is well known that

the ground state geometry of the biphenyl molecules has the two phenyl rings twisted ~

43° out of the plane.[91] Also important to note is that there is approximately a 20° dihedral

angle between the two pyridine planes in 2,2'-bipyridine when it is in it's transoid-like

conformation.[92] This lack of planarity causes a significant conjugation break within the

backbone of the oligomer. The biphenyl conjugation breaks do not allow further

delocalization and, consequently additional red-shifting with increased oligomer length.

An oligomer size increase may not bring a corresponding conjugation length increase. However, the increased overall size of oligomer still increases the electronic transition dipole, which in turn increases the oscillator strength of both π,π^* transitions, resulting in the observed intensity increase. So the largest conjugation enhancement is expected between the smaller oligomers 1 and 2 respectively, due to the fact that they are mostly planar; with only 2 having a biphenyl spacer on its periphery.

It is also anticipated that metallation of the oligomers would also increase the effective conjugation length. This is because incorporation of a metal ion forces the bipyridine rings from a transoid conformation to the necessary cisoid conformation needed for coordination to the metal center. This geometric change should help to increase the conjugation within the oligomer backbone. However, the peripheral of subunits are likely twisted as illustrated in Figure 2-30. For the $(L)Ru^{II}(bpy)_2$ complexes, following an initial increase and red-shift from Ru-1 to Ru-2, the oscillator strength and wavelength of the lower energy π,π^* transition band remains relatively constant as the oligomer size increases. The red-shifted π,π^* transition with respect to the free oligomer is due to the forced oligomer bipyridine planarity and the resulting conjugation increase (Figure 2-30), in addition to potential contributions from a charge transfer band. There is little change in the oscillator strength of this transition for the larger ruthenium oligomers, leading us to conclude that this transition is largely composed of the central bis (phenylethynyl-dialkoxyphenylethynyl)-capped bipyridine portion of the oligomer. This chromophore is likely confined by the twisting of the first biphenyl unit in the oligomer backbone, restricting any further delocalization into the peripheral segment of the oligomer. In general the larger oligomers, notably Ru-4 seems to behave as a dual

component system, one, an organic segment composed of the outer periphery of the conjugated oligomer, followed by a metal-organic central segment, restricted by the twisting of the first biphenyl unit. The similarity of absorption spectra of $(L)Ru^{II}(bpy)_2$ complexes with those of $(L)Re^{I}(CO)_3Cl$ complexes,[93] further proves that absorption spectra are dominated by the π,π^* transition of the ligand.

Figure 2-30: Diagram depicting the chromophore length prior to and after metallation.

A distinct shoulder is observed ($\lambda \approx 485$ nm, $\varepsilon \approx 8000$ $M^{-1}cm^{-1}$) in the spectrum of **Ru-1** which is very likely the $d\pi(Ru) \rightarrow \pi^*(1)$ MLCT transition. A similar MLCT band is not observed in the spectra of **Ru-2** - **Ru-4** because it is obscured by the more intense π,π^* transition that occurs at a lower energy in these oligomers. The excitation polarization spectra further confirm this statement. A value of $r(\lambda) = -0.10$ across the π,π^* transition of the ligand (360 – 470 nm) indicates almost orthogonal absorption and emission polarization. The $r(\lambda)$ values rise rapidly and becomes positive across the entire

^{1}MLCT transition (470 – 600 nm). This fact confirms that emission and charge transfer absorption are dominantly linear process.

Photophysics of the Metal-Organic Oligomers

The variable temperature emission spectra of **Ru-1 – Ru-4** are qualitatively similar (Figure 2-18). Vibronic structure is observed for all of the complexes. The emission band blue shifts with decreasing temperature which is characteristic for charge transfer emission. The thermally-induced Stokes shift is typical for MLCT emission in metal complexes; it arises because as temperature increases the solvent dipoles are able to reorganize around the polar MLCT state more efficiently.[93-95] So as the temperature increases, the emission energy decreases. The noteworthy feature for **(L)Ru^{II}(bpy)$_2$** complexes is seen by comparing the temperature dependence of the MLCT emission from **Ru-2-C7** and **Ru-2-C18**. The rather smaller thermally-induced Stokes shift for **Ru-2-C18** signals that the C18 alkoxy side chains disturb the solvation environment of the complex and preclude solvent dipole reorganization around the MLCT excited state. Selective solvation of the alkyl side chains makes thermally-induced Stokes shift bigger in 2-MTHF solvent compared to 4:1 (v/v) EtOH/MeOH solvent. EtOH/MeOH is a more polar solvent and stabilizes the MLCT excited state more efficiently.

The contributions to the emission spectral profile by low-frequency modes and the solvent are included in the bandwidth parameter $\Delta v_{1/2}$.[96] In principle, it is possible to separate the contributions to $\Delta v_{1/2}$ from low-frequency modes and the solvent by temperature dependent studies. The bandwidth is related to the solvent reorganizational energy χ_0, and the temperature by the relationship in equation 2-9.[96]

$$(\Delta v_{1/2})^2 \sim C + (7.71\chi_0)T \qquad\qquad 2\text{-}9$$

The squares of the resulting band widths, are plotted vs. T in Figure 2-31 for all of the complexes. The χ_0 values obtained from slopes are listed in Table 2-7. From Table 2-7 we can see that 2-MTHF solvent has bigger reorganization energy than 4:1 (v/v) EtOH/MeOH. It is consistent with the bigger Stokes shift in 2-MTHF since the Stokes shift is proportional to the outer-sphere reorganization energy for the MLCT excited state.[97]

Table 2-7: χ_0 values obtained from plots of $(\Delta v_{1/2})^2$ vs. T.

complex	Temperature Range / K	solvent	χ_0 / cm^{-1}
Ru-1	80 - 285	E/M	792
Ru-2-C7	80 - 285	E/M	297
		2-MTHF	826
Ru-2-C18	80 - 285	E/M	493
		2-MTHF	770
Ru-3	80 - 285	E/M	526
		2-MTHF	988
Ru-4	80 - 285	2-MTHF	617

Lifetimes for the $(L)Ru^{II}(bpy)_2$ complexes in CH_3CN solution at room temperature can be fit to a single exponential. The emission lifetime of all the complexes is on the order of 1 μs. This is consistent with MLCT transitions. In this polar solvent, the MLCT excited state is lowest in energy because it can be further stabilized by the polar solvent. While in the same polar solvent 4:1 (v/v) EtOH/MeOH, the lifetime of all of the

complexes show multiexponential fit besides **Ru-1** which are probably due to the bad solubility of **Ru-2 – Ru-4** in this solvent. The equilibrium between π,π^* transition and MLCT excited state, aggregation of molecules and the conformation change of phenyl ring of ligand all can cause addition decay channel for the excited state.

Lifetimes for the **(L)Ru^{II}(bpy)$_2$** complexes in Table 2-4 are remarkably long given the low excited state energies. The origin of the effect is the decrease in S_M (and ΔQ_e) which decrease vibrational overlap and k_{nr}.[62]

dd States

There is no evidence for dd state involvement. This is understandable qualitatively. Compared to Ru(bpy)$_3^{2+}$, the low lying π^* acceptor orbital at ligand **L** decreases the energy of the lowest MLCT and the dd state is not accessible.

Figure 2-31: Plots of $(\Delta\nu_{1/2})^2$ vs. T for $(\mathbf{L})\mathbf{Ru}^{\mathrm{II}}(\mathbf{bpy})_2$ complexes.

Energy Gap Correlation

Plots of $\ln k_{nr}$ vs. E_0 for $(L)Ru^{II}(bpy)_2$ complexes using data from 80 to 298 K are shown in Figure 2-32. E_0 is the energy of emission maxima for the emission. Slopes and intercepts obtained from least-squares fits of the data are shown in Table 2-8. Besides **Ru-2-C18**, it is clear that energy gap law behavior is observed. This suggests that d-d states do not influence the decay kinetics which is consistent with the low energy of the MLCT state in the metal-oligomers. The exception of energy gap correlation for **Ru-2-C18** is probably due to the perturbations of the long alkoxy side chains.

Energy gap law has been applied to nonradiative decay in MLCT excited states of $[Os^{II}(bpy)_2(CO)(Py)]^{2+}$ complex, where the energy gap was changed by glass to fluid transition.[63] From the spectral fitting results, the primary origin of the decrease in emission energies as the temperature is increased is in E_{00} and the influence of changes in solvent dipole orientations on the energy gap between the excited and ground states. As a consequence, the temperature-dependent data provide an additional experimental basis for testing the energy gap law. The slope and intercept obtained are similar with values obtained from $Ru(bpy)_3^{2+}$ complex by varying the surrounding medium (see Table 2-8). This suggests that the same pattern of acceptor vibrations and electronic coupling factors are involved in nonradiative decay induced by the glass-to-fluid transition.

The energy gap law was also observed for $Os(bpy)_3^{2+}$ complex by changing the temperature.[63] But the slope and intercept are much bigger than other systems (Table 2-8). The increase in slope is probably a consequence of the convolution of at least two contributions to k_{nr}, one from the glass-to-fluid transition and a second from the transition between the third and fourth states.

For our metal-organic complexes, we also got bigger slopes especially for **Ru-2-C7** in EtOH/MeOH solvent (Table 2-8). In our system, besides MLCT excited states, there is π,π^* excited state which is very close in energy of MLCT excited state. The increase in slope is probably due to the equilibrium between MLCT and π,π^* excited state.

Table 2-8: Slopes and intercepts obtained from plots of lnk_{nr} vs. E_0.

Complex	Variation made	Temperature Range / K	solvent	slope $1/cm^{-1} \times 10^3$	intercept
Ru(bpy)$_3$$^{2+ a}$	solvent			-0.93	29.1
[Os(bpy)$_2$(CO)(Py)]$^{2+ b}$	glass/fluid	90 - 170	E/M	-0.97	29.5
Os(bpy)$_3$$^{2+ c}$	glass/fluid	90 - 170	E/M	-1.82	40.3
Ru-1	glass/fluid	80 – 298	E/M	-1.40	34.8
Ru-2-C7	glass/fluid	80 – 298	E/M	-1.87	41.1
			2-MTHF	-1.22	30.7
Ru-2-C18	glass/fluid	80 – 298	E/M	–	–
			2-MTHF	–	–
Ru-3	glass/fluid	80 – 298	E/M	-1.47	35.2
			2-MTHF	-0.90	26.3
Ru-4	glass/fluid	80 – 298	2-MTHF	-1.25	31.5

[a] Data from ref.[66]. [b] Data from ref.[63]. [c] Data from ref.[63]

Figure 2-32: Energy gap law plots (lnk$_{nr}$ vs. E$_0$) over the temperature range 80 to 298 K. The energy values plotted are the energies of the band maxima of the emission.

Nature of the Lowest Excited States

Based on the spectroscopic assignment for the absorption and luminescence data, we can conclude that the lowest excited state is ^{3}MLCT. The electron transfer quenching experiments further prove this statement. The excitation of (L)Ru^{II}(bpy)$_2$ complexes with 355 nm light leads to the formation of MLCT excited state which has triplet character. This state exhibits strong reducing and oxidizing properties. Thus, in CH$_3$CN solution, it is capable of reducing PQ^{2+} or oxidizing DMA. However, from previous work we know that $^3\pi,\pi^*$ is close in energy to ^{3}MLCT, so its involvement cannot be ruled out. Transient absorbance spectra for (L)Ru^{II}(bpy)$_2$ complexes are very similar to (L)Re^I(CO)$_3$Cl systems where the transient absorption is believed to arise from $^3\pi,\pi^*$ state.[98] All of the above evidence suggests that there may be an equilibrium and/or mixing of MLCT and π,π^* states.

To further examine the relative energies of the ^{3}MLCT and $^3\pi,\pi^*$ state, quenching of both of the T$_1 \rightarrow$ T$_n$ absorption and ^{3}MLCT emission of Ru-3 was examined, using a series of aromatic hydrocarbons of known triplet energy (E$_T$) as quenchers. Table 2-9 lists quenching rate constants obtained assuming Stern – Volmer kinetics, and Figure 2-33 shows ln(k$_q$) as a function of the triplet energy for each complex. Results for quenching of both transient absorbance and luminescence of Ru-3 are nearly identical. Although the data are relatively limited, the $^3\pi,\pi^*$ energy is between that of 9,10-dibromoanthracene (14060 cm^{-1}) and 1-chloroanthracene (14750 cm^{-1}). We can estimate that $^3\pi,\pi^*$ energy is around 14500 cm^{-1} which is very close to that of the ^{3}MLCT emission maxima (14492 cm^{-1}). Quenching of Ru-3 with PQ^{2+}, which can only react with the ^{3}MLCT state via electron transfer, results in quenching of both ^{3}MLCT emission

and intraligand transient absorption at comparable rates (Table 2-9). This observation

suggests the two states are in equilibrium. The small prefactor and low activation barrier

obtained from temperature-dependent luminescence decays of **Ru-3** may result from

equilibrium internal conversion between the emitting ^{3}MLCT state and $^3\pi,\pi^*$ state.

Table 2-9: Rate constants for quenching of transient absorbance and luminescence of **Ru-3** in CH_3CN solution.

quencher	E_T / cm^{-1}	$k_q^{em} \times 10^{-9}$ M^{-1}s^{-1}	$k_q^{abs} \times 10^{-9}$ M^{-1}s^{-1}	lnk_q^{em}	lnk_q^{abs}
Acridine	15900	0.38	—	19.76	—
Phenazine	15400	0.75	—	20.43	—
Anthracene	15000	2.32	1.78	21.56	21.3
1-chloroanthracene	14750	4.20	4.45	22.16	22.2
9,10-dibromoanthracene	14060	6.73	—	22.63	—
perylene	12300	11.59	11.44	23.17	23.16
PQ^{2+}	—	0.53	0.47	20.09	—

Figure 2-33: Rates for triplet quenching of transient absorbance (Δ) and luminescence (o) of **Ru-3** as a function of quencher triplet-state energy in CH_3CN at room temperature. The solid line in the region of decreasing $\ln(k_q)$ vs E_T represents the best-fit straight line through the points.

Consideration of the molecular and electronic structure of the linear metal-organic oligomers provides insight into the nature of the excited states that give rise to their photoluminescence and transient absorption features. First, the metal-organic complexes feature two important chromophores: 1) The π-conjugated PPE system, and 2) the d^6 transition metal bpy-diyl unit. Each chromophore introduces characteristic excited states into the composite metal-organic molecular systems. Specifically, $^1\pi,\pi^*$ and $^3\pi,\pi^*$ states are expected for the PPE chromophore, while ^1MLCT and ^3MLCT states based on charge transfer from the metal to the bpy-diyl unit are expected for the metallated oligomers. Figure 2-34 shows a general state diagram for **Ru-3**, where the energies of the various are defined as accurately as possible. The $^3\pi,\pi^*$ lies in 1.90 eV which is approximated from

the triplet quenching experiments. Based on the absorption spectra, we estimated that $^1\pi,\pi^*$ state lies in the 2.71 eV. For **Ru-3** complex the emission likely originated from the ^{3}MLCT state, so based on the wavelength of the emission at room temperature (≈ 691 nm) we estimated that this state lies at ≈ 1.80 eV. It is somewhat more problematic to pinpoint the energies of the ^{1}MLCT state, due to the fact that the MLCT absorptions are obscured by the π,π^* bands. Based on the absorption spectra of the parent complex, $Ru(bpy)_3^{2+}$ ($\lambda_{max} \approx 450$ nm), we estimate that the ^{1}MLCT states lies at approximately 2.71 eV.

Figure2-34: **Ru-3** complex Jablonski diagram.

The energy level diagram in Figure 2-34 provides considerable insight into the rather complex photophysics observed for the **(L)Ru^{II}(bpy)$_2$** complexes. First, since the oligomers' absorption spectra are dominated by allowed π,π^* transitions, it is clear that photoexcitation initially affords $^1\pi,\pi^*$ states localized on the PPE backbone. However, given that fluorescence is not observed, relaxation from the $^1\pi,\pi^*$ manifold into lower energy states must occur very rapidly. The important feature which is common to the **(L)Ru^{II}(bpy)$_2$** complexes is that the ^{3}MLCT and $^3\pi,\pi^*$ are very close in energy. Due to this close energetic proximity, we conjecture that the ^{3}MLCT and $^3\pi,\pi^*$ manifolds are in equilibrium. Thus, for **(L)Ru^{II}(bpy)$_2$** complexes MLCT photoluminescence is observed, but the transient absorption is dominated by the $^3\pi,\pi^*$ state. The transient absorption spectra are dominated by the latter state because the optical transitions localized on the PPE oligomer have considerably stronger oscillator strength.

<u>Experimental</u>

<u>Photophysical Measurements</u>

All sample solutions studied are in THF, 2-methyltetrahydrofuran (2-MTHF), acetonitrile (CH$_3$CN) or dichloromethane (CH$_2$Cl$_2$). All solvents were distilled according to typical laboratory practices. All photophysical studies were conducted in 1 cm square quartz cuvettes unless otherwise noted. All room temperature studies were conducted on argon bubble-degassed solutions, and all low temperature studies were conducted on solvent glasses degassed by four freeze-pump-thaw cycles (ca. 10^{-4} Torr) unless otherwise noted. For the emission measurements, sample concentrations were adjusted to produce "optically dilute" solutions (i.e., A < 0.20 at all wavelengths; typical final

concentration is ca. 1.5 x 10^{-6} M). Transient absorption measurements were routinely performed on solutions with higher concentrations (i.e., A ≈ 0.8 – 1.0, ca. 7.5 x 10^{-6} M).

UV-Visible Spectra

Steady state absorption spectra were recorded on either an HP 8452A diode-array or Varian Cary 100 dual-beam spectrophotometer.

Steady-state Emission Spectra

Corrected steady state emission, excitation and polarization spectroscopic measurements were conducted on a SPEX F-112 spectrophotometer. Emission correction factors were generated by using a 1000 W tungsten primary standard lamp. Variable temperature studies were conducted in 1 cm diameter glass tubes contained in an Oxford Instruments cryostat interfaced to an Omega CYC3200 automatic temperature controller.

Emission Lifetimes

Time-resolved fluorescence decays were measured with time-correlated single photon counting (FLI, Photochemical Research Associates; Excitation filter Schott UG-11/H$_2$ spark (350 nm maximum); or 405 nm IBH NanoLED-07 laser diode; Emission filter: 650 nm interference filter). Lifetimes were determined from the observed decays with DECAN fluorescence lifetime deconvolution software.[99]

Transient Absorption Spectroscopy

Transient absorption spectra were obtained on previously described instrumentation,[100] with the third harmonic of a Nd:YAG laser (Spectra Physics GCR-14, 355 nm, 10 ns fwhm, 5 mJ pulse^{-1}) as the excitation source. The sample was contained in a recirculating flow cell that was degassed with argon. Global analysis of the

multiwavelength transient absorption data was effected using the SPECFIT factor analysis software.[101]

Emission Quantum Yield

Emission quantum yields were determined at room temperature in CH_3CN using samples of known optical density, compared to a standard sample of $[Ru(bpy)_3]Cl_2$ in H_2O for which $\phi_{em} = 0.055$.[102] Quantum yield values were calculated by using equation 2-10.

$$\phi_u = \phi_s(n_{D,u}/n_{D,s})^2 (OD_s/OD_u)(A_u/A_s) \qquad 2\text{-}10$$

In equation 2-10, the emission efficiency (ϕ_s), optical density (OD_s), index of refraction ($n_{D,s}$), and integrated emission intensity (A_s) of a known standard (s) are related to the same quantities of a complex of unknown efficiency (u). At low temperatures, ϕ_{em} values were calculated by reference against values at 298 K (ϕ_{298}) by using simplified equation 2-11,[96]

$$\phi_{LT} = \phi_{298}\left(\frac{A_{LT}}{A_{298}}\right) \qquad 2\text{-}11$$

where ϕ_{LT} is the emission quantum yield at low temperature.

Quenching Experiments

Samples for quenching measurements in CH_3CN contained $(L)Ru^{II}(bpy)_2$ with the appropriate concentration of added quencher. In a typical experiment, solutions containing six different concentrations of quencher were placed in quartz cells closed by rubber serum caps. The solutions were bubble degassed with argon for 15 minutes. Stern-Volmer luminescence quenching experiments were carried out by monitoring the

emission lifetime or emission intensity of the complexes as a function of the concentration of **PQ^{2+}** and **DMA**.

<u>Electrochemical Measurements</u>

All electrochemical measurements were conducted on CH_3CN or dichloromethane solutions with 0.1 M tetrabutylammonium hexafluorophosphate (TBAH, Aldrich) as the supporting electrolyte. Cyclic voltammetry measurements were performed on nitrogen bubble-degassed solutions with a BAS CV-27 Voltammograph and MacLab Echem software or a BAS CV-50W Voltammetric Analyzer and accompanying software. Platinum disk and glassy carbon working electrodes, platinum wire auxiliary electrode, and silver wire quasi-reference electrode were used, and potentials were corrected to values versus SCE via an internal ferrocene standard. A scan rate of 100 mV sec^{-1} was employed in all measurements.

<u>General Synthetic</u>

Diisopropylamine was distilled from KOH and tetrahydrofuran was distilled from sodium benzophenone ketyl and stored under nitrogen. Copper(I) iodide, PdCl$_2$, Pd(PPh$_3$)$_4$, 4,4-diiodobiphenyl, 4-bromobiphenyl and RuCl$_3$·3H$_2$O were purchased from Aldrich Chemical Co. and used without further purification. Trimethylsilylacetylene and 2-methyl-3-butyn-2-ol were obtained from GFS chemicals and used without further purification. All cross-coupling reactions using Pd catalyst were carried out under standard Schlenk and vacuum line techniques. ^{1}H and ^{13}C NMR was recorded on Gemini-300 and VXR-300 NMR spectrometers. High-resolution mass spectrometry was performed by the University of Florida analytical service. The matrix used for MALDI analysis is α-cyanohydroxycinnamic acid in THF solvent.

Synthesis

Pd(PPh₃)₂Cl₂

Commercial PdCl₂ (1.02 g, 5.78 mmol), triphenylphosphine (3.05 g, 1.16 mmol) were heated at reflux in reagent grade dimethylformamide (10 mL) for 8 hr. During the course of reaction, the solution color changed to yellow. After the reaction mixture was cooled to room temperature, and the resultant solution was cooled at 0°C overnight. Filtering yielded a fine yellow solid. The solid was washed three times with 10 mL portions of Et₂O, and then it was dried by suction. Yield: 3.2 g (78%).

cis-Ru(bpy)₂Cl₂

Commercial RuCl₃·3H₂O (62.0 mg, 0.24 mmol), 2,2'-bipyridine (75.0 mg, 0.48 mmol), and LiCl (20 mg, 0.43 mmol) were heated at reflux in reagent grade dimethylformamide (4 mL) for 8 hr. The reaction was stirred magnetically throughout this period. After the reaction mixture was cooled to room temperature, and the resulting solution was cooled at 0°C overnight. Filtering yielded a red to red-violet solution and a dark green-black microcrystalline product. The solid was washed three times with 10 mL portions of water followed by three 10 mL portions of Et₂O, and then it was dried by suction. Yield: 81 mg (70%). ¹H-NMR (300 MHz, CD₃OD) δ 7.08 (t, 2H), 7.64 (d, 2H), 7.74 (t, 4H), 8.04 (t, 2H), 8.40 (d, 2H), 8.56 (d, 2H), 10.04 (d, 2H).

Commercial RuCl₃·3H₂O (500 mg, 1.91 mmol) was dissolved in a mixture of EtOH (15 mL) and H₂O (10 mL) which was then degassed with argon for 0.5 hr. The solution was refluxed under nitrogen for 3-4 hr. During this period the solution color changes from brown to blue color (Ruthenium blue). To the hot blue solution was added 2,2'-bipyridine (595 mg, 3.82 mmol) in EtOH (6 mL), along with concentrated HCl (2

mL). The mixture was refluxed for 1.5 hr, during which time the solution color changed from blue to dark brown. The hot solution was filtered through a bed of celite to remove some insoluble materials. Then the volume of the solution was reduced to 10 mL by using a rotary evaporator and the resultant solution cooled at 0°C overnight. The deep red-brown solid deposited were collected by filtration, washed with acetone and then Et_2O. Yield: 980 mg (84%). The ^{1}H-NMR data is the same as above.

Protonated 2,2'-bipyridine (5)

Acetyl bromide (35.5 mL, 0.480 mol) was slowly added dropwise to 15.0 g of 2,2-bipyridine (0.096 mol) in 400 mL of methanol over a period of 1 hr. A yellow precipitate formed late in the reaction period. The solution was allowed to stir for one additional hour, and then it was then carefully filtered and washed with acetone, yielding 29.3 g of protonated 2,2'-bipyridine (5) (96%). ^{1}H-NMR (300 MHz, D_2O) δ 3.35 (s, 2H), 7.90 (m, 2H), 8.45 (s, 4H), 8.85 (d, 2H).

5,5'-Dibromo-2,2'-bipyridine (6)[72]

Protonated bipyridine (5) (2.3 g, 0.0073 mol), and Br_2 (5.0 g, 0.0313 mol) were added to a glass reinforced tube and the tube was placed under vacuum for three consecutive free-pump-thaw cycles. The tube was then sealed and heated at 180°C for four days. The tube was allowed to cool to room temperature and carefully cracked behind a face shield with a hammer. The resulting orange solid was allowed to sit in the fume hood overnight, which allowed the excess bromine to evaporate. The resulting solid was dissolved in 125 mL of a 1 M NaOH solution to deprotonate the brominated bipyridine. The resulting aqueous solution was then extracted with 200 mL of chloroform three times, and the chloroform layers were combined. The solvents were dried over

$MgSO_4$ and then removed under vacuum, yielding a light tan solid. To the resulting tan solid was added 30 mL of acetone, and the solid that does not dissolve was collected by vacuum filtration. The white solid was then rinsed with 10 mL of acetone one more time and allowed to dry, yielding pure 5,5'-dibromo-2,2'-bipyridine. The acetone rinse solutions were combined and the solvent removed under vacuum, these solids are a mixture of unreacted 2,2'-bipyridine, 5,5'-dibromo-2,2'-bipyridine and 5-bromo-2,2'-bipyridine. Overall yield is 1.10 g of 5,5'-dibromo-2,2'-bipyridine (48%). ^{1}H-NMR (300 MHz, $CDCl_3$) δ 7.95 (dd, 2H), 8.28 (d, 2H), 8.70 (s, 2H). ^{13}C-NMR (75.4 MHz, $CDCl_3$) δ 121.2, 122.0, 139.3, 150.0, 153.4.

5-Bromo-2,2'-bipyridine is isolated by chromatograpy on silica gel. The remaining solids (2,2'-bipyridine and 5-bromo-2,2'-bipyridine) were dissolved in a minimum amount of chloroform and loaded onto a column. The column was first eluted with 200 mL of hexane. The solvent polarity was then increased by adding Et_2O (20%) and the first product off the column was 2,2'-bipyridine. The band immediately following the 2,2'-bipyridine is the mono-bromo product, 5-bromo-2,2'-bipyridine, 0.3 g (25 %). 1H-NMR (300 MHz, $CDCl_3$) δ 7.30 (dd, 1H), 7.79 (td, 1H), 7.92 (dd, 2H), 8.32 (d, 1H), 8.36 (d, 1H), 8.62 (d, 1H), 8.70 (d, 1H). ^{13}C-NMR (75.4 MHz, $CDCl_3$) δ 121.7, 122.1, 123.2, 125.0, 137.9, 140.4, 150.2, 151.1, 156.1.

<u>5,5'-Trimethylsilylethynyl-2,2'-bipyridine (7)</u>[72]

5,5'-Dibromo-2,2'-bipyridine (0.4 g, 1.27 mmol), trimethylsilylacetylene (0.72 mL, 5 mmol), tetrahydrofuran (5 mL) and diisopropylamine (5 mL) were combined in a Schlenk flask which was then degassed for 0.5 hr. $Pd(PPh_3)_2Cl_2$ (54 mg, 0.07 mmol) and CuI (29 mg, 0.15 mmol) were added to the Schlenk flask and the resulting solution was

heated at 70°C for 20 hr, with heavy ammonium iodide salts forming immediately. The solution was allowed to cool and the solvent was removed under vacuum. The crude tan solid was purified by chromatography on silica gel with 100/1 hexane/ether solution affording 7 as a pale yellow solid, yield 200 mg (75%). ^{1}H-NMR (300 MHz, CDCl$_3$) δ 0.28 (s, 18H), 7.85 (dd, 2H), 8.35 (d, 2H), 8.71 (d, 2H). ^{13}C-NMR (75.4 MHz, CDCl$_3$) δ -0.2, 99.3, 101.8, 120.2, 120.4, 139.6, 151.9, 154.1.

5,5'-Diethynyl-2,2'-bipyridine (8)

5,5'-Trimethylsilylethynyl-2,2'-bipyridine (7) (0.2 g, 0.57 mmol) was dissolved in 10 mL of THF and then 5 mL of MeOH was added. To this solution was added 4 mL of 1 M KOH solution. The resulting solution was stirred at room temperature for 4 hr. The THF and MeOH solvent were removed under vacuum. The reaction mixture was diluted with 20 mL of water and extracted with 30 mL CHCl$_3$. The organic layer was separated, dried and the solvent evaporated leaving a brown pure solid 110 mg (95%) yield. ^{1}H-NMR (300 MHz, CDCl$_3$) δ 3.30 (s, 2H), 7.89 (dd, 2H), 8.38 (d, 2H), 8.76 (d, 2H). ^{13}C-NMR (75.4 MHz, CDCl$_3$) δ 99.5, 102.3, 119.5, 120.6, 140.0, 152.3, 154.5.

5,5'-Bis((2,5-dimethoxyphenyl)ethynyl]-2,2'-bipyridine (1)

1-Iodo-2,5-dimethoxybenzene (233 mg, 0.88 mmol), 5,5'-diethynyl-2,2'-bipyridine (8) (90 mg, 0.44 mmol), THF (10 mL) and diisopropylamine (8 mL) were combined in a Schlenk flask which was then degassed with argon for 0.5 hr. Pd(PPh$_3$)$_2$Cl$_2$ (15 mg, 0.022 mmol) and CuI (8.5 mg, 0.044 mmol) were added to the Schlenk flask and the resulting solution was heated at 70°C for 20 hr. The solution was allowed to cool and after evaporation of the solvent the product was purified by chromatography on silica gel with 100:10 ether/hexane affording 1 as a pale yellow solid, yield 157 mg (75%). ^{1}H-

NMR (300 MHz, CDCl₃) δ 3.80 (s, 6H), 3.90 (s, 6H), 6.85 (m, 4H), 7.05 (d, 2H), 7.96 (dd, 2H), 8.42 (d, 2H), 8.83 (s, 2H). ^{13}C-NMR (75.4 MHz, CDCl₃) δ 55.8, 56.4, 90.1, 90.3, 111.9, 112.1, 116.5, 117.9, 120.5, 120.7, 139.3, 151.6, 153.2, 153.9, 154.5. APCI MS calculated for $C_{30}H_{25}N_2O_4$ [M+H$^+$]: 477; found 477.

(5,5'-Bis((2,5-dimethoxyphenyl)ethynyl]-2,2'-bipyridine)Ru(bpy)₂ (Ru-1)

cis-Ru(bpy)₂Cl₂ (18 mg, 0.037 mmol) was dissolved in 20 mL of CH₃OH and the solution was refluxed under N₂ for 2 hr. The color of solution changes from green to wine-red. Oligomer 1 (18 mg, 0.037 mmol) which was dissolved in 5 mL of THF was added to the cis-Ru(bpy)₂Cl₂ solution and then refluxed for another 20 hr. During the course of the reaction the blue fluorescence characteristic of 1 disappeared. The solution was cooled to room temperature. Upon addition of 2 mL saturated aqueous NH₄PF₆ solution, the PF₆⁻ salt of the complex was precipitated. The product was collected by centrifugation. The complex was purified by repeated rinsing with H₂O and diethyl ether. The pure metallated oligomer was obtained as an orange solid, yield 21 mg (48%). ^{1}H-NMR (300 MHz, CDCl₃) δ 3.74 (s, 6H), 3.78 (s, 6H), 6.94 (d, 2H), 6.95 (d, 2H), 6.99 (d, 2H), 7.44 (br t, 4H), 7.70 (d, 2H), 7.75 (s, 2H), 7.82 (d, 2H), 8.50 (br t, 6H), 8.10 (br m, 6H). ^{13}C-NMR (75.4 MHz, CD₃CN) δ 56.3, 56.8, 88.6, 94.5, 114.48, 113.5, 118.9, 125.2, 125.4, 128.6, 138.9, 140.2, 152.73, 153.05, 154.04, 154.17, 155.72, 156.15, 157.77, 157.92. FAB-MS calculated for $C_{50}H_{40}RuO_4N_6$ (M-2PF₆) 890.2148, found 890.2124.

1,4- Diheptyloxybenzene (8)

1,4-Hydroquinone (8.0 g, 0.07 mol) and 1-bromoheptane (26.0 g, 0.146 mol) were placed in a 250 mL round bottom flask. To the solids was added 125 mL of DMF and NaOH (12.0 g, 0.3 mol) and the solution was heated at reflux for 2 days. The resulting

solution was cooled and poured into 150 mL of concentrated HCl with 400 g of ice. Ether extraction was conducted. The ether layer was washed with H_2O 5 times, dried over $MgSO_4$ and discolored with charcoal and the solvents were removed under reduced pressure. The resulting light brown solid was recrystalized from cold EtOH. Yield: 14.3 g (67%). ^{1}H-NMR (300 MHz, $CDCl_3$) δ 0.82 (br t, 6H), 1.3 (br s, 12H), 1.5 (br m, 4H), 1.75 (br m, 4H), 3.90 (t, 4H), 6.9 (s, 4H).

1,4-Diiodo-2,5-diheptyloxybenzene (9)

In a 500 mL round bottom flask was added 100 mL of acetic acid, 1 mL of concentrated sulfuric acid and 10 mL of water. To this solution was added 1,4-diheptyloxybenzene (5.0 g, 0.016 mol), I_2 (20.5 g, 0.08 mol) and KIO_3 (17.0 g, 0.04 mol) and the resulting solution was stirred at reflux for 24 hr. The solution was allowed to cool and 150 mL of 20% aqueous $Na_2S_2O_4$ was added to neutralize the iodine. At this time, the red color of iodine totally disappeared. A 100 mL solution of 2 M NaOH was added to quench the excess acid and the 300 mL of $CHCl_3$ was added to extract the product. The resulting chloroform layer was dried over $MgSO_4$ and the solvent removed under reduced pressure. The resulting light brown solid was recrystallized from hot MeOH. Yield: 4.9 g (55%). ^{1}H-NMR (300 MHz, $CDCl_3$) δ 0.82 (br t, 6H), 1.3 (br s, 12H), 1.5 (br m, 4H), 1.75 (br m, 4H), 3.90 (t, 4H), 7.14 (s, 2H).

1,4-diiodo-2,5-dimethoxybenzene (10)

In a 1 L round bottom flask was added 300 mL of acetic acid, 3 mL of concentrated sulfuric acid and 30 mL of water. To this solution was added 1,4-dimethoxybenzene (5.0 g, 0.036 mol), I_2 (41.4 g, 0.163 mol) and KIO_3 (15.5 g, 0.073 mol) and the resulting solution was stirred at reflux for 24 hr. The solution was allowed

to cool and 300 mL of a 20% aqueous $Na_2S_2O_4$ was added to neutralize the iodine. At this time a yellow/tan solid precipitated out of solution. This solid was collected by vacuum filtration and dissolved in 200 mL of chloroform. A 200 mL solution of 2 M NaOH was added to quench the excess acid and the resulting chloroform layer was dried over $MgSO_4$ and the solvent removed under reduced pressure. The resulting white solid was allowed to dry, yielding 11.8 g of 2,5-diiodo-1,4-dimethoxybenzene (84%). ^{1}H-NMR (300 MHz, $CDCl_3$) δ 3.88 (s, 6H), 7.18 (s, 2H). ^{13}C-NMR (75.4 MHz, $CDCl_3$) δ 57.0, 85.3, 121.4, 153.1.

1,4-Diiodo-2,5-hydroquinone (11)

2,5-Diiodo-1,4-dimethoxybenzene (10) (10.0 g, 0.025 mol) was dissolved in 150 mL of dichloromethane and cooled to –80°C in an acetone/dry ice bath. To this stirred solution was slowly added neat BBr_3 (10 mL, 0.10 mol) and after the addition the solution was allowed to warm up to room temperature. The solution was stirred for 12 hr at which time 100 mL of water was added to quench the excess BBr_3, a precipitate formed immediately. To the resulting precipitate and aqueous/dichloromethane solution was added 200 mL of a 2M NaOH solution, at which time the aqueous layer turned dark black. The aqueous layer was poured off and cooled in an ice bath. A concentrated solution of HCl was then added dropwise (100 mL), and once the NaOH was neutralized, a brown precipitate began to form. Once the solution was significantly acidic, pH ~ 1, the brown solid was filtered and allowed to dry under vacuum overnight, yielding 8.56 g of 1,4-diiodo-2,5-hydroquinone (93%). ^{1}H-NMR (300 MHz, acetone-d[6]) δ 7.27 (s, 2H), 8.98 (s, 2H). ^{13}C-NMR (75.4 MHz, acetone-d[6]) δ 84.4, 124.6, 151.5.

1,4-Diiodo-2,5-dioctadecyloxybenzene (12)

1,4-Diiodo-2,5-hydroquinone (11) (5.0 g, 0.0138 mol) and 1-bromooctadecane (10.6 g, 0.0317 mol) were placed in a 100 mL round bottom flask. To the solids was added 60 mL of DMF and NaOH (10.0 g, 0.250 mol) and the solution was heated at reflux for 2 hr. The resulting solution was cooled and the solid filtered. The filtered solid was then rinsed with excess water and dissolved in 100 mL of chloroform and again extracted with 200 mL of water three times. The resulting chloroform layer was dried over MgSO$_4$ and the solvents removed under reduced pressure. The crude brown solid was recrystallized from EtOH/chloroform twice to yield a white solid, 10.4 g (87%). ^{1}H-NMR (300 MHz, CDCl$_3$) δ 0.88 (t, 6H), 1.23 (br s, 56H), 1.58 (m, 4H), 1.88 (m, 4H), 3.96 (t, 4H), 7.16 (s, 2H). ^{13}C-NMR (75.4 MHz, CDCl$_3$) δ 25.8 (multiple), 29.4, 31.7, 70.1, 86.0, 122.5, 152.6.

Compound 13[103]

1,4-Diiodo-2,5-dioctadecyloxybenzene (0.8 g, 1.0 mmol), tetrahydrofuran (25 mL) and diisopropylamine (25 mL) were combined in a Schlenk flask which was then degassed with argon for 0.5 hr. The 2-methyl-3-butyn-2-ol (0.05 mL, 1 mmol), Pd(PPh$_3$)$_2$Cl$_2$ (36 mg, 0.05 mmol) and CuI (20 mg, 0.1 mmol) were added to the Schlenk flask which caused the solution to change from a pale white to a dark black color. The resulting solution was heated at 70°C for 20 hr. The reaction mixture was allowed to cool to room temperature and after evaporation of the solvent the product was purified by chromatography on silica gel with 6:1 hexane/ether affording 13 as a yellow solid, yield 315 mg (44%). The first product that elutes off of the column (R$_f$ = 1) is unreacted 1,4-diiodo-2,5-dioctadecyloxybenzene (12), followed by compound 13 (R$_f$ = 0.4) and finally

the bis-substituted alcohol, (R_f = 0.05). ^{1}H-NMR (300 MHz, CDCl$_3$) δ 0.88 (t, 6H), 1.26 (br s, 56H), 1.49 (br m, 4H), 1.62 (s, 6H), 1.80 (br m, 4H), 2.18 (s, 1H), 3.93 (t, 4H), 6.80 (s, 1H), 7.27 (s, 1H). ^{13}C-NMR (75.4 MHz, CDCl$_3$) δ 14.1, 22.7, 26.0, 29.4, 29.7, 31.4, 31.9, 65.7, 69.7, 70.0, 78.2, 87.4, 98.6, 112.9, 116.1, 123.7, 151.7, 154.3. EI-MS calculated for C$_{47}$H$_{83}$IO$_3$: 822; found 822.

Protected oligomer 14

5,5'-Diethynyl-2,2'-bipyridine (0.138 g, 0.678 mmol), **13b** (1.15 g, 1.39 mmol), tetrahydrofuran (60 mL) and diisopropylamine (40 mL) were combined in a Schlenk flask which was then degassed with argon for 0.5 hr. Pd(PPh$_3$)$_2$Cl$_2$ (0.029 g, 0.04 mmol) and CuI (0.016 g, 0.082 mmol) were added to the Schlenk flask and the resulting solution was heated at 70°C for 20 hr. The solution was allowed to cool and after evaporation of the solvent the product was purified by chromatography on silica gel with 30:70 hexane/ether affording **14** as a yellow solid, yield 832 mg (77%). ^{1}H-NMR (300 MHz, CDCl$_3$) δ 0.88 (t, 12H), 1.26 (br s, 112H), 1.58 (br m, 8H), 1.62(s, 12H), 1.88 (br m, 8H), 2.18 (br s, 2H), 4.0 (m, 8H), 6.92 (s, 4H), 7.92 (dd, 2H), 8.43 (dd, 2H), 8.80 (s, 2H). ^{13}C-NMR (75.4 MHz, CDCl$_3$) δ 14.1, 22.6, 26.0, 29.3, 29.7, 31.4, 31.9, 65.7, 69.4, 69.5, 78.4, 90.4, 91.5, 99.5, 113.0, 114.0, 116.7, 116.9, 120.6, 139.2, 151.6, 153.6, 153.7, 153.9. APCI MS calculated for C$_{108}$H$_{173}$N$_2$O$_6$ [M+H$^+$]: 1595.5; found 1595.5.

Oligomer 15

Protected oligomer **14** (700 mg, 0.438 mmol) was dissolved in 10 mL of toluene and the solution was thoroughly degassed with argon for 1 hr. Crushed potassium hydroxide (0.196 g, 3.50 mmol) was added and the Schlenk tube that contained the solution was immersed for 5 minutes into an oil bath that had been pre-heated to 110°C.

The reaction mixture was cooled and then extracted with $CHCl_3$. Evaporation the solvent afforded compound **15**, yield 589 mg (91%). ^{1}H-NMR (300 MHz, $CDCl_3$) δ 0.88 (t, 12H), 1.23 (br s, 112H), 1.58 (br m, 8H), 1.85 (br m, 8H), 3.36 (s, 2H), 4.0 (br t, 8H), 6.99 (s, 2H), 7.01 (s, 2H), 7.92 (dd, 2H), 8.43 (dd, 2H), 8.80 (s, 2H).

Oligomer **2-C$_{18}$**[103]

4-bromobiphenyl (0.189 g, 0.812 mmol), **15** (0.3 g, 0.203 mmol), tetrahydrofuran (20 mL) and diisopropylamine (20 mL) were combined in a Schlenk flask which was then degassed with argon for 0.5 hr. $Pd(PPh_3)_2Cl_2$ (0.008 g, 0.012 mmol) and CuI (0.005 g, 0.024 mmol) were added to the Schlenk flask and the resulting solution was heated at 70°C for 20 h. The solution was allowed to cool and after evaporation of the solvent the product was purified by chromatography on silica gel with 30:70 hexane/$CHCl_3$ affording **2-C$_{18}$** as a bright yellow solid, yield 246 mg (68%). ^{1}H-NMR (300 MHz, $CDCl_3$) δ 0.88 (t, 12H), 1.26 (br s, 112H), 1.58 (br m, 8H), 1.88 (br m, 8H), 4.04 (m, 8H), 7.05(s, 4H), 7.37(d, 2H), 7.46 (d, 4H), 7.60 (m, 12H), 7.92 (dd, 2H), 8.43 (dd, 2H), 8.80 (s, 2H). ^{13}C-NMR (75.4 MHz, $CDCl_3$) δ 14.1, 22.6, 26.0, 26.1, 29.3, 29.7, 31.9, 69.5, 69.7, 86.6, 90.6, 91.7, 95.2, 113.0, 114.8, 116.7, 116.9, 120.6, 120.8, 121.7, 122.2, 126.9, 127.6, 128.8, 132.0, 139.1, 140.3, 141.0, 151.7, 153.6, 153.8, 153.9. APCI MS calculated for $C_{126}H_{177}N_2O_4$ [M+H$^+$]: 1783.6; found 1783.6.

Metal-Organic Oligomer **Ru-2-C18**

$Ag(CF_3SO_3)$ (24 mg, 0.09 mmol) was added to a solution of *cis*-**Ru(bpy)$_2$Cl$_2$** (12 mg, 0.024 mmol) in 10 mL of acetone. The mixture was refluxed for 2 hr. The AgCl precipitate that formed was filtered off and the filtrate was allowed to react under reflux with 1 equivalent of the oligomer **2-C$_{18}$** in 5 mL of 2-methoxyethanol for 20 hr. During

the course of reaction the blue-green fluorescence characteristic of 2-C18 disappeared. After cooling down to room temperature, the solution was dropped into 5 mL of saturated aqueous NH_4PF_6 solution. The orange solid that precipitated was filtered and washed with H_2O and diethyl ether and then dried in vacuum to yield 21 mg of **Ru-2-C18** (40%). ^{1}H-NMR (300 MHz, CDCl$_3$) δ 0.92 (br t, 12H), 1.30 (br s, 112H), 1.58 (br m, 8H), 1.85 (br m, 8H), 4.04 (br t, 8H), 6.99 (s, 4H), 7.37 (br t, 2H), 7.44 (br t, 4H), 7.52 (t, 2H), 7.60 (br m, 14H), 7.70 (s, 2H), 7.78 (br m, 4H), 8.06 (br m, 6H), 8.52 (br m, 6H). ^{13}C-NMR (75.4 MHz, CDCl$_3$) δ 14.1, 22.7, 25.8, 26.1, 29.3, 29.7, 31.9, 69.4, 69.7, 86.3, 88.3, 95.5, 96.0, 111.1, 116.2, 116.4, 117.0, 122.0, 124.1, 124.5, 124.6, 125.0, 127.0, 127.7, 128.4, 128.9, 132.0, 138.0, 138.4, 140.2, 141.2, 151.4, 151.6, 152.1, 153.6, 153.8, 154.7, 156.3, 156.5. MALDI-MS calculated for $C_{102}H_{104}RuPON_6F_6$ (M-PF$_6$): 2340.43, found 2340.42.

Oligomer 16

5,5'-Diethynyl-2,2'-bipyridine (**8**, 100 mg, 0.5 mmol), 1,4-diiodo-2,5-diheptoxybenzene (1.116 g, 2 mmol), tetrahydrofuran (5 mL) and diisopropylamine (10 mL) were combined in a Schlenk flask which was then degassed with argon for 0.5 hr. Pd(PPh$_3$)$_2$Cl$_2$ (20 mg, 0.028 mmol) and CuI (11 mg, 0.057 mmol) were added to the Schlenk flask and the resulting solution was heated at 70°C for 20 hr. The solution was allowed to cool and the solvents removed under vacuum. The solid was dry packed on to a silica gel column in hexane. The resulting column was flushed with hexane to remove excess 1,4-diiodo-2,5-diheptoxybenzene. When all the excess starting compound was separated from column, the solvent polarity was increased to 20:1 hexane/ether solution and a yellow band was collected, yielding 170 mg of compound **16** (35%). ^{1}H-NMR (300 MHz, CDCl$_3$) δ 0.87 (br t, 12H), 1.30 (br s, 24H), 1.58 (br m, 8H), 1.85 (br m, 8H), 4.04

(br t, 8H), 6.92 (s, 2H), 7.31 (s, 2H), 7.91 (d, 2H), 8.48 (d, 2H), 8.82 (s, 2H); ^{13}C-NMR (75.4 MHz, CDCl$_3$) δ 14.9, 23.4, 26.8, 30.0, 32.5, 70.6, 70.9, 80.1, 89.5, 105.9, 115.8, 116.5, 121.8, 124.5, 129.8, 142.0, 145.5, 151.9, 152.7, 155.2. FAB-MS calculated for C$_{54}$H$_{70}$I$_2$N$_2$O$_4$: 1064.95, found 1065.0.

Compound Ru-2-C7-I

Ag(CF$_3$SO$_3$) (53 mg, 0.21 mmol) was added to a solution of *cis*-Ru(bpy)$_2$Cl$_2$ (46 mg, 0.094 mmol) in 10 mL acetone. The mixture was refluxed for 2 hr. The AgCl precitpitate that formed was filter out and the filtrate was allowed to react under reflux with 16 (100 mg, 0.094 mmol) in 5 mL of 2-methoxyethanol for another 20 hrs. During the course of reaction the blue-green fluorescence characteristic of compound 16 disappeared. After cooling to room temperature, the solution was dropped into 5 mL of saturated aqueous NH$_4$PF$_6$ solution. A dark red solid was filtered out and washed with H$_2$O and diethyl ether and dried in vacuum to yield 65 mg of Ru-2-C7-I (79%). ^{1}H-NMR (300 MHz, CDCl$_3$) δ 0.85 (br t, 12H), 1.25 (br s, 24H), 1.45 (br m, 8H), 1.75 (br m, 8H), 3.91 (br t, 8H), 6.88 (s, 2H), 7.28 (s, 2H), 7.51 (br q, 4H), 7.73 (br m, 6H), 8.01 (br m, 6H), 8.43 (br m, 6H). ^{13}C-NMR (75.4 MHz, CDCl$_3$) δ 14.1, 22.6, 25.7, 26.0, 29.1, 29.7, 31.7, 69.6, 70.1, 80.1, 90.3, 95.0, 111.0, 115.9, 123.5, 124.2, 124.5, 124.9, 128.3, 138.1, 138.4, 140.1, 151.2, 151.4, 151.9, 152.1, 154.3, 154.7, 156.3, 156.5. MALDI-MS calculated for C$_{74}$H$_{86}$N$_6$O$_4$I$_2$Ru (M-2PF$_6$): 1478.48, found 1478.25.

Compound 17

4-Bromobiphenyl (1.92 g, 8.24 mmol), tetrahydrofuran (25 mL) and diisopropylamine (25 mL) were combined in a Schlenk flask which was then degassed with argon for 0.5 hr. Then 2-methyl-3-butyn-2-ol (0.62 mL, 9 mmol), Pd(PPh$_3$)$_2$Cl$_2$ (300

mg, 0.4 mmol) and CuI (163 mg, 0.8 mmol) were added to the Schlenk flask which caused the solution to change from a pale white to a dark black color. The resulting solution was heated at 70°C for 20 hrs. The reaction mixture was allowed to cool and after evaporation of the solvent the product was purified by chromatography on silica gel with hexane/Et$_2$O (2:1) affording **17** as a pale yellow color solid, yield 500 mg (40 %).
^{1}H-NMR (300 MHz, CDCl$_3$) δ 2.18 (s, 2H), 4.52(s, 2H), 7.5 (m, 9H).

Compound **18**

Protected oligomer **17** (500 mg, 2.4 mmol) was dissolved in 10 mL of toluene and the solution was thoroughly degassed with argon for 1 hr. Crushed potassium hydroxide (1.3 g, 24 mmol) was added and the Schlenk tube that contained the solution was immersed for 5 minutes into an oil bath that had been pre-heated to 110°C. The reaction mixture was cooled and then extracted with CHCl$_3$. Evaporation the solvent afforded compound **18**, yield 350 mg (82%). ^{1}H-NMR (300 MHz, CDCl$_3$) δ 3.18 (s, 1H), 7.36 (t, 1H), 7.42 (t, 2H), 7.58 (br s, 6H).

Metal-Organic Oligomer **Ru-2-C7**

Compound **18** (22 mg, 0.013 mmol), **Ru-2-C7-I** (7 mg, 0.03 mmol), tetrahydrofuran (2 mL) and diisopropylamine (2 mL) were combined in a Schlenk flask which was then degassed with argon for 0.5 hr. Pd(PPh$_3$)$_4$ (1.2 mg, 0.001 mmol) and CuI (0.2 mg, 0.002 mmol) were added to the Schlenk flask. The resulting solution was heated at 70°C for 20 hr. The solution was allowed to cool and the solvent removed under vacuum. The crude product was dissolved in 50 mL of chloroform. The combined organic phase was washed with NH$_4$·OH (50%), H$_2$O and dried over MgSO$_4$. Most of the solvent was evaporated under vacuum and the concentrated solutions poured into ether.

The red precipitate was collected by centrifuge, washed with diethyl ether and dried in vacuum to yield **Ru-2-C7** 17 mg (70%). ^{1}H-NMR (300 MHz, CDCl$_3$) δ 0.92 (br t, 12H), 1.30 (br s, 24 H), 1.58 (br m, 8H), 1.85 (br m, 8H), 4.04 (br t, 8H), 7.0 (s, 4H), 7.38 (br t, 2H), 7.48 (br t, 4H), 7.60 (br m, 16H), 7.73 (s, 2H), 7.82 (t, 4H), 8.02 (br t, 4H), 8.10 (br d, 2H), 8.47 (br t, 4H), 8.57 (br d, 2H). ^{13}C-NMR (75.4 MHz, CDCl$_3$) δ 14.1, 22.6, 25.8, 26.1, 29.1, 29.7, 31.9, 69.4, 69.7, 86.3, 88.7, 95.5, 96.0, 111.1, 116.2, 116.5, 117.1, 121.8, 124.3, 124.7, 124.9, 125.0, 127.0, 127.7, 128.5, 128.9, 132.0, 138.1, 138.5, 140.2, 141.2, 151.4, 151.6, 152.1, 153.6, 153.8, 154.7, 156.3, 156.5. FAB-MS calculated for C$_{102}$H$_{105}$F$_{12}$N$_2$N$_6$O$_4$P$_2$Ru (M+H$^+$) 1869.64, found 1869.65.

Compound 19

4,4'-Diiodobiphenyl (3.19 g, 7.8 mmol), tetrahydrofuran (10 mL) and diisopropylamine (10 mL) were combined in a Schlenk flask which was then degassed with argon for 0.5 hr. Trimethylsilylacetylene (1.1 mL, 7.8 mmol), Pd(PPh$_3$)$_2$Cl$_2$ (250 mg, 0.35 mmol) and CuI (150 mg, 0.78 mmol) were added to the Schlenk flask and the resulting solution was heated at 70°C for 2 hr. Heavy ammonium iodide salt formed immediately. After 2 hr 2-methyl-3-butyn-2-ol (3 mL, 31.2 mmol) was added. The solution turned from light yellow to dark black and heating was continued for an additional 18 hr. The solution was allowed to cool and after evaporation of the solvent the product was purified by chromatography on silica gel with 150:50 CHCl$_3$/hexane affording 19 as a white solid, yield 673 mg (26%). ^{1}H-NMR (300 MHz, CDCl$_3$) δ 0.27 (s, 9H), 1.64 (s, 6H), 2.18 (s, 1H), 7.51 (m, 8H). ^{13}C-NMR (75.4 MHz, CDCl$_3$) δ -0.05, 31.4, 81.8, 94.6, 95.2, 104.8, 121.9, 122.3, 126.6, 126.7, 132.1, 132.4, 139.9, 140.1. EI-MS calculated for C$_{22}$H$_{24}$OSi: 332.51; found 332.17.

Compound 20

Methanol (10 mL), tetrahydrofuran (20 mL) and KOH (600 mg, 10.8 mmol) were added to **19** (1.22 g, 3.67 mmol) and the resulting solution was stirred at room temperature for 4 hr. The methanol and tetrahydrofuran were removed by vacuum. The residue was diluted with 20 mL of water and extracted with 30 mL of $CHCl_3$. The organic layer was separated, dried and the solvent evaporated leaving a yellow solid 845 mg (yield 90%). ^{1}H-NMR (300 MHz, $CDCl_3$) δ 1.64 (s, 6H), 2.18 (s, 1H), 7.54 (m, 8H). ^{13}C-NMR (75.4 MHz, $CDCl_3$) δ 31.4, 65.6, 78.1, 81.8, 83.4, 94.7, 121.3, 122.1, 126.6, 126.7, 132.0, 132.6, 139.8, 140.5. EI-MS calculated for $C_{19}H_{16}O$: 260.33; found 260.30.

Compound 21

1-Iodo-2,5-dimethoxybenzene (155 mg, 0.588 mmol), compound **20** (169 mg, 0.588 mmol), tetrahydrofuran (6 mL) and diisopropylamine (4 mL) were combined in a Schlenk flask which was then degassed with argon for 0.5 hr. $Pd(PPh_3)_2Cl_2$ (22 mg, 0.03 mmol) and CuI (12 mg, 0.06 mmol) were added to the Schlenk flask. The resulting solution was heating at 70°C for an additional 18 hr. The solution was allowed to cool and the solvent removed under vacuum. Chromatography on silica gel with 1:1 hexane/ether afforded **21** as a yellow solid, yield 153 mg (61%). ^{1}H-NMR (300 MHz, $CDCl_3$) δ 1.64 (s, 6H), 2.18 (s, 1H), 3.8 (s, 3H), 3.9 (s, 3H), 6.9 (m, 2H), 7.1 (d, 1H), 7.6 (m, 8H).

Compound 22

Protected oligomer **21** (230 mg, 0.58 mmol) was dissolved in 10 mL of toluene and the solution was thoroughly degassed with argon for 1h. Crushed potassium hydroxide (200 mg, 3.6 mmol) was added and the Schlenk tube that contained the

solution was immersed for 5 minutes into an oil bath that had been pre-heated to 110°C. The reaction mixture was cooled and then extracted with $CHCl_3$ (2 × 100 mL). Evaporation the solvent afforded compound **22**, yield 150 mg (76 %). ^{1}H-NMR (300 MHz, $CDCl_3$) δ 3.19 (s, 1H), 3.81(s, 3H), 3.9 (s, 3H), 6.85 (br d, 2H), 7.5 (s, 1H), 7.61 (m, 8H). ^{13}C-NMR (75.4 MHz, $CDCl_3$) δ 56.1, 56.8, 78.3, 83.7, 87.0, 93.4, 112.1, 113.1, 116.2, 118.3, 127.1, 128.7, 128.9, 132.4, 132.9, 133.3, 140.0, 140.9, 153.5, 154.7. MALDI-MS calculated for $C_{24}H_{18}O_2$: 338.1306; found 338.1284.

Metal-Organic Oligomer **Ru-3**

Compound **22** (14 mg, 0.04 mmol), compound **Ru-2-C7-I** (36 mg, 0.02 mmol), tetrahydrofuran (2 mL) and diisopropylamine (2 mL) were combined in a Schlenk flask which was then degassed with argon for 0.5 hr. Then $Pd(PPh_3)_4$ (1.2mg, 0.001 mmol) and CuI (0.2 mg, 0.002 mmol) were added to the Schlenk flask. The resulting solution was heated at 70°C for 20 hr. The solution was allowed to cool and the solvent removed under vacuum. The crude product was dissolved in 50 mL of $CHCl_3$. The combined organic phase was washed with NH_4· OH (50%) aqueous solution, H_2O and then dried over $MgSO_4$. Most of the solvent was evaporated under vacuum and the concentrated solution was poured into ether. The formed red solid was collected by centrifugation, washed with diethyl ether and then dried in vacuum to yield **Ru-3** 40 mg (70%). ^{1}H-NMR (300 MHz, $CDCl_3$) δ 0.92 (br t, 12H), 1.30 (br s, 24H), 1.71 (br m, 8H), 1.81 (br m, 8H), 3.82 (s, 6H), 3.91 (s, 6H), 4.06 (br m, 8H), 6.86 (br d, 4H), 7.01 (s, 4H), 7.06 (br s, 2H), 7.61 (br s, 16H), 7.72 (br s, 4H), 7.80 (br tr, 6H), 8.06 (br m, 6H), 8.5 (br m, 6H). ^{13}C-NMR (75.4 MHz, CD_3COCD_3) δ 14.35, 23.22, 26.52, 26.77, 32.59, 55.99, 56.61, 69.97, 70.13, 87.56, 88.01, 90.12, 93.38, 94.87, 96.25, 112.5, 113.2, 113.5, 116.7, 117.5, 117.6, 118.7, 123.3,

123.9, 125.1, 125.4, 125.6, 127.7, 127.8, 128.8, 132.8, 139.2, 140.4, 140.6, 140.98, 152.7, 153.12, 153.84, 154.2, 154.4, 154.9, 155.5, 156.4, 157.9, 158.1. MALDI-MS calculated for $C_{122}H_{121}N_6O_8Ru$ (M-2PF$_6$) 1898.96, found 1898.68.

Compound 23

Compound 20 (1.0 g, 3.84 mmol), 1,4-diiodo-2,5-dioctadecylbenzene (3.33 g, 3.84 mmol), tetrahydrofuran (50 mL) and diisopropylamine (50 mL) were combined in a schlenk flask which was then degassed with argon for 0.5 hr. Pd(PPh$_3$)$_2$Cl$_2$ (0.08 g, 0.115 mmol) and CuI (0.044 g, 0.23 mmol) were added to the Schlenk flask. The resulting solution was heated at 70°C for 20 hr. The solution was allowed to cool and after evaporation of the solvent the product was purified by chromatography on silica gel with 7:3 CHCl$_3$/hexane to afford 1.07 g of 23 (28%). The first product to elute off of the column (R_f=1), is the non-polar unreacted 1,4-diiodo-2,5-dioctadecylbenzene (12), followed by compound 23 (R_f = 0.4). ^{1}H-NMR (300 MHz, CDCl$_3$) δ 0.88 (t, 6H), 1.25 (br s, 56H), 1.51 (br m, 4H), 1.64 (s, 6H), 1.83 (br m, 4H), 2.18 (s, 1H), 3.98 (m, 4H), 6.92 (s, 1H), 7.31 (s, 1H), 7.54 (m, 8H). ^{13}C-NMR (75.4 MHz, CDCl$_3$) δ 14.1, 22.7, 26.0, 29.3, 29.7, 31.4, 31.9, 65.6, 69.8, 70.1, 81.9, 86.6, 87.6, 93.9, 94.6, 113.5, 115.8, 121.9, 122.7, 123.8, 126.7, 126.8, 131.9, 132.1, 139.9, 140.0, 151.8, 154.3. FAB-MS calculated for $C_{61}H_{91}IO_3$ 999.28, found 999.1.

Protected Oligomer 24

Compound 22 (140 g, 0.204 mmol), compound 23 (400 mg, 0.204 mmol), tetrahydrofuran (15 mL) and diisopropylamine (15 mL) were combined in a Schlenk flask which was then degassed with argon for 0.5 hr. Then Pd(PPh$_3$)$_4$ (12 mg, 0.01 mmol) and CuI (4 mg, 0.02 mmol) were added to the Schlenk flask. The resulting solution was

heated at 70°C for 20 hr. The solution was allowed to cool and after evaporation of the solvent the product was purified by chromatography on silica gel with 5:1 hexane/ether to afford 180 mg of 24 (75% yield). ^{1}H-NMR (300 MHz, CDCl$_3$) δ 0.88 (t, 6H), 1.25 (br s, 56H), 1.51 (br m, 4H), 1.64 (s, 6H), 1.83 (br m, 4H), 2.18 (s, 1H), 3.81 (s, 3H), 3.90 (s, 3H), 4.06 (m, 4H), 6.92 (m, 2H), 7.06 (s, 1H), 7.10 (s, 2H), 7.60 (m, 16H).

Oligomer 25

Protected oligomer 24 (180 mg, 0.15 mmol) was dissolved in 10 mL of toluene and the solution was thoroughly degassed with argon for 1 hr. Crushed potassium hydroxide (63 mg, 1.12 mmol) was added and the Schlenk tube that contained the solution was immersed for 5 minutes into an oil bath that had been pre-heated to 110°C. The reaction mixture was cooled and then extracted with CHCl$_3$. Evaporation the solvent afforded compound 24, yield 139 mg (50%). ^{1}H-NMR (300 MHz, CDCl$_3$) δ 0.88 (t, 6H), 1.25 (br s, 56H), 1.51 (br m, 4H), 1.83 (br m, 4H), 3.10 (s, 1H), 3.81 (s, 3H), 3.90 (s, 3H), 4.06 (m, 4H), 6.92 (m, 2H), 7.06 (s, 1H), 7.10 (s, 2H), 7.60 (m, 16H).

Metal-Organic Oligomer Ru-4

Compound 25 (25 mg, 0.02 mmol), compound Ru-2-C7-I (18 mg, 0.01 mmol), tetrahydrofuran (2 mL) and diisopropylamine (2 mL) were combined in a Schlenk flask which was then degassed with argon for 0.5 hr. Then Pd(PPh$_3$)$_4$ (0.6 mg, 0.0005 mmol) and CuI (0.1 mg, 0.001 mmol) were added to the schlenk flask. The resulting solution was heated at 70°C for 20 hr. The solution was allowed to cool and the solvent removed under vacuum. The crude product was dissolved in 50 mL of CHCl$_3$. The combined organic phase was washed with NH$_4$· OH (50%) (50 mL × 2), H$_2$O (50 mL × 2) and dried over MgSO$_4$. Most of the solvent was evaporated under vacuum and the concentrated

solution poured into ether. The formed red solid was collected by centrifugation, wash with diethyl ether and dried in vacuum to yield **Ru-4** 18 mg (70%). ^{1}H-NMR (300 MHz, CDCl$_3$) δ 0.92 (br t, 24H), 1.24 (br s, 136H), 1.40 (br m, 16H), 1.85 (br m, 16H), 3.80 (s, 6H), 3.89 (s, 6H), 4.06 (br t, 16H), 6.86 (br d, 4H), 7.0 (s, 4H), 7.04 (br s, 4H), 7.06 (br s, 2H), 7.61 (br s, 32H), 7.72 (br s, 4H), 7.81 (br t, 6H), 8.09 (br t, 6H), 8.45 (br 4, 6H). ^{13}C-NMR (75.4 MHz, CDCl$_3$) δ 14.1 22.6, 26.1, 29.1, 29.4, 31.9, 56.8, 56.5, 69.4, 69.6, 86.7, 86.9, 88.7, 93.2, 94.7, 94.8, 95.5, 95.9, 111.2, 112.1, 112.9, 113.9, 114.0, 115.8, 116.1, 116.4, 116.9, 117.0, 118.1, 122.3, 122.7, 122.9, 124.1, 124.5, 124.6, 125.0, 126.7, 128.5, 132.1, 138.0, 138.4, 139.9, 140.0, 140.3, 151.5, 151.6, 152.0, 153.2, 153.7, 153.8, 154.5, 154.6, 156.3, 156.5. ESI-MS calculated for C$_{238}$H$_{288}$N$_6$O$_{12}$Ru (M-2PF$_6$)$^{2+}$ 3526.03, found 1762.7.

CHAPTER 3
SYNTHESIS AND PHOTOPHYSICS OF 5,5'-BIPHENYL OLIGOMERS THAT CONTAIN $Os^{II}(bpy)_2$ AND $Ru^{II}(R-bpy)_2$ CHROMOPHORES

Introduction

The photophysical work on the $(L)Ru^{II}(bpy)_2$ complexes led to insight

concerning the nature of the interaction between π-conjugated systems and MLCT

chromophores, providing us with a wealth of knowledge with regard to the photophysics

of the substituted oligomers. One of the most interesting aspects of $(L)Ru^{II}(bpy)_2$ is the

equilibrium between the $d\pi(Ru) \rightarrow \pi^*(L)$ MLCT and ligand centered $^3\pi,\pi^*$ states. It

would be of interest to increase the energy separating the MLCT state and $^3\pi,\pi^*$ state and

to examine the effect on the photophysical properties of the metal-oligomers. There are

two ways to decrease the energy of MLCT excited state. Both the metal and ligands can

affect the energy of excited state. Introduction of electron withdrawing substituents on

bipyridine will influence the energetics of the ligand – centered π^* orbitals and offer the

possibility of decreasing the energy of the MLCT excited state relative to the $^3\pi,\pi^*$ state

because the excited electron will be promoted to the lower energy electron acceptor, and

therefore lower energy of MLCT excited state (Figure 3-1b). Here the π_L and π_L^* are the

π-bonding and π^*-antibonding orbitals of aromatic system of the ligand, and σ_L is the σ-

bonding orbital of ligand. The $d\pi$ and σ_M are the t_{2g} and e_g levels originating of 4d orbital
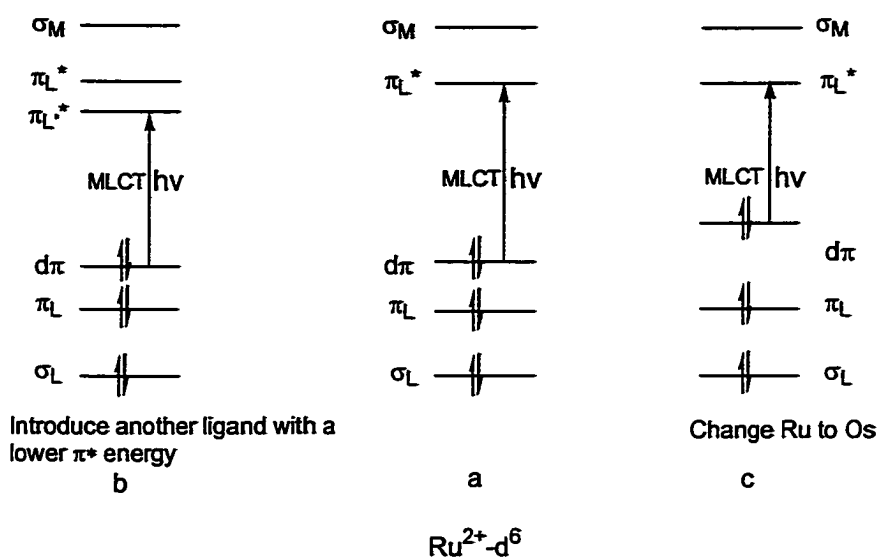
of the metals.

Figure 3-1: Simplified molecular orbital diagram.

A trifluoromethyl group is a good candidate for the electron withdrawing substituent group on bipyridine because of its σ-accepting power and excellent chemical stability (Figure 3-2). From electrochemical data, it can be seen that $[Ru(tfmb)_2(bpy)]^{2+}$ has a lower first reduction potential than **Ru-1** (Table 3-1).[104] This indicates that the energy of the π* orbital of **tfmb** is lower than that of oligomer 1. 4,4'-bis(ethylcarboxy)-2,2'-bipyridine is also a good choice as electron acceptor because of its low reduction potential (Figure 3-2).[105]
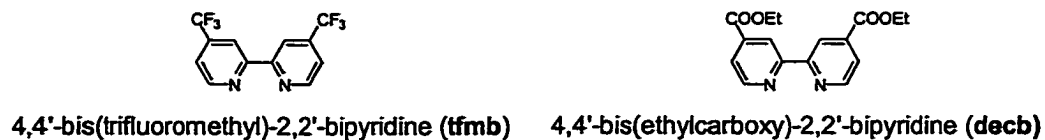

4,4'-bis(trifluoromethyl)-2,2'-bipyridine (**tfmb**)   4,4'-bis(ethylcarboxy)-2,2'-bipyridine (**decb**)

Figure 3-2: Structure of ligand.

Table 3-1: Redox properties of complexes in CH_3CN.

Complex	$E_{1/2}(M^{2+/3+})$ / V	$E_{1/2}(L^{0/0-})$ / V		
$[Ru(bpy)_3]^{2+}$ [a]	1.27	-1.31	-1.50	-1.77
$[Ru(decb)(bpy)_2]^{2+}$ [b]	1.38	-0.93	-1.36	-1.56
$[Ru(tfmb)_2(bpy)]^{2+}$ [c]	1.63	-0.83	-1.02	-1.51
$[Os(bpy)_3]^{2+}$ [d]	0.85	-1.25	-1.46	-1.77
Ru-1	1.41	-1.04	-1.55	-1.91

[a] Data from ref.[84]. [b] Data from ref.[105]. [c] Data from ref.[104]. [d] Data from ref.[106].

Another way to separate the MLCT and $^3\pi,\pi^*$ states is to change the metal from ruthenium to osmium. Osmium has a lower third ionization energy compared to ruthenium which leads to a lower potential for the Os(II/III) couple in complexes of Os(II). This decrease in the oxidation potential decreases the energy of the luminescent ^{3}MLCT level of an Os(II) complex relative to that of an analogous Ru(II) complex (Figure 3-1c). As one can see from the electrochemical data gathered in Table 3-1, $[Os(bpy)_3]^{2+}$ is oxidized at a less positive potential than $[Ru(bpy)_3]^{2+}$, whereas the first reduction potential of the two complexes is almost the same.

This chapter describes the synthesis and characterization of the $(L)Ru^{II}(R-bpy)_2$ and $(L)Os^{II}(bpy)_2$ complexes. The structures of these complexes are shown in Figure 3-3. Since the conjugation length is defined early in the series of Ru-1 – Ru-4, we made corresponding complexes with oligomer 1 and 2. Extensive photophysical studies were conducted on these molecules, and the results are presented in this chapter.

R = COOEt, Ru-1-COOEt
R = CF₃, Ru-1-CF₃

R = COOEt, **Ru-1-COOEt**
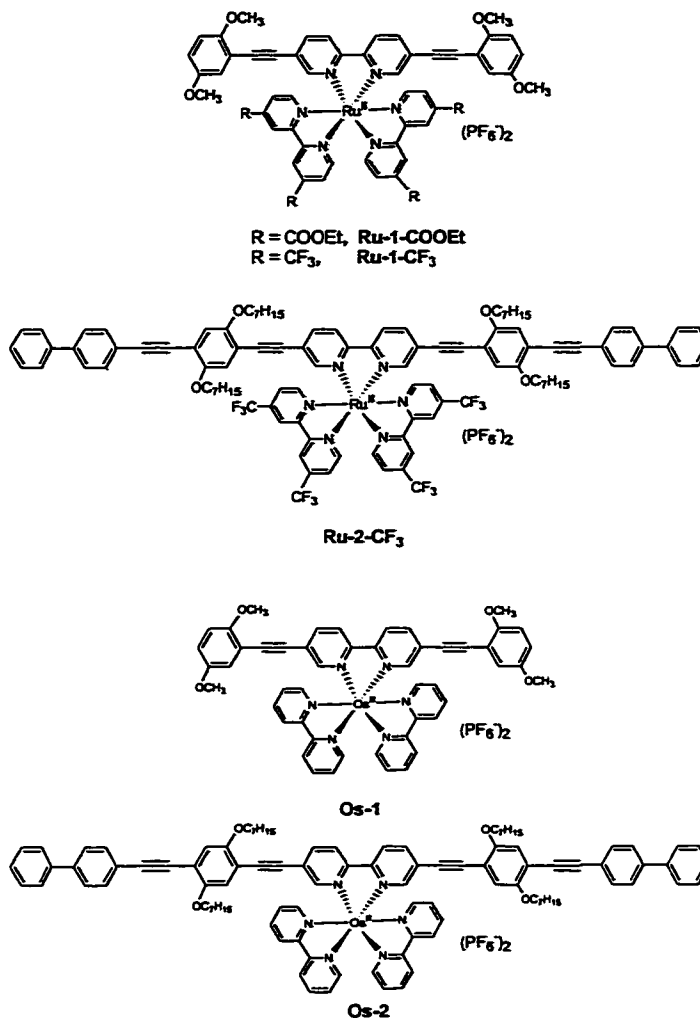R = CF₃, **Ru-1-CF₃**

Ru-2-CF₃

Os-1

Os-2

Figure 3-3: Structure of complexes.

<u>Synthesis</u>

The ligand 1 was synthesized as described in Chapter 2. The metal complex **Ru-1-CF₃** was prepared by modification of the literature method (Figure 3-4).[104] Metallation of oligomer 1 with *cis*-**Ru(tfmb)₂Cl₂** which was obtained from Prof. Furue's group

affords **Ru-1-CF₃**. During synthesis of **(L)Ru^{II}(bpy)** complexes, the use of Ag$^+$ to

remove chloride ligands to form labile solvated complex intermediates was a very useful

synthetic technique. However, the use of Ag$^+$ did not succeed for this analog.
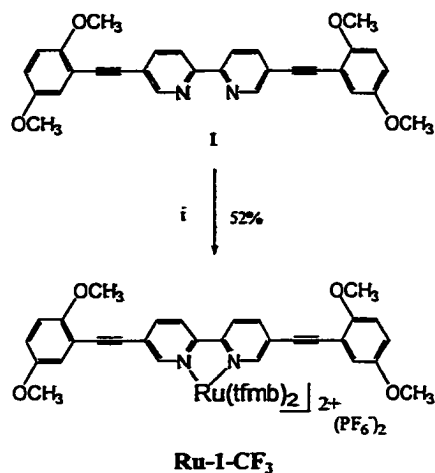
i. *cis*-**Ru(tfmb)₂Cl₂** , ethylene glycol/2-methoxyethanol, heat, 24 hr.

Figure 3-4: Synthesis of **Ru-1-CF₃**.

For the synthesis of **Ru-2-CF₃**, we applied the same strategy that was used for

synthesis of **Ru-2-C7** (Chapter 2). First compound **16** was metallated with *cis*-

Ru(tfmb)₂Cl₂ (Figure 3-5). This was followed by a Sonogashira coupling reaction with

biphenyl acetylene **18** (Figure 3-6). Surprisingly reaction of compound **16** with *cis*-

Ru(tfmb)₂Cl₂ takes place much more slowly compared to metallation of **1**. The reason

for the sluggishness of this reaction is uncertain, but it may be due to steric hinderence

due to the C₇ chains on the alkoxy phenyl rings.

Ru-2-C7-I-CF₃
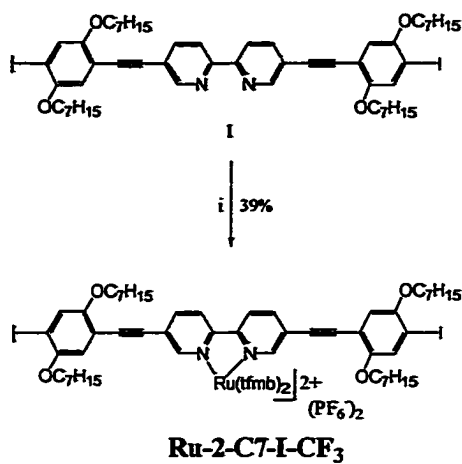
i. *cis*-**Ru(tfmb)₂Cl₂**, ethylene glycol/2-methoxyethanol, heat, 5 days.
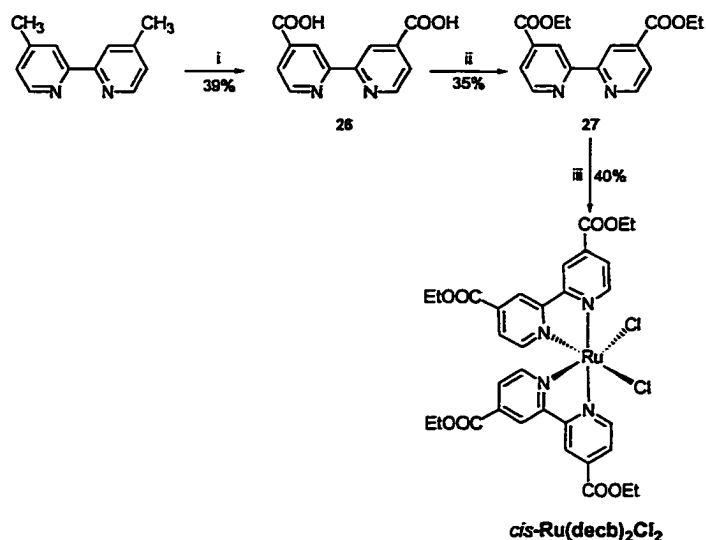
Figure 3-5: Synthesis of model compounds.

Ru-2-C7-I-CF₃
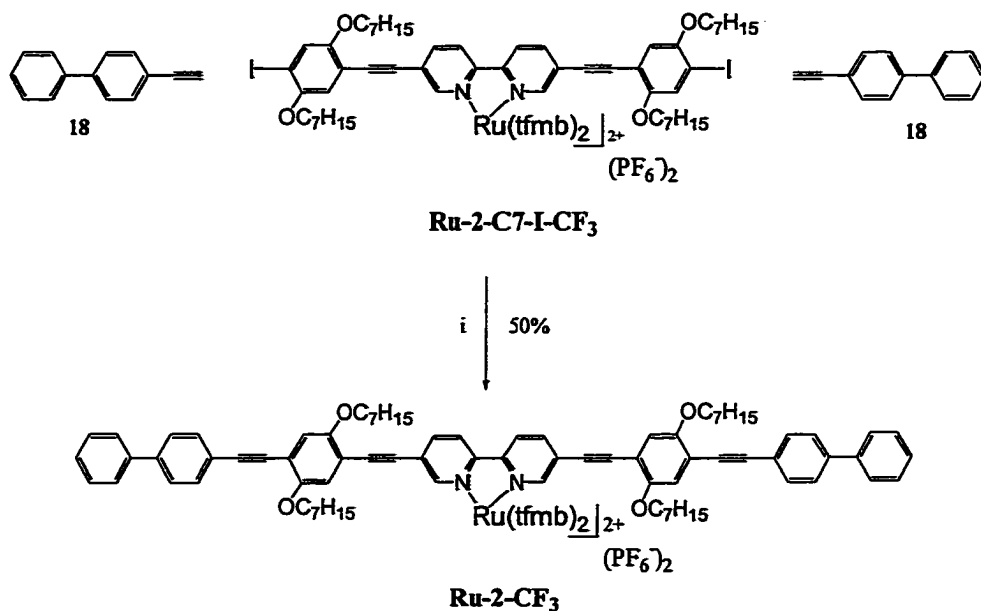
Ru-2-CF₃

i. Pd(PPh₃)₄, CuI, THF, (*i*-Pr)₂NH.

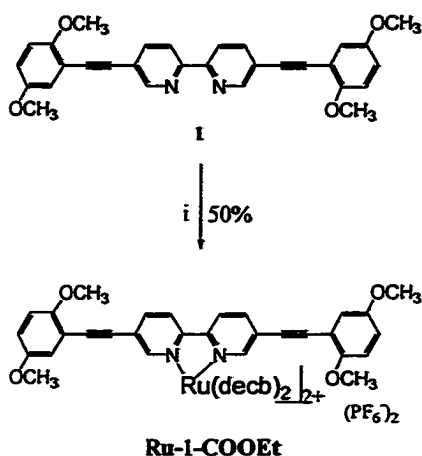Figure 3-6: Synthesis of **Ru-2-CF₃**.

Figure 3-7 – 3-8 illustrate the overall synthetic routes to prepare the complex **Ru-1-COOEt**. The key compound in these schemes is *cis*-**Ru(decb)₂Cl₂** which is obtained by modification of a procedure described by Montague (Figure 3-7).[107] Oxidation of 4,4'-dimethyl-2,2'-bipyridine using $KMnO_4$ produced compound **26** in reasonable yield. Then **26** was converted to the ester by treatment with ethanol followed by reaction of the ligand with $RuCl_3 \cdot 3H_2O$ to make *cis*-**Ru(decb)₂Cl₂** without difficulty. Reaction of *cis*-**Ru(decb)₂Cl₂** with ligand **1** produces **Ru-1-COOEt** in moderate yield (Figure 3-8). For this reaction, the addition of 2-methoxyethanol was very important. It can increase both the solubility of **1** and the reaction temperature which makes reaction go smoothly. But this metallation takes 4 days to finish which is much longer than required to synthesize the **Ru-1** and **Ru-1-CF₃** complexes. Attempts to synthesize the longer oligomer complex **Ru-2-COOEt** were unsuccessful. The reaction yielded only the tris complex **[Ru(decb)₃]²⁺**.

cis-Ru(decb)₂Cl₂

i. $KMnO_4$, H_2O, heat, 4 hr; ii. concentrated H_2SO_4, EtOH, heat, 10 hr; iii. $RuCl_3 \cdot 3H_2O$, DMF, heat, 8 hr.

Figure 3-7: Synthesis of model compound.

i. *cis*-**Ru(decb)₂Cl₂**, EtOH/acetone/2-methoxyethanol, heat, 4 days.

Figure 3-8: Synthesis of **Ru-1-COOEt**.

The synthesis of **Os-1** and **Os-2** is outlined in Figure 3-9 – 3-12. The starting

material *cis*-**Os(bpy)₂Cl₂** was prepared by modification of the literature method.[79,108]

$(NH_4)_2OsCl_6$ and 2,2'-bipyridine were refluxed in ethylene glycol to yield *cis*-

Os(bpy)₂Cl₂ in high yield (Figure 3-9). The use of Ag^+ was not useful for the synthesis of

the osmium complexes. Thus metallation of ligand **1** with *cis*-**Os(bpy)₂Cl₂** required more

vigorous reaction conditions. A high reaction temperature was required and therefore

ethylene glycol was used as the solvent. Refluxing ligand **1** with *cis*-**Os(bpy)₂Cl₂** in

ethylene glycol produced **Os-1** in high yield (Figure 3-10). **Os-2** was prepared by first

synthesizing metal complex **Os-2-C7-I**, and then endcapping this complex with biphenyl

acetylene **18** (Figure 3-11, 3-12). However for **Os-2**, extraction and rinsing with solvent

did not afford a pure product and therefore chromatography on activated alumina was

used to purify the final product.

$(NH_4)_2OsCl_6$ + [structure: 2,2'-bipyridine] $\xrightarrow[90\%]{i}$ cis-Os(bpy)$_2$Cl$_2$
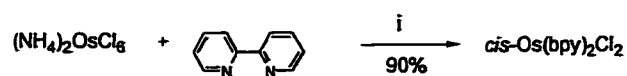
i. ethylene glycol, heat, 2.5 hr.

Figure 3-9: Synthesis of starting compound.

I

i | 91%

Os-1
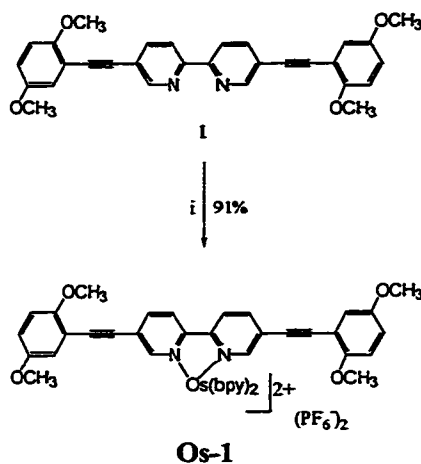
i. *cis*-**Os(bpy)₂Cl₂**, ethylene glycol, heat, 30 hr.

Figure 3-10: Synthesis of **Os-1**.

I

i | 68%

Os-2-C7-I
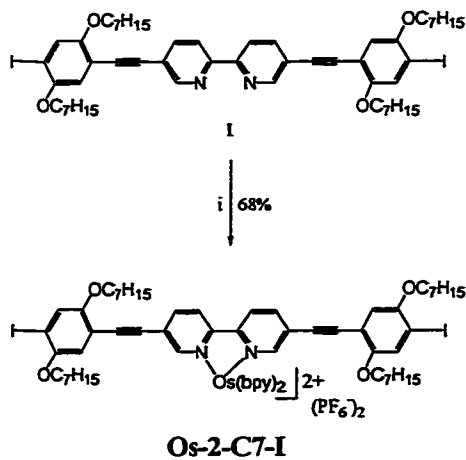
i. Ethylene glycol/2-methoxyethanol, heat, 3 days.

Figure 3-11: Synthesis of model compound.

Os-2-C7-I

i, ii | 42%

Os-2
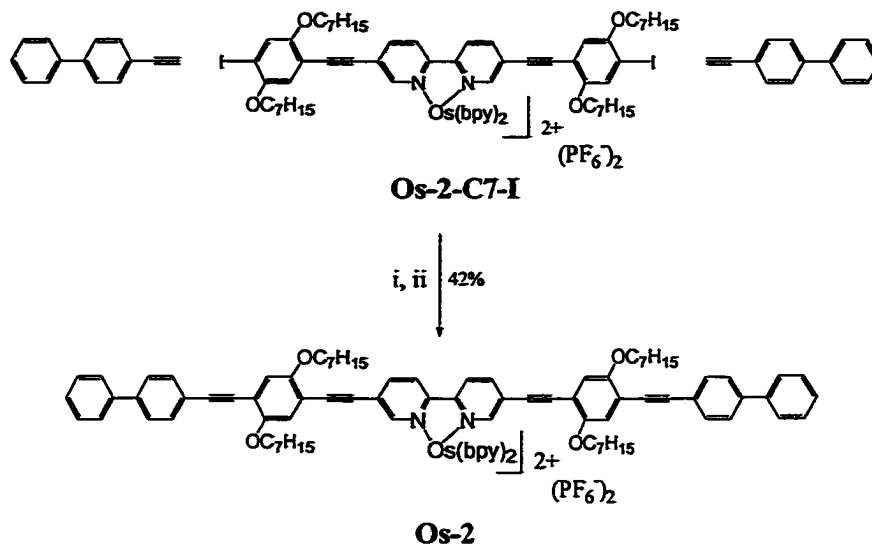
i. Pd(PPh$_3$)$_4$, CuI, THF, (*i*-Pr)$_2$NH; ii. Chromatography on alumina.

Figure 3-12: Synthesis of **Os-2**.

Results

Electrochemistry

Cyclic voltammetry was performed on the **(L)Ru^{II}(R-bpy)$_2$** and **(L)Os^{II}(bpy)$_2$** complexes in CH$_3$CN with 0.1 M TBAH as the supporting electrolyte (Figure 3-13, 14, 15). Quasi-reversible reduction waves were observed in all cases, and relevant oxidation and reduction half-wave potentials are listed in Table 3-2. For comparison, redox potentials for Ru(bpy)$_3^{2+}$, Ru(decb)(bpy)$_2^{2+}$, Ru(tfmb)$_2$(bpy)$^{2+}$ and Os(bpy)$_3^{2+}$ in the same solvent medium are also included.

Replacement of the two bpy ligands of **(1)Ru^{II}(bpy)$_2$** with **tfmb** and **decb** did not shift the first oxidation potential of complexes. For **Ru-1, Ru-1-COOEt** and **Ru-1-CF$_3$** these three complexes display an anodic wave at 1.42 V. This wave was reversible for

Ru-1 and Ru-1-CF$_3$, but not for Ru-1-COOEt. The anodic wave is assigned to oxidation of ligand 1 instead of oxidation of Ru^{II} metal center for Ru-1-CF$_3$ and Ru-1-COOEt. The electron withdrawing ability of -CF$_3$ and -COOEt substituent is expected to shift the oxidation potential of Ru^{II} to a more positive value. As shown in Table 3-2, the Ru(II/III) couple for Ru(tfmb)$_2$(bpy) and Ru(decb)$_2$(bpy) moves to 1.63 V and 1.38 V, respectively, compared to 1.27 V for Ru(bpy)$_3$. In (1)Ru^{II}(R-bpy)$_2$, the first reduction potential is observed at –0.9 for Ru-1-COOEt and at –0.86 for Ru-1-CF$_3$, indicating reduction of coordinated decb and tfmb ligands. The second reduction potential of Ru-1-COOEt and Ru-1-CF$_3$ occurs at –1.04 and –1.02, respectively, which is very close the first reduction potential of Ru-1. Thus, we assign the second reduction of these complexes to reduction of ligand 1. The first reduction and oxidation potential of Ru-2-CF$_3$ is almost the same as that of Ru-2-C7. We believe that the anodic wave is ascribed to the oxidation of the conjugated ligand 2. It is difficult to determine whether the cathodic wave is caused by the reduction of oligomer 2 or tfmb, but the energy level of π* orbital of oligomer 2 and tfmb must be very close.

Both Os-1 and Os-2 display a reversible anodic wave at ≈ 0.91 V. This wave is assigned to the Os(II)/Os(III) couple by analogy to Os(bpy)$_3$. The osmium complexes also display a second reversible anodic wave near 1.40 V. The anodic wave is assigned to oxidation of the ligands 1 and 2. The similarity of the oxidation potentials of Ru-1-CF$_3$ and Ru-2-CF$_3$ further support this assignment. Os-1 also exhibits three reversible cathodic waves which occur in the potential region –0.99 to –1.52 V and Os-2 exhibits two reversible cathodic waves which occur in the potential region –0.94 to –1.27 V. In

both complexes the first wave is ascribed to reduction of the conjugated ligand and the
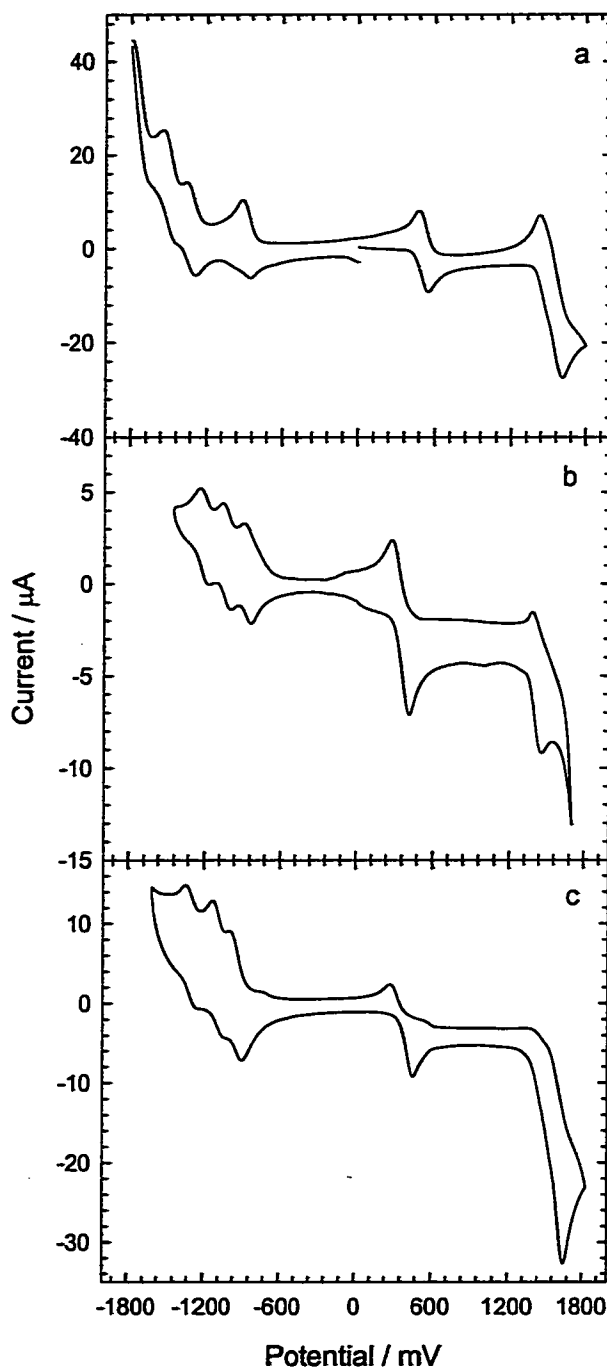
second one is due to reduction of **bpy**.

Figure 3-13: Cyclic voltammetry of **(1)Ru^{II}(R-bpy)$_2$** in CH$_3$CN. (a) **Ru-1**; (b) **Ru-1-CF$_3$**; (c) **Ru-1-COOEt**.

Table 3-2: Electrochemical data for $(L)Ru^{II}(R\text{-}bpy)_2$ and $(L)Os^{II}(bpy)_2$ complexes.[a]

compound	$E_{1/2}^{ox}$	$E_{1/2}^{red}$
$[Ru(decb)(bpy)_2]^{2+}$ [b]	1.38 $(Ru^{II/III})$	-0.93 $(decb^{0/-})$
		-1.36 $(decb^{0/-})$
		-1.56 $(bpy^{0/-})$
$[Ru(tfmb)_2(bpy)]^{2+}$ [c]	1.63 $(Ru^{II/III})$	-0.83 $(tfmb^{0/-})$
		-1.02 $(tfmb^{0/-})$
		-1.51 $(bpy^{0/-})$
Ru-1	1.43 $(Ru^{II/III})$	-0.98 $(1^{0/-})$
		-1.41 $(bpy^{0/-})$
Ru-1-COOEt	1.44 $(1^{0/+})$	-0.88 $(decb^{0/-})$
		-1.02 $(1^{0/-})$
		-1.19 $(decb^{0/-})$
Ru-1-CF$_3$	1.44 $(1^{0/+})$	-0.84 $(tfmb^{0/-})$
		-1.00 $(1^{0/-})$
		-1.19 $(tfmb^{0/-})$
Ru-2-C7[d]	1.37 $(2^{0/+})$	-0.91 $(2^{0/-})$
Ru-2-CF$_3$	1.34 $(2^{0/+})$	-0.95 $(2^{0/-})$
$[Os(bpy)_3]^{2+}$ [e]	0.85 $(Os^{II/III})$	-1.25 $(bpy^{0/-})$
		-1.46 $(bpy^{0/-})$
		-1.77 $(bpy^{0/-})$
Os-1	0.98 $(Os^{II/III})$	-0.97 $(1^{0/-})$
	1.51 $(1^{0/+})$	-1.29 $(bpy^{0/-})$
		-1.51 $(bpy^{0/-})$
Os-2	0.93 $(Os^{II/III})$	-0.92 $(2^{0/-})$
	1.41 $(2^{0/+})$	-1.25 $(bpy^{0/-})$

[a] Estimated error in $E_{1/2}$ values is ± 0.05 V for reversible waves. Recorded in CH_3CN solution with 0.1 M TBAH as supporting electrolyte with a Pt working electrode, a Pt auxiliary electrode, and Ag/Ag$^+$ reference electrode. Potentials are referenced to a ferrocene internal standard and reported in V vs. SCE along with their assigned redox couples. Fc$^+$/Fc = 0.425 V was assumed in CH_3CN, and 0.45 V in CH_2Cl_2.[86] [b] Data from ref.[105]. [c] Data from ref.[104]. [d] CH_2Cl_2-0.1 M TBAH solution. [e] Data from ref.[106].
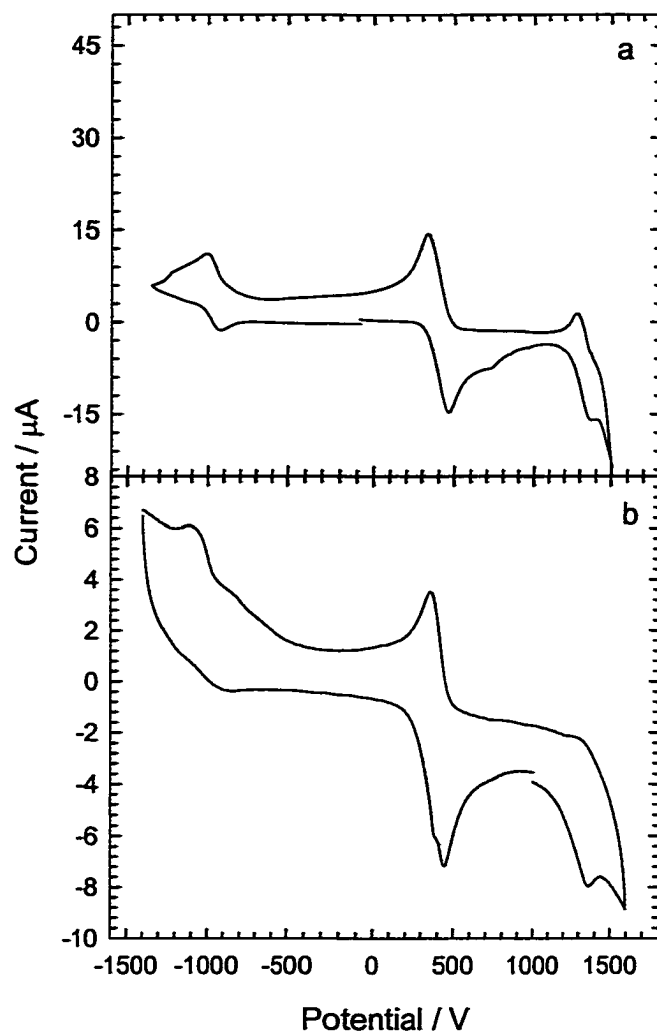
Figure 3-14: Cyclic voltammetry of (2)Ru^{II}(R-bpy)$_2$. (a) Ru-2-C7 in CH$_2$Cl$_2$; (b) Ru-2-CF$_3$ in CH$_3$CN.
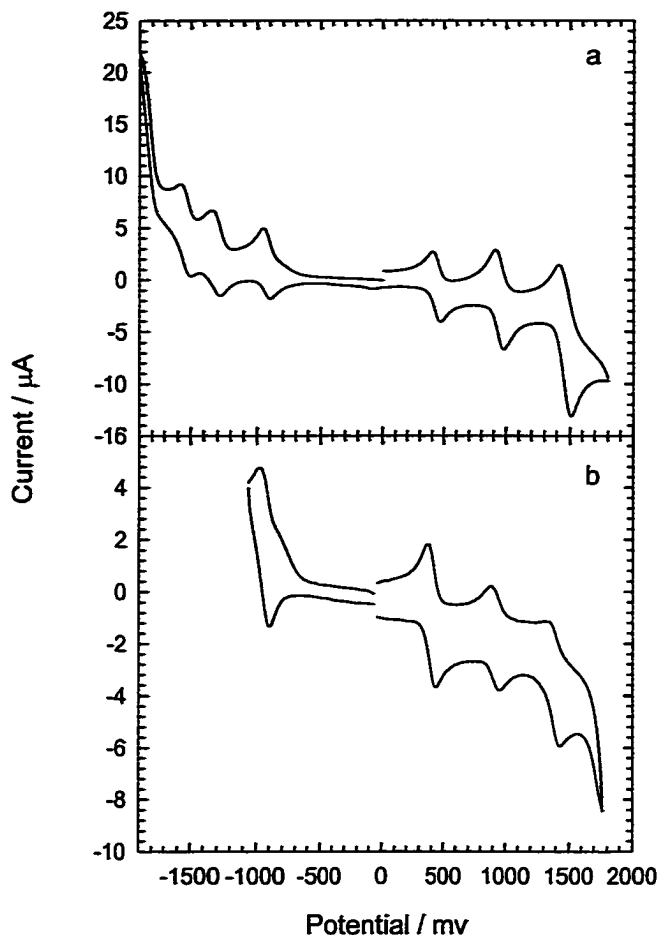
Figure 3-15: Cyclic voltammetry of **(L)Os^{II}(bpy)$_2$** in CH$_3$CN. (a) **Os-1**; (b) **Os-2**.

Absorption Spectra of (L)Ru^{II}(R-bpy)$_2$

Absorption spectra were obtained on dilute CH$_3$CN solutions of the **(L)Ru^{II}(R-bpy)$_2$** complexes. Absorption spectra for these complexes are shown in Figure 3-16 and Table 3-3 contains a listing of the absorption bands and extinction coefficients. Each complex features a high-energy band in the near UV region due to the π,π^* transition of the **R-bpy** ligand. This band is red-shifted with the electron withdrawing groups in the complexes. For **Ru-1-COOEt**, this band is more red-shifted because of conjugation of

the carboxylate substituent which also obscures the higher energy π,π^* transition of

ligand 1. The spectra exhibit the same two strong π,π^* transitions as observed in the

$(L)Ru^{II}(bpy)_2$ series. A distinct shoulder around 480 nm is observed in the spectra of

both Ru-1-COOEt and Ru-1-CF₃ which is blue shifted compared to the $d\pi(Ru) \rightarrow \pi^*$

(1) MLCT band of Ru-1. This band is clearly due to the $d\pi(Ru) \rightarrow \pi^*(R\text{-bpy})$ transition.

A second small shoulder is also observed for these two complexes which probably arises

from $d\pi(Ru) \rightarrow \pi^*(1)$. The blue shift in the $d\pi(Ru) \rightarrow \pi^*(R\text{-bpy})$ transition compared to

$d\pi(Ru) \rightarrow \pi^*(1)$ transition is related to the cumulative inductive effect of the σ-

withdrawing and π-withdrawing ligand orbitals. The absorption spectra of Ru-2-CF₃ is

almost the same as Ru-2. Like the Ru-2 spectrum, the MLCT-based absorptions of Ru-

2-CF₃ are obscured by the more intense oligomer π,π^* transitions.

Table 3-3: Absorption bands of $(L)Ru^{II}(R\text{-bpy})_2$ complexes in CH_3CN solutions.

Complex	λ_{max} /nm	$\varepsilon_{max}/$ mM^{-1}cm^{-1}	Assignment
Ru-1	287	80.4	π,π^* (bpy)
	318	53.3	π,π^* (1)
	398	46.6	π,π^* (1)
	485	8.4	MLCT
Ru-1-COOEt	308	89.6	
	409	34.9	π,π^* (decb)
	480	19.9	π,π^* (1)
			MLCT
Ru-1-CF₃	297	98.3	π,π^* (tfmb)
	318	52.3	π,π^* (1)
	408	41.3	π,π^* (1)
	470	19.1	MLCT
Ru-2-CF₃	297	134.5	π,π^* (tfmb)
	329	105.5	π,π^* (2)
	436	55.6	π,π^* (2) & MLCT
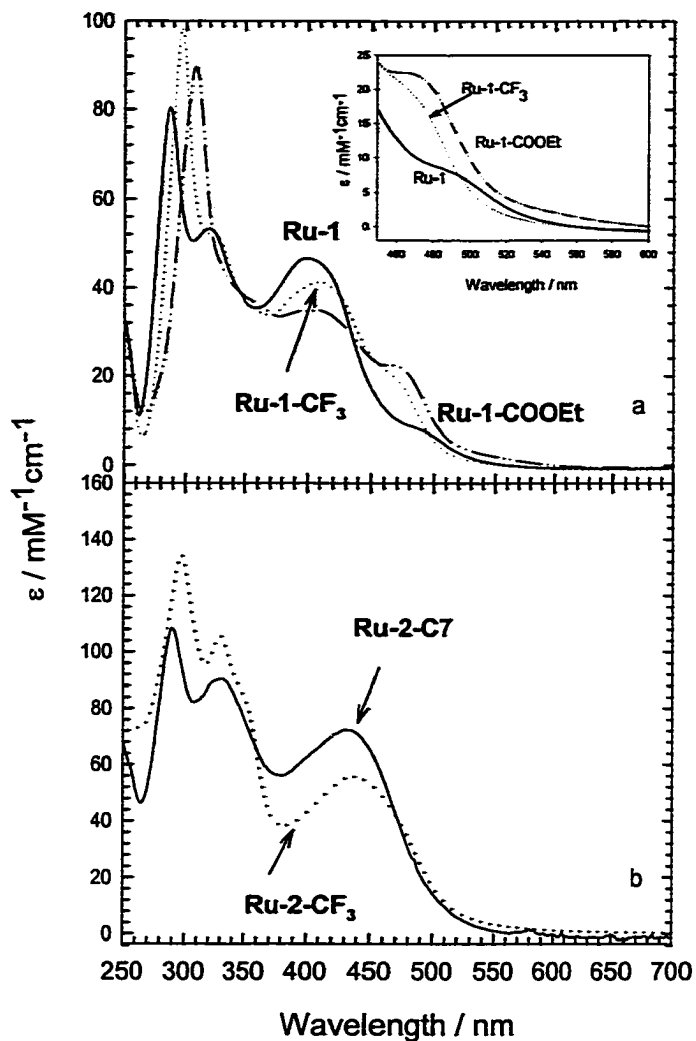
Figure 3-16: Absorption spectra in CH₃CN. (a) **Ru-1** (solid line), **Ru-1-CF₃** (dotted line), **Ru-1-COOEt** (dash-dot-dot line); (b) **Ru-2-C7** (solid line), **Ru-2-CF₃** (dotted line).

Emission Spectra of (L)Ru^{II}(R-bpy)$_2$

In Figure 3-17a are shown emission spectra of **Ru-1-COOEt** and **Ru-1-CF₃** in CH₃CN at room temperature. At room temperature, a broad structureless emission is observed.

But the spectrum of **Ru-1** has a larger bandwidth and a noticeable vibronic shoulder compared to other two. The **tfmb** and **decb** ligands are much easier to reduce than ligand 1, and thus **Ru-1-CF₃** and **Ru-1-COOEt** might be expected to exhibit a lower emission energy than **Ru-1**. However, in contrast to that prediction, both emission and absorption band energies increase as the electron withdrawing ability of the substituent increases. In the multiple chelate complexes, both emission and low-energy absorption are dominated by MLCT transitions to the ligand with the lowest lying π^* level. For our complexes containing both the conjugated ligand 1, and **R-bpy**, the emitting MLCT states are expected to be localized on **R-bpy** by electrochemical data. The influence on the energy gap of the electron withdrawing group -CF₃ and -COOEt comes from the destabilization of the $(d\pi)^5$ core in the $(d\pi)^5(\pi^*)^1$ excited state. This leads to a blue shift in the emission and absorption bands. The same effect can be observed in the emission of **Ru(tfmb)₂(bpy)** which appears at a higher energy ($\lambda_{max} = 653$ nm) than that of **Ru(tfmb)(bpy)₂** ($\lambda_{max} = 677$ nm).[104]

The emission spectrum of **Ru-2-CF₃** is shown in Figure 3-17b. The spectrum of **Ru-2-CF₃** has a vibronic shoulder which is probably due to mixing of two MLCT states ($d\pi(Ru) \rightarrow \pi^*(tfmb)$ and $d\pi(Ru) \rightarrow \pi^*(2)$). The emission band is also blue-shifted compared to that of **Ru-2-C7**.
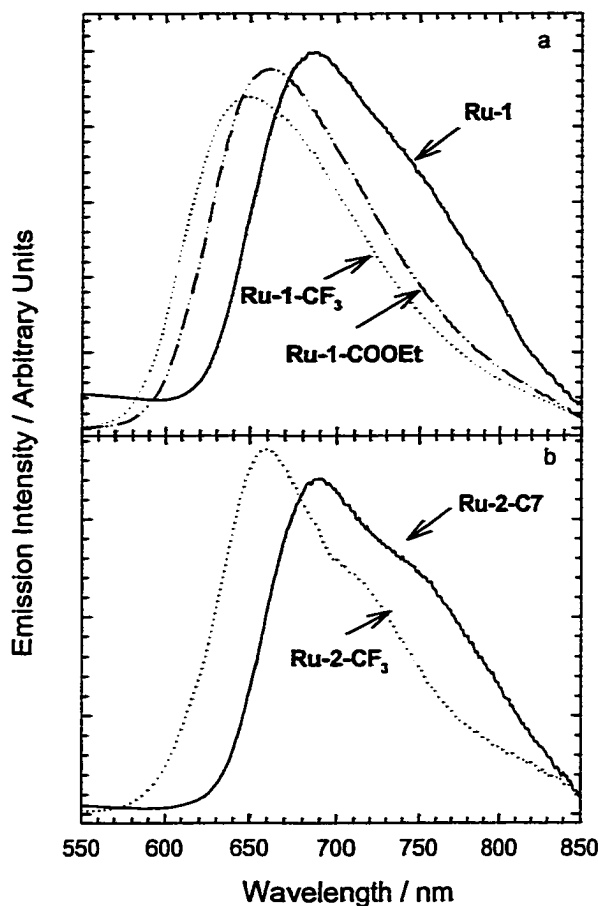
Figure 3-17: Emission spectra of the (1)Ru^{II}(R-bpy)$_2$ complexes in argon bubble-degassed CH$_3$CN at room temperature. (a) **Ru-1** (solid line), **Ru-1-CF$_3$** (dotted line), **Ru-1-COOEt** (dash-dot-dotted line); (b) **Ru-2-C7** (solid line), **Ru-2-CF$_3$** (dotted line).

The emission spectra of **(L)Ru^{II}(R-bpy)$_2$** in optically dilute 4:1 (v/v)

EtOH/MeOH solutions at temperature ranging from room temperature to 80 K are shown

in Figure 3-18 and the spectrum of **Ru-1** is also shown in this figure for comparison.

Emission maxima at 80 K are listed in Table 3-4. The **(L)Ru^{II}(R-bpy)$_2$** complexes

exhibit a strong, low-energy emission that blue-shifts with decreasing temperature.

Similar to that of **(L)Ru^{II}(bpy)$_2$** complexes, the emission band structure at 80 K shows a

structured (0,0) band with a vibronic (0,1) shoulder which is caused by the vibrational

progression. The similarity of these emission spectra suggests that in all cases the MLCT excited state is responsible for the observed emission.

The emission peak of **Ru-1-COOEt** is much narrower compared to **Ru-1** and **Ru-1-CF₃**. The interesting part is that for temperatures close to 200 K, **Ru-1-CF₃** and **Ru-1-COOEt** show only a slight temperature dependence. The emission maximum and emission intensity remains relative constant and actually shift to slightly higher energies when temperature moves closer to room temperature. Above freezing point, conformation change of biphenyl ring and the alkyl chain may disturb the excited state properties.

Table 3-4: Photophysical properties of $(L)Ru^{II}(R\text{-}bpy)_2$ complexes.

| Compound | 298 K [a] | | | | | | λ_{max}^{em} / nm [b] | |
	λ_{max}^{em} nm	τ_{em} μs	ϕ_{em}	$10^4\, k_r^{e}$ s^{-1}	$10^5\, k_{nr}^{e}$ s^{-1}	τ_{TA}^{f} μs	80 K	298 K
Ru-1	687	0.67 [c]	0.039	5.9	14	0.65	647	677
Ru-2-C7	690	0.71 [c]	0.034	4.4	13	0.99	664	686
Ru-1-COOEt	662	1.7 [c]	0.087	5.0	5.3	1.7	626	650
Ru-1-CF₃	646	1.1 [c]	0.054	4.8	8.4	0.96	617	641
Ru-2-CF₃	661	3.2 [d]	0.018	0.57	3.1	3.4	633	661

[a] Measurements were conducted on argon bubble-degassed CH_3CN solution at 298 K. [b] Measurements were conducted on freeze-pump-thaw degassed 4:1 (v/v) EtOH/MeOH. [c] The lifetimes are monoexponential . [d] Lifetime is biexponential (0.8 μs (15%) and 3.6 μs (85%)) and this is mean decay lifetime calculated using equation 2-3. [e] $k_r = \phi_{em} / \tau$; $k_{nr} = 1/\tau_{em}(1-\phi_{em})$. It is assumed that the emitting state is produced with $\phi = 1$. [f] Decay lifetimes of transient absorption.

127
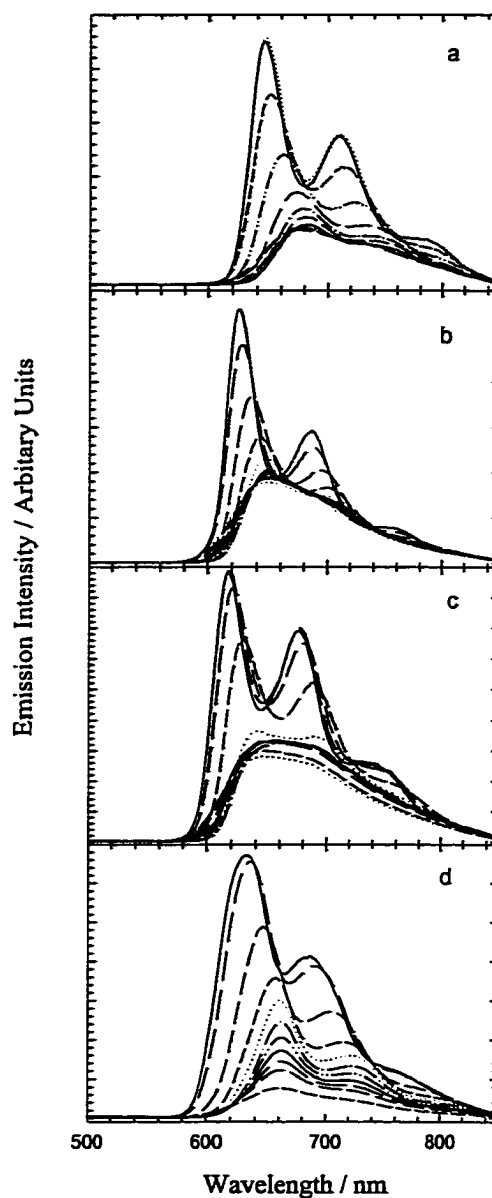
Figure 3-18: Emission spectra of **(L)Ru**^{II}**(R-bpy)**$_2$ complexes in 4:1 (v/v) EtOH/MeOH solvents (450 nm excitation) at temperatures varying from 80 to 298 K. Emission intensity increases with decreasing temperature, and spectra are in 20 K increments. (a) **Ru-1**; (b) **Ru-1-COOEt** (c) **Ru-1-CF$_3$**; (d) **Ru-2-CF$_3$**.

Emission Lifetimes of (L)Ru^{II}(R-bpy)$_2$

The emission decay of (L)Ru^{II}(R-bpy)$_2$ complexes in CH$_3$CN at room

temperature were measured and the lifetimes are listed in Table 3-4. For **Ru-1-CF$_3$** and

Ru-1-COOEt, the decays are monoexponential. Both of them have longer lifetimes

compared to that of **Ru-1** because of the higher energy gap between ground and excited

states. For **Ru-2-CF$_3$** a biexponential decay was observed. The lifetime of one component

is 0.8 μs (15%) which is very close to that of **Ru-2-C7**. The second component has a

longer lifetime which is around 3.6 μs (85%). The mixing of MLCT and $^3\pi,\pi^*$ excited

states probably contributes to the two components lifetime and these two excited states

must be very close in energy. Figure 3-19 shows the decay observed for **Ru-1-CF$_3$** and

Ru-2-CF$_3$ in CH$_3$CN solution on a logarithmic scale along with the excitation lamp

profile and the computer calculated fit.
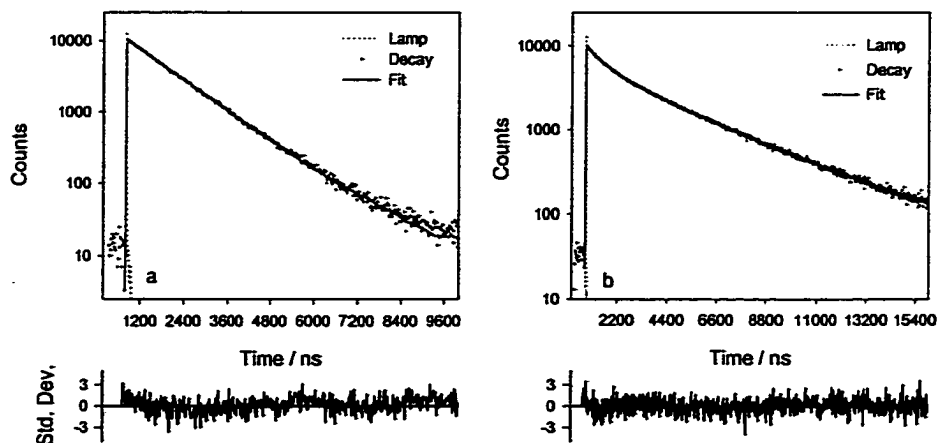
Figure 3-19: Time resolved emission decay in CH$_3$CN at room temperature. Upper box shows the emission decay (Δ) and the excitation lamp profile (dot line) along with the computer-calculated fit (solid line). Lower box show plots of the residuals indicating the quality of the calculated fit. (a) **Ru-1-CF$_3$**; (b) **Ru-2-CF$_3$**.

The luminescence quantum yields (ϕ_{em}) were measured for **(L)Ru^{II}(R-bpy)$_2$** complexes in CH$_3$CN at 298 K, and the values are listed in Table 3-4. Radiative and apparent nonradiative decay rates (k_r and k_{nr}) were computed for all these complexes from equation 2-1 using the ϕ_{em} and τ_{em} values, and these parameters are also listed in the table. The decrease in k_{nr} rates of **(L)Ru^{II}(R-bpy)$_2$** complexes compared to **(L)Ru^{II}(bpy)$_2$** complexes are due to the higher energy gap between ground and excited states of **(L)Ru^{II}(R-bpy)$_2$** complexes.

Lifetimes for the **(L)Ru^{II}(R-bpy)$_2$** complexes were measured as a function of temperature in 4:1 (v/v) EtOH/MeOH. For all of these complexes, both monoexponential and biexponential decays were observed. Multiexponential fits were performed using equation 2-2,[82,83] yielding decay times (τ_i) and normalized amplitudes (α_i) of **(L)Ru^{II}(R-bpy)$_2$** complexes in 4:1 (v/v) EtOH/MeOH solutions. Table 4-4 contains a listing of parameters recovered from multi-component fits of the emission decays for the complexes at 80 K and 298 K. The lifetime data obtained at other temperatures are listed in appendix C. For **Ru-1-COOEt**, the emission decays were characterized by a short-lived component ($\tau \approx 2$ ns) and a component with a considerably longer lifetime. The long-lived component amplitude increases with increasing temperature. We believe that this emission is mostly from MLCT luminescence. For **Ru-1-CF$_3$**, at low temperature, the emission decays were characterized by two components. Both of them have quite long lifetime which is possibly due to overlapping of two MLCT emissions (dπ(Ru) $\rightarrow$ π*(tfmb) and dπ(Ru) $\rightarrow$ π*(1)). At room temperature, the emission is dominated by dπ $\rightarrow$ π*(tfmb) MLCT emission. For **Ru-2-CF$_3$**, the emission decay at 80 K is dominated by a very long-lived component ($\tau \approx 11$ μs, $\alpha = 62\%$) and a low amplitude component

with a shorter lifetime ($\tau \approx 2.9$ µs, $\alpha = 38\%$). Since only phosphorescence is expected to have such long lifetime, this low temperature emission is believed to be overlapping MLCT emission and oligomer $^3\pi,\pi^*$ phosphorescence.

Figure 3-20 shows the decay observed for **Ru-1-COOEt, Ru-1-CF₃** and **Ru-2-CF₃** in 4:1 (v/v) EtOH/MeOH glass at 80 K on a logarithmic scale along with the excitation lamp profile and the computer calculated fit.
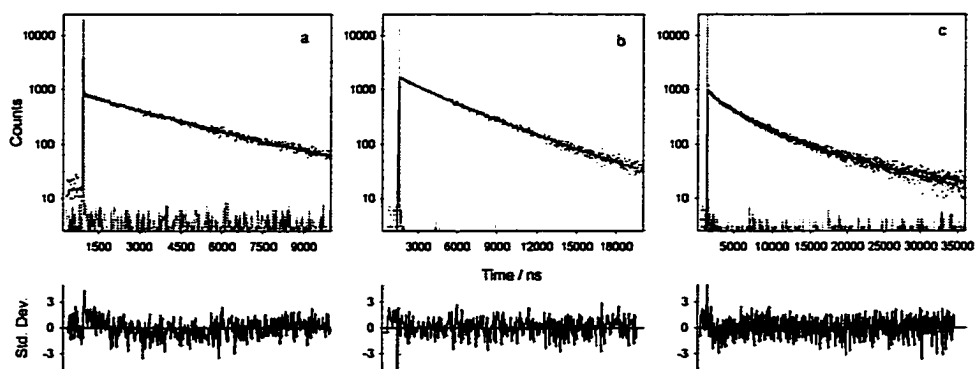
Figure 3-20: Time resolved emission decay in 4:1 (v/v) EtOH/MeOH glass at 80 K. Upper box shows the emission decay (Δ) and the excitation lamp profile (dot line) along with the computer-calculated fit (solid line). Lower box show plots of the residuals indicating the quality of the calculated fit. (a) **Ru-1-COOEt**; (b) **Ru-1-CF₃**; (c) **Ru-2-CF₃**.

Table 3-5: Emission lifetime data of $(L)Ru^{II}(R\text{-bpy})_2$ complexes in 4:1 (v/v) EtOH/MeOH.[a]

Complex	80 K				298 K				
	τ_1, ns	τ_2, ns	$<\tau>$ [b]	$\chi^{2\,c}$	τ_1, ns	τ_2, ns	τ_3, ns	$<\tau>$ [b]	$\chi^{2\,c}$
	$(\alpha_1, \%)$	$(\alpha_2, \%)$	ns		$(\alpha_1, \%)$	$(\alpha_2, \%)$	$(\alpha_3, \%)$	ns	
Ru-1-COOEt	2.9 (77)	3160 (22)	697	1.3	1.7 (29)	1500 (71)	—	1065	1.1
Ru-1-CF₃	2520 (23)	5060 (77)	4465	1.2	1300	—	—	1300	1.2
Ru-2-CF₃	2930 (38)	10830 (62)	7855	1.1	4 (25)	700 (27)	2680 (48)	1450	1.2

[a] 405 nm Excitation. Decays were recorded at 650 nm. Samples were free-pump-thaw degassed. Lifetime and relative biexponential fits were performed with equation 2-2. [b] The mean decay lifetime,$<\tau>$, was calculated using the multiexponential decay data according to the equation 2-3. [c] χ^2 is used to evaluate the quality of the calculated fit. $\chi^2 = 1$ means the best fit.

132

Transient Absorption Spectra of $(L)Ru^{II}(R\text{-}bpy)_2$

Transient absorption spectra were recorded for all the complexes in CH_3CN solutions. Transient absorption spectra of $(L)Ru^{II}(R\text{-}bpy)_2$ following pulsed laser excitation at 355 nm are shown in Figure 3-21. Excited state lifetimes (τ_{TA}) obtained from factor analysis and global decay fitting are listing in Table 3-4. All of the absorbance difference spectra feature the bleaching of the ground state absorption bands in the 350 – 450 nm region which is similar to that of their $(L)Ru^{II}(bpy)_2$ analoges. However, the absorption band is different. For **Ru-1**, it features a strong mid-visible absorption band in the 450 – 500 nm region and a broad, featureless absorption in the red that continues into the near-IR region. The absorption is clearly due to the $d\pi(Ru) \rightarrow \pi^*$ (1) MLCT state. For **Ru-1-COOEt**, the spectrum shows a broad excited-state absorption extending into the near-IR region above 500 nm region. The decay lifetime and that of the luminescence are identical. This suggests that this absorption arises from the $d\pi(Ru) \rightarrow \pi^*(\text{decb})$. For **Ru-1-CF$_3$**, it has small absorption peak at 480 nm similar to **Ru-1** which has tail extends into red region. And the decay lifetime is shorter than that of the luminescence decay. The transient absorption of **Ru-1-CF$_3$** is probably due to superposition of $d\pi(Ru) \rightarrow \pi^*(\text{tfmb})$ and $d\pi(Ru) \rightarrow \pi^*(1)$. There is probably an equilibrium between $d\pi(Ru) \rightarrow \pi^*(\text{tfmb})$ and $d\pi(Ru) \rightarrow \pi^*(1)$ two states. The transient absorption spectra of **Ru-2-CF$_3$** is different from **Ru-2-C7** too. Since the two states of $d\pi(Ru) \rightarrow \pi^*(\text{tfmb})$ and $d\pi(Ru) \rightarrow \pi^*(2)$ are very close in energy, we conclude that the absorption is due to π,π^* transition of ligand **2** instead of MLCT. Also the transient absorption of **Ru-2-CF$_3$** is very similar to **Re-2**,[98] which is known to $^3\pi,\pi^*$. This further confirmed that absorption is due to π,π^* transition of ligand **2**.
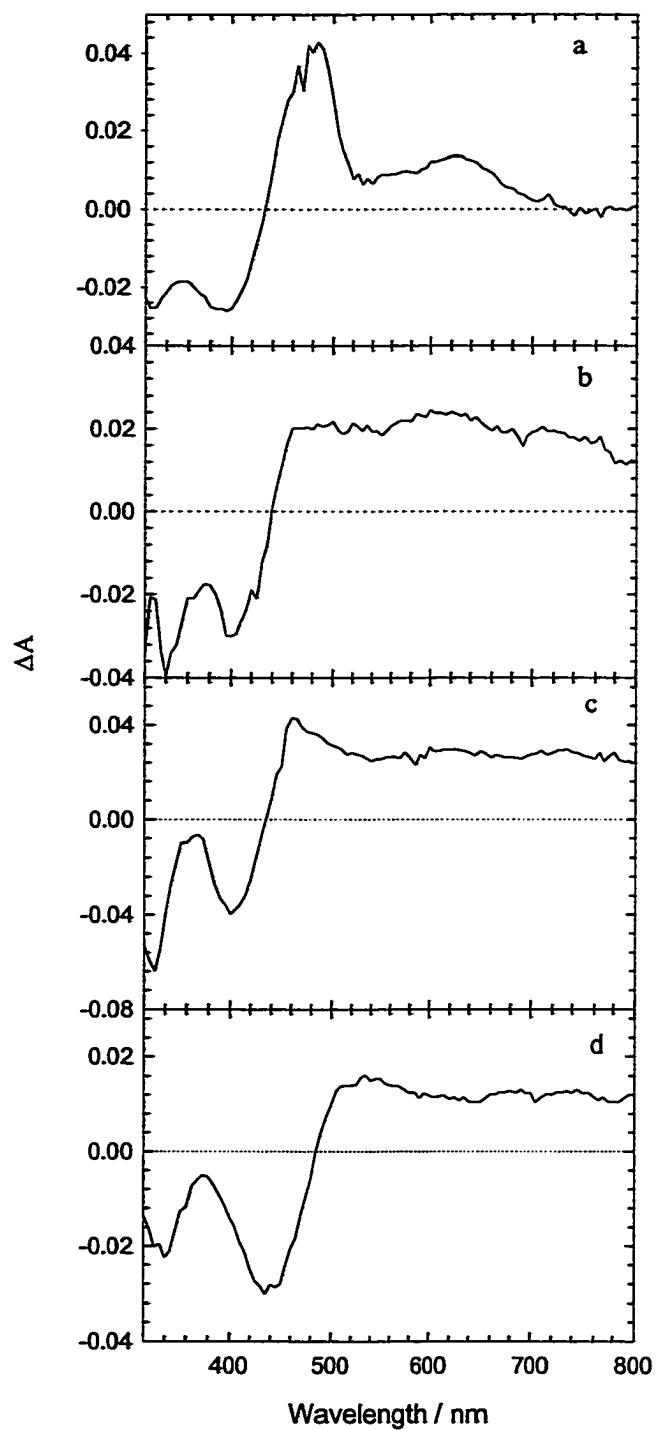
Figure 3-21: Transient absorption difference following 355 nm pulsed laser excitation (5 mJ dose) acquired from argon bubble degassed CH_3CN solution. (a) **Ru-1**; (b) **Ru-1-COOEt**; (c) **Ru-1-CF$_3$**; (d) **Ru-2-CF$_3$**.

Absorption Spectra of $(L)Os^{II}(bpy)_2$

Absorption spectra were obtained on dilute CH_3CN solutions of the $(L)Os^{II}(bpy)_2$ complexes (Figure 3-22).
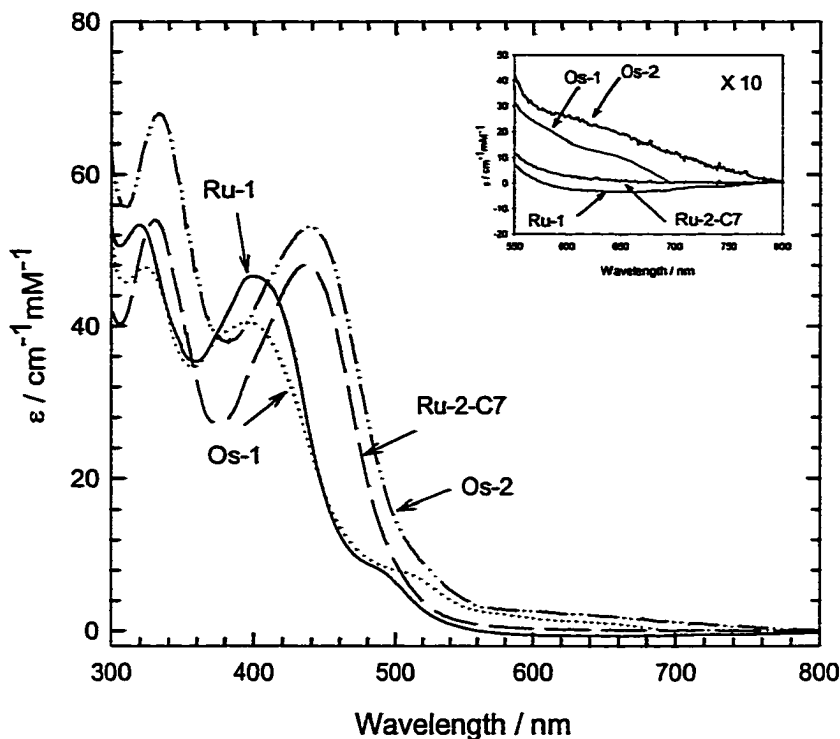
Figure 3-22: Absorption spectra in CH_3CN. **Ru-1** (solid line), **Ru-2-C7** (long dashed), **Os-1** (dotted line), **Os-2** (dash-dot-dotted).

The spectra are dominated by oligomer π,π^* transitions. A distinct shoulder around 520 nm is observed in the spectrum of **Os-1** which is assigned to ^{1}MLCT state. This MLCT band is red-shifted compared to that of **Ru-1** due to the higher energy $d\pi$ orbitals of osmium. Unlike **Ru-2**, the ^{1}MLCT-based absorption of **Os-2** is red-shifted and is not completely obscured by the more intense oligomer π,π^* transitions. A small shoulder around 530 nm can be observed in the spectrum of **Os-2** due to ^{1}MLCT band.

For both **Os-1** and **Os-2**, a small tail absorption extending from 600 nm to 700 nm is observed which is due to the spin-forbidden transition to ^{3}MLCT state. Because of the significant spin-orbital coupling of osmium, the MLCT excited-state manifold includes MLCT transitions to states both largely singlet and largely triplet in character with the "triplet" components appearing on the low-energy side of the spectra with diminished intensities.[106] This behavior is also observed in $Os(bpy)_3^{2+}$, where the forbidden transitions to ^{3}MLCT occur in the same spectral region.[79]

Emission Spectra of $(L)Os^{II}(bpy)_2$

In Figure 3-23 are shown emission spectra of **Os-1** and **Os-2** in CH_3CN at room temperature. Since the emission band of osmium complexes extends into the near-IR region, the CCD spectrometer was used instead of PMT spectrometer. Emission maxima, quantum yields and decay lifetimes are listed in Table 3-6. The emission band is red-shifted quite a lot compared to ruthenium analogues because of the low oxidation potential of osmium. The luminescence is assigned to the MLCT state. Osmium complexes feature a relatively weak emission which has very short lifetime and low quantum yield (Table 3-6). This is due to the very low energy gap between ground and excited states and greater spin-orbital coupling which enhance nonradiative decay rates for triplet-singlet transitions.
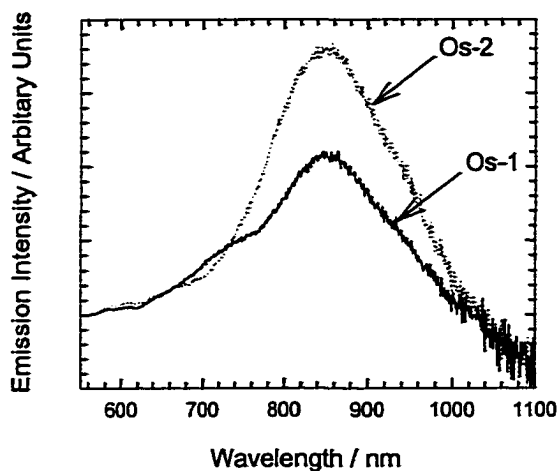
Figure 3-23: Emission spectra of the **(L)Os^II(bpy)2** complexes in argon bubble-degassed CH3CN at room temperature. **Os-1** (solid line), **Os-2** (dotted line).

The **(L)Os^II(bpy)2** complexes emission spectra in optically dilute 2-MTHF and

4:1 (v/v) EtOH/MeOH solutions at temperature at 80 K and 298 K are shown in Figure 3-

24. At cryogenic temperatures, the emission of **Os-1** in 4:1 (v/v) EtOH/MeOH solutions

appears to consist of two bands; one is around 786 nm, and another one is around 722

nm. The high energy band is possibly caused by the transition of $d\pi(Os) \rightarrow \pi^*(bpy)$ since

Os(bpy)3 emits at 720 nm at 77 K in 4:1 (v/v) EtOH/MeOH solution.[108] The low energy

band is due to $d\pi(Os) \rightarrow \pi^*(1)$ MLCT state. The emission band of **Os-2** is red-shifted

compared to **Os-1** and its also shows a structured band with the same shoulder around

720 nm. In 2-MTHF at 80 K **Os-2** shows a structured (0,0) band with a vibronic (0,1)

shoulder which is caused by the vibrational progression. For both of these two

complexes, monoexponential decays were observed. The lifetimes of the

photoluminescence for **(L)Os^II(bpy)2** complexes are approximately 20 ns at ambient

temperature, and they increase up to several hundred nanoseconds at cryogenic

temperatures.
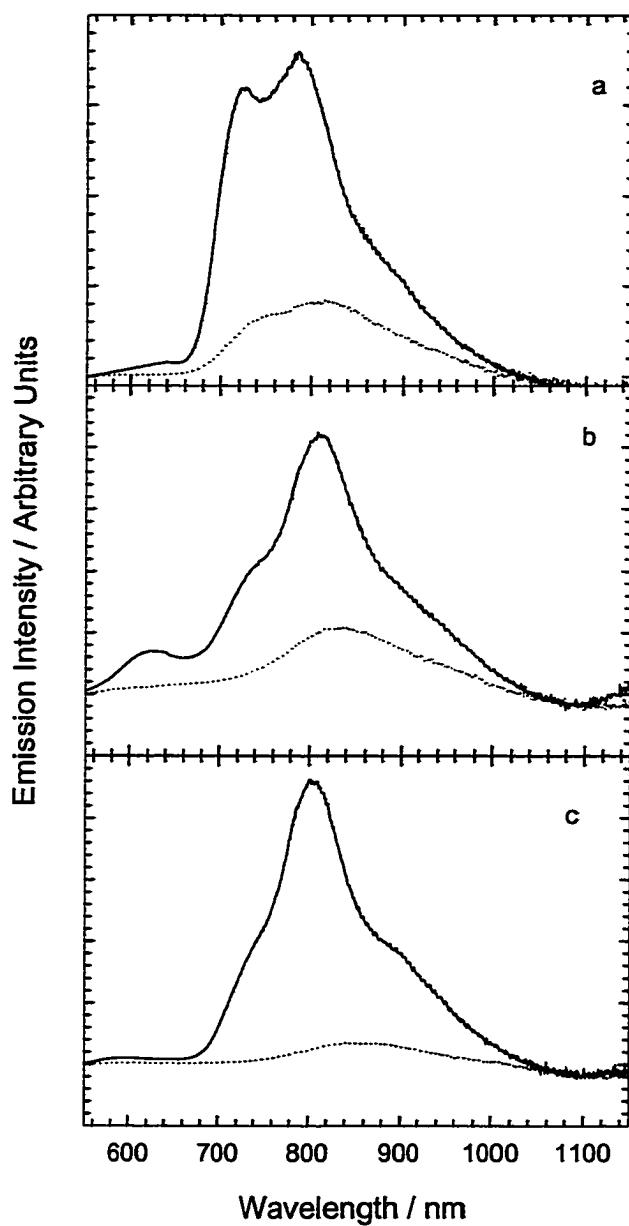
Figure 3-24: Emission spectra of the $(L)Os^{II}(bpy)_2$ complexes (450 nm excitation) at 298 K (dot line) and 80 K (solid line). (a) **Os-1** in 4:1 (v/v) EtOH/MeOH; (b) **Os-2** in 4:1 (v/v) EtOH/MeOH; (c) **Os-2** in 2-MTHF.

Table 3-6: Photophysical properties of $(L)Os^{II}(bpy)_2$ complexes.

	298 K[a]						80 K[b]		80 K[c]	
	λ_{max}^{em} nm	ϕ_{em}	τ ns	$10^4 k_r^d$ s^{-1}	$10^6 k_{nr}^d$ s^{-1}	τ_{TA}^e ns	λ_{max}^{em} nm	τ_{em} ns	λ_{max}^{em} nm	τ_{em} ns
Os(bpy)$_3$[f]	746	0.005	60	8.3	16.6	–	720	–	–	–
Os-1	848	0.00072[g]	21[h]	3.4	33	17	722, 786	355[h]	–	–
Os-2	848	0.00073[g]	32[h]	2.3	50	15	806	527[h]	787	518[h]

[a] Measurements were conducted on argon bubble-degassed CH_3CN solution at 298 K. [b] Measurements were conducted on freeze-pump-thaw degassed 4:1 (v/v) EtOH/MeOH. [c] Measurements were conducted on freeze-pump-thaw degassed 2-MTHF. [d] $k_r = \phi_{em} / \tau$; $k_{nr} = 1/\tau_{em}(1-\phi_{em})$. It is assumed that the emitting state is produced with $\phi = 1$. [e] Decay lifetimes of transient absorption. [f] Data from ref.[106, 109]. [g] Measurements were conducted on CCD spectrometer. The actinometer uses a standard sample of $[Os(bpy)_3](PF_6)_2$ in CH_3CN for which $\phi_{em} = 0.005$.[106] [h] The decays are monoexponential.

Transient Absorption Spectra of $(L)Os^{II}(bpy)_2$

Transient absorption spectra were recorded for **Os-1** and **Os-2** in CH_3CN

solutions. Transient absorption spectra of these two complexes following pulsed laser

excitation at 355 nm are shown in Figure 3-25. Excited state lifetimes obtained from

factor analysis and global decay fitting are approximately equivalent with that of those of

the luminescence and listed in Table 3-6. The spectra of **Os-1** and **Os-2** exhibit a ground-

state bleaching and the mid-visible absorption that are similar to that observed in the

spectra of **Ru-1** and **Ru-2-C7**; however, the excited-state absorption of osmium

complexes in the 550-800 nm region is much less prominent than that of the

corresponding ruthenated complexes. Also the absorption bands of **Os-1** and **Os-2** are red

shifted to 512 nm and 534 nm compared to 486 nm of **Ru-1** and 520 nm of **Ru-2-C7**.

Clearly the absorption is due to the MLCT excited state.

Spectroelectrochemistry

In order to further probe the electrochemistry and electronic absorption

spectroscopy of $(L)Ru^{II}(R\text{-}bpy)_2$ and $(L)Os^{II}(bpy)_2$ complexes, spectroelectrochemistry

was conducted at 298 K in $CH_3CN/0.1$ M TBAH solutions. In this experiment the

complex is oxidized or reduced and the changes in the electronic absorption spectrum are

monitored. This oxidation or reduction results in dramatic changes in any transitions

involving the orbital that is involved in the electrochemical process. Oxidation of a metal

will cause a dramatic shift in the energy of any MLCT transitions involving that metal.

Metal oxidation will also tend to stabilize the π^* orbitals of the ligands coordinated to

that metal, giving rise to slight red shifts in transitions involving the acceptor orbital.[110]

The reduction of the ligand results in the electron formally residing in the π^* orbital of

the ligand. This results in a dramatic shift in the energy of any MLCT transitions involving that ligand. Ligand centered $\pi \rightarrow \pi^*$ transitions involving the reduced ligand also shift in energy. Reduction of the ligand can also cause the appearance of new ligand $\pi^* \rightarrow \pi$ transitions in the visible region of the spectrum.
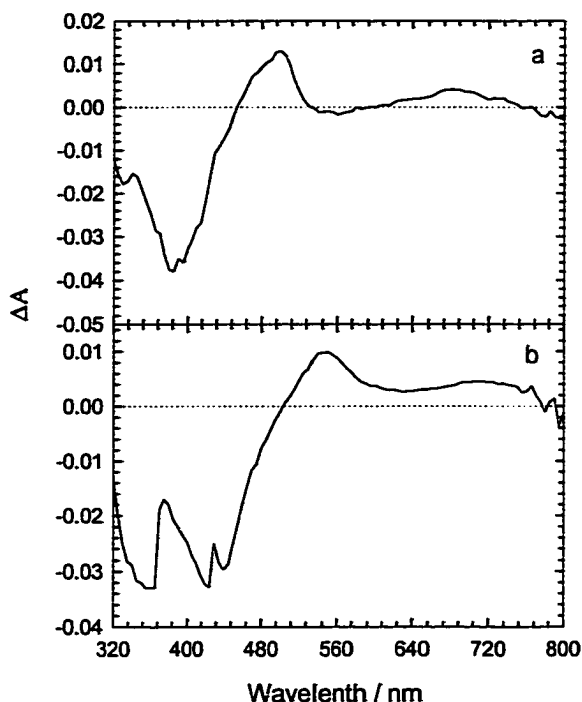
Figure 3-25: Transient absorption difference following 355 nm pulsed laser excitation (5 mJ dose) acquired from argon bubble degassed CH₃CN solution. (a) **Os-1**; (b) **Os-2**.

The spectroelectrochemistry of **Ru-1-CF₃** is shown in Figure 3-26. When **Ru-1-CF₃** is reduced by one electron, one would expect that the added electron would formally reside on the **tfmb** π^* orbital. The loss of shoulder peak at 304 nm upon reduction of the complex supports the assignment of this transition as **tfmb** $\pi \rightarrow \pi^*$ based. Since the band in the 460 - 500 nm region represents overlapping $d\pi(Ru) \rightarrow \pi^*(tfmb)$ and $d\pi(Ru) \rightarrow$

$\pi^*(1)$ MLCT bands, this band should decrease in intensity upon **tfmb** reduction due to

the loss of $d\pi$(Ru) $\rightarrow \pi^*$(**tfmb**) MLCT component. The new absorbances appear in the

visible upon **tfmb** reduction and can be attributed to new **tfmb** $\pi \rightarrow \pi^*$ transitions.

Follow this reduction, the parent complex can be regenerated with > 75% efficiency.
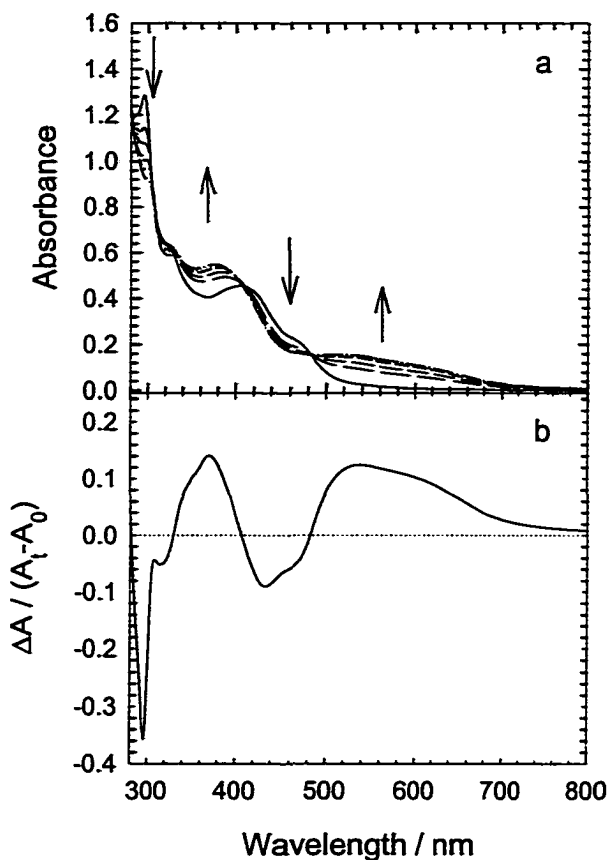
Figure 3-26: UV-Vis spectroelectrochemical response upon the reversible reduction of **Ru-1-CF$_3$** in CH$_3$CN/0.1 M TBAH at 298 K. (a) **Ru-1-CF$_3$** is reduced at –0.7 V; (b) Absorption spectrum difference upon reduction.

The spectroelectrochemistry of **Ru-1-CF$_3$** upon oxidation was also tried (Figure

3-27). Since the first oxidation potential of **Ru-1-CF$_3$** is assigned as oxidation of ligand 1,

the MLCT absorption band and the **tfmb** $\pi \rightarrow \pi^*$ based absorption around 290 nm

remains constant as expected. The absorbances at 410 nm is assigned as $\pi \rightarrow \pi^*$

transitions of ligand **1**. Upon oxidation this peak blue shifts to 370 nm. The oxidation of

ligand possibly causes the complex to decompose and consequently the oxidative

spectroelectrochemistry is irreversible.
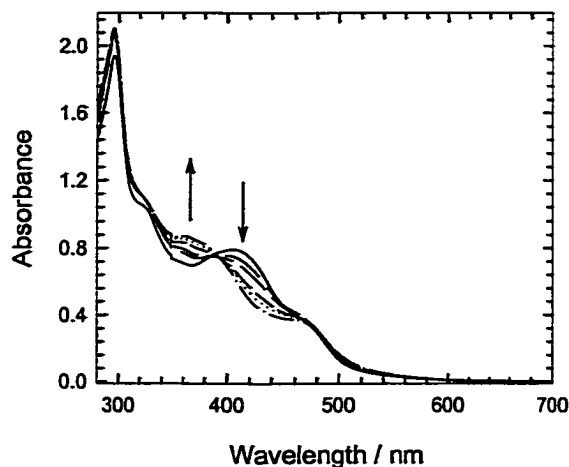
Figure 3-27: UV-Vis spectroelectrochemical response upon the oxidation of **Ru-1-CF₃** at
1.4 V in CH₃CN/0.1 M TBAH at 298 K.

The reductive spectroelectrochemistry of **Ru-1-COOEt** is shown in Figure 3-28.

The loss of shoulder peak at 308 nm, the red shift of $\pi \rightarrow \pi^*$ transitions of ligand **1**, and

the appearance of small new **decb** $\pi \rightarrow \pi^*$ transitions were observed. Follow this

reduction, the parent complex can be regenerated with around 75% efficiency.
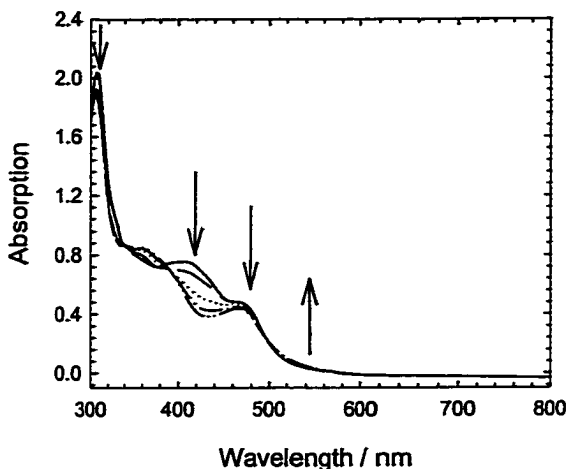
Figure 3-28: UV-Vis spectroelectrochemical response upon the reduction of **Ru-1-COOEt** at −0.9 V in CH_3CN/0.1 M TBAH at 298 K.

The spectroelectrochemistry of **Os-1** is shown Figure 3-29. Upon oxidation of the osmium metal center, a number of spectroscopic changes are evident. The loss of the band centered at 520 nm upon oxidation of Os^{II} to Os^{III} is consistent with the previous assignment of this transition as Os → 1 MLCT transition. Peaks in 550-750 nm region are lost upon oxidation consistent with the ^{3}MLCT assignment. Oxidation of the osmium would also be expected to lower the energy of the π^* orbital of the oligomer 1 resulting in slight red shifts of the ligand 1 $\pi \rightarrow \pi^*$ transitions. This effect is seen in the ligand 1 $\pi \rightarrow \pi^*$ transitions at 400 nm. When the oxidation is complete, this peak red shifts to 424 nm. Reduction of the oxidized complex gave > 95% regeneration of the parent complex as assed by the final spectrum. The absorption spectrum change upon reduction of **Os-1** was also attempted too. But we were unable to obtain reversible reductive spectroelectrochemsitry. We still don't know what causes this irreversibility.

Figure 3-29 also contains the spectroelectrochemical results for **Os-2**. Same trend is observed for this complex. The absorbances at 331 nm and 436 nm are assigned as π → π^* transitions of oligomer **2**. Upon oxidation these two peaks red shift to 343 and 461 nm, respectively. This new peaks at 461 nm obscure MLCT band changes in this region. But peaks in 550-750 nm region are lost upon oxidation consistent with this ^{3}MLCT assignment. Again the reduction of ligand was irreversible.

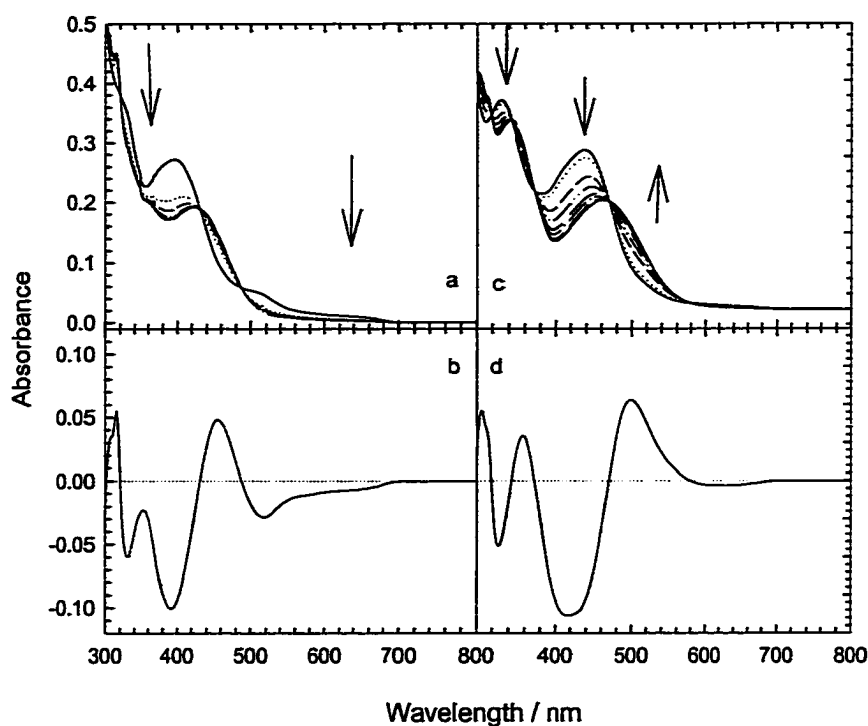

Figure 3-29: UV-Vis spectroelectrochemical response upon the reversible oxidation in CH$_3$CN/0.1 M TBAH at 298 K. (a) **Os-1** oxidized at 0.8 V; (b) Absorption spectrum difference of **Os-1** upon oxidation; (c) **Os-2** oxidized at 0.95 V; (d) Absorption spectrum difference of **Os-2** upon oxidation.

Discussion

Excited-State Energetics and Interconversion in (L)Ru^{II}(R-bpy)$_2$ Complexes

For **Ru-1-COOEt**, the absorption and emission spectra show that the lowest excited state is MLCT and the excited electron is localized on π* orbital of **decb**. Transient absorption and lifetime further prove this statement. The lowest excited state of **Ru-1-CF$_3$** is MLCT (dπ(Ru) → π*(**tfmb**)). From the transient absorption spectrum, we know that dπ(Ru) → π*(**1**) state is very close in energy of dπ(Ru) → π*(**tfmb**) state. For **Ru-2-CF$_3$**, the three excited states of dπ(Ru) → π*(**tfmb**), dπ(Ru) → π*(**2**) and π,π*(**2**) are very close in energy. At low temperature, solvent dipole can not reorganize around polar MLCT state effectively and π,π*(**2**) becomes dominant.

To further probe the relative energy of each state, the emission and its decay of (L)Ru^{II}(R-bpy)$_2$ complexes in CH$_2$Cl$_2$ solvent were tested and listed in Table 3-7. For comparison, the decay data in CH$_3$CN is also listed. Compared to CH$_3$CN solvent, the emission decay kinetics in CH$_2$Cl$_2$ solvent becomes more complicated. In CH$_3$CN solution, the emission of both of **Ru-1-COOEt** and **Ru-1-CF$_3$** exhibit single exponential decay. It's clear that this decay is due to MLCT (dπ(Ru) → π*(R-bpy)) emission. While in CH$_2$Cl$_2$ solution, the emission band of **Ru-1-COOEt** blue shifts from 655 nm in CH$_3$CN to 640 nm in CH$_2$Cl$_2$. The emission decay of **Ru-1-COOEt** becomes two components. It is characterized by a large amplitude long-lived component (τ = 2650 ns, α = 97%) and a low amplitude with a shorter lifetime (τ = 440 ns, α = 3%). We believe that this short-lived component is due to dπ(Ru) → π*(**1**). In less polar solvent, ligand **1** has better solubility and the energy of dπ(Ru) → π*(**1**) is decreased and becomes closer to the energy of dπ(Ru) → π*(**decb**) state. But dπ(Ru) → π*(**decb**) state is still

dominant. The situation is similar to **Ru-1-CF₃**. In CH₂Cl₂ solvent, the emission decay features three components with similar amplitudes. The long-lived one is still due to $d\pi(Ru) \rightarrow \pi^*(1)$, the middle one is maybe due to $d\pi(Ru) \rightarrow \pi^*(\textbf{tfmb})$.

The remarkable feature is for **Ru-2-CF₃**. In CH₂Cl₂ solution, the complex exhibits a weak, broad emission with a maximum at 687 nm (Figure 3-30). This band is considerably weaker and is red-shifted compared to that in CH₃CN. The emission decay of complex in CH₂Cl₂ becomes triexponential.
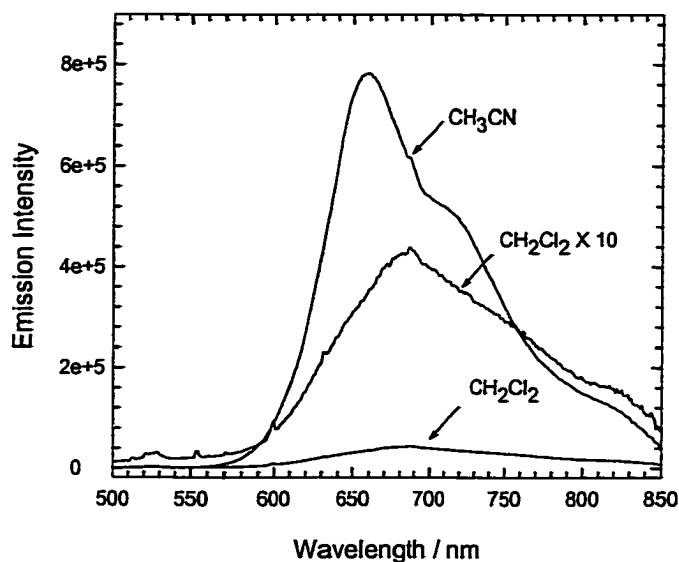
Figure 3-30: Emission spectra of **Ru-2-CF₃** in CH₃CN and CH₂Cl₂ at 298 K. The spectra reflect relative intenstities.

Table 3-7: Emission lifetime data of $(L)Ru^{II}(R\text{-bpy})_2$ at room temperature.[a]

Compound	Solvent	τ_1, ns (α_1, %)	τ_2, ns (α_2, %)	τ_3, ns (α_2, %)	$<\tau>$ [b] ns	χ^{2} [c]	τ_{TA} [d] ns
Ru-1-COOEt	CH_3CN	1700 (100)	–	–	1700	1.3	1700
	CH_2Cl_2	445 (3)	2450 (97)	–	2580	1.2	–
Ru-1-CF$_3$	CH_3CN	1100 (100)	–	–	1100	1.2	960
	CH_2Cl_2	221 (39)	502 (37)	1460 (24)	620	1.5	–
Ru-2-CF$_3$	CH_3CN	800 (15)	3600 (85)	–	3180	1.1	3400
	CH_2Cl_2	8.5 (16)	584 (21)	3150 (63)	2108	1.2	1240

[a] 405 nm Excitation. Decays were recorded at 650 nm. Samples were argon bubble degassed. Lifetime and relative biexponential fits were performed with equation 2-2. [b] The mean decay lifetime ,$<\tau>$, was calculated using the multiexponential decay data according to the equation 2-3. [c] χ^{2} is used to evaluate the quality of the calculated fit. χ^{2} =1 means the best fit. [d] Decay lifetimes of transient absorption.

148

This solvent-induced excited-state quenching also happens to [(bpy)Re^I(CO)$_3$DMABN]$^+$ complex (where DMABN = 4-(dimethylamino)benzonitrile).[111] Strong dπ(Re) → π^* (bpy) MLCT emission is observed in CH$_2$Cl$_2$, but not in CH$_3$CN. The MLCT quenching process is attributed to the presence of a ligand-to-ligand charge-transfer state in the excited-state manifold. From electrochemical data, ligand **2** is easier to be oxidized than Ru^{II} metal center and **tfmb** is a strong electron acceptor. It is possible that ligand-to-ligand charge-transfer (LLCT) state, *[(2^{+})Ru^{II}(tfmb$^-$)]$^{2+}$, can be introduced into the excited-state manifold.

The energy of the LLCT excited state (E$_{LLCT}$) can be estimated for these complexes by the following equation 3-1:[112]

$$E_{LLCT} = E_{1/2}(2^+) - E_{1/2}(tfmb^-) - 14.45/\varepsilon R_{DA} \qquad 3\text{-}1$$

In equation 3-1, E$_{1/2}$(2$^+$) is the oxidation potential of the ligand **2** and E$_{1/2}$(tfmb$^-$) is the reduction potential of the **tfmb** ligand. The last term represents the Coulombic stabilization energy of the LLCT excited state that results from interaction of the electron and hole at separation distance R$_{DA}$ (in angstrom units) in a solvent of dielectric constant ε. The first two terms in equation 3-1 are available from electrochemical measurements. The last term is estimated by using the respective dielectric constants and taking R$_{DA}$ = 5.0 Å.[112] Table 3-8 lists calculated values of E$_{LLCT}$ for the **Ru-2-CF$_3$** complex in CH$_3$CN and CH$_2$Cl$_2$ solutions. It is clear that the energy of this state in CH$_2$Cl$_2$ is much lower than the energy in CH$_3$CN and is comparable to the energy of the lowest MLCT state.

Table 3-8: Estimated energies for the LLCT state for **Ru-2-CF₃**.[a]

Complex	E_{LLCT} CH_3CN	E_{LLCT} CH_2Cl_2	E_{MLCT} CH_3CN	E_{MLCT} CH_2Cl_2
Ru-2-CF₃	2.21	1.99	1.88	_

[a] Energies in eV calculated by using equation 3-1.

The red-shifted band observed for **Ru-2-CF₃** in CH_2Cl_2 can be assigned to emission from the LLCT state. The new short-lived emission lifetime component (8.5 ns (16%) which is close to the lifetime of LLCT state in [(bpy)Re^I(CO)₃DMABN]$^+$ complex[111] is due to the LLCT excited state.

To gain more insight into this LLCT excited state, the transient absorption spectra of **Ru-2-CF₃** was recorded in CH_2Cl_2 and shown in Figure 3-31. It still features the bleaching of the ground state absorption bands in the 300 – 500 nm region. However, the absorption band is different from that in CH_3CN. It exhibits a strong absorbance around 580 nm, and a second broad absorption band that extends into the near-IR. This strong absorption band is probably due to the absorption of oxidized ligand 2. Excited state lifetime obtained from factor analysis and global decay fitting is around 1.2 μs (Table 3-7) which is much short than that in CH_3CN.
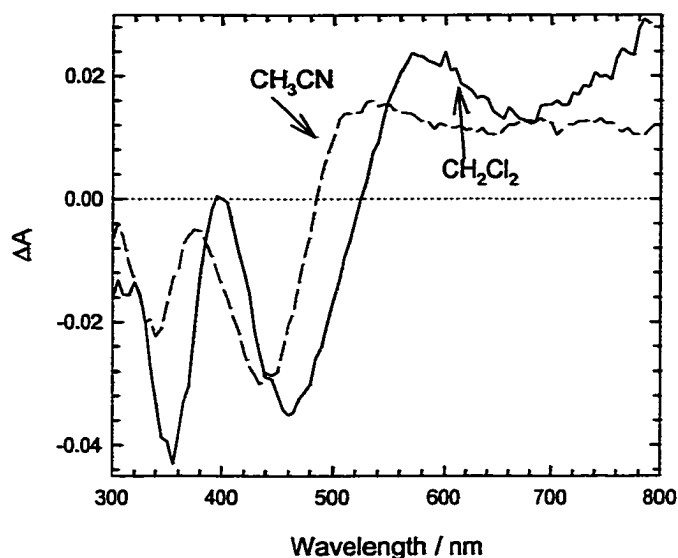
Figure 3-31: Transient absorption difference following 355 nm pulsed laser excitation (5 mJ dose) for **Ru-2-CF$_3$** acquired from argon bubble degassed solution. CH$_3$CN (dash line), CH$_2$Cl$_2$ (solid line).

For **Ru-2-CF$_3$**, we conclude that energy level of three states, $d\pi$(Ru) $\rightarrow$ π*(2),

$d\pi$(Ru) $\rightarrow$ π*(**tfmb**), and π $\rightarrow$ π*(**2**) are all very close in energy. And which state is

dominant dependents on the solvent and temperature. Figure 3-32 shows the general

energy diagram of **Ru-2-CF$_3$**. It is hard to calculate the relative energy of each MLCT

state because $d\pi$(Ru) $\rightarrow$ π*(**2**) and $d\pi$(Ru) $\rightarrow$ π*(**tfmb**) are mixed together. The energy

of ^{3}MLCT was estimated based on the emission in CH$_3$CN at room temperature. We

estimate the $^3\pi,\pi$* lies in 1.90 eV which is approximated from the triplet quenching

experiments. Based on the absorption spectra, we estimated that $^1\pi,\pi$* state lies in the

2.71 eV. The ^{1}MLCT is estimated based on the absorption spectra of the parent complex,

Ru(tfmb)$_3$$^{2+}$ (λ_{max} $\approx$ 455 nm), we estimate that the ^{1}MLCT states lie at approximately

2.72 eV.

Photoexcitation initially affords $^1\pi,\pi^*$ states, followed by relaxation to ^{3}MLCT

state, $*[(2)Ru^{III}(R\text{-bpy}^-)]^{2+}$. The interconversion between ^{3}MLCT, LLCT and $^3\pi,\pi^*$

depends on the medium. The photoluminescence of ^{3}MLCT can be observed and the

LLCT state is nonluminescent and it apparently decays back to the ground state via

ligand charge recombination (Figure 3-32).
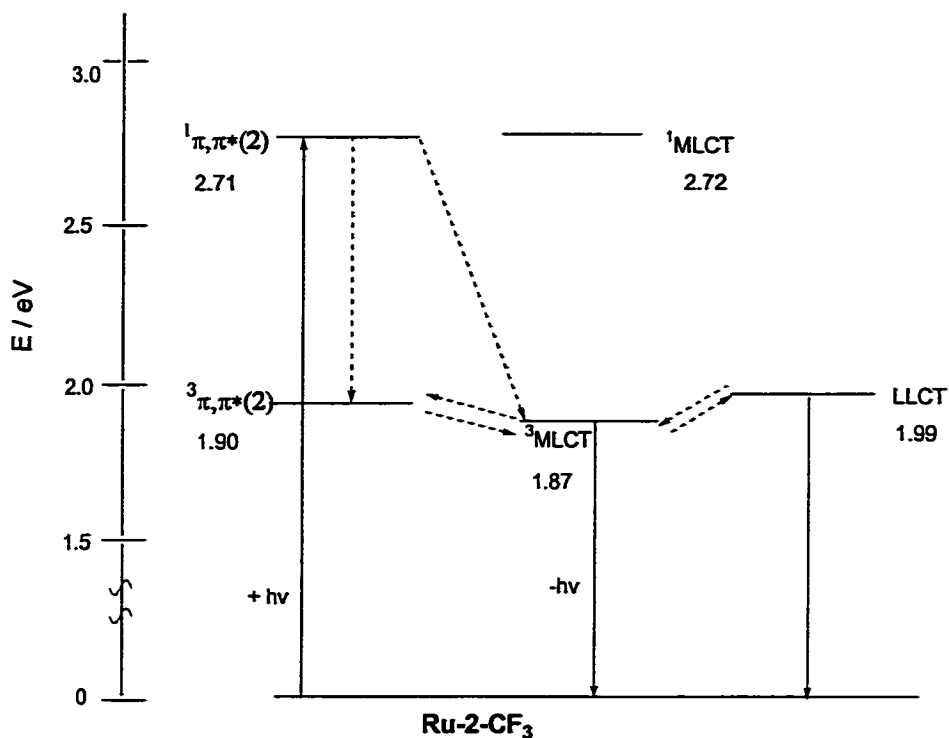
Figure 3-32: Energy level diagram of **Ru-2-CF₃**.

<u>Energy Gap Correlation</u>

Plots of $\ln k_{nr}$ vs E_0 for **(L)Ru^{II}(R-bpy)₂** complexes using data from 80 to 298 K

are shown in Figure 3-33. It is clear that for **Ru-1-COOEt** and **Ru-1-CF₃** the energy gap

law behavior is observed through glass to fluid transition temperature. Slopes and

intercepts obtained from least-squares fits of the data are shown in Table 3-9. The

increase in slope for **Ru-1-CF₃** is probably due to more involvement of $d\pi \to \pi^*(1)$ in

the $d\pi \to \pi^*$(**tfmb**) excited state. For **Ru-2-CF₃**, the presence of low-lying MLCT states

suggests a thermally activated MLCT $\to$ dd transition is not adequate to account for the

exception of energy gap law. This probably arises from an additional decay channel

involving the population and decay of an additional MLCT state and $^3\pi,\pi^*$ state.

Table 3-9: Slopes and intercepts obtained from plots of $\ln k_{nr}$ vs. E_0.

complex	Variation made	Temperature Range / K	solvent	slope $1/cm^{-1} \times 10^3$	intercept
Ru-1	glass/fluid	80 - 298	E/M	-1.40	34.8
Ru-1-COOEt	glass/fluid	80 - 298	E/M	-1.19	31.5
Ru-1-CF₃	glass/fluid	80 - 298	E/M	-1.83	42.0

Excited-State Energetics and Interconversion in (L)Os^{II}(bpy)₂ Complexes

On the basis of the luminescence and transient absorption spectroscopy, the

excited-state scheme for osmium complexes is outlined in the Jablonski digram on the

Figure 3-34. Thus, near-UV and visible excitation of the complexes affords the $^1\pi,\pi^*$

state of the PPE backbone. This state rapidly relaxes to the Os $\to$ oligomer MLCT state,

which is the lowest excited state of the complexes. The MLCT state then relaxes by

normal radiative and nonradiative decay pathways, giving rise to the luminescence

spectrum and lifetime that are typical for the Os(bpy)₃ chromophore.
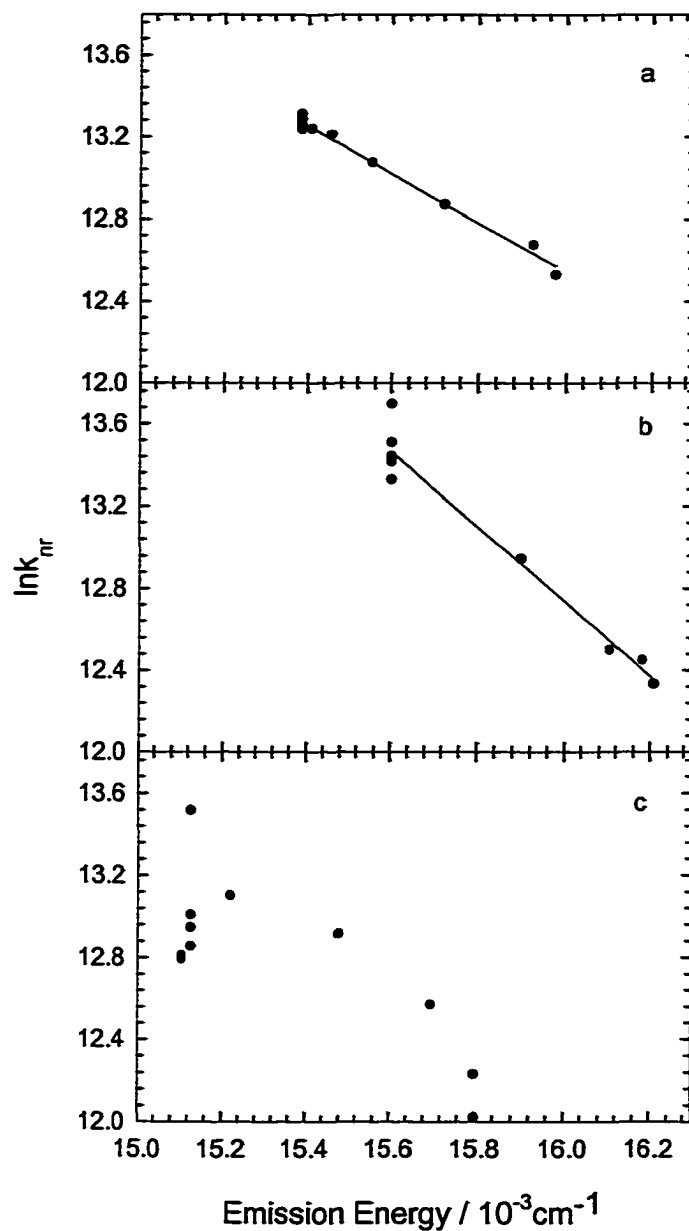
Figure 3-33: Energy gap law plots ($\ln k_{nr}$ vs. E_0) over the temperature range 80 to 298 K of $(L)Ru^{II}(R\text{-bpy})_2$ in 4:1 (v/v) EtOH/MeOH solvents. (a) **Ru-1-CF$_3$**; (b) **Ru-1-COOEt**; (c) **Ru-2-CF$_3$**.
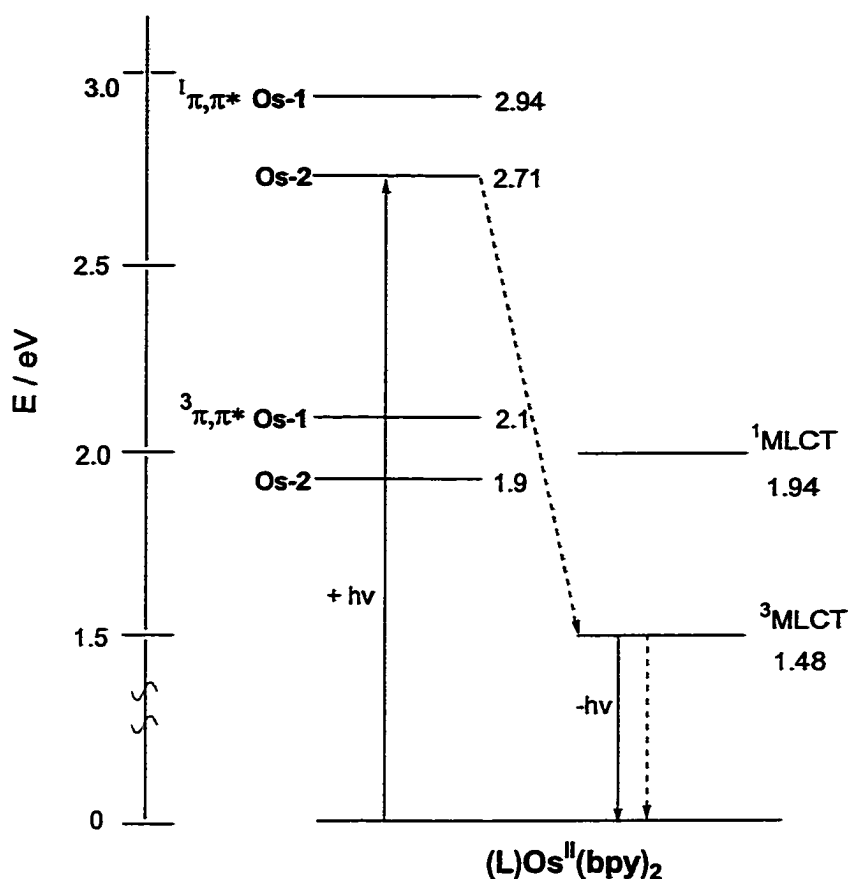
Figure 3-34: (L)Os^{II}(bpy)$_2$complexes Jablonski diagram.

Experimental

Photophysical Measurements

All room temperature studies were conducted in CH_3CN or CH_2Cl_2 and low

temperature studies were conducted in either 4:1 (v/v) EtOH/MeOH or 2-MTHF. All

solvents were distilled according to typical laboratory practices. All photophysical studies

were conducted with the same instrumentation and techniques described in chapter 2.

Fluorescence spectra were measured on a SPEX Fluorolog-2 or on a spectrometer

consisting of an ISA-SPEX Triax 180 spectrograph equipped with a LN2 cooled CCD

detector (Hamamatsu CCD, 1024 x 64 pixels).

Emission Quantum Yield

Emission quantum yields were determined at room temperature in CH_3CN using

samples of known optical density, compared to a standard sample of $[Os(bpy)_3](PF_6)_2$ in

CH_3CN for which $\phi_{em} = 0.005$.[106] Quantum yield values were calculated by using

equation 2-10.

Electrochemical Measurements

All electrochemical measurements were conducted on CH_3CN solutions with

TBAH as the supporting electrolyte. Cyclic voltammetry measurements were performed

with the same procedures on the same instrumentation described in chapter 2.

Spectroelectrochemical Measurements

Electronic spectra of electrogenerated oxidized or reduced species were recorded

using an H-cell, a modification of a literature reported cell. The working compartment

was a 1 cm glass cuvette and contained the analyte in 0.1 M TBAH in CH_3CN, a

platinum mesh working electrode, and a Ag reference electrode. The other compartment

of the H-cell contained a platinum mesh auxiliary electrode and 0.1 M TBAH in CH_3CN.

The two compartments are separated by a fine porosity glass frit. The working

compartment was bubbled with nitrogen for 10 min prior to and during each experiment.

The potential was controlled using a BAS CV-27 electrochemical analyzer. The analyte

was electrochemically oxidized or reduced and the redox process monitored by UV-vis

spectroscopy. The measurements were conducted on HP 8452A diode-array or Varian

Cary 100 dual-beam spectrophotometer. All processes gave clean isosbestic points. The

oxidation or reduction was considered complete when there was no further change in the

UV-vis spectra. After the completion of the bulk electrolysis, the complex was returned electrochemically to its parent charge to determine the reversibility of the oxidation or reduction process.

General Synthetic

Diisopropylamine was distilled from KOH and tetrahydrofuran was distilled from sodium benzophenone ketyl and stored under nitrogen. The synthesis of oligomer **1** and **2** and compound **16** and **18** are described in chapter 2. Copper(I) iodide, Pd(PPh$_3$)$_4$, 4,4-diiodobiphenyl, 4-bromobiphenyl, RuCl$_3$·3H$_2$O, (NH$_4$)$_2$OsCl$_6$ and 4,4-dimethyl-2,2'-bipyridine were purchased from Aldrich Chemical Co. and used without further purification. *cis*-**Ru(tfmb)$_2$Cl$_2$** was donated by Prof. M. Furue of Fukuoka University. All cross-coupling reactions using Pd catalyst were carried out under standard Schlenk and vacuum line techniques. ^{1}H and ^{13}C NMR was recorded on Gemini-300 and VXR-300 NMR spectrometers. High-resolution mass spectrometry was performed by the University of Florida analytical service. The matrix used for MALDI analysis is α-cyanohydroxycinnamic acid in THF solvent.

Synthesis

Metal-Organic Oligomer **Ru-1-CF$_3$**

cis-**Ru(tfmb)$_2$Cl$_2$** (22.0 mg, 0.0428 mmol) and 1 equivalent of **1** (15.0 mg, 0.04 mmol) were dissolved in 5 mL of ethylene glycol and 2 mL of 2-methoxyethanol and the solution was refluxed under N$_2$ for 24 hr. During the course of reaction the color of solution changes from purple to brown-red and the blue fluorescence characteristic of **1** disappeared. The reaction was monitored by TLC (silica, CH$_2$Cl$_2$-CH$_3$CN 5:1 v:v) and heating was discontinued when the yellow fluorescent spot due to **1** disappeared. The

solution was allowed to cool to room temperature. Upon addition of 5 mL of saturated NH$_4$PF$_6$ aqueous solution, the red PF$_6^-$ salt of the complex precipitated. The crude product was collected by centrifuge. Then it was dissolved in 50 mL of dichloromethane and washed with 50 mL of water to remove the residual high boiling point ethylene glycol and 2-methoxyethanol solvents. The organic phase was dried over MgSO$_4$ and removed under vacuum to yield red solid. The product was further purified by rinsing with Et$_2$O remove traces of unreacted oligomer 1 and then it was dried in vacuum to yield 32 mg of **Ru-1-CF$_3$** (52%). ^{1}H-NMR (300 MHz, CD$_3$CN) 3.51 (s, 6H), 3.53 (s, 6H), 6.68 (m, 6H), 7.5 (m, 6H), 7.7 (d, 2H), 7.75 (d, 2H), 7.92 (d, 2H), 8.26 (d, 2H), 8.58 (d, 2H). ^{13}C-NMR (75.4 MHz, CD$_3$CN) 56.2, 56.6, 87.5, 94.8, 111.3, 113.3, 118.8, 122.5, 124.8, 125.4, 138.8, 141/3, 153.9, 154.5, 154.8, 155.3, 155.5, 158.4. FAB-MS Calculated for C$_{54}$H$_{35}$F$_{12}$N$_6$O$_4$Ru (M-2PF$_6$)1161.1565, found 1161.1579.

Ru-2-C7-I-CF$_3$

Compound **16** (40 mg, 0.0376 mmol) and 1 equivalent of *cis*-**Ru(tfmb)$_2$Cl$_2$** (29 mg, 0.038 mmol) were dissolved in 10 mL of ethylene glycol and 5 mL of 2-methoxyethanol and the solution was refluxed for 5 days. During the course of reaction the blue-green fluorescence characteristic of **16** disappeared. The reaction was monitored by TLC (silica, CH$_2$Cl$_2$-CH$_3$CN 5:1 v:v) and heating was discontinued when the yellow fluorescent spot due to **16** disappeared. The solution was cooled to room temperature and the reaction mixture was filtered through a frit to remove impurities. Upon addition of 5 mL of saturated NH$_4$PF$_6$ aqueous solution, the red PF$_6^-$ salt of the complex precipitated. The crude product was collected by centrifugation. Then it was dissolved in 50 mL of dichloromethane and washed with 50 mL of water to remove residual high boiling point ethylene glycol and 2-methoxyethanol solvents. The organic phase was dried over

MgSO$_4$ and removed under vacuum to yield a red-brown solid. The product was further

purified by rinsing with Et$_2$O and dried in vacuum to yield 30 mg of **Ru-2-C7-I-CF$_3$**

(39%). ^{1}H-NMR (300 MHz, CD$_3$COCD$_3$) δ 0.9 (m, 12H), 1.4 (br m, 32H), 1.8 (br m,

8H), 3.95 (t, 4H), 4.1 (t, 4H), 6.85 (s, 2H), 7.5 (s, 2H), 7.85 (d, 2H), 7.95 (d, 2H), 8.20 (s,

2H), 8.35 (d, 2H), 8.62 (d, 4H), 8.90 (d, 2H), 9.50 (s, 4H). ^{13}C-NMR (75.4 MHz,

CD$_3$COCD$_3$) δ 14.8, 23.7, 23.8, 27.0, 27.3, 33.0, 70.1, 89.2, 90.7, 94.7, 111.9, 116.2,

122.5, 124.8, 125.2, 139.8, 141.5, 152.5, 154.5, 155.0, 155.2, 155.8, 158.9. MALDI-MS

calculated for C$_{78}$H$_{82}$F$_{12}$I$_2$N$_6$O$_4$Ru (M-2PF$_6$)1750.38, found 1750.08.

Ru-2-CF$_3$

Compound **Ru-2-CF$_3$-I** (25.6 mg , 0.012 mmol), 2 equivalents of compound **18**

(4.2 mg), THF (10 mL) and diisopropylamine (8 mL) were combined in a Schlenk flask

which was then degassed with argon for 0.5 hr. Pd(PPh$_3$)$_2$Cl$_2$ (0.4 mg , 0.006 mmol) and

CuI (0.2 mg , 0.012 mmol) were added to Schlenk flask. The resulting solution was

heated at 70°C for 12 hr. The solution was allowed to cool to room temperature and the

solvent removed under vacuum. The crude product was dissolved in 50 mL of

chloroform. The combined organic phase was washed with NH$_4$OH (50%), H$_2$O and

dried over over MgSO$_4$. The solvent was removed under vacuum to yield a red-orange

solid. The complex was reprecipitated by dissolving it in a minimum amount of

dichloromethane and adding the solution dropwise to 30 mL of Et$_2$O under stirring. The

product was collected by centrifugation and washed with Et$_2$O and dried in vacuum to

yield 10 mg of **Ru-2-CF$_3$** (50%). ^{1}H-NMR (300 MHz, CD$_3$COCD$_3$) δ 0.9 (m, 12H), 1.4

(br m, 32H), 1.8 (br m, 8H), 3.95 (t, 4H), 4.08 (t, 4H), 6.89 (s, 2H), 7.16 (s, 2H), 7.40 (t,

2H), 7.46 (t, 4H), 7.60 (d, 4H), 7.69 (m, 8H), 7.90 (d, 4H), 8.20 (s, 2H), 8.28 (d, 2H),

8.62 (m, 4H), 8.92 (d, 2H), 9.42 (s, 4H). ^{13}C-NMR (75.4 MHz, CD$_3$COCD$_3$) δ 14.3,

14.9, 23.2, 26.6, 26.7, 31.5, 66.0, 69.9, 87.1, 95.1, 96.4, 116.8, 117.5, 122.7, 124.9, 125.7, 127.6, 127.8, 128.7, 129.8, 132.7, 140.6, 141.5, 154.3, 154.7, 155.2, 155.3, 155.9, 159.2 ESM-MS calculated for $C_{106}H_{100}F_{12}N_6O_4Ru$ (M-2PF$_6$) 1850.67, found 1850.64.

Compound 26

To a solution of potassium permanganate (55.0 g, 0.35 mol) in water (950 mL), 4,4'-dimethyl-2,2'-bipyridine (4.0 g, 21.7 mmol) is added and heated to reflux until the solution becomes colorless (about 4 hr). After filtering off the precipitated manganese dioxide, the solution is extracted with three 200 mL portions of diethyl ether to remove any unreacted 4,4-dimethyl-2,2'-bipyridine. Concentrated hydrochloric acid is added to the aqueous phase until acidic to precipitate an insoluble white powder which is collected by filtration. Yield for the crude 2,2'-bipyridine-4,4'-dicarboxylic acid after drying is 5.1 g (39%).

Compound 27

2,2'-bipyridine-4,4'-dicarboxylic acid (1.0 g, 4.1 mmol) is refluxed with 10 mL of concentrated sulfuric acid in 25 mL of absolute ethanol for 10 hr. The solution is cooled and poured over ice (about 40 g) followed by neutralization with 25% NaOH (~ 10 g). Upon neutralization the solution turns light pink and a white bulky precipitate forms which is collected by filtration, washed with H_2O and dried under vacuum. Recrystallizing once from 95% ethanol and drying under vacuum yields 0.35 g of white crystal 350 mg (35%). ^{1}HNMR (300 MHz, CDCl$_3$) δ 1.45 (t, 6H), 4.46 (q, 4H), 7.91 (d, 2H), 8.87 (d, 2H), 8.95 (s, 2H). mp = 158.5°– 160.5°, Lit – 159° –160.5°.

cis-Ru(decb)$_2$Cl$_2$

RuCl$_3$· 3H$_2$O (102 mg, 0.49 mmol) and **decb** (298 mg, 0.99 mmol) are refluxed in 60 mL of DMF for 3 hr. The volume is reduced to 10 mL under vacuum at 100°C.

Acetone is added while hot, and the flask is capped and stored at 0°C for 8 hr. Black

crystals are collected by filtration, recrystallized from dichloromethane / acetonitrile, and

dried under vacuum, yielding 300 mg of product (40%). ^{1}H-NMR (300 MHz, CDCl$_3$) δ

1.4 (t, 6H), 1.5 (t, 6H), 4.4 (q, 4H), 4.6 (q, 4H), 7.5 (d, 2H), 7.7 (d, 2H), 8.2 (d, 2H), 8.7

(s, 5H), 8.82 (s, 2H). 10.5 (d, 2H).

Ru-1-COOEt

cis-**Ru(decb)$_2$Cl$_2$** (33 mg, 0.042 mmol) and 1 equivalent of **1** (20 mg, 0.042

mmol) were dissolved in 20 mL of 95% (v/v) EtOH/Acetone and refluxed under nitrogen

for 4 days. During the course of reaction, 5 mL of 2-methoxyethanol is added and the

color of the solution changed from purple to red yellow and the blue fluorescence

characteristic of **1** disappeared. The solution was allowed to cool to room temperature

and the ethanol was removed by vacuum. Upon addition of 5 mL of saturated NH$_4$PF$_6$

aqueous solution to the reaction mixture, the red PF$_6$⁻ salt of the complex precipitated.

The crude product was collected by centrifugation and washed with H$_2$O to remove traces

of high boiling point 2-methoxyethanol solvent. The complex was reprecipitated by

dissolving it in a minimum amount of acetone and adding the solution dropwise to 30 mL

of Et$_2$O under stirring. The product was collected by centrifuge and repeatedly with Et$_2$O

to get rid of the traces of ligand **1**. The product was dried in vacuum to yield 23 mg of

Ru-1-COOEt (50%). ^{1}H-NMR (300 MHz, CD$_3$COCD$_3$) δ 1.4 (m, 12H), 3.77 (s, 6H),

3.79 (s, 6H), 4.5 (m, 8H), 6.84 (s, 2H), 7.04 (br s, 4H), 7.94 (d, 2H), 8.05 (d, 2H), 8.13 (s,

2H), 8.35 (d, 2H), 8.38 (d, 2H), 8.90 (d, 2H), 9.35 (s, 4H). ^{13}C-NMR (75.4 MHz,

CD$_3$COCD$_3$) δ 14.3, 56.0, 56.5, 63.3, 88.5, 94.5, 113.3, 118.0, 118.7, 124.8, 124.9, 125.4,

125.6, 127.7, 140.2, 141.3, 154.1, 154.3, 155.6, 155.8, 158.5, 158.8, 164.0. MALDI-MS calculated for $C_{62}H_{56}N_6O_{12}Ru$ (M-2PF$_6$)1178.3, found 1178.5.

cis-Os(bpy)$_2$Cl$_2$

(NH$_4$)$_2$OsCl$_6$ (100 mg, 0.22 mmol) and 2,2'-bypyridine (72 mg, 0.45 mmol) were combined in 5 mL of ethylene glycol and refluxed for 2.5 hr under N$_2$. During the course of the reaction, the color of the solution changed from red to red-brown. Since the crude reaction mixture contains Os(bpy)$_2$Cl$_2$ and Os(bpy)$_2$Cl$_2^+$, upon cooling 5 mL of saturated aqueous Na$_2$S$_2$O$_4$ (Sodium hydrosulfite) was added to the reaction mixture to reduce Os(bpy)$_2$Cl$_2^+$ and Os(bpy)$_2$Cl$_2$ was precipitated as a purple-black solid. The mixture was allowed to cool at 0°C for 0.5 hr. The black precipitate was collected and washed copiously with water and diethyl ether. The product was dried in vacuum to yield 120 mg of Os(bpy)$_2$Cl$_2$ (92%). ^{1}H-NMR (300 MHz, CD$_3$Cl$_3$) δ 6.62 (t, 2H), 7.18 (t, 2H), 7.44 (m, 6H), 7.92 (d, 2H), 8.18 (d, 2H), 10.1 (d, 2H).

Os-1

cis-Os(bpy)$_2$Cl$_2$ (40 mg, 0.07 mmol) and 1 equivalent of oligomer 1 (32 mg, 0.07 mmol) were dissolved in 7 mL of ethylene glycol and refluxed under nitrogen for 30 hr. During the course of the reaction, the blue luminescence characteristic of 1 disappeared completely. The solution was cooled to room temperature. Upon addition of 10 mL of saturated aqueous NH$_4$PF$_6$ solution, the dark-green colored PF$_6^-$ salt of the complex precipitated. The product was collected and washed with H$_2$O to remove ethylene glycol and unreacted cis-Os(bpy)$_2$Cl$_2$. The complex was reprecipitated by dissolving it in a minimum amount of dichloromethane and adding the solution dropwise to 30 mL of Et$_2$O under stirring. The product was collect by filtration and washed with excess Et$_2$O to remove unreacted free ligand 1. Yield: 80 mg (91%). ^{1}H-NMR (300 MHz, CD$_3$CN) δ

3.71 (s, 6H), 3.75 (s, 6H), 6.95 (br m, 6H), 7.36 (t, 4H), 7.65 (br d, 6H), 7.88 (br m, 6H), 8.47 (br m, 6H). ^{13}C-NMR (75.4 MHz, CD$_3$CN) δ 57.1, 57.6, 89.0, 95.5, 112.2, 114.2, 119.6, 126.1, 126.2, 126.3, 129.7, 129.8, 139.1, 140.2, 152.5, 153.0, 154.0, 154.9, 156.5, 159.3, 160.4. HRFAB-MS, calculated for C$_{50}$H$_{40}$N$_6$O$_4$Os (M-2PF$_6$) 980.2725, found 980.2728.

Os-2-C7-I

Compound **16** (43 mg, 0.043 mmol) and **Os(bpy)$_2$Cl$_2$** (25.3 mg, 0.044 mmol) were combined in 5 mL of 2-methoxyethanol and 10 mL of ethylene glycol and the solution refluxed under N$_2$ for 3 days. During the course of the reaction, 2-methoxyethanol was added from time to time to prevent the reaction from evaporating to dryness. During the course of the reaction the blue-green fluorescence characteristic of **16** almost disappeared. The reaction mixture was allowed to cool to room temperature. Upon addition of 10 mL of saturated aqueous NH$_4$PF$_6$ solution, the dark-green colored PF$_6^-$ salt of the complex precipitated. The product was collected and washed with H$_2$O to remove ethylene glycol and unreacted cis-**Os(bpy)$_2$Cl$_2$**. The complex was reprecipitated by dissolving it in a minimum amount of dichloromethane and adding the solution dropwise to 30 mL of Et$_2$O under stirring. The product was collect by filtration and washed with excess Et$_2$O to remove unreacted free ligand **16**. Yield: 50 mg (68%). ^{1}H-NMR (300 MHz, CD$_3$CN) 0.85 (br t, 12H), 1.25 (br s, 24H) 1.45 (br m, 8H), 1.75 (br m, 8H), 3.9 (br t, 8H), 6.86 (s, 2H), 7.25 (s, 2H), 7.42 (br m, 4H), 7.62 (br m, 4H), 7.80 (br m, 8H), 8.38 (br m, 8H). FAB-MS calculated for C$_{45}$H$_{56}$N$_2$O$_3$I$_2$Os (M-2PF$_6$), 926.24, found 926.3.

Os-2

Compound **Os-2-C7-I** (44 mg, 0.024 mmol), 2 equivalents of compound **18** (12 mg, 0.048 mmol), THF (10 mL) and diisopropylamine (8 mL) were combined in a Schlenk flask which was then degassed with argon for 0.5 hr. $Pd(PPh_3)_2Cl_2$ (0.85 mg, 0.0012 mmol) and CuI (0.45 mg, 0.0024 mmol) were added to the Schlenk flask. The resulting solution was heated at 70°C for 12 hr. The solution was allowed to cool to room temperature and the solvent removed under vacuum. The crude product was dissolved in 50 mL of chloroform. The combined organic phase was washed with aqueous NH_4OH (50%), H_2O and dried over over $MgSO_4$. The solvent was removed under vacuum to yield a red-orange solid. The complex was reprecipitated by dissolving it in a minimum amount of dichloromethane and adding the solution dropwise to 30 mL of Et_2O under stirring. The product was collected by centrifugation and washed with Et_2O and hexane. The material was purified by chromatography on a small activated alumna column packed in toluene. The solid was dissolved in a minimum of the CH_3CN and dry packed on onto the column. Upon elution with the 100:3 toluene/CH_3CN, a strong fluorescent impurity band was eluted. After removal of the impurity, the desired product was eluted by changing the eluant to 9:3 toluene/CH_3CN. The dark green band was collected and taken to dryness by rotary evaporation. Yield: 20 mg (42%). ^{1}H-NMR (300 MHz, $CDCl_3$) δ 0.85 (br t, 12H), 1.30 (br s, 24H), 1.58 (br m, 8H), 1.85 (br m, 8H), 3.98 (br t, 8H), 6.98 (s, 4H), 7.38 (br t, 2H), 7.48 (br t, 8H), 7.60 (br m, 18H), 7.90 (br m, 6H), 8.40 (br m, 6H). ^{13}C-NMR (75.4 MHz, $CDCl_3$) δ 14.1, 22.6, 25.8, 28.9, 29.7, 31.8, 69.3, 69.6, 86.7, 88.8, 96.0, 96.4, 110.5, 116.2, 116.4, 117.1, 122.2, 124.1, 124.6, 125.0, 125.7, 127.0, 127.9, 128.9, 130.1, 132.1, 138.0, 139.5, 140.7, 141.2, 150.8, 151.1, 152.5, 153.2,

153.8, 157.0, 157.8, 158.3. MALDI-MS calculated for $C_{102}H_{104}N_6O_4Os$ (M-2PF$_6$),

1668.7, found 1668.67.

CHAPTER 4
SYNTHESIS AND PHOTOPHYSICS OF 5,5'-BIPHENYL OLIGOMERS THAT CONTAIN Re(CO)₃ MOIETY

Introduction

After extensive photophysical work with ruthenium and osmium complexes,

another important family of luminescent complexes that contain rhenium

$[(b)Re^I(CO)_3Cl]^+$ (where b is a bidentate diimine ligand) were considered. From the

synthetic point of view, the Re^I-based complexes offer several advantages. These include

the ease of exchange of Cl⁻ for other ligands and the ability to incorporate substituted

pyridine ligands. Substituted pyridine ligands may not only shift the energy of the MLCT

state, but they can also act as an oxidative or reductive quencher, thereby providing a tool

to "tune" the photophysical properties. When Cl⁻ is replaced by electron-acceptor or

electron-donor, this complex is called chromophore-quencher (C-Q) molecule. The

electronically excited state of the $(b)Re^I(CO)_3$ chromophore can be quenched by

intramolecular electron transfer (ET). For example, Meyer and co-workers have studied

the photophysical properties of $[(bpy)Re^I(CO)_3(MQ^+)]^{2+}$ complex (MQ^+ = N-methyl-

4,4'-bipyridinium cation).[113] They found that MLCT emission from dπ(Re) → π*(bpy)

was quenched at room temperature and a weak new emission appeared at lower energies

from the dπ(Re) → π*(MQ^+) MLCT state. Continued research[114] on

$[(dmb)Re^I(CO)_3(MQ^+)]^{2+}$ (dmb = 4,4'-dimethyl-2,2'-bipyridine), showed that excitation

of the molecule produces a mixture of dπ(Re) → π*(bpy) and dπ(Re) → π*(MQ^+)

166

MLCT states (Figure 4-1, route 1 and 2). The dπ(Re) → π*(bpy) MLCT state undergoes a **bpy⁻** → **MQ⁺** interligand electron transfer to produce a relatively long-lived dπ(Re) → π*(MQ⁺) MLCT excited state (Figure 4-1, route 3).
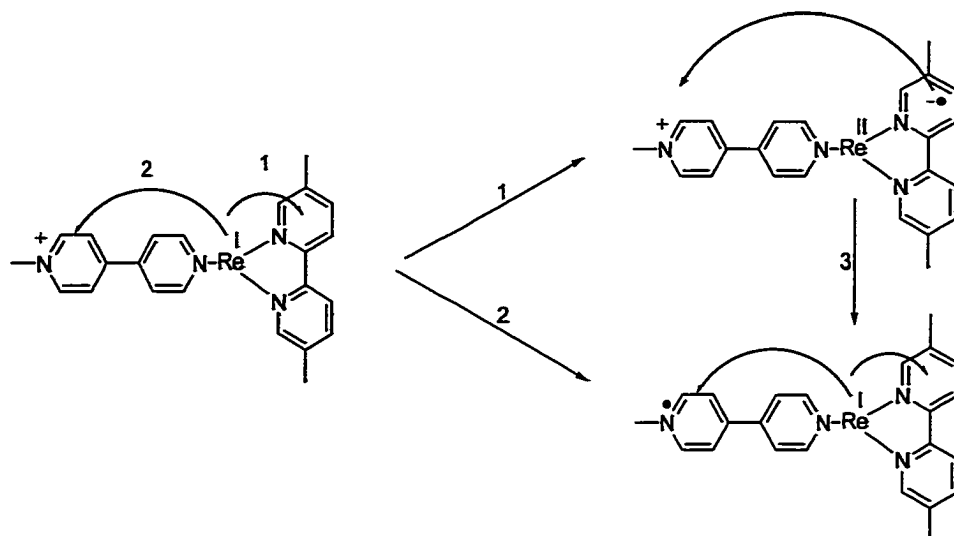
Figure 4-1: Photoinduced intraligand ET in **[(MQ⁺)Re(CO)₃(dmb)]²⁺** complex (Ref.114).

The driving force (ΔG) of this intramolecular ET depends on the relative energy level of two charge transfer (CT) states which are determined by the reduction potentials of the acceptor ligand. The relative reduction potentials of electron acceptor sites can be controlled by substituent changes at **bpy**. Meyer's group have tested the role of ΔG on intramolecular ET by turning to the bpy-modified CQ complexes, [(4,4'-(X)₂-bpy)Reᴵ(CO)₃(MQ⁺)]²⁺ (X = COOEt, NH₂).[115] The electron-donating –NH₂ groups increase the energy of the lowest π*(bpy) level and the electron-withdrawing ester groups lower the energy. ΔG for intramolecular quenching is - 0.1 eV for X = COOEt, -0.49 eV for X = H, and -1.0 eV for X = NH₂. For the diester complex, a fairly intense MLCT emission that arises mainly from the bpy-ester-based state is observed. It is clear

that very little intramolecular ET quenching occurs during the lifetime of the MLCT excited state. For the amino complex MLCT emission is completely quenched in solution at room temperature and quenching still occurs in the glass at 77 K. The emission that does occur from the CQ complex at 77 K arises from MQ^+ -based state.

Based on above idea, a new intramolecular CQ complex $[(2)Re^I(CO)_3(MQ^+)]$ was prepared. The reduction potential of MQ^+ is at -0.96 V which has lower reduction potential than oligomer 2. By introduction of this electron acceptor into the molecule, we hope to see how the photophysical properties were affected. The structures of this complex and related model complexes are illustrated in Figure 4-2. In this chapter the synthesis of $[(2)Re^I(CO)_3(MQ^+)]$ and model complexes is presented as well as their optical properties.

Re-2

Re-2-MQ

(PF$_6$)$_2$

Re-2-Py

(PF$_6$)

Re-2-bpy-Re-2

(PF$_6$)$_2$
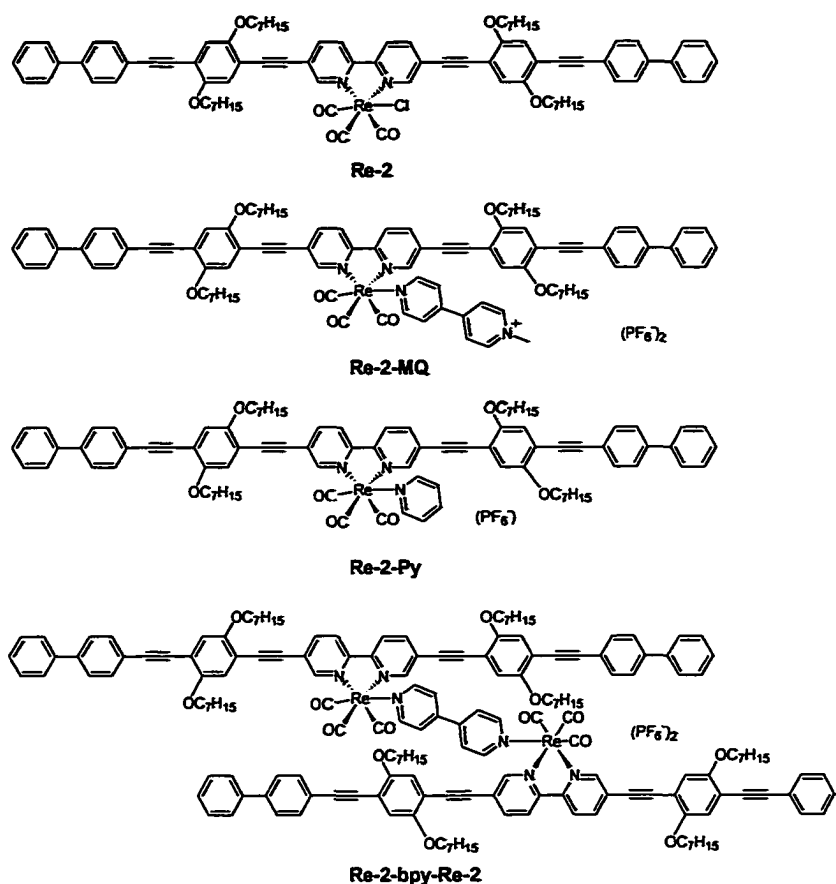
Figure 4-2: Structures of [(2)Re^I(CO)$_3$(X)] complexes.

Synthesis

In developing a synthetic methodology for the **Re-2-MQ** complex a number of strategies were investigated. The four synthetic strategies applied for the synthesis of **Re-2-MQ** complex are summarized in Figure 4-3 to 4-6. Route I is similar to our previous synthesis method for preparing for ruthenium complexes (Figure 4-3). The central core, **[(bpy-Br)Re^I(CO)$_3$(MQ$^+$)]**, was made first, followed by coupling reaction to endcapping group A.
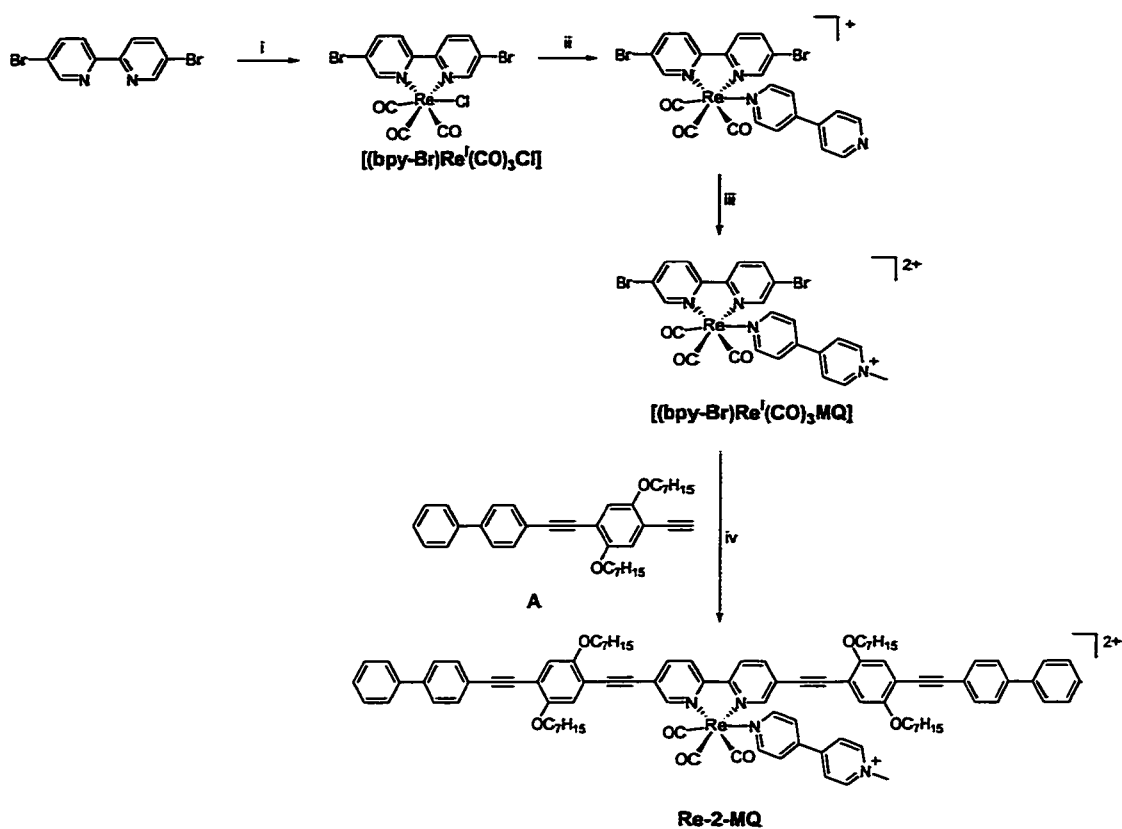
i. Re(CO)$_5$Cl, toluene, Δ; ii. Ag(CF$_3$SO$_3$), 4,4'-bipyridine, THF/EtOH, Δ; iii. (CH$_3$)$_3$O$^+$(BF$_4^-$), CH$_2$Cl$_2$; iv. 4-ethynylbiphenyl, Pd/Cu (Cat.), THF, (i-Pr)$_2$NH, heat.

Figure 4-3: Route I for synthesis of **Re-2-MQ**.

Route II applied Meyer and coworkers' synthetic strategy[116] for making

[(L)Re^I(CO)$_3$(MQ$^+$)] by the reaction of [Re^I(CO)$_5$(MQ$^+$)] with corresponding diimine

ligand (Figure 4-4).

$$[Re(CO)_5Cl] \xrightarrow{i} [Re(CO)_5(CF_3SO_3)] \xrightarrow{ii} [Re(CO)_5(MQ^+)](CF_3SO_3)(PF_6)$$

$$\downarrow iii$$

$$[(L)Re(CO)_3(MQ^+)](PF_6)_2$$
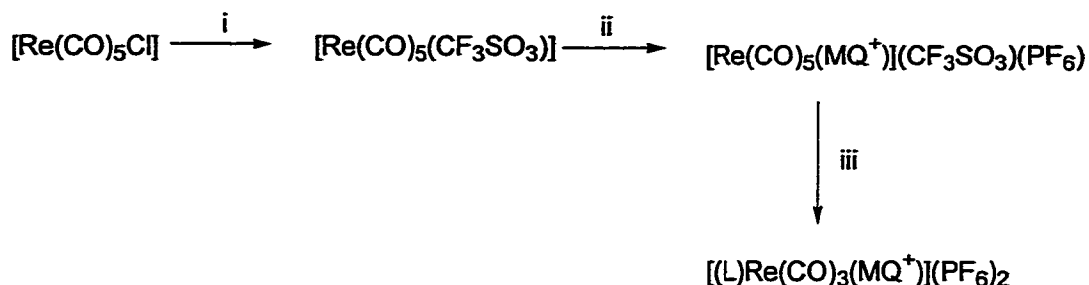
i. $Ag(CF_3SO_3)$, CH_2Cl_2, dark; ii. MQ^+, toluene, Δ; iii. Oligomer 2, toluene, Δ.

Figure 4-4: Route II for synthesis of **Re-2-MQ**.

Route III is quite straightforward, and is based on methylation of the precursor complex **Re-2-bpy** to afford **Re-2-MQ** (Figure 4-5). This precursor can be prepared by treatment of **Re-2** with $Ag(CF_3SO_3)$ followed by reaction with excess 4,4'-bipyridine to afford **Re-2-bpy**. **Re-2-MQ** is then prepared by methylation of **Re-2-bpy** using $(CH_3)_3O^+(BF_4^-)$.

Route IV is even more straightforward. The starting compound **Re-2** reacted readily with MQ^+ to afford the **Re-2-MQ**.

172

Re-2

i

Re-2-bpy

ii
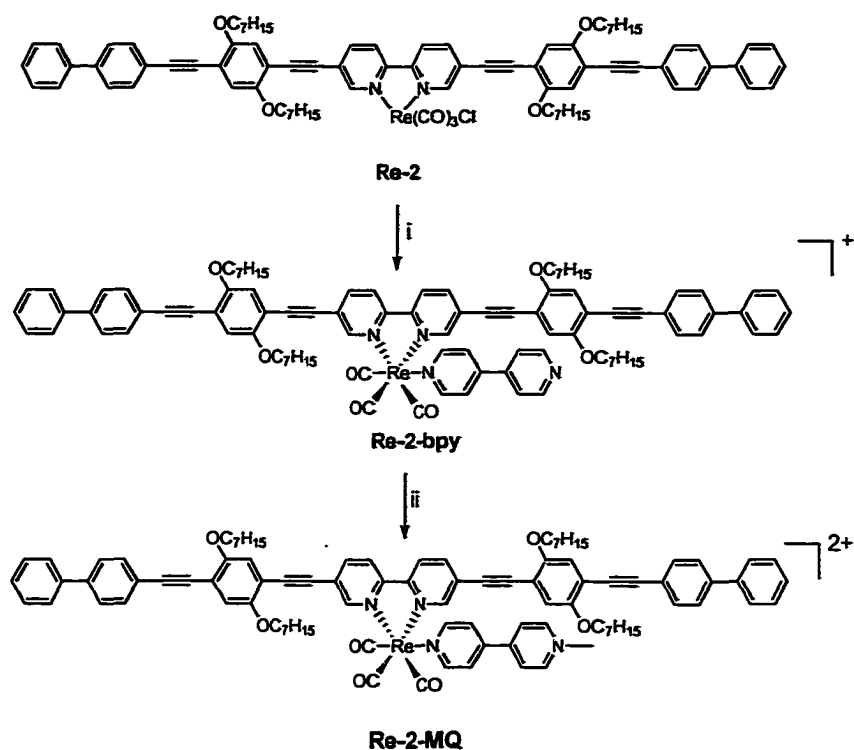
Re-2-MQ

i. 4,4'-bipyridine, THF/EtOH, Δ; ii. (CH₃)₃O⁺(BF₄⁻), CH₂Cl₂.

Figure 4-5: Route III of synthesis of **Re-2-MQ**.

Re-2

i
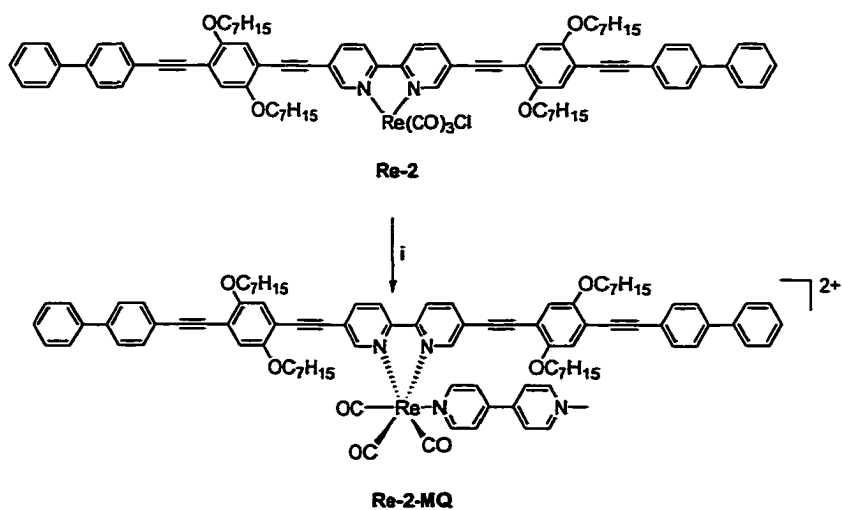
Re-2-MQ

i. Ag(CF₃SO₃), **MQ⁺(PF₆⁻)**, THF, EtOH, Δ.

Figure 4-6: Route IV of synthesis of **Re-2-MQ**.

We will discuss all the synthesis routes we have tried in the following. The first intermediate in Route I was [(bpy-Br)Re^I(CO)$_3$Cl] which then reacted with 7 equivalent 4,4'-bipyridine to get [(bpy-Br)Re^I(CO)$_3$(bpy)] with good yield. Methylation of [(bpy-Br)Re^I(CO)$_3$(bpy)] with (CH$_3$)$_3$O$^+$(BF$_4^-$) yielded [(bpy-Br)Re^I(CO)$_3$(MQ$^+$)] without difficulty. However, coupling reaction of endcapping group with [(bpy-Br)Re^I(CO)$_3$(MQ$^+$)] proved unsatisfactory because MQ$^+$ was replaced by diisopropylamine solvent.
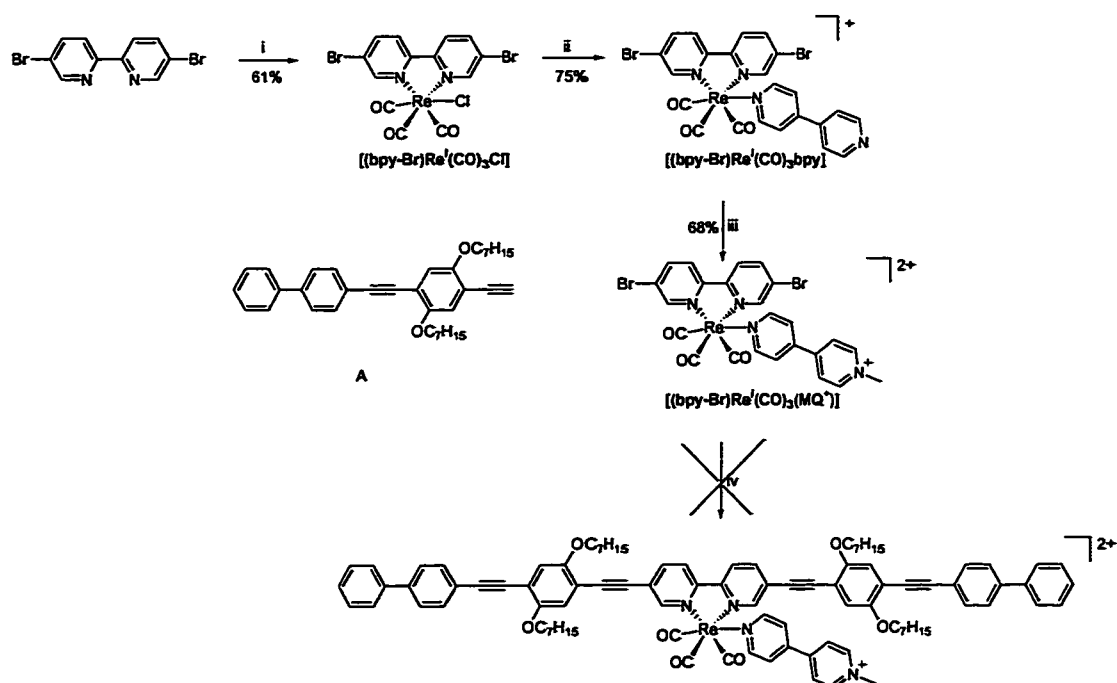
i. Re(CO)$_5$Cl, toluene, Δ; ii. Ag(CF$_3$SO$_3$), 4,4'-bipyridine (7 eq.), THF/EtOH, Δ; iii. (CH$_3$)$_3$O$^+$(BF$_4^-$) (1.2 eq.), CH$_2$Cl$_2$; iv. 4-ethynylbiphenyl, Pd/Cu (Cat.), THF, (i-Pr)$_2$NH, heat.

Figure 4-7: Synthesis of Re-2-MQ.

While route II may have provided a pathway to **Re-2-MQ**, the synthesis of

[Re^I(CO)$_5$(MQ$^+$)] proved difficult to reproduce because the reaction and workup has to

run in the dark.

In the Route III the starting material for **Re-2-MQ** complex is **Re-2** which can be

readily prepared from ClRe(CO)$_5$ and oligomer **2-C7** (Figure 4-8). Reaction of compound

16 with 2 equivalents of 4-ethynylbiphenyl gave oligomer **2-C7** without difficulty, and

subsequent metallation with ClRe(CO)$_5$ yielded **Re-2** .
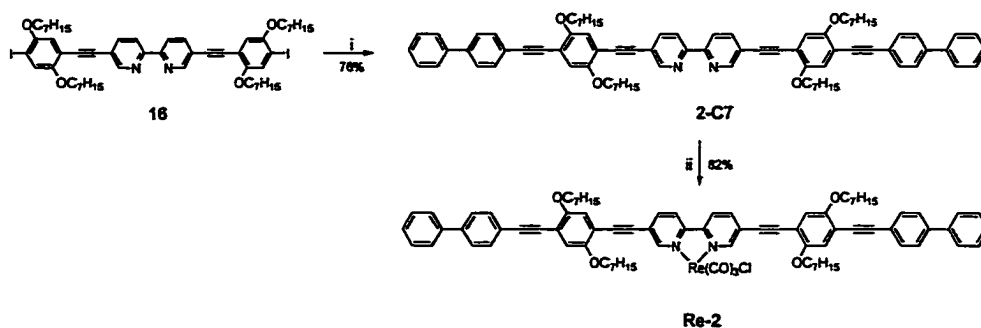
i. 4-ethynylbiphenyl, Pd/Cu (Cat.), THF, (i-Pr)$_2$NH, heat; ii. Re(CO)$_5$Cl, toluene, Δ.

Figure 4-8: Synthesis of **Re-2**.

By modification of the procedure described by Schanze and co-workers,[117] **Re-2**

was first treated with Ag(CF$_3$SO$_3$) to replace Cl$^-$ with CF$_3$SO$_3^-$ in which the lability of

CF$_3$SO$_3^-$ group was used. Then 5 equivalent 4,4'-bipyridine was added to the reaction

mixture. Surprisingly, the only product was **Re-2-bpy-Re-2** (Figure 4-9). Dimer was an

"accidental" but still of interest. Meyer's group[118] has prepared similar dimer [(4,4'-(X)$_2$-

2,2'-bpy)(CO)$_3$Re(4,4'-bpy)Re(CO)$_3$[(4,4'-(X)$_2$-2,2'-bpy)]$^{2+}$. They found that when X =

NH$_2$ the excited electron is localized on the bridging 4,4'-bpy ligand. When X = COOEt

which lower the energy of π^* level and lead to localization of the excited electron on the

2,2'-bpy ligand. When X = H, a solvent-dependent equilibrium exists between the 2,2'-bpy and 4,4'-bpy states. It will be interesting to see this bridging 4,4'-bpy group affect the electron transfer and any interaction between two oligomers.

Re-2

i | 50%
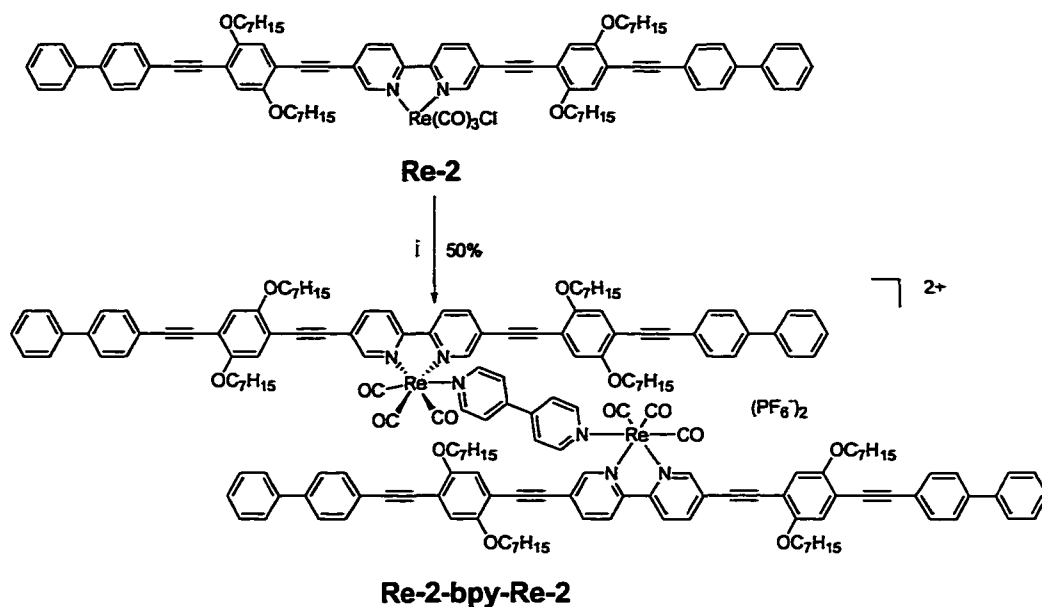
Re-2-bpy-Re-2

i. Ag(CF$_3$SO$_3$), 4,4'-bipyridine (5 eq.), THF, EtOH, heat.

Figure 4-9: Synthesis of **Re-2-bpy-Re-2**.

Since none of these alternatives proved satisfactory, Route IV was finally tried (Figure 4-10). Although **MQ$^+$** seems to be not a good coordinated ligand, surprisingly we still got **Re-2-MQ** with a reasonable yield. The synthesis of **MQ$^+$(PF$_6^-$)** is shown in Figure 4-11.
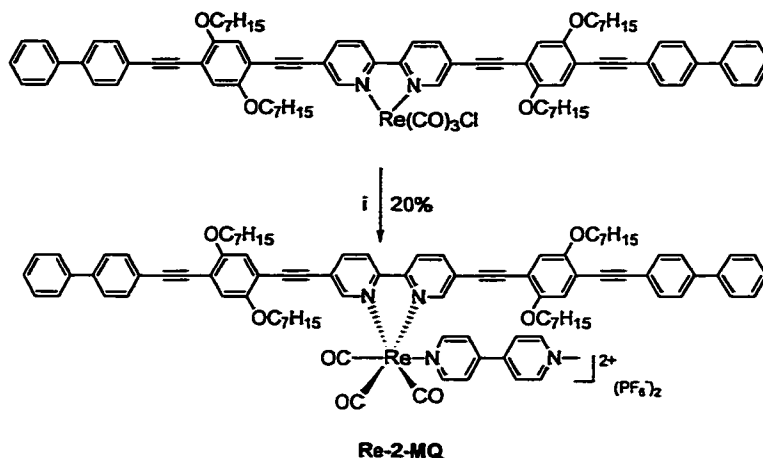
i. Ag(CF₃SO₃), **MQ⁺(PF₆⁻)** (1.5 eq.), THF, EtOH, heat.

Figure 4-10: Synthesis of **Re-2-MQ**.
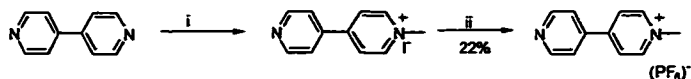
i. methyl iodide, ethyl acetate; ii. NH₄PF₆.

Figure 4-11: Synthesis of N-methyl-4,4'-bipyridium (**MQ⁺**).

Re-2-Py was also prepared as a model compound (Figure 4-12). **Re-2** was first treated with Ag(CF₃SO₃), then excess pyridine was added to the reaction mixture to afford **Re-2-Py** with moderate yield.
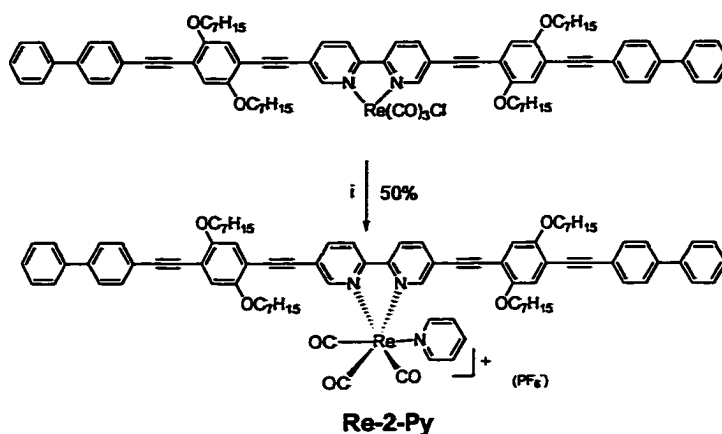
Re-2-Py

i. Ag(CF$_3$SO$_3$), Pyridine (excess), THF, EtOH, heat.
Figure 4-12: Synthesis of model complex **Re-2-Py**.

Results

Electrochemistry

Cyclic voltammetry was carried out on each of the **[(2)Re^I(CO)$_3$X]** complexes.

Electron transfer-induced exchange reaction is observed for **[(bpdz)Re^I(CO)$_3$(MQ)]$^{2+}$**

(bpdz = 3,3'-bipyridazine) in CH$_3$CN (equation 4-1),[119]

$$[(bpy)Re^I(CO)_3(MQ)]^{2+} + CH_3CN \rightarrow [(bpy)Re(CO)_3(CH_3CN)]^+ + MQ^+ \quad 4-1$$
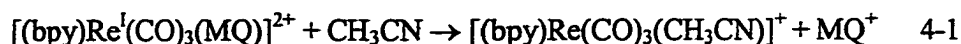
To avoid electron transfer-induced exchange reaction, all measurements were

performed in CH$_2$Cl$_2$ solution instead of CH$_3$CN. The cyclic voltammetrys are shown in

Figure 4-13. The relevant oxidation and reduction half-wave potentials are listed in Table

4-1. For comparison, redox potentials for bpy-based model complexes in 0.1 M

CH$_3$CN/TBAH are also included. The one-electron oxidation is generally reversible in

the cyclic voltammograms of all complexes with a half-wave potential (E$_{1/2}$^{ox}) in the

region of 1.3 – 1.4 V vs. SCE. Since Re^I oxidation potential should appear at much more

positive potential,[119] this oxidation peak must correspond to the oxidation of oligomer **2**.
This same oxidation value is observed in the oxidation of ligand **2** for **Os-2**.

All of three **[(2)Re^I(CO)$_3$X]** complexes display a characteristic, reversible
cathodic wave at $E_{1/2} \approx -0.81$ V which is due to reduction of the coordinated acceptor
ligand **2**. In addition, **Re-2-MQ** also displays a reversible cathodic wave at $E_{1/2} \approx -0.58$ V,
which is consistent with the rather chemical stability of the radical, **MQ$^{+\cdot}$**. Accordingly,
the electron acceptor in **Re-2-bpy-Re-2** and **Re-2-Py** upon excitation should be
conjugated ligand **2**. For **Re-2-MQ**, the electron acceptor is **MQ$^+$**.

Table 4-1: Electrochemical potentials of **[(2)Re^I(CO)$_3$X]** complexes.[a]

compound	$E_{1/2,}^{ox}$	$E_{1/2,}^{red}$
[Re(bpy)(CO)$_3$(Py)]$^{+}$ [b]	1.74 (Re$^{I/II}$)	-1.09 (bpy$^{0/\cdot-}$)
		-1.39 (Py$^{0/\cdot-}$)
[(bpy)(CO)$_3$Re(4,4'-bpy)Re(CO)$_3$(bpy)]$^{2+}$ [c]	1.90 (Re$^{I/II}$)	-1.06 (4,4'-bpy$^{0/\cdot-}$)
		-1.20 (bpy$^{0/\cdot-}$)
MQ$^+$ [d]		-0.96 (MQ$^+$/MQ$^{+\cdot}$)
[(bpy)Re(CO)$_3$(MQ$^+$)]$^{2+}$ [d]		-0.68 (MQ$^+$/MQ$^{+\cdot}$)
		-1.17 (bpy$^{0/\cdot-}$)
Re-2-Py	1.34 (2$^{0/\cdot+}$)	-0.81 (2$^{0/\cdot-}$)
Re-2-bpy-Re-2	1.36 (2$^{0/\cdot+}$)	-0.81 (2$^{0/\cdot-}$)
Re-2-MQ	1.40 (2$^{0/\cdot+}$)	-0.58 (MQ$^+$/MQ$^{+\cdot}$)
		-0.81 (2$^{0/\cdot-}$)

[a] Estimated error in $E_{1/2}$ values is ± 0.05 V for reversible eaves. Recorded in CH$_2$Cl$_2$ solution with 0.1 M TBAH as supporting electrolyte with a Pt working electrode, a Pt auxiliary electrode, and Ag/Ag$^+$ reference electrode. Potentials are referenced to a ferrocene internal standard and reported in V vs. SCE along with their assigned redox couples. Fc$^+$/Fc = 0.425 V was assumed in CH$_3$CN, and 0.45 V in CH$_2$Cl$_2$.[86] [b] Data from ref.[120] [c] Data from ref.[118] [d] Data from ref.[121]

179
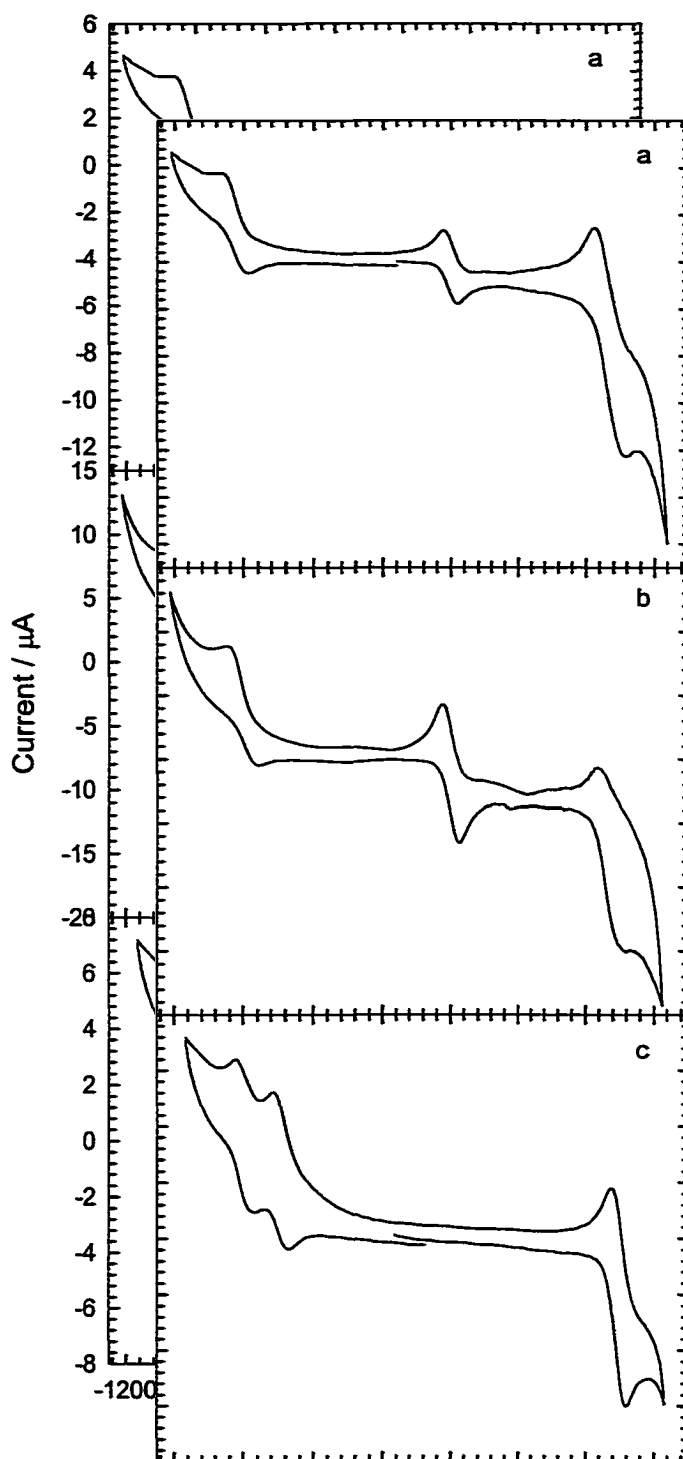
Figure 4-13: Cyclic voltammogram of [(2)Re^{I}(CO)$_3$X] in CH$_2$Cl$_2$/TBAH electrolyte solution (υ = 100 mv·s^{-1}). (a) **Re-2-Py**; (b) **Re-2-bpy-Re-2**; (c) **Re-2-MQ**.

Absorption Spectra

Absorption spectra were obtained on dilute CH_2Cl_2 solutions of the

$[(2)Re^I(CO)_3X]$ complexes. Absorption spectra for these complexes are shown in Figure

4-14 and Table 4-2 contains a listing of absorption bands and extinction coefficients. The

electronic spectra of these three complexes retain the same shape as that of **Re-2**. The

spectra are dominated by the strong π,π^* transition of ligand **2**. The MLCT-based

absorption is obscured by the more intense oligomer π,π^* transitions. Compared to **Re-2**,

there is a small red shift of the absorption peaks with the **Re-2-Py** being the most red-

shifted.
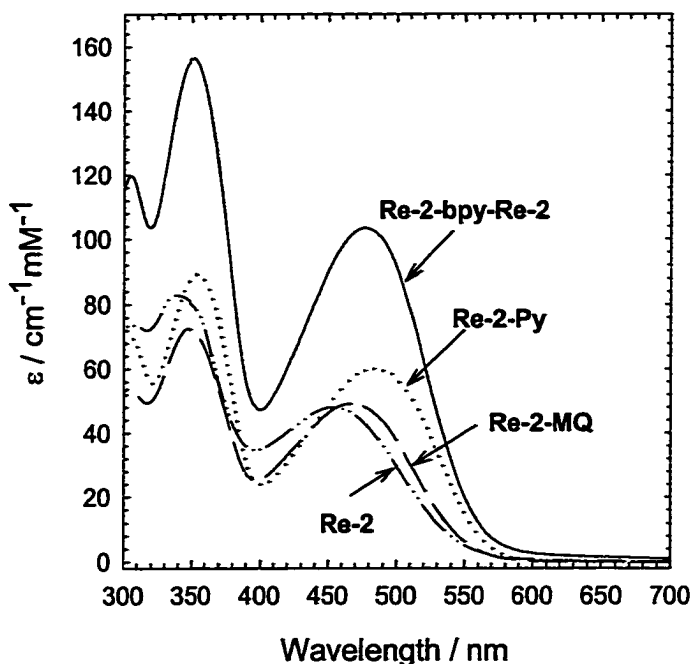
Figure 4-14: Absorption spectra of $[(2)Re^I(CO)_3X]$ complexes in CH_2Cl_2. **Re-2** (dash-dotted line), **Re-2-Py** (dotted line), **Re-2-bpy-Re-2** (solid line), **Re-2-MQ** (long dashed line).

Table 4-2: Near UV-visible absorption bands of $[(2)Re^I(CO)_3X]$ complexes in CH_2Cl_2 solution.

Complex	λ_{max} /nm	ε_{max}/ mM^{-1}cm^{-1}	Assignment
Re-2	338	83.3	π,π^* (2)
	454	48.1	π,π^* (2) & MLCT
Re-2-Py	352	88.9	π,π^* (2)
	484	60.0	π,π^* (2) & MLCT
Re-2-bpy-Re-2	348	72.6	π,π^* (2)
	467	49.1	π,π^* (2) & MLCT
Re-2-MQ	352	157	π,π^* (2)
	477	104	π,π^* (2) & MLCT

Emission Spectra

Emission studies were carried out on each of the $[(2)Re^I(CO)_3X]$ complexes. The room-temperature emission spectra of $[(2)Re^I(CO)_3X]$ complexes in CH_2Cl_2 are shown in Figure 4-15. For comparison, the emission spectrum of **Re-2** is also shown in Figure 4-15. Emission maxima and quantum yields are given in Table 4-3. All of the Re(I) complexes exhibit a weak, broad room-temperature luminescence with a maximum in the 650-680 nm region.

Attempts to measure the luminescence quantum yields of **Re-2** were not attempted since the emission was too weak to be effectively measured ($\phi_{em} < 10^{-4}$).[98] As expected, the quantum yields of **Re-2-Py** and **Re-2-bpy-Re-2** do increase one order of magnitude, but the emission is still very weak.

The emission spectra of $[(2)Re^I(CO)_3X]$ in 2-MTHF solution at temperatures ranging from 80 K to room temperature are shown in Figure 4-16. The emission spectra of all of three complexes exhibit very similar structure at all temperature range. At 80 K,

the spectra exhibit a highly structured band. As temperature increases, the emission band red shift and becomes broad and structureless. For comparison, the emission spectra of $[(bpy)Re(CO)_3(Py)]^{2+}$ and $[(bpy)Re(CO)_3(MQ^+)]^{2+}$ in 2-MTHF at 80 K are also measured and the data are shown in Table 4-3.
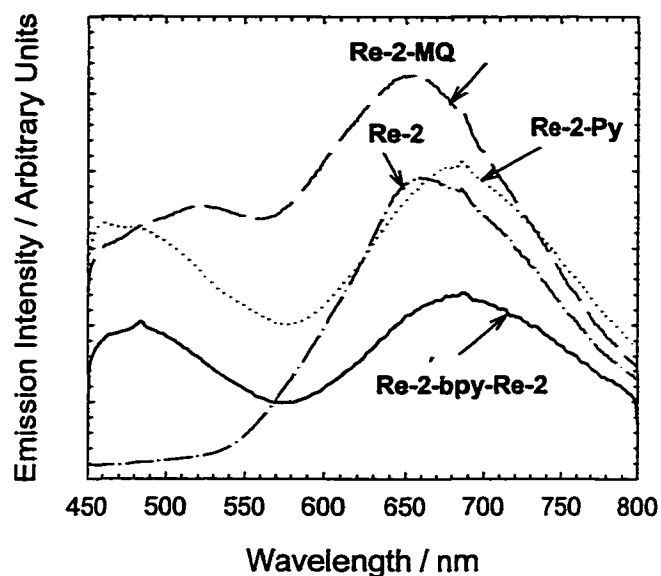
Figure 4-15: Room-temperature emission spectra of $[(2)Re^I(CO)_3X]$ complexes in CH_2Cl_2. **Re-2** (dash-dot line), **Re-2-Py** (dot line), **Re-2-bpy-Re-2** (solid line), **Re-2-MQ** (long dash line).

Table 4-3: Photophysical properties for the $[(2)Re^I(CO)_3X]$ complexes.

Compound	298 K [a]				80 K [b]
	λ_{max}^{em} / nm	ϕ_{em}	τ_{em} [c] μs	τ_{TA} [d] μs	λ_{max}^{em} / nm
Re-2	656			0.15	659
[(bpy)Re(CO)₃(Py)]⁺ [e]	558	0.16	0.669		490
[(bpy)Re(CO)₃(MQ⁺)]²⁺					540
Re-2-Py	676	0.004	4.7	4.1	520, 556, 635
Re-2-bpy-Re-2	676	0.009	3.4	3.5	529, 582, 638
Re-2-MQ	649	0.0002	3.0	0.74	525, 558, 629, 686

[a] Measurements were conducted on argon bubble-degassed CH_2Cl_2 solution at 298 K. [b] Measurements were conducted on freeze-pump-thaw degassed 2-MTHF. [c] The mean decay lifetime ,<τ>, was calculated using the multiexponential decay data according to the equation 2-3. [d] Decay lifetimes of transient absorption. [e] Data from ref.[120].

183
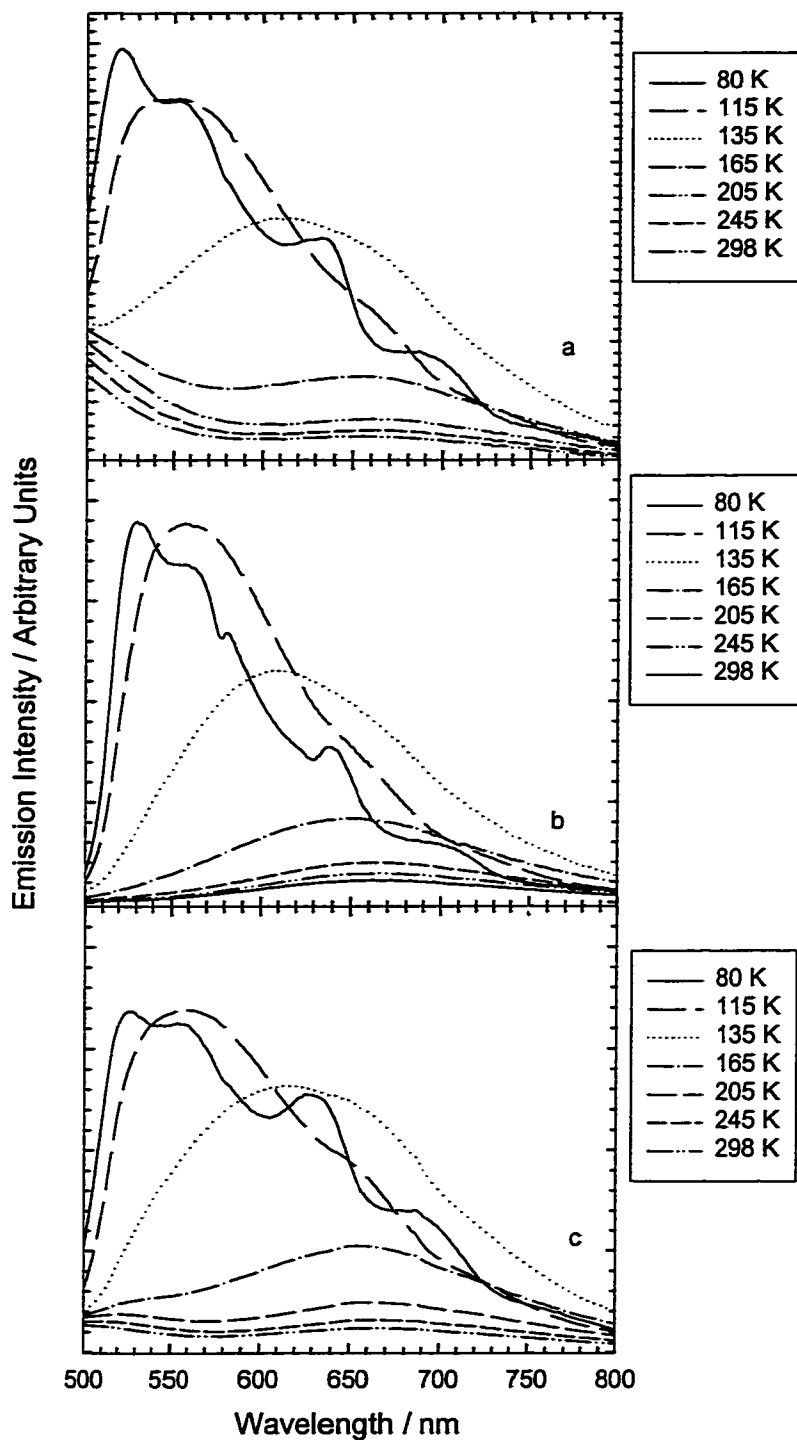
Figure 4-16: Emission spectra of [(2)Re^I(CO)$_3$X] complexes (450 nm excitation) in 2-MTHF at various temperatures from 298 K to 80 K. Emission intensity increases with decreasing temperature. (a) Re-2-Py; (b) Re-2-bpy-Re-2; (c) Re-2-MQ.

Emission Lifetimes

Emission decay lifetimes were recorded for the $[(2)Re^{I}(CO)_3X]$ complexes in 2-MTHF at 80 K and in CH_2Cl_2 at 298 K. The emission decay profiles are multiexponential. Table 4-4 contains a listing of parameters recovered from multi-component fits of the emission decays for the complexes at 80 K and 298 K. The emission decay profiles of each of three complexes are quite similar at 298 K. The decays are fit to a three-component exponential with lifetime of 78 – 180 , 830 -1000, and 5600 – 6850 ns; each lifetime has a significant amplitude (10% - 14%, 26% - 40 %, and 45% - 65%). The short-lived component is due to ^{3}MLCT excited state and the long-lived component is due to $^3\pi,\pi^*$ phosphorescence. It is clear that the MLCT state in **Re-2-bpy-Re-2** and **Re-2-Py** is from $d\pi(Re) \rightarrow \pi^*(2)$. The lowest excited state of **Re-2-MQ** will be discussed below. Figure 4-17a shows the decay observed for **Re-2-MQ** in CH_2Cl_2 on a logarithmic scale along with the excitation lamp profile and the computer calculated fit.

At 80 K in a rigid solvent glass the emission decays at 650 nm for three complexes are characterized by a large amplitude, very short-lived component ($\tau \approx 2 - 7$ ns, $\alpha \approx 94 - 99\%$) and a low amplitude component with a very long lifetime ($\tau \approx 13 - 18$ μs, $\alpha \approx 1 - 6\%$). Figure 4-17b also shows decay observed for **Re-2-MQ** in 2-MTHF at 80 K on a logarithmic scale along with the excitation lamp profile and the computer calculated fit.

Table 4-4: Emission lifetime data of $[(2)Re^I(CO)_3X]$ complexes.[a]

Complex	298 K [b]					80 K [c]		
	τ_1, ns (α_1, %)	τ_2, ns (α_2, %)	τ_2, ns (α_3, %)	$<\tau>$ [d] ns	χ^2 [e]	τ_1, ns (α_1, %)	τ_2, ns (α_2, %)	χ^2 [e]
Re-2-Py	78 (10)	830 (26)	6840 (65)	4.7	1.04	2.6 (99.84)	18200 (0.16)	1.8
Re-2-bpy-Re-2	85 (10)	994 (40)	5930 (50)	3.4	1.1	6.3 (94)	15266 (6)	1.2
Re-2-MQ	177 (14)	951 (40)	5600 (46)	3.0	1.1	5.2 (95)	13420 (5)	1.2

[a] 405 nm Excitation. Decays were recorded at 650 nm. Lifetime and relative biexponential fits were performed with equation 2-2. [b] Samples were measured on argon-bubble degassed CH_2Cl_2. [c] Samples were measured on free-pump-thaw degassed 2-MTHF. [d] The mean decay lifetime, $<\tau>$, was calculated using the multiexponential decay data according to the equation 2-3. [e] χ^2 is used to evaluate the quality of the calculated fit. $\chi^2 = 1$ means the best fit.

186
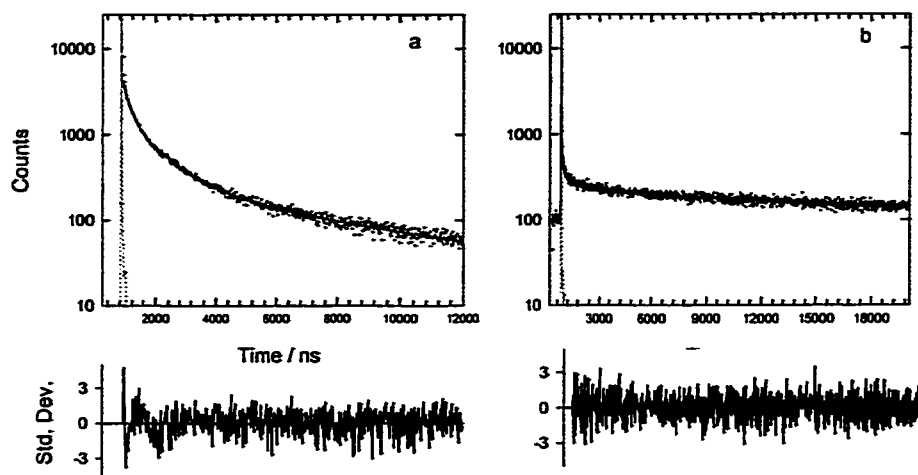
Figure 4-17: Time resolved emission decay of **Re-2-MQ**. Upper box shows the emission decay (Δ) and the excitation lamp profile (dash line) along with the computer-calculated fit (solid line). Lower box show plots of the residuals indicating the quality of the calculated fit. (a) CH_2Cl_2 at room temperature; (b) 2-MTHF at 80 K.

Transient Absorption Spectra of [(2)Re^I(CO)$_3$(X)]

Transient absorption spectra of [(2)Re^I(CO)$_3$(X)] complexes following pulsed laser excitation at 355 nm are shown in Figure 4-18. Spectra were recorded in CH_2Cl_2 to prevent CH_3CN ligand photosubstitution. Generally, equivalent first order decays were observed for all features of the various transient absorption spectra. The difference absorption spectra of these complexes are very similar in appearance to that of **Re-2**. Ground state π,π^* absorption bleaching was observed at 350 nm and 450 nm, along with a strong absorption band around 550 nm and a broader absorption band extending into the near-IR. For **Re-2**, it is believed that the transient absorption spectrum is dominated by the $^3\pi,\pi^*$ state. The similarity of the transient absorption spectra of the [(2)Re^I(CO)$_3$(X)] complexes to **Re-2** suggests that the lowest energy excited state is $^3\pi,\pi^*$ state.[98] Excited

state lifetimes obtained from factor analysis and global decay fitting are listing in Table 4-3. The transition absorption decay lifetimes and that of the luminescence (mean decay lifetime) are approximately equivalent for **Re-2-Py** and **Re-2-bpy-Re-2** which further confirms that the transient absorptions of these two complexes are due to $^3\pi,\pi^*$ state. However, for **Re-2-MQ** the transition absorption decay lifetime is considerably shorter than emission decay lifetime. Surprisingly, for **Re-2-MQ** we didn't see the appearance of the $-$**MQ**$^{+\cdot}$ radical which is formed via intramolecular-electron-transfer quenching probably because the absorption extinction coefficient of π,π^* state is two strong which mask the absorption of $-$**MQ**$^{+\cdot}$.
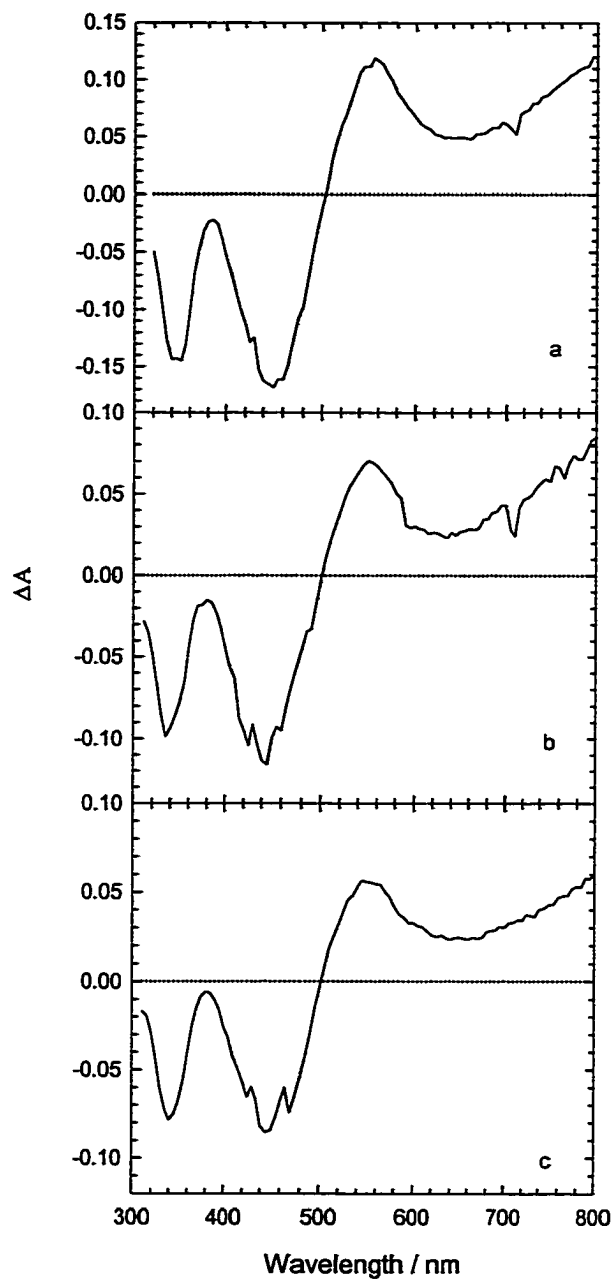
Figure 4-18: Transient absorption difference following 355 nm pulsed laser excitation (5 mJ dose) acquired from argon bubbled degassed CH_2Cl_2 solution. (a) **Re-2-Py**; (b) **Re-2-bpy-Re-2**; (c) **Re-2-MQ**.

<u>Discussion</u>

<u>Excited State Energetics of [(2)Re^I(CO)$_3$(X)] Complexes</u>

It is first necessary to establish the energies for the various low-lying excited

states in the [(2)Re^I(CO)$_3$(X)] complexes in order to explain the photophysical data.

For **Re-2**, the energies of $^3\pi,\pi^*$ and ^{3}MLCT states are ≈ 1.90 eV and 1.7 eV,

respectively. These two states are very close in energy and both of them are responsible

for its photoluminescence. The decay via ^{3}MLCT state is the main deactivation mode,

and the rate of this process controls the overall lifetime of the excited state population.[122]

Since it is anticipated that substitution of Cl$^-$ for a chromophoric ligand will not

affect the energies of the π,π^* state for the π-system, the $^1\pi,\pi^*$ and $^3\pi,\pi^*$ states are

positioned the same in [(2)Re^I(CO)$_3$(X)] complexes as in **Re-2**. It is more problematic to

pinpoint the energies of the ^{1}MLCT and ^{3}MLCT states in [(2)Re^I(CO)$_3$(X)] complexes,

because the MLCT absorptions are obscured by the π,π^* bands and the luminescence

spectra are complicated. Thus, in the absence of direct spectroscopic evidence, the state

energies are estimated based on several known facts. (1) The energy of the ^{3}MLCT state

of the parent complex, [(bpy)Re^I(CO)$_3$(Py)] is ≈ 2.35 eV.[123,124] (2) The energies of the

MLCT manifold in [(2)Re^I(CO)$_3$(X)] complexes will scale with the difference in

reduction potentials between the oligomer complexes and [(bpy)Re^I(CO)$_3$(Py)]. The

reduction potential of [(bpy)Re^I(CO)$_3$(Py)] is ≈ -1.09 eV (Table 4-1). The difference in

the reduction potentials between [(bpy)Re^I(CO)$_3$(Py)] and **Re-2-Py** is 0.28 V. Thus, the

energy of dπ(Re) → π^*(2) MLCT state in **Re-2-Py** is 2.07 eV. There are two sets of

MLCT states in **Re-2-bpy-Re-2**, the first based on dπ(Re) → π^*(2) transition and the

second on a dπ(Re) → π^*(4,4'-bpy) transition. The energy of the former one lies at ≈

2.07 eV . And the energy of $d\pi(Re) \rightarrow \pi^*(4,4'\text{-bpy})$ MLCT state is $\approx$ 2.32 eV based on

the electrochemical data of model complex $[(bpy)(CO)_3Re(4,4'\text{-bpy})Re(CO)_3(bpy)]^{2+}$, -

1.06 V, Table 4-1). For **Re-2-MQ**, there are also two possible MLCT states, $d\pi(Re) \rightarrow$

$\pi^*(MQ^+)$ transition and $d\pi(Re) \rightarrow \pi^*(2)$ transition. These two states are placed at 1.84

and 2.07 eV, respectively. These energies are used in the energy diagram of

$[(2)Re^I(CO)_3(X)]$ complexes shown in Figure 4-19.

This analysis raises several important issues regarding the lowest excited states in

the metal-organic complex. First, it is evident that the ^{3}MLCT and $^3\pi,\pi^*$ states are in

close energetic proximity. This close proximity makes it possible that both states will

contribute to the observed photophysics. Second, it is also clear that for **Re-2-Py** and **Re-

2-bpy-Re-2**, $^3\pi,\pi^*$ states is lowest in energy, while for **Re-2-MQ**, ^{3}MLCT ($d\pi(Re) \rightarrow$

$\pi^*(MQ^+)$) is lowest.
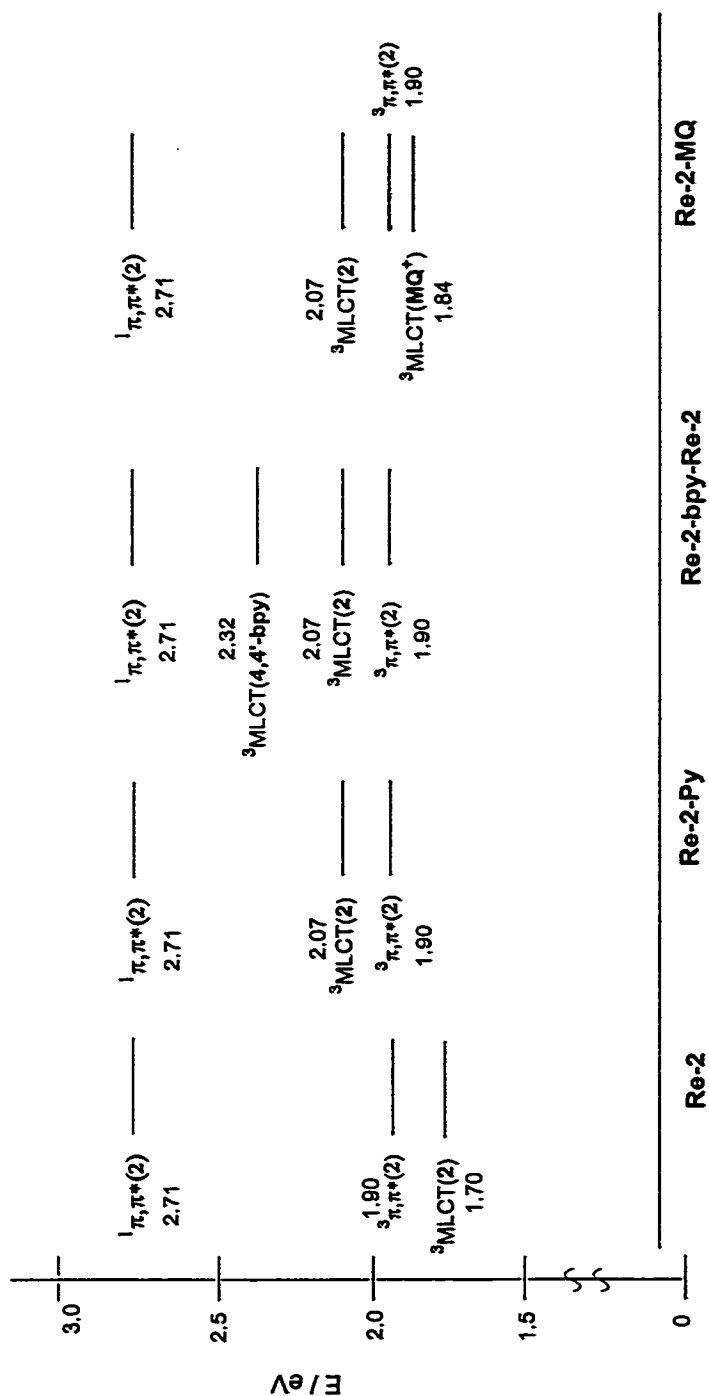
Figure 4-19: Energy diagram of $[(2)Re^I(CO)_3(X)]$ complexes.

Photophysics of Re-2-Py

When the Cl⁻ is replaced by pyridine, it is expected that this N-donor ligand will increase the electron density on rhenium metal center. Therefore it will decrease the energy of the MLCT state.[125] As expected, the emission spectrum of **Re-2-Py** at room temperature is very similar to that of **Re-2** and red-shifted. The lifetime decay profile indicated that both ^{3}MLCT and $^3\pi,\pi^*$ states contribute to this emission. Both of these two low-lying excited states, ^{3}MLCT and $^3\pi,\pi^*$, are populated to a significant extent following excitation. The dual emission implies that these two excited states are in equilibrium. Since the $^3\pi,\pi^*$ state is lowest in energy, the equilibrium favors the $^3\pi,\pi^*$ state and at long times after excitation the excited state population resides mainly in this state. Consequently, the transient absorption spectrum is dominated by $^3\pi,\pi$ state which has a considerably long lifetime.

The emission spectrum of **Re-2-Py** at 80 K is quite different from that of **Re-2** which shows a superposition of a structureless 600 nm band and a structured (0,0) 650 nm band with a vibronic (0,1) shoulder. For **Re-2**, the low energy emission is assigned as ligand centered $^3\pi,\pi^*$ phosphorescence with the mixing of ^{3}MLCT emission.[98] **Re-2-Py** exhibits a structured lowest energy band at 525 nm with a vibronic (0,1) shoulder and a 650 nm structured band. The low energy band arises in the same energy region as that of $^3\pi,\pi^*$ phosphorescence band of **Re-2**. And the emission decay kinetics of this band is dominated by a large amplitude, short-lived component and a low amplitude component with a very long lifetime. We believe that this emission band is due to ligand centered $^3\pi,\pi^*$ phosphorescence. The origin of fast emission decay components corresponds to establishment of the equilibrium between $^3\pi,\pi^*$ and ^{3}MLCT states. The blue side

emission band arises from the ^{3}MLCT (Re(dπ) → π*(2)) state since the ligand 2 is the only electron acceptor in this molecule. This MLCT state shifts to lower energy going from low temperature glasses to room temperature fluid solution because of rigidochromic effect,[81] whereas $^3\pi,\pi$* state is hardly influenced (Figure 4-20). So the pure MLCT emission and $^3\pi,\pi$* phosphorescence can be observed separately at low temperature.
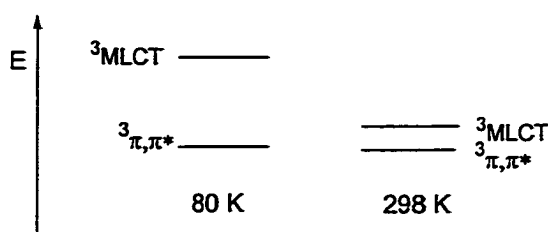
Figure 4-20: State diagram for the lowest excited states of **Re-2-Py**.

Photophysics of Re-2-bpy-Re-2

Both of the emission spectrum and emission decay kinetics of **Re-2-bpy-Re-2** at room temperature is similar to that of **Re-2-Py**. Consequently there is no significant electronic interactions between two rhenium metal centers in the dimer. This is consistent with the relative energies of two MLCT states since MLCT (dπ(Re) → π*(4,4'-bpy)) state lies at much higher energy than MLCT (dπ(Re) → π*(2)) state. So the photophysics of **Re-2-bpy-Re-2** is similar to that of **Re-2-Py**.

Photophysics of Re-2-MQ

For **Re-2-MQ** the low temperature emission spectrum and emission decay profile are similar to that of **Re-2-Py** and **Re-2-bpy-Re-2**. The high energy emission band arises from the ^{3}MLCT (Re(dπ) → π*(2)) state, and the red side of the band arises from $^3\pi,\pi$*

phosphorescence. It is understandable for **Re-2-MQ** that excited electron lies on ligand 2

instead of MQ^+ upon excitation at low temperature. At 80 K for $[(\text{bpy})\text{Re}^I(\text{CO})_3(MQ^+)]$,

the excited electron is localized on **bpy**. In a frozen 2-MTHF glass at 80 K, a strong bpy-

based MLCT emission ($\lambda_{max} \approx 551$ nm) is observed from $[(\text{bpy})\text{Re}^I(\text{CO})_3(MQ^+)]^{2+}$

(Figure 4-21). There is no evidence for a significant amount of intramolecular ET in the

glass.[113,115] At room temperature, $[(\text{bpy})\text{Re}^I(\text{CO})_3(MQ^+)]$ displays only a very weak

luminescence at long wavelength ($\lambda_{max} \approx 600$ nm). The photophysical data implies that

MQ^+ ligand is only able to "quench" this excited state in fluid media. The energy of the

$d\pi(\text{Re}) \rightarrow \pi^*(MQ^+)$ MLCT state is a strong function of the dihedral (twist) angle (θ)

between the planes defined by the two pyridyl rings of the MQ^+ ligand. The energy of

$d\pi(\text{Re}) \rightarrow \pi^*(MQ^+)$ MLCT state is at a minimum when the $\theta = 0°$ (e.g., when MQ^+ is

planar). This effect is due to the increased delocalization of the odd electron on **MQ**,

which is imparted by $\text{Re} \rightarrow MQ^+$ MLCT excitation. Another important piece of

information comes from the X-ray crystal structure of $[(\text{bpy})\text{Re}^I(\text{CO})_3(MQ^+)]$ which

indicates that in the ground-state complex the inter-ring dihedral angle is approximately

45°.[116] In the relaxed ground state, the MQ^+ ligand is twisted and the $d\pi(\text{Re}) \rightarrow \pi^*(\text{bpy})$

MLCT state is lowest in energy. In fluid solution, near UV photoexcitation produces the

$d\pi(\text{Re}) \rightarrow \pi^*(\text{bpy})$ MLCT state and rapidly thereafter intramolecular bpy $\rightarrow MQ^+$ ET

occurs to produce the $d\pi(\text{Re}) \rightarrow \pi^*(MQ^+)$ MLCT state. By contrast, in a rigid

environment (80 K solvent) rotation around the inter-ring bond in MQ^+ is slow or

completely inhibited and intermolecular bpy $\rightarrow MQ^+$ ET does not occur.
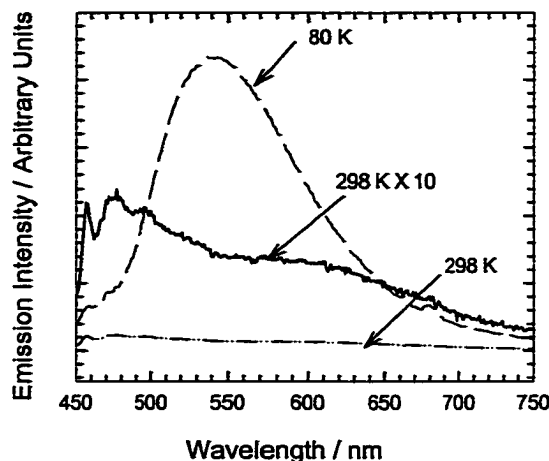
Figure 4-21: Emission spectra of [(bpy)Re^I(CO)$_3$(MQ$^+$)]complex (400 nm excitation) in 2-MTHF at various temperatures from 298 K to 80 K.

For **Re-2-MQ**, it is believed that the lowest excited state is MLCT (dπ(Re) →

π*(**MQ$^+$**)) state (Table 4-19). Although we did not see characteristic peak of reduced

MQ$^+$ ligand, **MQ^{+-}** in the transient absorption spectrum, we still believe that the MLCT

(dπ(Re) → π*(**MQ$^+$**)) state is present. The decay lifetime of transient absorption of this

complex is 5-fold shorter than that of **Re-2-Py** and **Re-2-bpy-Re-2**. This is due to the

short-lived MLCT (dπ(Re) → π*(**MQ$^+$**)) state. Since the energy of MLCT state is so

close to ^{3}π,π* state, there is equilibrium between these two state. It is likely that the

difference molar absorptivity (Δε) for the ^{3}π,π* state is very large, and this also may

account for the fact that this state dominates the transient absorption spectrum, i.e., the

absorption of **MQ^{+-}** is obscured by the strong absorbance of ^{3}π,π*.

In an effort to characterize the spectroscopic properties of the reduced forms of

complex, transient absorption studies were carried out on [(bpy)Re^I(CO)$_3$(MQ$^+$)], **Re-2-**

Py and **Re-2-MQ** in the presence of N,N'-dimethylaniline (**DMA**). **DMA** quenches the

transient absorption of all of the complexes. Moreover, quenching leads to the production

of long-lived transient absorptions that clearly arise from the products of bimolecular

photoinduced ET.
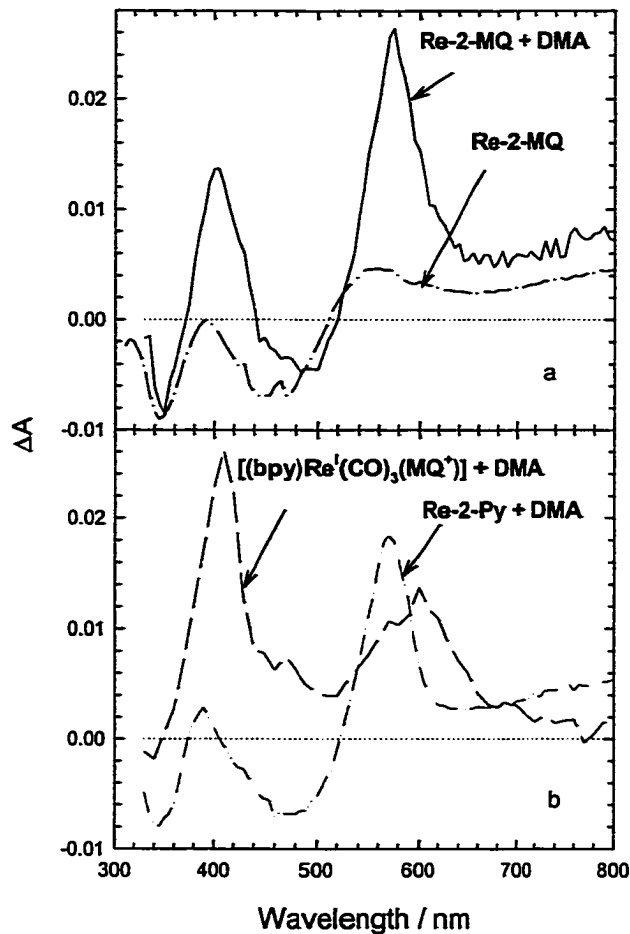
Figure 4-22: Transient absorption spectra of complexes with 10 mM DMA. (a) **Re-2-MQ** + DMA (solid line), **Re-2-Py** + DMA (solid-dot-dot line); (b) [(bpy)Re^I(CO)$_3$(MQ$^+$)] + DMA (long dashed line), **Re-2-MQ** (dash-dotted line).

The transient absorption spectra of model complex **Re-2-Py** in the presence of 10

mM DMA are illustrated in Figure 4-22b. For **Re-2-Py**, the oligomer **2** coordinated to

rhenium metal center is expected to be reduced by **DMA** following excitation, i.e.,

$$[(2)Re^I(CO)_3Py]^* + DMA \rightarrow [(2^-)Re^I(CO)_3Py] + DMA^{\cdot+}$$
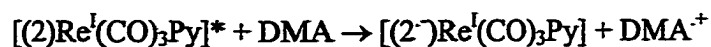
The difference absorption spectrum featured a new band at 600 nm which is due to the absorption of the reduced ligand (2$^-$).

The transient absorption spectra of **Re-2-MQ** in the presence of 10 mM **DMA** are illustrated in Figure 4-22a. The difference absorption features a characteristic peak at 390 nm of MQ$^{\cdot+}$ nm and 600 nm of DMA$^{\cdot+}$. These species are produced by photoinduced ET, i.e.

$$[(2)Re^I(CO)_3(MQ^+)]^* + DMA \rightarrow [(2)Re^I(CO)_3(MQ^+)] + DMA^{\cdot+}$$
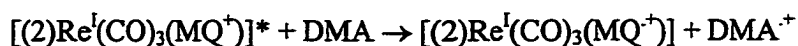
The transient absorption decays on a longer time scale ($\tau_{1/2} \approx 31.4$ µs), consistent with disappearance of the radical ions via diffusion-controlled back-ET. The transient absorption spectra of **Re-2-Py** and **Re-2-MQ** in the presence of DMA are very similar besides the new peak at 390 nm for **Re-2-MQ** which is assigned to the absorption of MQ$^{\cdot+}$. Also compare the transient absorption of **Re-2-MQ** and **[(bpy)Re^I(CO)$_3$(MQ$^+$)]** in the presence of **DMA** (Figure 4-22), difference absorption peak at 550 – 650 nm region of **Re-2-MQ** is not only caused by **DMA**$^{\cdot+}$ but also due to the strong absorption band characteristic of the reduced ligand **2**. Upon photoinduced ET, two species which are in equilibrium are produced (Figure 4-23).
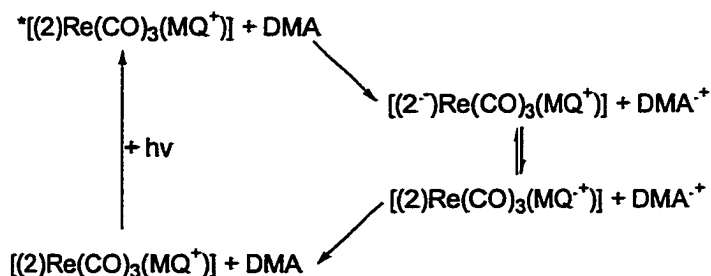
Figure 4-23: Photoinduced electron transfer reactions of **Re-2-MQ**.

In this case we believe that at room temperature the $d\pi(Re) \rightarrow \pi^*(2)$ MLCT state is competitive with $d\pi(Re) \rightarrow \pi^*(MQ^+)$ MLCT state and two states are in equilibrium. It is understandable because these two states are quite close in energy (Figure 4-19).

Based on above discussion, we know initial excitation populates the $^1\pi,\pi^*$ state of **Re-2-MQ** which followed by ultrafast energy transfer and intersystem crossing ensues to afford $^3\pi,\pi^*$ state and a mixture of $d\pi(Re) \rightarrow \pi^*(2)$ and $d\pi(Re) \rightarrow \pi^*(MQ^+)$ states. Then most of $d\pi(Re) \rightarrow \pi^*(2)$ state undergoes $2^{\cdot-} \rightarrow MQ^+$ intreligand electron transfer to produce $d\pi(Re) \rightarrow \pi^*(MQ^+)$ state.

Experimental

Photophysical Measurements

All room temperature studies were conducted in CH_3CN and low temperature studies were conducted in 2-MTHF. All solvents were distilled according to typical laboratory practices. All photophysical studies were conducted with the same instrumentation and techniques described in Chapter 2.

Electrochemical Measurements

All electrochemical measurements were conducted on CH_2Cl_2 solutions with TBAH as the supporting electrolyte. Cyclic voltammetry measurements were performed with the same procedures on the same instrumentation described in Chapter 2.

General Synthetic

Diisopropylamine was distilled from KOH and tetrahydrofuran was distilled from sodium benzophenone ketyl and stored under nitrogen. The synthesis of compound 16

and **18** are described in chapter 2. Copper(I) iodide, Pd(PPh$_3$)$_4$, trimethyloxonium tetrafluorborate and 4,4'-bipyridine were purchased from Aldrich Chemical Co. and used without further purification. All cross-coupling reactions using Pd catalyst were carried out under standard Schlenk and vacuum line techniques. ^{1}H and ^{13}C NMR was recorded on either Gemini-300 or VXR-300 NMR spectrophotometers. High-resolution mass spectrometry was performed by the University of Florida analytical service. The matrix used for MALDI analysis is α-cyanohydroxycinnamic acid in THF solvent.

Synthesis

[(bpy-Br)Re^I(CO)$_3$Cl]

5,5'-dibromobipyridine (100 mg, 0.32 mmol) and Re(CO)$_5$Cl (173 mg, 0.43 mmol) were dissolved in 30 mL of toluene, the solution was purged with argon and then was heated at 90°C for 2 hr. The solution color changed to bright yellow. The solution was allowed to cool to room temperature and the toluene was removed under vacuum. The complex was purified by repeated rinsing with acetone. The metallated oligomer was obtained as a bright yellow solid, 197 mg (61%). ^{1}H-NMR (300 MHz, CD$_3$COCD$_3$) δ 8.45 (d, 2H), 8.70 (d, 2H), 9.22 (s, 2H).

[(bpy-Br)Re^I(CO)$_3$(bpy)]

(bpy-Br)Re^I(CO)$_3$Cl (260 mg, 0.42 mmol) and Ag(CF$_3$SO$_3$) (129 mg, 0.5 mmol) were combined in 20 mL of 1:1 dry THF / 2-MTHF mixture (v:v). The solution was stirred and refluxed for 2 hr in the dark and the white AgCl precitpitate was removed by filtration through a pad of celite. Then 4,4'-bipyridine (467 mg, 2.94 mmol) in 10 mL of EtOH was added. The reaction mixture was refluxed overnight under nitrogen, resulting a yellow solution. The solution was allowed to cool to room temperature and the solvent

was removed under vacuum. Collect the solid and dissolve in acetone. Upon addition of 5 mL of saturated aqueous NH$_4$PF$_6$ solution, the red PF$_6^-$ salts of the complexes were precipitated. The solid was collected by centrifugation and wash with H$_2$O and hexane. Yield: 280 mg (75%). ^{1}H-NMR (300 MHz, CD$_3$Cl$_3$) δ 7.48 (d, 2H), 7.70 (d, 2H), 8.18 (d, 2H), 8.40 (d, 2H), 8.48 (d, 2H), 8.72 (d, 2H), 9.02 (s, 2H).

[(bpy-Br)Re^I(CO)$_3$(MQ$^+$)]

To a solution of 100 mg of **(bpy-Br)Re(CO)$_3$(bpy)** (100 mg, 0.113 mmol) in CH$_2$Cl$_2$ was added trimethyloxonium tetrafluorborate (20 mg, 0.13 mmol). The reaction mixture was stirred under argon for 12 hr at room temperature. During the course of reaction, there was some oil residue fallen out of the solution. Collect this precipitate and dissolve in acetone. Upon addition of 5 mL of saturated aqueous NH$_4$PF$_6$ solution, the red PF$_6^-$ salts of the complexes were precipitated. The solid was collected by centrifugation and wash with H$_2$O and Et$_2$O. Yield: 80 mg (68%). ^{1}H-NMR (300 MHz, CD$_3$COCD$_3$) δ 4.64, (s, 3H), 8.04 (d, 2H), 8.55 (d, 2H), 8.67 (m, 4H), 9.03 (d, 2H), 9.19 (d, 2H), 9.65 (s, 2H).

2-C7

Compound **16** (80 mg, 0.0756 mmol), compound **18** (28 mg, 0.16 mmol), tetrahydrofuran (8 mL) and diisopropylamine (5 mL) were combined in a Schlenk flask which was then degassed with argon for 0.5 hr. Pd(PPh$_3$)$_4$ (4.8 mg, 0.004 mmol) and CuI (0.8 mg, 0.008 mmol) were added to the Schlenk flask. The resulting solution was heating at 70°C for 20 hr. The solution was allowed to cool and the solvent removed under vacuum. The crude product was dissolved in 50 mL of chloroform. The combined organic phase was washed with NH$_4$·OH (50%), H$_2$O and dried over MgSO$_4$. Most of the

solvent was evaporated under vacuum and the concentrated solutions poured into ether. The formed red solid was collected by centrifugation, washed with hexane and dried in vacuum to yield 2-C7 41 mg (76%). ^{1}H-NMR (300 MHz, CDCl$_3$) δ 0.88 (br t, 12H), 1.35 (br s, 24H), 1.58 (br m, 8H), 1.88 (br m, 8H), 4.06 (br t, 8H), 7.06 (s, 4H), 7.40 (t, 2H), 7.51 (t, 4H), 7.61 (m, 12H), 7.91 (d, 2H), 8.44 (d, 2H), 8.81 (s, 2H).

Re-2

Oligomer 2-C7 (77 mg, 0.067 mmol) and Re(CO)$_5$Cl (36 mg, 0.1 mmol) were dissolved in 30 mL of toluene, the solution was purged with argon and then was heated at 90°C for 2 hr. The solution color changed from light yellow to deep red. During the course of the reaction the blue-green fluorescence characteristic of 2-C7 disappeared. The solution was allowed to cool to room temperature and the toluene was removed under vacuum. The complex was purified by repeated rinsing with acetone. The metallated oligomer was obtained as a dark red solid, 80 mg (82%). ^{1}H-NMR (300 MHz, CDCl$_3$) δ 0.88 (br t, 12H), 1.25 (br s, 24H), 1.58 (br m, 8H), 1.85 (br m, 8H), 4.06 (br t, 8H), 7.08 (s, 4H), 7.36 (s, 2H), 7.42 (d, 4H), 7.55 (m, 12H), 7.90 (d, 2H), 8.01 (d, 2H), 9.12 (s, 2H). ^{13}C-NMR (75.4 MHz, CDCl$_3$) δ 14.1, 22.5, 25.9, 26.1, 29.3, 29.8, 31.9, 69.4, 69.5, 86.5, 88.9, 95.5, 95.8, 111.3, 116.0, 116.4, 116.6, 122.1, 122.6, 122.9, 124.4, 126.9, 127.6, 128.8, 132.0, 140.1, 140.3, 141.0, 152.8, 153.5, 154.2, 154.7, 189.0 (CO), 196.7 (CO).

Re-2-bpy-Re-2

Re-2 (46 mg, 0.0312 mmol) and Ag(CF$_3$SO$_3$) (32 mg, 0.12 mmol) were combined in 20 mL of 1:1 dry THF / 2-MTHF mixture (v:v). The solution was stirred and refluxed for 2 hr in the dark and the white AgCl precitpitate was removed by filtration through a pad of celite. Then 4,4'-bipyridine (25.0 mg, 0.16 mmol, 5 × excess) in 10 mL of EtOH

was added. The reaction mixture was refluxed overnight under nitrogen, resulting in a deep organge-red solution. There is a little bit of blue fluorescence characteristic of the free ligand which was probably caused by the decomposing of **Re-2**. After the solution was cooled to room temperature, the solvent was evaporated under vacuum. Crude product was dissolved in 5 mL of acetone. Upon addition of 5 mL of saturated aqueous NH_4PF_6 solution, the red PF_6^- salt of the complex precipitated. The solid was collected by centrifuge and washed with H_2O and Et_2O. The solid was further purified by chromatography on a small activated alumna column packed in hexane. The solid was dissolved in a minimum of the dichloromethane and loaded into the column through a pipet. Upon elution with neat Et_2O, the strong fluorescent impurity band was eluted. After remove of the impurity, the desired product was eluted by changing the eluant to 5:1 Et_2O/dichloromethane. The dark red band was collected and taken to dryness by rotary evaporation. Yield: 25 mg (50%). ^{1}H-NMR (300 MHz, $CDCl_3$) δ 0.88 (br t, 24H), 1.23 (br s, 48H), 1.58 (br m, 16H), 1.85 (br m, 16H), 4.06 (br t, 16H), 7.06 (s, 4H), 7.08 (s, 4H), 7.36 (t, 6H), 7.46 (t, 6H), 7.63(m, 28H), 8.19 (d, 4H), 8.24(d, 4H), 8.37 (d, 4H), 9.06 (s, 4H). ^{13}C-NMR (75.4 MHz, $CDCl_3$) δ14.1, 25.9, 26.1, 29.3, 29.7, 31.9, 69.4, 69.6, 86.4, 88.6, 96.0, 96.6, 110.9, 116.4, 116.8, 122.3, 125.1, 125.5, 125.9, 126.9, 127.7, 128.8, 131.8, 132, 140.2, 141.2, 142.1, 152.3, 153.0, 153.5, 154.0, 154.2, 195.1. MALDL-MS calculated for $C_{180}H_{185}N_6O_{14}Re$ 3028.91325, found 3028.8. IR (mineral oil): 2201.5, 2034.4, 1925.8, 1886.9, 1472.2, 1416.6, 1285.4, 1219.8.

N-methyl-4,4'-bipyridium (MQ$^+$)

4,4'-bipyridine (5.0 g, 32 mmol) and methyl iodide (4.09 g, 29 mmol) were dissolved in 100 mL of ethyl acetate, and the solution was stirred under nitrogen for 4 hr. The solution became yellowish and there were a copious amount of yellow solid formed

during the course of reaction. The solid was collected by vacuum filtration and washed with Et$_2$O. The solid was dissolved in minimum amount of water and 10 mL of saturated NH$_4$PF$_6$ aqueous solution was added to the solution. The resulting solid was collected and washed with excess water and Et$_2$O to yield 2.0 g of white solid product (22%). ^{1}H-NMR (300 MHz, CD$_3$CN$_3$) δ 4.36 (s, 3H), 7.81 (d, 2H), 8.36 (d, 2H), 8.70 (d, 2H), 8.84 (d, 2H).

Re-2-MQ

Re-2 (70 mg, 0.0476 mmol) and Ag(CF$_3$SO$_3$) (18 mg, 0.07 mmol) were combined in 20 mL of dry THF. The solution was stirred and refluxed for 2 hr in the dark and a white AgCl precipitate was removed by filtration through a pad of celite. Then excess N-methyl-4,4'-bipyridium (24 mg, 0.07 mmol) in 10 mL of EtOH was added. The reaction mixture was refluxed overnight under nitrogen, resulting a deep orange-red solution. There is a weak blue fluorescence characteristic of free ligand which was probably due to the decomposing of **Re-2**. After the solution was cooled to room temperature, the solvent was evaporated under vacuum. Crude product was dissolved in 5 mL of acetone and 20 mL of Et$_2$O was added to precipitate most of excess **MQ$^+$**. The liquid phase was collected by vacuum filtration and concentrated to dryness. The product was further purified by chromatography on a small activated alumna column packed in hexane. The solid was dissolved in a minimum of the dichloromethane and loaded into the column through pipet. Upon elution with the Et$_2$O and dichloromethane sequentially, the unreacted starting compound was eluted. After removed of the impurity, the desired product was eluted by changing the eluant to 1:1 CH$_2$Cl$_2$/CH$_3$CN (v:v). The dark red band was collected and taken to dryness by rotary evaporation. Yield: 18 mg (20%). ^{1}H-NMR (300 MHz, CDCl$_3$) δ 0.88 (t, 12H), 1.25 (br s, 24H), 1.58 (br m, 8H), 1.85 (br m, 8H), 4.06 (br

t, 8H), 4.15 (s, 3H), 7.08 (s, 2H), 7.11 (s, 2H), 7.37 (t, 4H), 7.48 (t, 2H), 7.61 (m, 12H),

7.93 (d, 2H), 8.24 (d, 2H), 8.40 (t, 4H), 8.48 (d, 2H), 8.89 (d, 2H), 9.12 (s, 2H). ^{13}C-NMR

(75.4 MHz, CDCl$_3$) δ 14.4, 22.9. 26.1, 26.3, 29.4, 32.1, 69.9. 96.5, 104.5, 117.1, 126.8,

127.3, 129.1, 132.3, 142.2, 143.6, 146.1, 154.5, 173.8, 188.8, 192.7. MALDI-MS

Calculated for C$_{96}$H$_{99}$N$_4$O$_7$Re (M-2PF$_6$) 1607.04, found 1607.2. IR (mineral oil): 2204,

2033, 1921, 1504, 1417, 1255.9, 1220.4, 1159.8, 1029.7.

Re-2-Py

Re-2 (23 mg, 0.0156 mmol) and Ag(CF$_3$SO$_3$) (16 mg, 0.062 mmol) were

combined in 20 mL of 1:1 dry THF / 2-MTHF mixture (v:v). The solution was stirred and

refluxed for 2 hr in the dark and a white AgCl precipitate was removed by filtration

through a pad of celite. Then excess pyridine (5 mL) in 10 mL of EtOH was added. The

reaction mixture was refluxed overnight under nitrogen, resulting in a deep organge-red

solution. There is a little bit blue fluorescence characteristic of free ligand which was

probably the decomposing of Re-2. After the solution was cooled to room temperature,

the solvent was evaporated under vacuum. Crude product was dissolved in 5 mL of

acetone. Upon addition of 5 mL of saturated aqueous NH$_4$PF$_6$ solution, the red PF$_6^-$ salt of

the complex precipitated. The solid was collected by centrifuge and washed with H$_2$O.

The complex was reprecipitated by dissolving it in a minimum amount of

dichloromethane and adding the solution dropwise to 30 mL of hexane under stirring.

The product was further purified by chromatography on a small activated alumna column

packed in hexane. The solid was dissolved in a minimum of the dichloromethane and

loaded into the column through pipet. Upon elution with the 2:1 hexane/Et$_2$O (v:v), the

strong fluorescent impurity band was eluted. After removing the impurity, the desired

206

product was eluted by changing the eluant to neat Et$_2$O. The dark red band was collected and taken to dryness by rotary evaporation. Yield: 13 mg (50%). ^{1}H-NMR (300 MHz, CDCl$_3$) δ 0.86 (br t, 12H), 1.25 (br s, 24H), 1.58 (br m, 8H), 1.85 (br m, 8H), 4.06 (br t, 8H), 7.08 (s, 4H), 7.39 (br m, 8H), 7.89 (t, 1H), 8.13 (d, 2H), 8.29 (d, 2H), 8.59 (d, 2H), 9.05 (s, 2H). ^{13}C-NMR (75.4 MHz, CDCl$_3$) δ14.6, 23.1, 26.3, 26.5, 29.3, 29.5, 29.8, 30.2, 32.2, 69.9, 70.1, 86.7, 88.9, 96.6, 96.9, 111.3, 116.9, 117.3, 122.4, 126.3, 127.4, 127.8, 128.2, 129.3, 133.5, 140.7, 141.7, 143.2, 151.9, 153.6, 153.9, 154.2, 154.6, 190.7, 196.0. MALDI-MS Calculated for C$_{96}$H$_{99}$N$_4$O$_7$Re (M-PF$_6$) 1512.65, found 1512.64. IR (mineral oil): 1924.3, 1463, 1377.

CHAPTER 5
SYNTHESIS AND PHOTOPHYSICS OF PHENYLENE ETHYNYLENE VINYLENE OLIGOMERS THAT CONTAIN THE $Ru(bpy)_2^{2+}$ CHROMOPHORE

Introduction

Besides the PPE type oligomer described in Chapter 2, we also tried to extend this oligomer system to a polymer. But the solubility problem is always the issue due to the rigid PPE polymer chains. Bearing this in mind, it is reasonable to suggest that a polymer consisting of discrete aryleneethynylene moieties linked together by flexible spacers should increase the solubility. Incorporation of vinylene into backbone would be a good choice and it would be of interest to study the hybrid of two structure types (PPVE), i.e., PPV and PPE. In this chapter we will describe the synthesis and photophysics of the model complex of PPVE type polymer. The structures are listed in Figure 5-1.
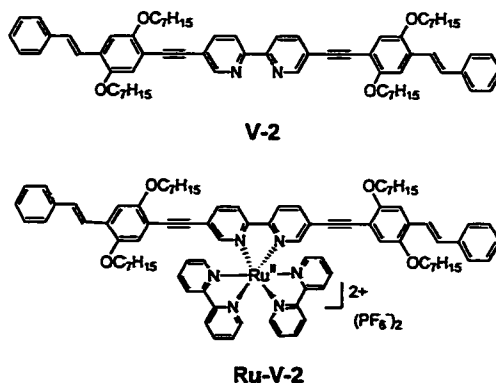
Figure 5-1: Structure of oligomers.

208

Synthesis

We applied the same synthesis strategy as synthesizing **Ru-2-C7** to make **V-2** and **Ru-V-2**. Central core **16** is coupled to outside segment styrene by Heck reaction (Figure 5-2). Heck reaction is found to be a very convenient method for forming carbon-carbon bonds at unsubstituted vinylic positions.[126] Recently, the Heck reaction has been utilized to prepare PPV from dibromobenzene and ethylene and other poly(arene vinylenes).[127-130]

Compound **16** was synthesized as described in Chapter 2. The coupling reaction followed the modification of procedure developed by Yu.[23] Reaction of compound **16** with 2 equivalent of styrene gave oligomer **V-2** with moderate yield (Figure 5-2). The metellation of **V-2** with *cis*-**Ru(bpy)₂Cl₂** to make **Ru-V-2** didn't work very well. Then the coupling reaction between **Ru-2-C7-I** and styrene was attempted (Figure 5-3). The desired product **Ru-V-2** was obtained in reasonable yield.
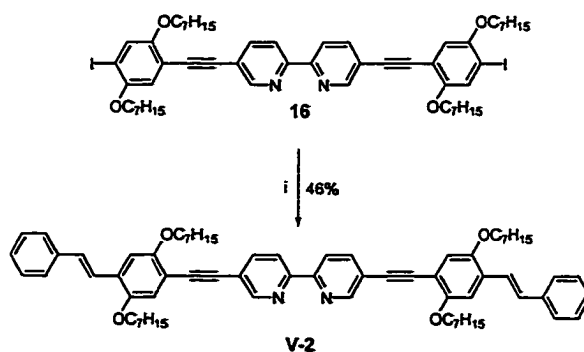
i. Styrene, DMF/Et₃N, Pd(OAc)₂, P(*o*-tol)₃, heat.

Figure 5-2: Synthesis of **V-2**.
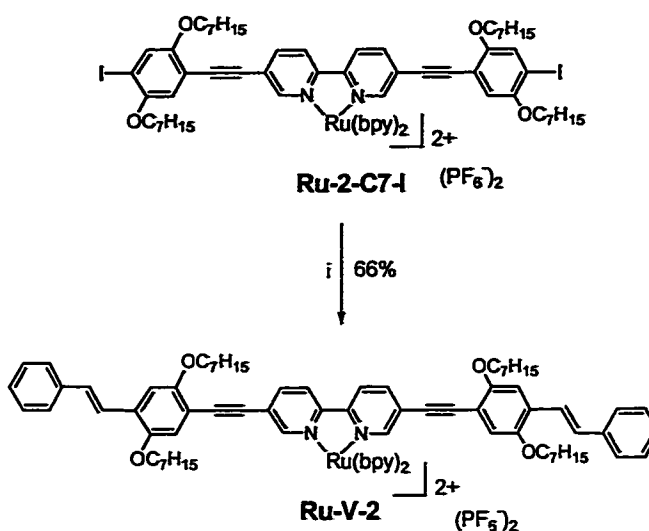
i. Styrene, DMF/Et$_3$N, Pd(OAc)$_2$, P(o-tol)$_3$, heat.

Figure 5-3: Synthesis of **Ru-V-2**.

Results

Electrochemistry

Cyclic voltammetry was performed on the **Ru-V-2** in CH$_2$Cl$_2$ with 0.1 M TBAH

as the supporting electrolyte. Figure 5-4 illustrates the cyclic voltammogram of **Ru-V-2**.

The relevant oxidation and reduction half-wave potentials are listed in Table 5-1. For

comparison, redox potentials of **Ru-2-C7** are also included.
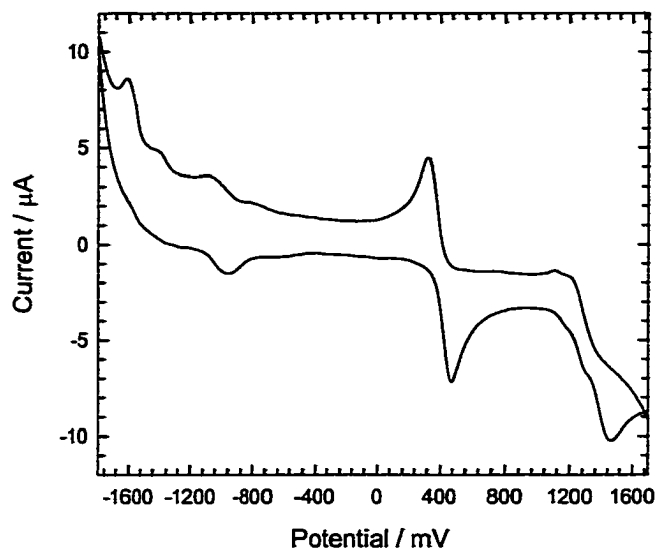
Figure 5-4: Cyclic voltammetry of **Ru-V-2** in CH_2Cl_2.

The one-electron oxidation is quasi-reversible with a half-wave potential at 1.36 V which is very similar to its **Ru-2-C7** analogue. It is still difficult to determine whether this oxidation wave corresponds to the Ru(II/III) couple or the oxidation of ligand. The first reduction occurs with $E_{1/2} \approx -1.0$ V which is also almost identical to **Ru-2-C7**. This wave is assigned to reduction of the **V-2** ligand. The second and third reduction waves are irreversible.

Table 5-1: UV-visible absorption bands and electrochemical results[a] in CH_2Cl_2 at 298 K.

Compound	λ_{max} / nm	ε_{max} / mM^{-1}cm^{-1}	$E_{1/2,}^{ox}$	$E_{1/2,}^{red}$
V-2	322	48.4		
	408	98.4		
Ru-V-2	289	80.9	1.36	-1.0 (V-2$^{0/-}$)
	346	58.5		
	469	54.1		
Ru-2-C7	290	78.5	1.32	-0.96 (2$^{0/-}$)
	342	64.3		
	454	48.8		

[a] Estimated error in $E_{1/2}$ values is ± 0.05 V for reversible waves. Recorded in CH_3CN solution with 0.1 M TBAH as supporting electrolyte with a Pt working electrode, a Pt auxiliary electrode, and Ag/Ag$^+$ reference electrode. Potentials are referenced to a ferrocene internal standard and reported in V vs. SCE along with their assigned redox couples. Fc$^+$/Fc = 0.425 V was assumed in CH_3CN, and 0.45 V in CH_2Cl_2.[86]

Absorption Spectra

Absorption spectra for the free oligomer and metal complex were obtained on dilute CH_2Cl_2 solutions. Absorption spectra are shown in Figure 5-5 and Table 5-1 contains a listing of the absorption bands and extinction coefficients. For comparison, the absorption spectrum of **Ru-2-C7** is also included in Figure 5-5.

The free oligomer exhibits two strong absorption bands in 300 – 450 nm region. The low energy band is due to the long-axis polarized π,π* transition, while the high energy band is due to the short-axis π,π* transition. Metallation of this oligomers also red-shifts the absorption band considerably due to the increase of conjugation length. And the Ru → V-2 MLCT band is buried under considerably more intense π,π* transition.
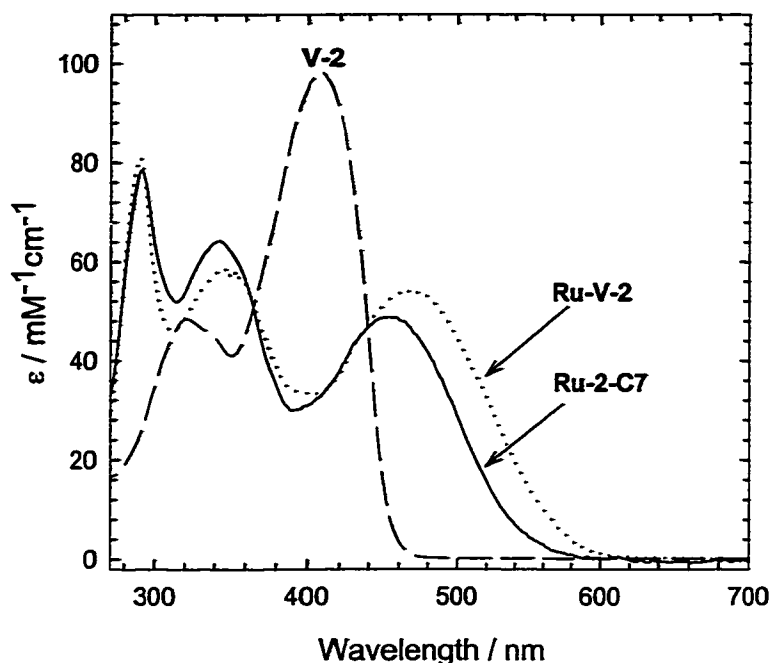
Figure 5-5: Absorption spectra in CH_2Cl_2. **V-2** (long dash line), **Ru-V-2** (dot line), and **Ru-2-C7** (solid line).

Emission Spectra

Emission studies were carried out on **V-2** and **Ru-V-2**; emission maixima at 298

and 80 K are given in Table 5-2. In Figure 5-6 are shown emission spectra of **Ru-V-2** and

V-2 in CH_3CN at room temperature. At room temperature, **V-2** features a structureless

strong emission band at 490 nm that exhibits a small Stokes shift (i.e., shift to lower

energies) from the lowest-energy absorption. On this basis, the emission is assigned to

the long-axis polarized $^1\pi,\pi^*$ state. This emission band is red-shifted compared to that of

2-C7. Excitation of **Ru-V-2** at 450 nm at room temperature in CH_3CN produces a

moderately intense emission at $\lambda_{max} \approx 690$ nm (Figure 5-6). It features a broad emission

bad with well-defined (0,0) and (0,1) vibronic components. This emission band is

probably due to the dπ(Ru) → π*(V-2) MLCT excited state because it is very similar to

that of **Ru-2-C7** besides a slight red shift on emission maxima.
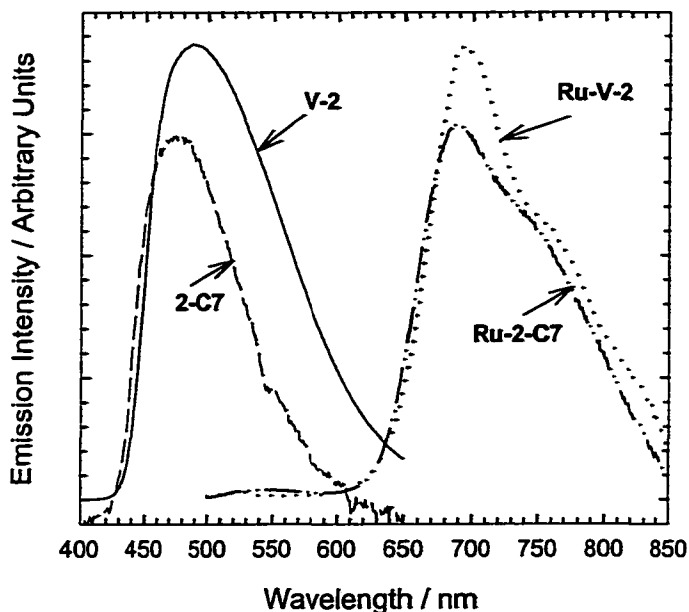
Figure 5-6: Emission spectra of the **V-2** and **Ru-V-2** in argon bubble-degassed CH_3CN at room temperature. **2-C7** (dash line), **V-2** (solid line), **Ru-V-2** (dotted line), and **Ru-2-C7** (dash-dot-dotted line).

Emission spectra of **V-2** in 2-MTHF solvents at temperatures ranging from 298 to

165 K is shown in Figure 5-7. At 298 K, the spectrum shows superposition of a 400 nm

band and a 450 nm band. The intensity of high energy band decreases with decreasing

temperature. And at the lowest examined temperatures the emission is dominated by a

broad band that lie to the red of the assigned "0-0" band.
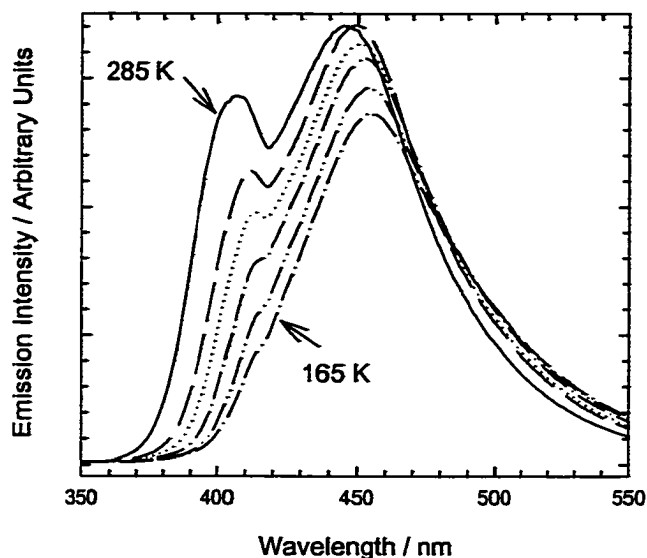
Figure 5-7: Corrected emission spectra of V-2 at 298, 265, 245, 225, 205, 185 and 165 K. Spectrum is acquired from 2-MTHF solution with an excitation wavelength of 300 nm.

In Figure 5-8 are shown temperature-dependent emission spectra of Ru-V-2 in 2-MTHF solutions through the glass-to-fluid transition region from 80 to 298 K. The emission intensity increases substantially upon cooling (a 5-fold increase on cooling from 298 to 80 K). As temperature increases, the band red-shifted and it becomes broad at 298 K. The appearance of emission spectra of Ru-V-2 at 80 K is different from that of Ru-2-C7. It features the superposition of a 650 nm band and a structured (0,0) 700 nm band with a vibronic (0,1) shoulder. When the temperature is above 125 K, the high energy band disappears and there was very little band shifting of the structure emission to higher or lower energies with increasing temperature. Excitation spectra probing this emission (not shown) agree well with the absorption spectra.
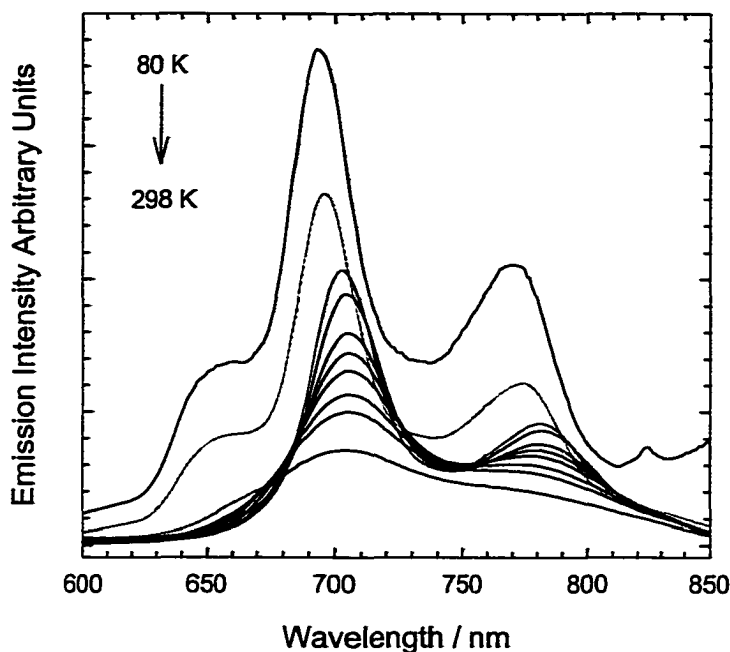
Figure 5-8: Emission spectra of **Ru-V-2** in 2-MTHF (450 nm excitation) at temperature varying from 298 to 80 K. Emission intensity decreases with increasing temperature, and spectra are in 20 K increments.

Table 5-2: Photophysical properties of **V-2** and **Ru-V-2**.

Compound	λ_{max}^{em} nm	ϕ_{em}[b]	τ_{em}[c] μs	298 K[a] $10^3 k_r$[d] s^{-1}	$10^5 k_{nr}$[d] s^{-1}	τ_{TA}[e] μs	80 K[e] λ_{max}^{em} nm
V-2	490						407, 443
Ru-V-2	690	0.009	1.0	8.7	9.6	2.4	694, 768
Ru-2-C7	690	0.034	0.7	44	13	0.99	658, 701

[a] Measurements were conducted on argon bubble-degassed CH_3CN solution at 298 K.
[b] The actinometer uses a standard sample of $[Ru(bpy)_3]Cl_2$ in H_2O for which $\phi_{em} = 0.055$.[102] [c] The mean decay lifetime obtained at 700 nm. [d] $k_r = \phi_{em} / \tau$; $k_{nr} = 1/\tau_{em}(1-\phi_{em})$. It is assumed that the emitting state is produced with $\phi = 1$. [e] Decay lifetimes of transient absorption. [f] Measurements were conducted on free-pump-thaw degassed 2-MTHF at 80 K.

<u>Emission Lifetime</u>

The emission decay of **Ru-V-2** complex in CH_3CN at room temperature was measured and the decay times at various emission wavelengths are listed in Table 5-3. The emission decay profiles are multiexponential. On the blue side of emission (650 nm), the emission decay was fit to a three-component exponential with lifetimes of 7.6, 700, 4100 ns; each lifetime had a significant amplitude (28%, 26%, and 41%). The long-lived component can only be contributed to the $^3\pi,\pi^*$ excited state at room temperature. On the low-energy side of the emission band (700 nm), the emission decay was fit to a three-component exponential with lifetimes of 19 (3%), 500 (36%), and 1400 ns (61%). The major component ($\tau \approx 1.4 \ \mu s$, $\alpha = 61\%$) is probably due to MLCT excited state. At both wavelength the emission decays feature a short-lived component which is possibly caused by the equilibrium between MLCT and $^3\pi,\pi^*$ states. Figure 5-9 shows the decay at 700 nm observed for **Ru-V-2** in CH_3CN solution on a logarithmic scale along with the excitation lamp profile and the computer calculated fit.

The luminescence quantum yields (ϕ_{em}) were measured for **Ru-V-2** complex in CH_3CN at 298 K, and the values are listed in Table 5-2. Radiative and apparent nonradiative decay rates (k_r and k_{nr}) were computed for this complex from equation 2-1 using the ϕ_{em} and τ_{em} values, and these parameters are also listed in the table. The additional rigidity in the **Ru-2-C7** compared to the **Ru-V-2** allowed for higher emission quantum yield. And k_r is smaller for **Ru-V-2** because of the more triplet π,π^* character of the excited state.
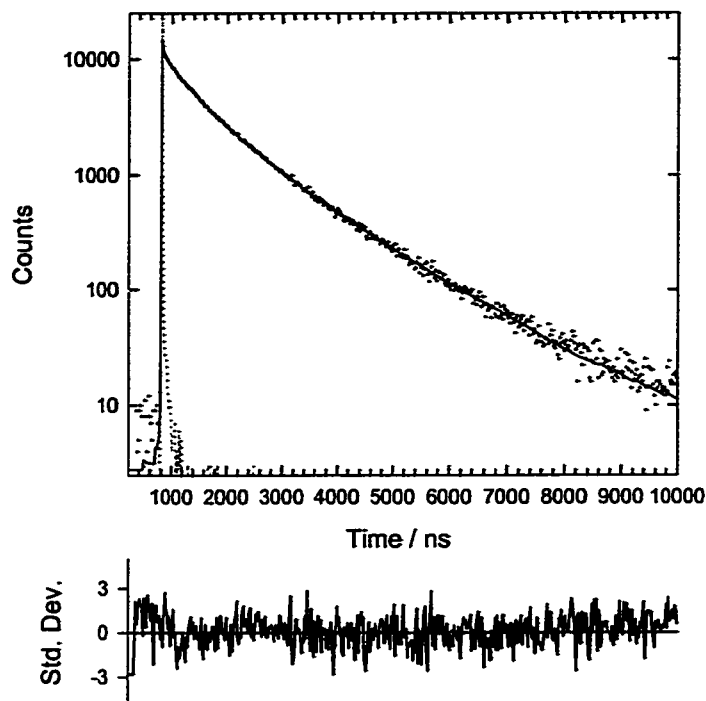
Figure 5-9: Time resolved emission decay of **Ru-V-2** in CH_3CN at room temperature. Decay was recorded at 700 nm. Upper box shows the emission decay (Δ) and the excitation lamp profile (dot line) along with the computer-calculated fit (solid line). Lower box show plots of the residuals indicating the quality of the calculated fit.

The decay times at various emission wavelengths for the **Ru-V-2** were obtained as a function of temperature in 2-MTHF. Multiexponential kinetics were observed for the emission decay, and parameters recovered from three-component fit of the emission decays are listed in Table 5-3.

At 80 K, the amplitudes and lifetimes obtained on the blue side of the emission (650 nm) are in contrast to those obtained at red side of the emission (700 nm). At 650 nm, the emission decay was fit to a three-component exponential with lifetimes of 15.8, 1084, and 3497 ns, and the long-lived component dominates emission decay ($\alpha = 81\%$)

which arises from ^{3}MLCT state. On the red side of emission (700 nm), the emission

decay was still fit to a three-component exponential with lifetimes of 18 (3%), 2033

(28%), and 10650 (69%) ns; and long-lived component has a significant amplitude which

is probably due to the $^3\pi,\pi^*$ state. We believe that the low temperature emission for **Ru-**

V-2 is due to overlapping MLCT emission and oligomer $^3\pi,\pi^*$ phosphorescence. Figure

5-10 shows the decay observed for **Ru-V-2** in 2-MTHF solvent on a logarithmic scale

along with the excitation lamp profile and the computer calculated fit. The decays in 2-

MTHF at room temperature were identical to those obtained in CH$_3$CN.
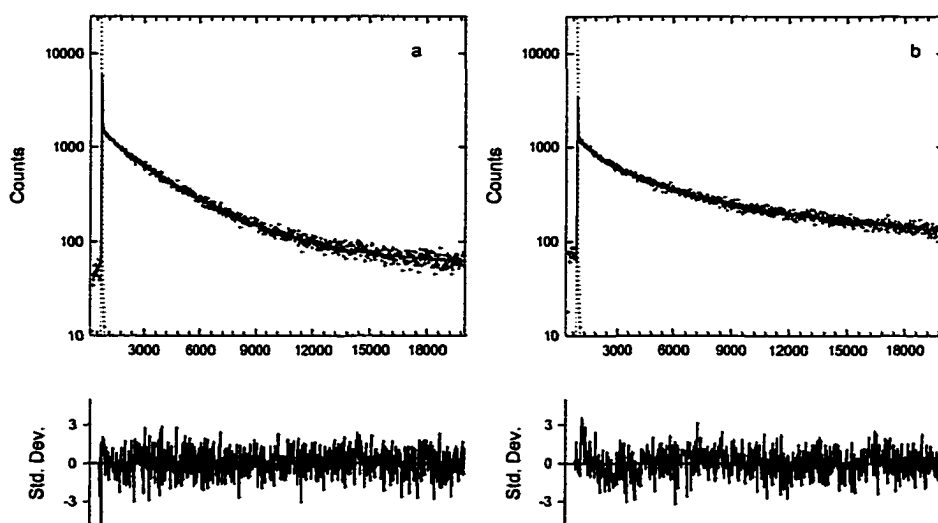
Figure 5-9: Time resolved emission decay of **Ru-V-2** in 2-MTHF at 80 K. Upper box shows the emission decay (Δ) and the excitation lamp profile (dot line) along with the computer-calculated fit (solid line). Lower box show plots of the residuals indicating the quality of the calculated fit. (a) Decay was recorded at 650 nm; (b) Decay was recorded at 700 nm.

Table 5-3: Variable temperature emission decay times of **Ru-V-2** complex [a].

T / K	650 nm					700 nm				
	τ_1, μs (α_1, %)	τ_2, μs (α_2, %)	τ_3, μs (α_2, %)	$<\tau>$ [b] μs	χ^{2} [c]	τ_1, μs (α_1, %)	τ_2, μs (α_2, %)	τ_3, μs (α_2, %)	$<\tau>$ [b] μs	χ^{2} [c]
80 [d]	0.016 (7)	1.1 (12)	3.5 (81)	2.7	1.04	0.018 (3)	2.0 (28)	10.6 (69)	7.9	1.05
298 [d]	0.01 (32)	0.6 (27)	3.4 (41)	1.6	1.89	0.01 (5)	0.5 (26)	2.6 (69)	1.9	1.08
298 [e]	0.0076 (28)	0.7 (26)	4.1 (46)	2.1	1.3	0.019 (3)	0.5 (36)	1.4 (61)	1.0	1.3

[a] 405 nm Excitation. Lifetime and relative triexponential fits were performed with equation 2-2. [b] The mean decay lifetime, $<\tau>$, was calculated using the multiexponential decay data according to the equation 2-3. [c] χ^2 is used to evaluate the quality of the calculated fit. $\chi^2 = 1$ means the best fit. [d] Samples were measured in free-pump-thaw degassed 2-MTHF. [e] Samples were measured in argon-bubble degassed CH_3CN.

<u>Transient Absorption Spectra</u>

Transient absorption spectra were recorded for **Ru-V-2** in CH_3CN solutions. The difference spectra following pulsed laser excitation at 355 nm is shown in Figure 5-11. Transient absorption decay lifetimes obtained from global (factor) analyses of the time-resolved absorption data are listed in Table 5-2. The spectrum exhibits ground state π,π^* absorption bleaching at 350 nm and 450 nm similar to that observed in the spectra of **Ru-2-C7**; however, the excited-state absorption of **Ru-V-2** in the 500 - 800 nm region is much less prominent than that of **Ru-2-C7** (i.e.; the absorption of **Ru-V-2** increase in intensity from 500 – 800 nm without any discernible maximum in this region). Furthermore, the transient absorption decay lifetime is in agreement with the luminescence decay lifetimes obtained at 650 nm. These features point to the possibility that, for **Ru-V-2**, the transient absorption arises from the $^3\pi,\pi^*$ state, not ^{3}MLCT state.
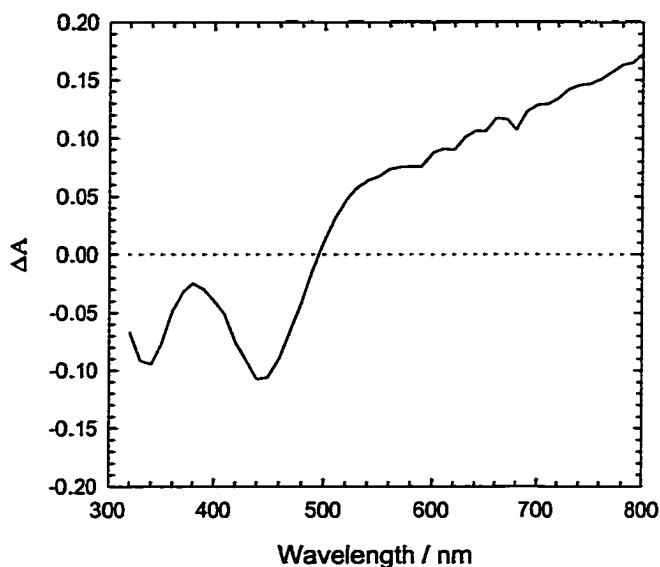
Figure 5-10: Transient absorption difference following 355 nm pulsed laser excitation (5 mJ dose) acquired from argon bubble degassed CH_3CN solution.

Discussion

Photophysics of Oligomer V-2

Although the fluorescence of oligomer V-2 at room temerpature is "typical", the variable-temperature emission data is uncommon. Specifically, the high-energy band decreases in intensity with decreasing temperature. The structurally similar oligomer 2-C18 also shows uncommon temperature dependence emission data. It's fluorescence decreases in intensity and red-shifts with decreasing temperature which is attributed to aggregation at low temperature.[98] For V-2, the aggregation can not explain the disappearance of high energy band at low temperature. It is possibly that unusual photoluminescence at different temperature arise from variation in the conformation of the oligomer backbone since the more flexible vinylene bond is introduced into the molecule.

Photophysics of Ru-V-2

Compared to Ru-2-C7, the absorption band of Ru-V-2 is red-shifted by 15 nm. We conclude that the energy gap of V-2 is lower than that of 2-C7. The same hybrid PPVE polymer has been synthesized by Bunz and coworkers[131] (Figure 5-12). The absorption spectra of PPVE are broad and unstructured but bathochromically shifted by 11 nm when compared to those of identically substituted PPEs. The introduction of vinylene band into PPE backbone decreases the energy gap.
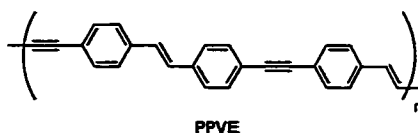
PPVE

Figure 5-12: Structure of PPVE polymer.

To better understand the remaining photophysical data, it is necessary to establish the energies for the various low-lying excited states for **Ru-V-2**. Figure 5-13 provides a general state diagram for this complex, where the energies of the various state are defined as accurately as possible. Based on the absorption spectrum, we estimate that $^1\pi,\pi$ state lies in the 2.64 eV. For **Ru-2-C7** the $^3\pi,\pi$ energy lies in 1.9 eV. Since the absorption spectra of **Ru-V-2** red shifts 15 nm compared to **Ru-2-C7**, we estimate the $^3\pi,\pi^*$ energy of **Ru-V-2** will also red-shifts the same amount. Then $^3\pi,\pi^*$ energy lies in 1.86 eV. For **Ru-V-2** the emission is mostly from the ^{3}MLCT state, so based on the wavelength of the emission at room temperature ($\approx$ 690 nm) we estimated that this state lies at $\approx$ 1.80 eV. The estimation of ^{1}MLCT state energy is still based on the absorption of Ru(bpy)$_3^{2+}$ (λ_{max} $\approx$ 450 nm), and ^{1}MLCT state lies at approximately 2.71 eV.

From this analysis, it is evident that $^3\pi,\pi^*$ and ^{3}MLCT states are in close energetic proximity. This close proximity makes that both states contribute to the observed photophysics. Initial photoexcitation populates the $^1\pi,\pi^*$ manifold since the absorption spectrum is dominated by intense $^1\pi,\pi^*$ transition. Subsequently, ultrafast energy transfer and intersystem crossing ensues to afford a non-equilibrium distribution of the $^3\pi,\pi^*$ and ^{3}MLCT states which are both emissive. For emission lifetime decay, the decay via $^3\pi,\pi^*$ and ^{3}MLCT states can always be observed. Since the $^3\pi,\pi^*$ and ^{3}MLCT states are very close in energy, there is an rapidly established equilibrium between $^3\pi,\pi^*$ and ^{3}MLCT states. So the origin of the fast emission decay components ($\tau \approx 7 - 20$ ns) corresponds to establishment of the equilibrium between the $^3\pi,\pi^*$ and ^{3}MLCT excited states. The

population remaining in the $^3\pi,\pi^*$ state is available to be excited into a higher triplet

excited state, produced the obtained transient absorption spectrum.
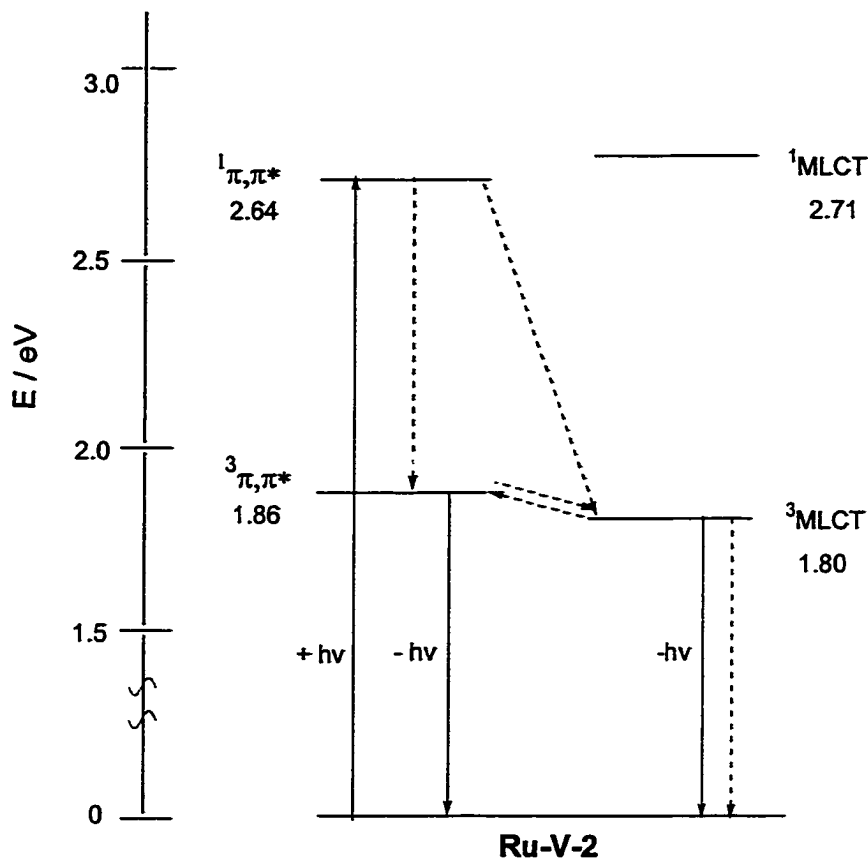
Figure 5-13: **Ru-V-2** complex Jablonski diagram.

Experimental

Photophysical Measurements

All room temperature studies were conducted in CH_2Cl_2 and CH_3CN and low

temperature studies were conducted in 2-MTHF. All solvents were distilled according to

typical laboratory practices. All photophysical studies were conducted with the same instrumentation and techniques described in Chapter 2.

Emission Quantum Yield

Emission quantum yields were determined at room temperature in CH_3CN using samples of known optical density, compared to a standard sample of [Ru(bpy)$_3$]Cl$_2$ in H_2O for which $\phi_{em} = 0.055$.[102] Quantum yield values were calculated by using equation 2-10.

Electrochemical Measurements

All electrochemical measurements were conducted on CH_2Cl_2 solutions with TBAH as the supporting electrolyte. Cyclic voltammetry measurements were performed with the same procedures on the same instrumentation described in Chapter 2.

General Synthetic

Triethylamine was distilled from KOH. The synthesis of compound 16 is described in chapter 2. Copper(I) iodide, Pd(OAc)$_2$, P(o-tol)$_3$ and Pd(PPh$_3$)$_4$were purchased from Aldrich Chemical Co. and used without further purification. All cross-coupling reactions using Pd catalyst were carried out under standard Schlenk and vacuum line techniques. ^{1}H and ^{13}C NMR was recorded on Gemini-300 and VXR-300 NMR spectrometers. High-resolution mass spectrometry was performed by the University of Florida analytical service. The matrix used for MALDI analysis is α-cyanohydroxycinnamic acid in THF solvent.

Synthesis

V-2

Compound 16 (68 mg, 0.064 mmol), styrene (15 mg, 0.14 mmol), DMF (10 mL) and triethylamine (5 mL) were combined in a Schlenk flask which was then degassed

Reproduced with permission of the copyright owner. Further reproduction prohibited without permission.

with argon for 0.5 hr. Pd(OAc)$_2$ (1.0 mg, 0.003 mmol) and P(o-tol)$_3$ (4.0 mg, 0.013 mmol) were added to the Schlenk flask. The resulting solution was heated at 90°C for 20 hr. The solution was allowed to cool and the triethylamine removed under vacuum. The remaining crude product and DMF were dissolved in 50 mL of chloroform. The combined organic phase was washed with NH$_4$·OH (50%), H$_2$O and dried over MgSO$_4$. Then the solvent was removed under vacuum to yield yellow solid. The material was purified by chromatography on a silica column packed in hexane. The solid was dissolved in a minimum of dichloromethane and dry packed onto the column. Upon elution with 60:1 hexane/Et$_2$O, the strong fluorescent starting compound band was eluted. After removal of the impurity, the desired product was eluted by changing the eluant to 30:1 hexane/Et$_2$O. The shining yellow band was collected and taken to dryness by rotary evaporation. Yield 30 mg (46%). ^{1}H-NMR (300 MHz, CDCl$_3$) δ 0.82 (br t, 12H), 1.32 (br s, 24H), 1.57 (br m, 8H), 1.85 (br m, 8H), 4.01 (t, 4H), 4.12 (t, 4H), 7.04 (s, 2H), 7.14 (s, 2H), 7.20 (d, 2H), 7.25 (t, 2H), 7.44 (t, 4H), 7.52 (d, 2H), 7.55 (d, 4H), 7.94 (d, 2H), 8.44 (d, 2H), 8.62 (s, 2H). ^{13}C-NMR (75.4 MHz, CDCl$_3$) δ14.7, 23.2, 26.7, 26.8, 29.8, 30.0, 32.4, 70.0, 70.3, 91.6, 111.1, 112.4, 117.5, 121.1, 121.5, 123.7, 127.2, 128.3, 129.2, 133.5, 130.7, 138.2, 139.7, 151.0, 152.2, 154.5, 154.9. FAB-MS calculated for C$_{70}$H$_{84}$N$_2$O$_4$ 1017.64 found 1017.65.

Ru-V-2

Compound **Ru-2-C7-I** (45 mg, 0.02 mmol), styrene (15 mg, 0.08 mmol), DMF (10 mL) and triethylamine (5 mL) were combined in a Schlenk flask which was then degassed with argon for 0.5 hr. Pd(OAc)$_2$ (0.3 mg, 0.0008 mmol) and P(o-tol)$_3$ (1.4 mg, 0.013 mmol) were added to the Schlenk flask. The resulting solution was heated at 90°C

for 20 hr. The solution was allowed to cool and the triethylamine removed under vacuum. The remaining crude product and DMF were dissolved in 50 mL of chloroform. The combined organic phase was washed with $NH_4 \cdot OH$ (50%), H_2O and dried over $MgSO_4$. Then the solvent was removed under vacuum to yield red solid. The complex was reprecipitated by dissolving it in a minimum amount of dichloromethane and adding the solution dropwise to 30 mL of hexane under stirring. The product was collected by centrifuge and repeated washing with hexane serves to remove most of the unreacted styrene. The material was further purified by chromatography on an activated alumina column packed in hexane. The solid was dissolved in a minimum of dichloromethane and loaded onto the column by pipet. Upon elution with neat CH_2Cl_2, the starting material was eluted. After removal of the impurity, the desired product was eluted by changing the eluant to 6:1 CH_2Cl_2/CH_3CN. The red band was collected and taken to dryness by rotary evaporation. Yield 20 mg (66%). ^{1}H-NMR (300 MHz, CD_3COCD_3) δ 0.82 (br t, 12H), 1.32 (br s, 24H), 1.58 (br m, 8H), 1.85 (br m, 8H), 4.01 (t, 4H), 4.12 (t, 4H), 6.96 (s, 2H), 7.0 (s, 2H), 7.16 (d, 2H), 7.30 (t, 2H), 7.39 (m, 4H0, 7.46 (d, 2H), 7.57 (d, 4H), 7.65 (t, 6H), 8.08 (m, 4H), 8.23 (m, 6H), 8.86 (m, 6H). ^{13}C-NMR (300 MHz, CD_3COCD_3) δ 14.9, 23.8, 27.2, 33.1, 70.6, 90.0, 98.8, 111.9, 118.2, 123.9, 125.9, 128.0, 129.4, 130.2, 132.5, 139.7, 141.0, 153.3, 158.7. MALDI-MS calculated for $C_{90}H_{100}F_6N_6O_4PRu$ 1575.0 found 1577.4.

CHAPTER 6
CONCLUSION

In the previous chapters, the synthesis and extensive photophysics of PPE-type and PPVE-type oligomers containing a central 2,2'-bipyridine unit with different MLCT chromophore incorporation into the π-backbone have been presented. The properties of these metal-organic materials clearly indicate that the metal center interacts strongly with the π-conjugated system. The interaction gives rise to properties that are not simply predictable on the basis of the sum of the component molecular electronic systems.

In **(L)Ru^{II}(bpy)$_2$** complexes, the MLCT excited state is slightly lower in energy than the $^3\pi,\pi^*$ state of the PPE backbone. There is an equilibrium between these two states. The photoluminescence and transient absorption are dominated by ^{3}MLCT excited states. All these complexes undergo photoinduced bimolecular electron transfer reactions with oxidative and reductive quenchers.

By putting electron withdrawing groups into the bipyridine group on Ru^{II}(bpy)$_2$ chromophore which introduce another low energy ligand **R-bpy** into the system for **(L)Ru^{II}(R-bpy)$_2$** complexes, the situation becomes more complicated. For **Ru-1-COOEt** the lowest energy ^{3}MLCT state (dπ(Ru) $\rightarrow$ π^*(**decb**)) is dominated in the emission and transient absorption spectra. For **Ru-1-CF$_3$**, the excited electron is believed to be localized on π^* orbital of **tfmb**. However, the involvement of ^{3}MLCT state (dπ(Ru) $\rightarrow$ π^*(**1**)) is observed in transient absorption spectrum. For **Ru-2-CF$_3$**, all three states, ^{3}MLCT (dπ(Ru) $\rightarrow$ π^*(**2**)), ^{3}MLCT (dπ(Ru) $\rightarrow$ π^*(**tfmb**)), and $^3\pi,\pi^*$ (**2**) are very close in

227

energy and which state is dominant depends on the medium and temperature. At low temperature, $^3\pi,\pi^*$ (2) is the major deactivation mode. When temperature increases, ^{3}MLCT state gets more and more involvement in the excited state. When the solvent is changed to CH_2Cl_2, the ^{3}MLCT state is quenched by electron transfer from ligand 2 to the Ru metal center. This process generates a ligand-to-ligand charge transfer state.

By incorporation of low oxidation potential osmium metal, the ^{3}MLCT state of $(L)Os^{II}(bpy)_2$ complexes is is lower in energy than the PPE-based $^3\pi,\pi^*$ state and the "unperturbed" MLCT emission is observed. The MLCT state gives rise to the luminescence and lifetime that are typical for the $Os(bpy)_3$ chromophore.

For chromophore quencher complex $[(2)Re^I(CO)_3(MQ^+)]$, the introduction of $Re(CO)_3(MQ^+)$ chromophore into the PPE backbone shifts the MLCT state to higher energy. At low temperature, a fairly intense ^{3}MLCT emission that arises mainly from $d\pi(Re) \rightarrow \pi^*(2)$ is observed. It is clear that very little intramolecular ET quenching occurs from MQ^+ during the lifetime of the MLCT excited state. And $^3\pi,\pi^*$ phosphorescence is also observed at lower energy side. At room temperature, there is mixing of MLCT and $^3\pi,\pi^*$ emission. And the transient absorption spectrum is dominant by $^3\pi,\pi^*$ state.

For **Ru-V-2**, with the introduction of vinylene bond into PPE backbone the energy level of $^3\pi,\pi^*$ state is decreased and the photoluminescence and transient absorption are dominated by $^3\pi,\pi^*$ phosphorescence.

APPENDIX A
SPECTRAL FITTING DIAGRAM OF (L)Ru^{II}(bpy) COMPLEXES

Ru-1 / EtOH/MeOH / 85 K
$E_o = 15455$ cm^{-1}, $\hbar\omega = 1390$ cm^{-1}, $S_m = 0.96$, $\Delta_{1/2} = 870$ cm^{-1}

Ru-1 / EtOH/MeOH / 285 K
$E_o = 14749$ cm^{-1}, $\hbar\omega = 1340$ cm^{-1}, $S_m = 0.95$, $\Delta_{1/2} = 1420$ cm^{-1}

Ru-2-C7 / EtOH/MeOH / 85 K
$E_o = 15060$ cm^{-1}, $\hbar\omega = 1350$ cm^{-1}, $S_m = 0.95$, $\Delta_{1/2} = 1025$ cm^{-1}

Ru-2-C7 / EtOH/MeOH / 285 K
$E_o = 14684$ cm^{-1}, $\hbar\omega = 1270$ cm^{-1}, $S_m = 0.99$, $\Delta_{1/2} = 1220$ cm^{-1}

229
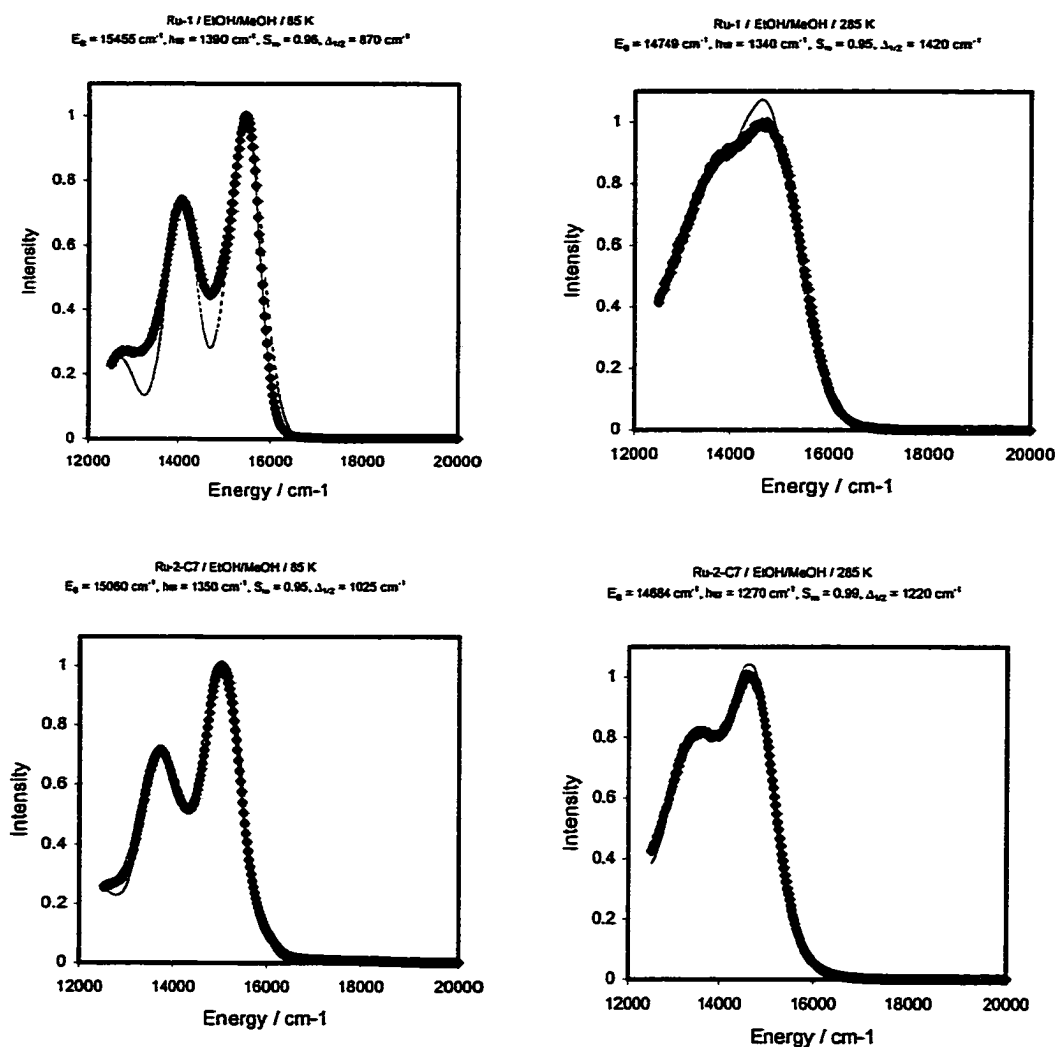
Ru-2-C7 / 2-Me-THF / 85 K
$E_0 = 15174$ cm^{-1}, $\hbar\omega = 1380$ cm^{-1}, $S_m = 0.85$, $\Delta_{1/2} = 830$ cm^{-1}
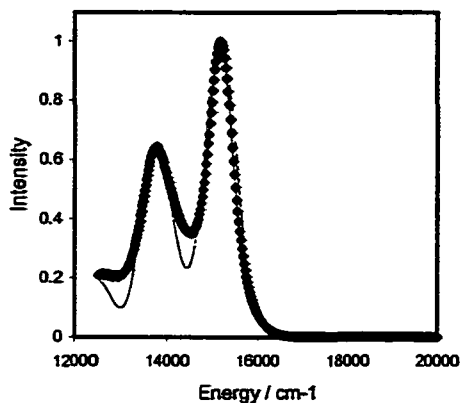
Ru-2-C7 / 2-Me-THF / 285 K
$E_0 = 14306$ cm^{-1}, $\hbar\omega = 1250$ cm^{-1}, $S_m = 0.92$, $\Delta_{1/2} = 1300$ cm^{-1}
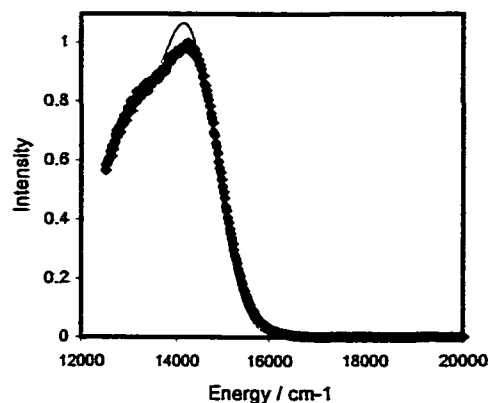
Ru-2-C18 / EtOH:MeOH 4:1 / 85 K
$E_0 = 14771$ cm^{-1}, $\hbar\omega = 1350$ cm^{-1}, $S_m = 0.9$, $\Delta_{1/2} = 920$ cm^{-1}
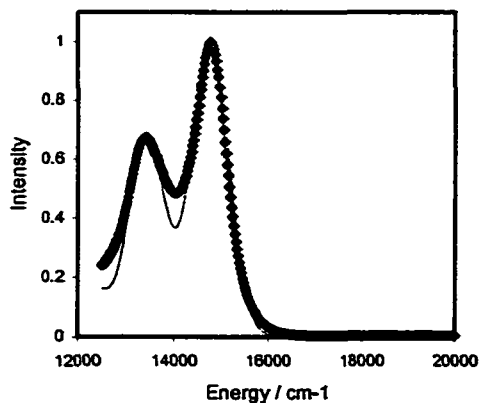
Ru-2-C18 / EtOH:MeOH 4:1 / 285 K
$E_0 = 14535$ cm^{-1}, $\hbar\omega = 1275$ cm^{-1}, $S_m = 1$, $\Delta_{1/2} = 1265$ cm^{-1}
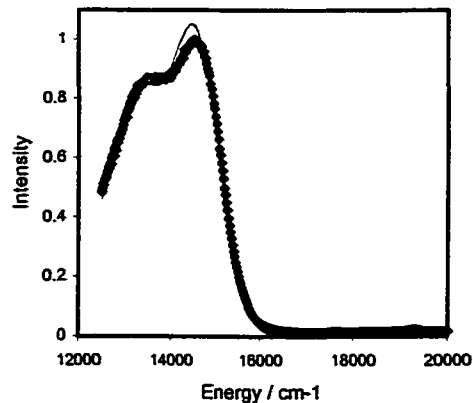
Ru-2-C18 / 2-MTHF / 80 K
$E_0 = 15220$ cm^{-1}, $\hbar\omega = 1360$ cm^{-1}, $S_m = 0.80$, $\Delta_{1/2} = 1200$ cm^{-1}
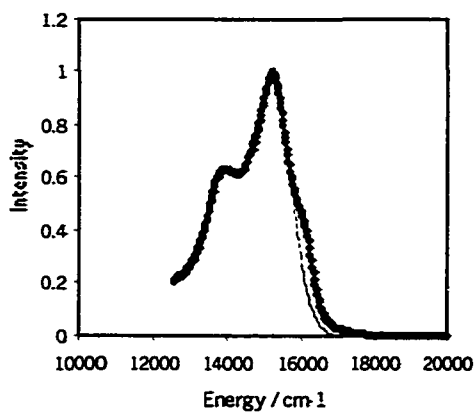
Ru-2-C18 / 2-MTHF / 285 K
$E_0 = 14420$ cm^{-1}, $\hbar\omega = 1530$ cm^{-1}, $S_m = 0.78$, $\Delta_{1/2} = 1600$ cm^{-1}

Ru-3 / EtOH:MeOH 4:1 / 85 K
$E_0 = 15151\ cm^{-1}$, $\hbar\omega = 1400\ cm^{-1}$, $S_m = 0.96$, $\Delta_{1/2} = 900\ cm^{-1}$

Ru-3 / EtOH:MeOH 4:1 / 285 K
$E_0 = 14728\ cm^{-1}$, $\hbar\omega = 1380\ cm^{-1}$, $S_m = 1$, $\Delta_{1/2} = 1280\ cm^{-1}$

Ru-3 / 2-Me-THF / 85 K
$E_0 = 15174\ cm^{-1}$, $\hbar\omega = 1400\ cm^{-1}$, $S_m = 0.85$, $\Delta_{1/2} = 780\ cm^{-1}$

Ru-3 / 2-Me-THF / 285 K
$E_0 = 14306\ cm^{-1}$, $\hbar\omega = 1350\ cm^{-1}$, $S_m = 0.9$, $\Delta_{1/2} = 1420\ cm^{-1}$

Ru-4 / 2-Me-THF / 85 K
$E_o = 15175\,cm^{-1}$, $\hbar\omega = 1360\,cm^{-1}$, $S_m = 0.92$, $\Delta_{1/2} = 950\,cm^{-1}$

Ru-4 / 2-Me-THF / 285 K
$E_o = 14340\,cm^{-1}$, $\hbar\omega = 1280\,cm^{-1}$, $S_m = 0.92$, $\Delta_{1/2} = 1330\,cm^{-1}$
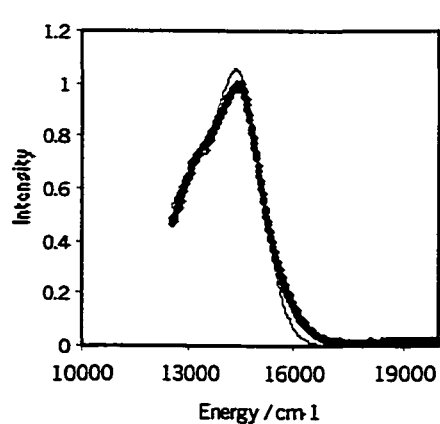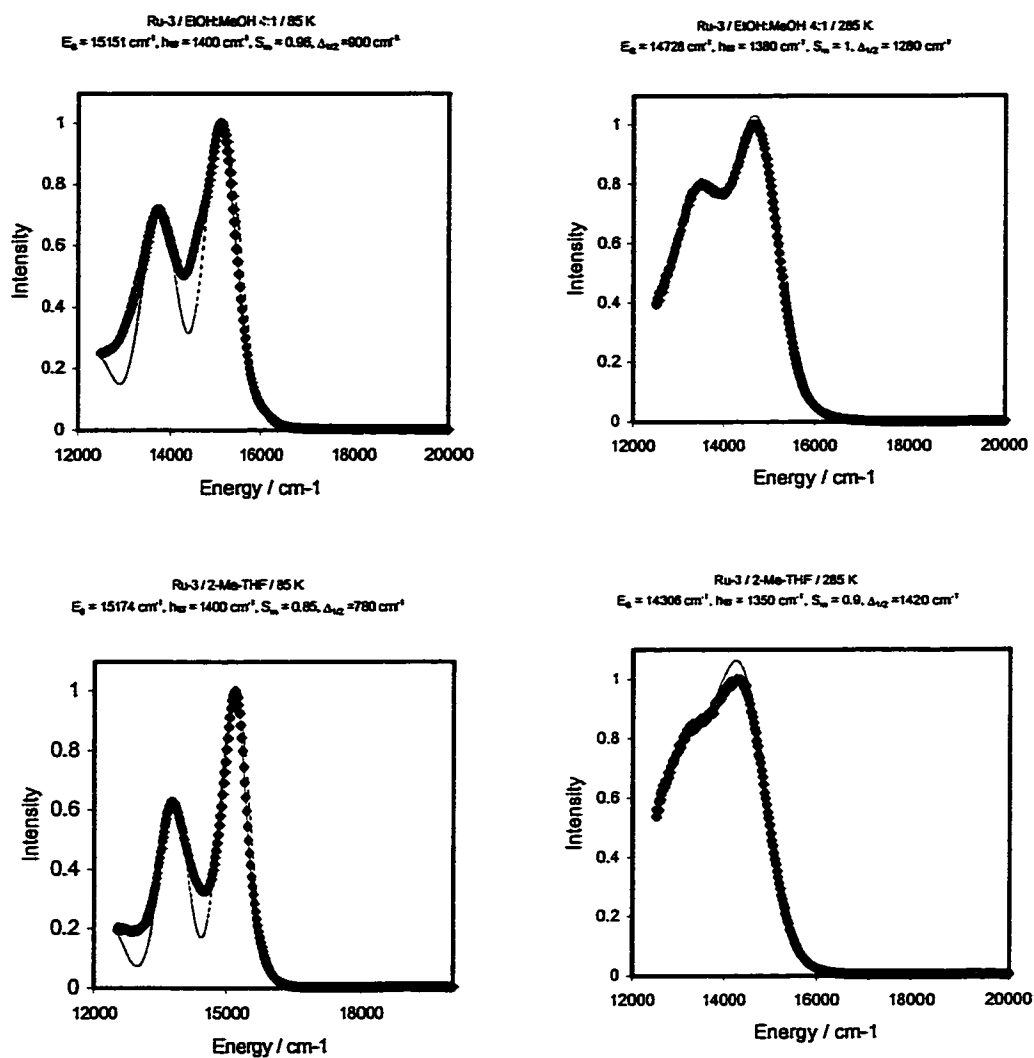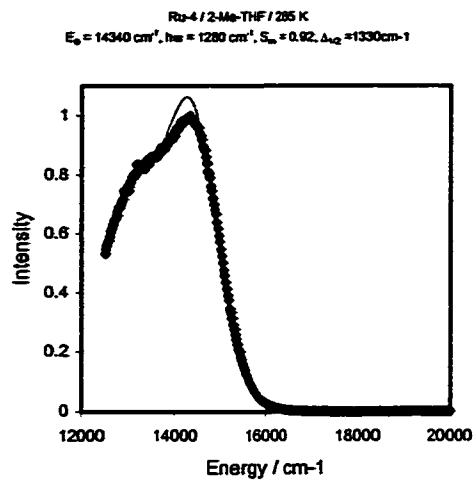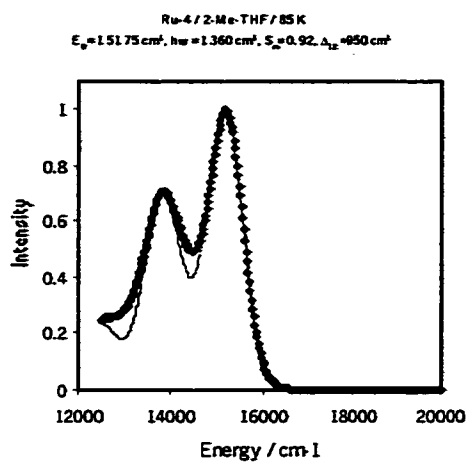
TRANSIENT ABSORPTION DIFFERENCE SPECTRA OF $(L)Ru^{II}(bpy)_2$ IN THE PRESENCE OF PQ^{2+} AND DMA
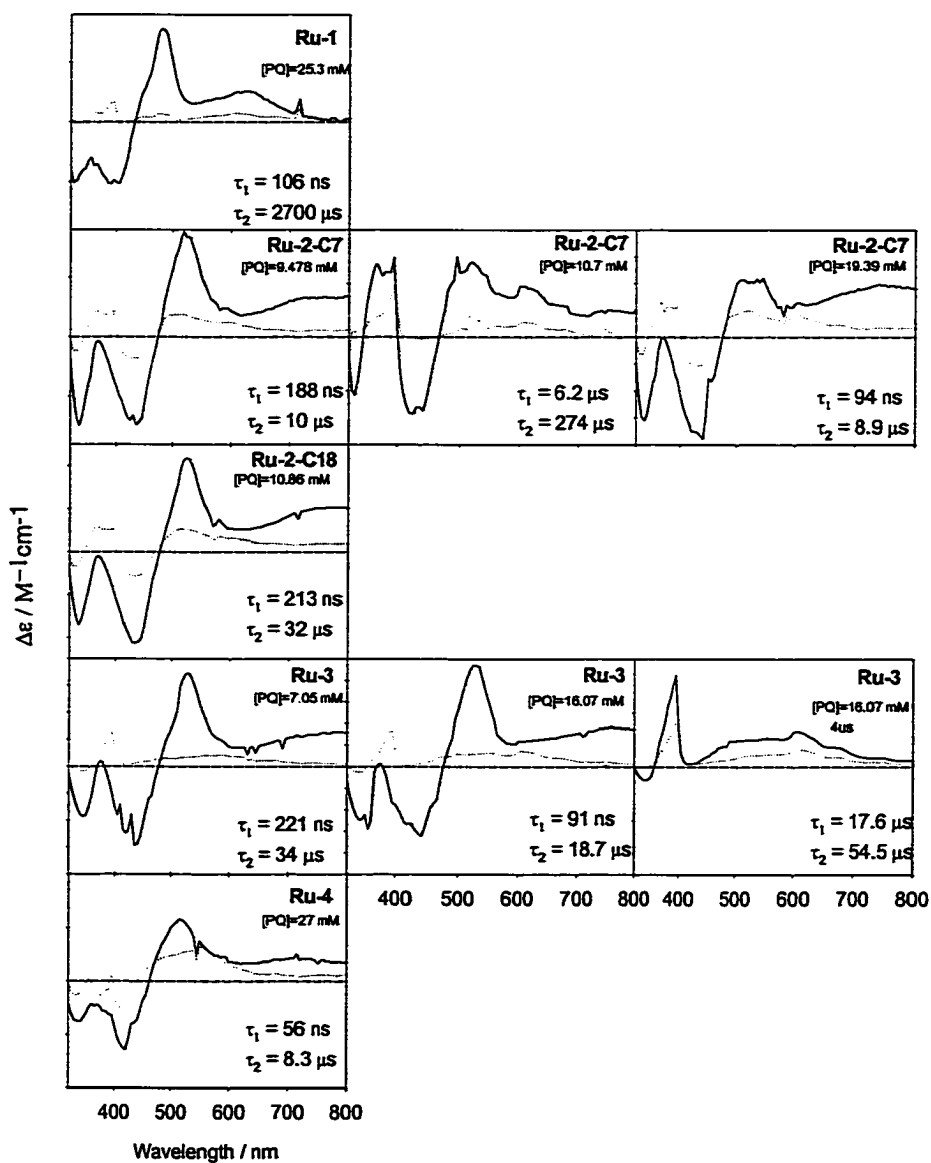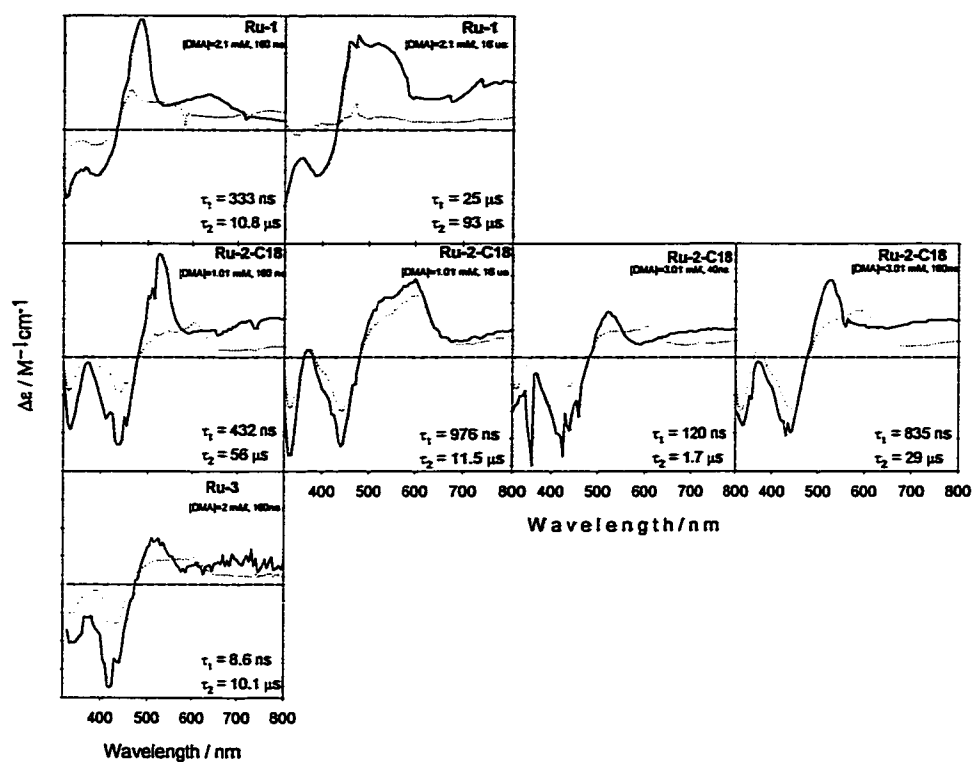
EMISSION LIFETIME DATA OF $(L)Ru^{II}(R-bpy)_2$ IN 4:1 (v/v) EtOH/MeOH FROM
80 K TO 298 K

Ru-1-CF$_3$

Temperature K	τ_1, ns (α_1, %)	τ_2, ns (α_2, %)	$<\tau>$ ns	χ^2
80	2520 (23)	5060 (77)	4465	1.2
125	1502 (40)	2956 (60)	2347	_
145	854 (27)	2019 (73)	1704	1.9
165	798 (22)	1676 (78)	1482	3.8
185	761 (22)	1671 (78)	1471	2.0
205	778 (20)	1659 (80)	1483	1.4
225	1441 (100)	_	1441	1.3
245	1424 (100)	_	1424	1.2
265	1311 (100)	_	1311	1.4
285	1300 (100)	_	1300	1.2

235

Ru-2-CF$_3$

Temperature K	τ_1, ns (α_1, %)	τ_2, ns (α_2, %)	τ_3, ns (α_2, %)	$<\tau>$ ns	χ^2
80	2930 (38)	10830 (62)	_	7855	1.2
105	3048 (48)	10830 (52)	_	7094	1.2
125	2256 (41)	9418 (59)	_	6071	2.6
145	1359 (32)	8197 (63)	144 (5)	5607	1.2
165	979 (24)	6196 (69)	8.2 (7)	4510	1.3
185	1124 (22)	6455 (56)	4.3 (22)	3862	0.94
205	1528 (31)	6259 (65)	343 (4)	4562	1.3
225	3172 (57)	9192 (28)	631 (15)	4453	1.2
245	991 (30)	4419 (70)	_	3390	1.3
285	700 (27)	2680 (47)	4 (25)	1450	1.2

237

Ru-1-COOEt

Temperature K	τ_1, ns (α_1, %)	τ_2, ns (α_2, %)	χ^2
80	2.9 (77)	3160 (22)	1.3
105	4.1 (24)	2952 (76)	1.2
125	2399 (36)	1872 (64)	1.1
145	957 (13)	1962 (87)	1.2
165	3.2 (4)	1714 (96)	1.1
185	2.6 (7)	1680 (96)	1.3
205	3.3 (4)	1651 (96)	1.3
225	3.4 (4)	1604 (94)	1.1
245	407 (3)	1627 (97)	1.7
285	1.7 (29)	1500 (71)	1.1

REFERENCES

1. Patil, A. O.; Heeger, A. J.; Wudl, F. "Optical Properties of Conducting Polymers." *Chem. Rev.* **1988**, *88*, 183.

2. Burroughes, J. H.; Bradley, D. D. C.; Brown, A. R.; Marks, R. N.; Mackay, K.; Friend, R. H.; Burn, P. L.; Holmes, A. B. "Light-Emitting-Diodes Based on Conjugated Polymers." *Nature* **1990**, *347*, 539.

3. Baigent, D. R.; Hamer, P. J.; Friend, R. H.; Moratti, S. C.; Holmes, A. B. "Polymer Electroluminescence in the Near-Infrared." *Synth. Met.* **1995**, *71*, 2175.

4. Joshi, N. V. *Photoconductivity Art, Science, and Technology*; Marcel Dekker: New York, 1990.

5. Moerner, W. E.; Silence, S. M. "Polymeric Photorefractive Materials." *Chem. Rev.* **1994**, *94*, 127.

6. Zhou, Q.; Swager, T. M. "Fluorescent Chemosensors Based on Energy Migration in Conjugated Polymers: The Molecular Wire Approach to Increased Sensitivity." *J. Am. Chem. Soc.* **1995**, *117*, 12593.

7. McQuade D. T., Pullen A. E., Swager T. M. "Conjugated Polymer-Based Chemical Sensors." *Chem. Rev.* **2000**, *100*, 2537

8. Wang, B.; Wasielewski, M. R. "Design and Synthesis of Metal Ion-Recognition-Induced Conjugated Polymers: An Approach to Metal Ion Sensory Materials." *J. Am. Chem. Soc.* **1997**, *119*, 12.

9. Jones, L.; Pearson, D. L.; Tour, J. M. "Synthesis of Well-Defined Conjugated Oligomers for Molecular Electronics." *Pure and Appl. Chem.* **1996**, *68*, 145.

10 Tour, J. M. "Conjugated Macromolecules of Precise Length and Constitution. Organic Synthesis for the Construction of Nanoarchitectures." *Chem. Rev.* **1996**, *96*, 537.

11. Sonogashira, K.; Tohda, Y.; Hagihara, N. "A Convenient Synthesis of Acetylenes: Catalytic Substitutions of Acetylenic Hydrogens with Bormoalkenes, Iodoarenes, and Bromopyridines." *Tet. Lett.* **1975**, *16*, 4467.

12.   Takahashi, S.; Kuroyama, Y.; Sonogashira, K.; Hagihara, N. "A Convenient Synthesis of Ethynylarenes and Diethynylarenes." *Synthesis 1980*, 627.

13.   Dieck, H. A.; Heck, R. F. J. "Palladium Catalyzed Synthesis of Aryl, Heterocyclic and Vinylic Acetylene Derivatives." *Organomet. Chem.* **1975**, *93*, 259.

14.   Cassar, I. "Synthesis of Aryl- and Vinyl-Substituted Acetylene Derivatives by the Use of Nickel and Palladium Complexes." *J. Organomet. Chem.* **1975**, *93*, 253.

15.   Bunz, U. "Poly(aryleneethylene)s: Synthesis, Properties, and Applications." *Chem. Rev.* **2000**, *100*, 1605.

16.   Tischler, A. N.; Lanza, T. J. "6-Substituted Indoles From Ortho-Halonitrobenzenes." *Tet. Lett.* **1986**, *27*, 1653.

17.   Taylor, R. J. K. *Organocopper Reagent s: a Practical Approach*; Oxford: New York, 1994.

18.   Deeter, G. A.; Moore, J. S. "A New Polymerization Reaction for the Synthesis of Aromatic Polyketones." *Macromolecules*, **1993**, *26*, 2535.

19.   Francke, V.; Mangel, T.; Müllen, K. "Synthesis of α,ω-Difunctionalized Oligo- and Poly(p-phenyleneethynylene)s." *Macromolecules*, **1998**, *31*, 2447.

20.   Ofer, D.; Swager, T. M.; Wrighton, M. S. "Solid-State Ordering and Potential Dependence of Conductivity in Poly(2,5-dialkoxy-p-phenyleneethynylene)." *Chem. Mater.* **1995**, *7*, 418.

21.   Steiger, D.; Smith, P.; Weder, C. "Liquid Crystalline, Highly Luminescent Poly(2,5-Dialkoxy- p-phenyleneethynylene)." *Macromol. Rapid Commun.* **1997**, *18*, 643.

22.   Alami, M.; Ferri, F.; Linstrumelle, G. "An Efficient Palladium-Catalyzed Reaction of Vinyl and Aryl Halides or Triflated with Terminal Alkynes." *Tet. Lett.* **1993**, *34*, 6403.

23.   Peng, Z.; Yu, L. "Synthesis of Conjugated Polymers Containing Ionic Transition Metal Complexes" *J. Am. Chem. Soc.* **1996**, *118*, 3777.

24.   Peng, Z.; Gharavi, A. R.; Yu, L. "Synthesis and Characterization of Photorefractive Polymers Containing Transition Metal Complexes as Photosensitizer." *J. Am. Chem. Soc.* **1997**, *119*, 4622.

25.   Ley, K. D.; Whittle, C. E.; Bartberger, M. D.; Schanze, K. S. "Photophysics of π-Conjugated Polymers that Incorporate Metal to Ligand Charge Transfer Chromophores." *J. Am. Chem. Soc.* **1997**, *119*, 3423.

26. Ley, K. D.; Schanze, K. S. "Photophysics of Metal-Organic π-Conjugated Polymers." *Coord. Chem. Rev.* **1998**, *171*, 287.

27. Tokura, S.; Yasuda, T.; Segawa, Y.; Kira, M. "Novel σ-π Alternating Polymers Having 2,2'-Bipyridyl in the Polymer Backbone and their Ruthenium Complexes." *Chem. Lett.* **1997**, 1163.

28. Ng, P. K.; Gong, X.; Wong, W. T.; Chan, W. K. "Quinoxaline-Based Conjugated Polymers Containing Rutheinum(II) Bipyridine Metal Complex." *Macromol. Rapid Commun.* **1997**, *18*, 1009.

29. Yamamoto, T.; Zhou, Z.; Kanbara, T.; Maruyama, T. "Preparation and Properties of Poly(2,2'-bipyridine-5,5'-diyl)." *Chem. Lett.* **1990**, 223.

30. Yamamoto, T.; Yoneda, Y.; Maruyama, T. "Ruthenium and Nickel Complexes of a π-Conjugated Electrically Conducting Polymer Chelate Ligand, Poly(2,2'-bipyridine-5,5'-diyl), and their Chemical and Catalytic Reactivity." *Chem. Commun.* **1992**, 1652.

31. Yamamoto, T.; Maruyana, T.; Zhou, A.; Ito, T.; Fukuda, T.; Yoneda, Y.; Begum, F.; Ikeda, T.; Sasaki, S.; Takezoe, H.; Fukuda, A.; Kubota, K. "π-Conjugated Poly(pyridine-2,5-diyl), Poly(2,2'-bipyridine-5,5'-diyl), and Their Alkyl Derivatives. Preparation, Linear Structure, Function as a Ligand to Form Their Transition Metal Complexes, Cata240ytic Reactions, n-Type Electrically Conducting Properties, Optical Properties, and Alignment on Substrates." *J. Am. Chem. Soc.* **1994**, *116*, 4832.

32. Maruyama, T.; Yamamoto, T. "New Copper Complex with π-Conjugated Electrically Conductive Polymer Chelating Ligand, poly(6,6'-dialkyl-2,2'-bipyridine-5,5'-diyl). Preparation and Optical Properties of the Complex." *Inorg. Chim. Acta* **1995**, *238*, 9.

33. Cameron C.G.; Pickup, P. G. "Metal-Metal Interactions in a Novel Hybrid Metallpolymer." *J. Am. Chem. Soc.* **1999**, *121*, 11773

34. Wang, Q.; Wang, L.; Yu, L. "Synthesis and Unusual Physical Behavior of a Photorefractive Polymer Containing Tris(bipyridyl)ruthenium(II) Complexes as a Photosensitizer and Exhibiting a Low Glass-Transition Temperature." *J. Am. Chem. Soc.* **1998**, *120*, 12860.

35. Wang, Q.; Yu, L. "Conjugated Polymers Containing Mix-Ligand Ruthenium (II) Complexes. Synthesis, Characterization, and Investigation of Photoconductive Properties." *J. Am. Chem. Soc.* **2000**, *122*, 11806.

36. Chen, L. X.; Jäger, W. J. H.; Gosztola, D. J.; Niemczyk, M. P.; Wasielewski, M. R. "Ionochromic Effects and Structures of Metalated Poly(p-phenylenevinylene) Polymers Incorporating 2,2'-Bipyridines." *J. Phys. Chem. B* **2000**, *104*, 1950.

37.   Kimura, M.; Horai, T.; Hanabusa, K.; Shira, H. " Fluorescence Chemosensor for Metal Ions Using Conjugated Polymers." *Adv. Mater.* **1998**, *10*, 459.

38.   Rasmussen, S. C.; Thompson, D. W.; Singh, V.; Petersen, J. D. "Controlled Synthesis of a New, Soluble, Conjugated Metallopolymer Containing Ruthenium Chromophoric Units." *Inorg. Chem.* **1996**, *35*, 3449.

39.   Zhu, S. S.; Swager, T. M. "Design of Conducting Redox Polymers: A Polythiophene-Ru(bipy)$_3^{n+}$ Hybrid Material." *Adv. Mater.* **1996**, *8*, 497.

40.   Zhu, S. S.; Kingsborough, R. P.; Swager, T. M. "Conducting Redox Polymers: Investigations of polythiophene-Ru(bpy)$_3^{2+}$ Hybrid Materials." *J. Mater. Chem.* **1999**, *9*, 2123.

41.   Zhu, S. S.; Carroll, P. J.; Swager, T. M. "Conducting Polymetallorotaxanes: A Supramolecular Approach to Transition Metal Ion Sensors." *J. Am. Chem. Soc.* **1996**, *118*, 8713.

42.   Zhu, S. S.; Swager, T. M. "Conducting Polymetallorotaxanes: Metal Ion Mediated Enhancements in Conductivity and Charge Localization." *J. Am. Chem. Soc.* **1997**, *119*, 12568.

43.   Trouillet, L., De Nicola, A., Guillerez, S. "Synthesis and Characterization of a New Soluble, Structurally Well-Defined Conjugated Polymer Alternating Regioregularly Alkylated Thiophene Oligomer and 2,2'-bipyridine Units: Metal-Free Form and Ru(II) Complex." *Chem. Mater.* **2000**, *12*, 1611.

44.   Walters, K. A.; Trouillet, L.; Guillerez, S.; Schanze, K. S. "Photophysics and Electron Transfer in Poly(3-octylthiophene) Alternationg with Ru(II)- and Os(II)-Bipyridine Complexes." *Inorg. Chem.* **2000**, *39*, 5496.

45.   Reddinger, J. L.; Reynolds, J. R. "Electroactive, π–Conjugated Polymers Based on Transition Metal-Containing Thiophenes." *Synth. Met.* **1997**, *84*, 225.

46.   Reddinger, J. L.; Reynolds, J. R. "Tunable Redox and Optical Properties Using Transition Metal-Complexed Polythiophenes." *Macromol.* **1997**, *30*, 673.

47.   Wittmann, H. F.; Friend, R. H.; Khan, M. S.; Lewis, J. "Optical Spectroscopy of Platinum and Palladium Containing Poly-ynes." *J. Chem. Phys.* **1994**, *101*, 2693.

48.   Davey, A. P.; Elliott, S.; O-Connor, O.; Blau, W. "New Rigid Backbone Conjugated Organic Polymers with Large Fluorescence Quantum Yields." *Chem. Commun.* **1995**, 1433.

49.   Swager, T. M.; Gil, C. J.; Wrighton, M. S. "Fluorescence Studies of Poly(*p*-phenyleneethynylene)s: The Effect of Anthracene Substitution." *J. Phys. Chem.* **1995**, *99*, 4886.

50.   Meyer, T. J. "Photochemistry of metal coordination complexes: metal to ligand charge transfer excited states." *Pure & Appl. Chem.* **1986**, *58*, 1193.

51.   Roundhill, D. M. *Photochemistry and Photophysics of Metal Complexes;* Plenum Press: New York, 1994.

52.   Ronbinson, G. W.; Frosch, R. R. "Theory of Electronic Energy Relaxation in the Solid Phase." *J. Chem. Phys.* **1962**, *37*, 1962.

53.   Ronbinson, G. W. "Electronic Excitation Transfer and Relaxation." *J. Chem. Phys.* **1963**, *38*, 1187.

54.   Gillipsie, G. D.; Lim, E. C. "Quantum and Excited-State yields in luminol chemiluminescence by Pulse Radiolysis." *Chem. Phys. Lett.* **1979**, *63*, 193.

55.   Griesser, H. J.; Wild, U. P. "The Energy Gap Dependence of the radiationless Transition Rates in Azulene and Its derivatives." *Chem. Phys.* **1980**, *52*, 117.

56.   Barltrop, J. A.; Coyle, J. D. *Excited States in Organic Chemistry;* John Wiley & Sons Press: London, 1975.

57.   Casper, J. V.; Kober, E. M.; Sullivan, B. P.; Meyer, T. J. "Application of the Energy Gap Law to the Decay of Charge-Transfer Excited States." *J. Am. Chem. Soc.* **1982**, *104*, 630.

58.   Englman, R.; Jortner, J. "The Energy Gap Law for Radiationless Transitions in Large Molecules." *Mol. Phys.* **1970**, *18*, 145.

59.   Free, K. F.; Jortner, J. "Multiphonon Process in the Nonradiative Decay of Large Molecules." *J. Chem. Phys.* **1970**, *52*, 6272.

60.   Jortner, J. "Temperature Dependent Activation Energy for Electron Transfer between Biological Molecules." *J. Chem. Phys.* **1976**, 64, 4860.

61.   Bunks, E.; Navon, G.; Bixon, M.; Jortner, J. "Spin Conversion Process in Solutions." *J. Am. Chem. Soc.* **1980**, *102*, 2918.

62.   Treadway, J. A. Loeb, B.; Lopez, R.; Anderson, P. A.; Keene, F. R.; Meyer, T. J. "Effect of Delocalization and Rigidity in the Acceptor Ligand on MLCT Excited-State Decay." *Inorg. Chem.* **1996**, *35*, 2242.

63.   Lumpkin, R. S.; Meyer, T. J. "Effect of the Glass-to-Fluid Transition on Excited-State Decay. Application of the Energy Gap Law." *J. Phys. Chem.* **1986**, *90*, 5307.

64.   Casper, J. V.; Meyer, T. J. "Application of the Energy Gap Law to Nonradiative, Excited-State Decay." *J. Phys. Chem.* **1983**, *87*, 952.

65. Vining, W. J.; Casper, J. V.; Meyer, T. J. "The Influence of Environmental Effects on Excited-State Lifetimes. The Effect of Ion Pairing on Metal-to-Ligand Charge Transfer Excited States." *J. Phys. Chem.* **1985**, *89*, 1095.

66. Casper, J. V.; Meyer, T. J. "Photochemistry of Ru(bpy)$_3^{2+}$. Solvents Effects." *J. Am. Chem. Soc.* **1983**, *105*, 5583.

67. Damrauer, N. H.; Boussie, T. R.; Devenney, M.; McCusker, J. K. " Effects of Intraligand Electron Delocalization, Steric Tuning, and Excited-State Vibronic Coupling on the Photophysics of Aryl-Substituted Bipyridyl Complexes of Ru(II)." *J. Am. Chem. Soc.* **1997**, *119*, 8253.

68. Strouse, G. f.; Schoonover, J. R.; Duesing, R.; Boyde, S.; Jones, W. E.; Meyer, T. J. "Influence of Electronic Delocalization in Metal-to-Ligand Charge Transfer Excited States." *Inorg. Chem.* **1995**, *34*, 473.

69. Ley, K. D.; Walters, K. A.; Schanze, K. S. "Photophysics of Metal-Organic π-Conjugated Oligomers and Polymers." *Synth. Metals* **1999**, 102, 1585.

70. Sullivan, B. P.; Salmon, D. J.; Meyer, T. J. "Mixed Phosphine 2,2'-Bipyrdine Complexes of Ruthenium." *Inorg. Chem.* **1978**, *17*, 3334.

71. Togano T.; Nagao N., Tsuchida, M.; Kumakura, H.; Hisamatsu, K.; Howell. F. S.; Mukaida, M. "One-Pot and Selective Synthesis of a Series of [RuCl$_{6-2n}$Ln] (L = Bidentate Ligand, n = 0 – 3) Types of Complexes with Polypyridyl Ligands; Another Example of the Synthetic Utility of "Ruthenium-Blue" Solution." *Inorg. Chim. Acta.* **1992**, *195*, 221.

72. Romero, F. M.; Ziessel, R. "Preparation of Novel Mixed Tritopic Oligopyridine Ligands Built with Chelating Spacers and Using Palladium (0) Catalyzed Coupling Reactions." *Tet. Lett.* **1994**, *35*, 9203.

73. Yang, J. S.; Swager, T. "Fluorescent Porous Polymer Films as TNT chemosensors: Electronic and Structural Effects." *J. Am. Chem. Soc.* **1998**, *120*, 11864.

74. Ley, K. D.; Li, Y.; Johnson, J. V.; Powell, D. H.; Schanze, K. S. "Synthesis and Characterization of π-Conjugated Oligomers that Contain Metal-to-Ligand Charge Transfer Chromophores." *Chem. Comm.* **1999**, 1749.

75. Jones, L. R.; Schumm, J. S.; Tour, J. M. "Rapid Solution and Solid Phase Synthesis of Oligio(1,4-phenyleneethynylene)s with Thioester Termini: Molecular Scale Wires with Alligator Clips. Derivation of Iterative Reaction Efficiencies on a Polymer Support." *J. Org. Chem.* **1997**, *62*, 1388.

76. Moroni, M.; LeMoigne, J.; Luzzati, S. "Rigid Rod Conjugated Polymers for Nonlinear Optics. 1. Characterization and Linear Optical Properties of Poly(aryleneethynylene) Derivatives." *Macromolecules.* **1994**, *27*, 562.

77.   Kukula, H.; Veit, S.; Godt, A. "Synthesis of Monodiperse Oligo(para-phenyleneethynylene)s Using Orthogonal Protecting Groups with Different Polarity for Terminal Acetylene Units." *Eur. J. Org. Chem.* **1999**, 277.

78.   Ziener, U.; Godt, A. "Synthesis and Characterization of Monodiperse Oligo(phenyleneethynylene)s." *J. Org. Chem.* **1997**, *62*, 6137.

79.   Casper, J. V. "Excited State Decay Processes in Osmium (II), Ruthenium (II) and Rhenium (I) Polypyridyl Complexes." Ph. D. Dissertation, University of North Carolina at Chapel Hill, 1982.

80.   Nakamaru, K. "Synthesis, Luminescence Quantum Yields, and Lifetimes of Trischelated Ruthenium(II) Mixed-ligand Complexes Including 3,3'-Dimethyl-2,2'-bipyridyl." *Bull. Chem. Soc. Jpn.* **1982**, *55*, 2697.

81.   Lees, A. "Luminescence Properties of Organometallic Complexes." *Chem. Rev.* **1987**, *87*, 711.

82.   O'Connor, D. V.; Phillips, D. Time-correlated Single Photon Counting,; Academic: New York, 1984.

83.   Lakowicz, J. R. *Principles of Fluorescence Spectroscopy*; Plenum Press: New York, 1983.

84.   Juris. A.; Balzani, V. "Ru(II) Polypyridine Complexes: Photophysics, Photochemistry, Electrochemistry, and Chemiluminescence." *Coord. Chem. Rev.* **1988**, *84*, 85.

85.   Murtaza, Z.; Graff, D. K.; Zipp, A. P.; Worl, L. A.; Jones, W. E.; Bates, W. D.; Meyer, T. J. "Energy Transfer in the Inverted Region: Calculation of Relative Rate Constants by Emission Spectral Fitting." *J. Phys. Chem.* **1994**, *98*, 10504.

86.   Leznoff, C. C.; Lever, A. B. P. *Phthalocyanines Properties and Applications*; VCH Press: New York, 1993.

87.   Bock, C. R.; Connor, J. A.; Gutierrez, A. R.; Meyer, T. J.; Whitten, D. G.; Sullivan, B. P.; Nagle, J. K. "Estimation of Excited-State Redox Potentials by Electron Transfer Quenching. Application of Electron-Transfer to Excited-State Redox Processes." *J. Am. Chem. Soc.* **1979**, *101*, 4816.

88.   Zweig, A.; Hodgson, W. G.; Jura, W. H. "The Oxidation of Methoxybenzenes." *J. Am. Chem. Soc.* **1964**, *86*, 4124.

89.   Dewar, M. J. S.; Hafner, K. *Topics in Current Chemistry*; Springe-Verlag Press: Berlin Heidelberg New York, 1978.

90.   Nagel, J. K.; Young, R. C.; Meyer, T. J. "Chemically Catalyzed Disproportionation of $Ru(bpy)_3^{2+*}$." *Inorg. Chem.* **1977**, *16*, 3366.

91. Ogata, Y.; Nakajima, K. "Ground State Geometry of Substituted Biphenyls." *Tetrahedron* **1964**, *20*, 43.

92. Cumper, C. W. N.; Ginman, R. F. A.; Vogel, A. I. "Physical Properties and Chemical Constitution. Part XXXV. The Electric Dipole Moments of Some Phenanthrolines and Bipyridyls." *J. Chem. Soc.* **1962**, *1188*.

93. Wrighton, M.; Morse, D. L. "The Nature of the Lowest Excited State in Tricarbonylchloro-1,10-phenanthroline rhenium(I) and Related Complexes." *J. Am. Chem. Soc.* **1974**, *96*, 998.

94. Meyer, T. J. "Excited State Electron Transfer." *Prog. Inorg. Chem.* **1983**, *30*, 389.

95. Chen. P.; Meyer, T. J. "Medium Effects on Charge Transfer in Metal Complexes." *Chem. Rev.* **1998**, *98*, 1439.

96. Worl, L. A.; Duesing, R.; Chen P.; Della Ciana, L.; Meyer, T. J. "Photophysical Properties of Polypyridyl Carbonyl Complexes of Rhenium(I)." *J. Chem. Soc. Dalton Trans.* **1991**, 849.

97. Kozik, M.; Sutin, N.; Winkler, J. R. "Energetics and Dynamics of Solvent Reorganization in Charge-Transfer Excited State." *Coord. Chem. Rev.* **1990**, *97*, 23.

98. Walters, K. A. "Photophysical Studies of π-Conjugated Oligomers and Polymer that Incorporate Inorganic MLCT Chromophores." Ph. D. Dissertation, University of Florida, 2000.

99. Boens, N.; De Roeck, T. DECAN; 1.0ed. Leuven, 1990.

100. Wang, Y.; Schanze, K. S. "Photochemical Probes of Intramolecular Electron and Energy Transfer." *Chem. Phys.* **1993**, *176*, 305.

101. Binstead, R. A.; Zuberbuhler, A. d. *SPECFIT*; 2.1 ed.; Spectrum Software Associates: Chapel Hill, 1996.

102. Surfactant Derivative of Tris(2,2'-bipyridyl)ruthenium (II)." *J. C. S. Chem. Comm.* **1997**, *777*.

103. Ley, K. D. "Photophysics of π-Conjugated Polymers and Oligomers that Incorporate Metal to Ligand Charge Transfer Chromophores." Ph. D. Dissertation, University of Florida, 2000.

104. Furue, M.; Maruyama, K.; Oguni, T.; Naiki, M.; Kamachi, M. " Trifluormethyl-Substituted 2,2'-Bipyridine Ligands. Synthetic Control of Excited-State Properties of Ruthenium(II) Tris-Chelate Complexes." *Inorg. Chem.* **1992**, 3792.

246

105. Elliott, C. M.; Hershenhart, E. J. "Electrochemical and Spectral Investigations of Ring-Substituted Bipyridine Complexes of Ruthenium." *J. Am. Chem. Soc*, **1982**, *104*, 7519.

106. Johnson, S. R.; Westmoreland, T. D.; Casper, J. V.; Barqawi, K. R.; Meyer, T. J. "Influence of Variations in the Chromophoric Ligand on the Properties of Metal-to-Ligand Charge-Transfer Excited States." *Inorg. Chem.* **1988**, *27*, 3195.

107. Montague, S. A. "Electrochemical and Intervalence Transfer Properties of New Mononuclear and Binuclear Ruthenium Complexes." Ph.D. Dissertation, University of Florida, 1984.

108. Wacholtz, W. F.; Auerbach, R. A.; Schmehl, R. H. "Independent Control of Charge-Transfer and Metal-Centered Excited States in Mixed-Ligand Polypyridine Ruthenium(II) Complexes via Specific Ligand Design." *Inorg. Chem.* **1986**, *25*, 227.

109. Pankuch, B. J.; Lacky, D. E.; Crosby, G. A. "Charge-Transfer Excited States of Osmium(II) Complexes. 1. Assignment of the Visible Absorption Bands." *J. Phys. Chem.* **1980**, *84*, 2061.

110. Jones. S. W.; Vrana, L. M.; Brewer, K. J. "Using Spectroelectrochemistry to Probe the Light Absorbing Properties of Polymetallic Complexes Containing the tridentate Bridging Ligand 2,3,5,6-tetrakis(2-pyridyl)pyrazine." *J. Organomet. Chem.* **1998**, *554*, 29.

111. Perkins, T. A.; Humer, W.; Netzel, T. L.; Schanze, K. S. "Solvent-Induced Excited-State Quenching in a Chromophore-Quencher Complex." *J. Phys. Chem.* **1990**, *94*, 2229.

112. Perkins, T. A.; Pourreau, D. B.; Netzel, T. L.; Schanze, K. S. "Ligand-Ligand Charge-Transfer Excited States of Os(II) Complexes." *J. Phys. Chem.* **1989**, *93*, 4511.

113. Westmoreland, T. D.; Le Bozec, H.; Murray, R. W.; Meyer, T. J. "Multiple-State Emission and Intramolecular Electron-Transfer Quenching in Rhenium(I) Bipyridine Based Chromophore-Quencher Complexes." *J. Am. Chem. Soc*, **1983**, *105*, 5952.

114. Liard, D. J.; Vlcek, A. Jr. "Picosecond Dynamics of Photoinduced Interligand Electron Transfer in $[Re(MQ^+)(CO)_3(dmb)]^{2+}$ (dmb = 4, 4'-Dimethyl-2,2'-bipyridine, MQ^+ = N-Methyl-4,4'-bipyridium)." *Inorg. Chem.* **2000**, *39*, 485.

115. Chen, P.; Danielson, E.; Meyer, T. J. "Role of Free Energy Change on Medium Effects in Intramolecular Electron Transfer." *J. Phys. Chem.* **1988**, *92*, 3708

116. Mecklenburg, S. L.; Opperman, K. A.; Chen, P.; Meyer, T. J. "Designed Intramolecular Competition in a Chromophore-Biquencher Complex." *J. Phys. Chem.* **1996,** *100,* 15145.

117. Schanze, K. S.; MacQueen, D. B.; Perkins, T. A.; Cabana, L. A. "Studies of Intramolecular Electron and Energy Transfer Using the *fac*-(diimine)Re^I(CO)$_3$ Chromophore." *Coord. Chem. Rev.* **1993,** *122,* 63.

118. Tapolsky, G.; Duesing, R.; Meyer, T. J. "Synthetic Control of Excited-State Properties in Ligand-Bridged Complexes of Rhenium(I). Intramolecular Energy Transfer by an Electron-Transfer / Energy-Transfer Cascade." *Inorg. Chem.* **1990,** *29,* 2285.

119. Berger, S.; Klein, A.; Kaim, W. "Variable Reduction Sequences for Axial (L) and Chelate Ligands (N^N)Re(CO)$_3$(L)]n." *Inorg. Chem.* **1998,** *37,* 5664.

120. Sacksteder, L.; Zipp, A. P.; Brown, E. A.; Streich, J.; Demas, J. N.; DeGraff, B. A. "Luminescence Studies of Pyridine α-Diimine Rhenium(I) Tricarbonyl Complexes." *Inorg. Chem.* **1990,** *29,* 4335.

121. Chen, P.; Curry, M.; Meyer, T. J. "Effects of Conformational Change in the Acceptor on Intramolecular Electron Transfer." *Inorg. Chem.* **1989,** *28,* 2271.

122. Walters, K. A.; Ley, K. D.; Cavalaheiro, C. S.; Miller, S. E.; Gosztola, D.; Wasielewski, M. R.; Bussandri, A. P.; Willigen, H. V.; Schanze, K. S. "Photophysics of π-Conjugated Metal-Organic Oligomers. Phenylene Ethynylenes that Contain the (bpy)Re(CO)$_3$Cl Chromophore." Submitted.

123. MacQueen D. B.; Schanze, K. S. "Free Energy and Solvent Dependence of Intramolecular Electron Transfer in Donor-Substituted Re(I) Complexes." *J. Am. Chem. Soc,* **1991,** 113, 7470.

124. Lucia, L. A.; Schanze, K. S. "Cage Escape Yields for Photoinduced Bimolecular Electron Transfer Reactions of Re(I) Complexes." *Inorg. Chim. Acta* **1994,** *225,* 41.

125. D. J. Stufkens, D. J. "The Remarkable Properties of α-Diimine Rhenium Tricarbonyl Complexes in Their Metal-to-Ligand Charge Transfer (MLCT) Excited States." *Comments Inorg. Chem.* **1992,** *13,*359.

126. Heck, R. F. "Palladium-Catalyzed Vinylation of Organic Halides." *Org. React.* **1981,** *27,* 345.

127. Heitz, W.; Brugging, W.; Freund, L.; Gailberger, M.; Greiner, A.; Jung, H.; Kampschutle, U.; Niebner, N.; Osan, F. "Structural Modifications of Poly(1,4,-Phenylenevinylene) to Soluble, Fusible, Liquid-Crystalline Products." *Makromol. Chem.* **1991,** *192,* 967.

128. Suzuki, M.; Lim, J. C.; Saegusa, T. "Polycondensation Catalyzed by a Palladium Complex. 2. Synthesis and Characterization of Main-Chain Type Liquid Crystalline Polymers Having Distyrylbenzene Mesogenic Group." *Macromolecules* **1990**, *23*, 1574.

129. Weitzel, H. P.; Mullen, K. "Polyarylenes and Poly(Arylenevinylene)s. 4. Novel Anthracene-Containing Poly(Arylenevinylene)s via Poly-Heck Reaction." *Makromol. Chem.* **1990**, *191*, 2837.

130. Bao, Z. N.; Chen, Y. M.; Cai, R. B.; Yu, L. "Conjugated Liquid-Crystalline Polymers-Soluble and Fusible Poly(Phenylenevinylene) By the Heck Coupling Reaction." *Macromolecules* **1993**, *26*, 5281.

131. Brizius, G.; Pshirer, N. G.; Steffen, W.; Stizer, K.; Loye, H, Z.; Bunz, U. H. "Alkyne Metathesis with Simple Catalyst Systems: Efficient Synthesis of Conjugated Plymers Containing Vinyl Groups in Main or Side Chain." *J. Am. Chem. Soc.* **2000**, *122*, 12435.
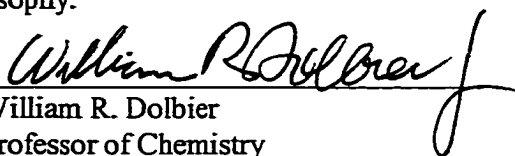
BIOGRAPHICAL SKETCH

Yiting Li was born on November 14, 1972, in Zhangzhou, China. In July 1994, she received her Bachelor of Science degree (major: chemistry) at Tsinghua University. Then she continued her study at the same school and received her Master of Science degree, major physical chemistry, in July 1997. After graduation, she came to the U.S. to further pursue graduate study under Dr. Kirk Schanze (major: organic chemistry) at the University of Florida in 1997.
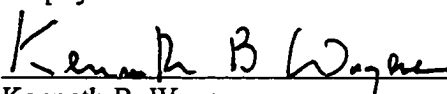
I certify that I have read this study and that in my opinion it conforms to acceptable standards of scholarly presentation and is fully adequate, in scope and quality, as a dissertation for the degree of Doctor of Philosophy.

Kirk S. Schanze, Chair
Professor of Chemistry

I certify that I have read this study and that in my opinion it conforms to acceptable standards of scholarly presentation and is fully adequate, in scope and quality, as a dissertation for the degree of Doctor of Philosophy.

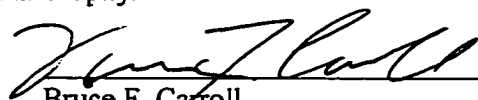William R. Dolbier
Professor of Chemistry

I certify that I have read this study and that in my opinion it conforms to acceptable standards of scholarly presentation and is fully adequate, in scope and quality, as a dissertation for the degree of Doctor of Philosophy.

Kenneth B. Wagener
Professor of Chemistry

I certify that I have read this study and that in my opinion it conforms to acceptable standards of scholarly presentation and is fully adequate, in scope and quality, as a dissertation for the degree of Doctor of Philosophy.

David, E. Richardson
Professor of Chemistry

I certify that I have read this study and that in my opinion it conforms to acceptable standards of scholarly presentation and is fully adequate, in scope and quality, as a dissertation for the degree of Doctor of Philosophy.

Bruce F. Carroll
Associate Professor of Aerospace
Engineering, Mechanics, and
Engineering Science

This thesis was submitted to the Graduate Faculty of the Department of Chemistry in the College of Liberal Arts and Sciences and to the Graduate School and was accepted as partial fulfillment of the requirements for the degree of Doctor of Philosophy.

August, 2001

Dean, Graduate School